Universitat Autònoma de Barcelona

Role of nuclear receptor RORγ1 in white adipose tissue

Maria Vilà Rovira

Role of nuclear receptor RORγ1 in white adipose tissue

Maria Vilà Rovira

Doctoral Thesis

Barcelona, 2022

Laboratory of Metabolism and Obesity
Unit of Diabetes and Metabolism
Vall d'Hebron Research Institute

Department of Biochemistry and Molecular Biology
Autonomous University of Barcelona

Role of nuclear receptor RORγ1 in white adipose tissue

Maria Vilà Rovira

Thesis submitted for the Degree of Doctor in Biochemistry, Molecular Biology and Biomedicine

Barcelona, 2022

Josep A. Villena Delgado
Thesis Director

Anna Meseguer Navarro
Tutor

Maria Vilà Rovira

TABLE OF CONTENTS

▼ ABBREVIATIONS

20α-OHC	20α-hydroxycholesterol
22R-OHC	22 R- hydroxycholesterol
24S-OHC	24 S-hydroxycholesterol
25-OHC	25-hydroxycholesterol

A

ACC	Acetyl-CoA carboxylase
Acox2	Acyl-Coenzyme A oxidase 2, branched chain
ADA	American Diabetes Association
AdipoQ	Adiponectin
AKT	Protein kinase B
AL	*Ad libitum*
AMPK	AMP kinase
Angptl8	Angiopoietin-like 8
ANO6	Anoctamin 6
ANOVA	Analysis of the variance
APCs	Antigen presenting cells
Apoa1	Apoliprotein A1
Apol6	Apolipoprotein L6
Apol9b	Apolipoprotein 9b
aP2	Adipocyte fatty acid-binding protein 4
Arg1	Arginase 1
AROS	Active regulator of SIRT1
ASP	Acylation-stimulating protein
ATF6	Activating transcription factor-6
Atgl	Adipose triglyceride lipase

B

BAT	Brown adipose tissue
BCA	Bicinchoninic Acid
Bcl-XL	Anti-apoptotic B-cell lymphoma-extra large
BCR	B cell receptor
Bmal1	Brain and muscle ARNT-like
BMI	Body Mass Index
BMPs	Bone morphogenetic proteins
Btla1	B and T lymphocyte associated

C

Ccl2	Chemokine (C-C motif) ligand 2
Ccl7	Chemokine (C-C motif) ligand 7
Ccl17	Chemokine (C-C motif) ligand 17
Ccl19	Chemokine (C-C motif) ligand 19
Ccl22	Chemokine (C-C motif) ligand 22
Ccr6	Chemokine (C-C motif) receptor 6

	cDNA	Complementary DNA
	Cd1d	Cluster of differentiation 1d
	Cd2	CD2 antigen
	Cd3e	CD3 antigen, epsilon polypeptide
	Cd4	CD4 antigen
	Cd8b1	CD8 antigen, beta chain 1
	Cd11c	Integrin alpha X
	CD32	Fc Fragment Of IgG Receptor IIa
	Cd37	CD37 antigen
	Cd206	Mannose receptor, C type 1
	Cd301	C-type lectin domain family 10, member A
	Clock	Circadian locomotor output cycles kaput
	COL6A3	*Collagen Type VI Alpha 3 Chain*
	CR	Calorie restriction
	Cre	Recombinase
	CRP	C reactive protein
	Cry1	Cryptochrome 1
	CLS	Crown-Like structures
	CT	Computed tomography
	Ctla4	Cytotoxic T-lymphocyte-associated protein 4
	Cxcl10	Chemokine (C-X-C motif) ligand 10
	Cyp8b1	Cytochrome P450 family 8 subfamily B member 1
	Cyp46	Cholesterol 24-hydroxylase
	CypA	Cyclophilin A
D	**DAMPs**	Host-cell-derived danger-associated molecular patterns
	DAVID	Database for Annotation, Visualitzation and Integrated Discovery
	DBD	DNA-binding domain
	DCs	Dendritic cells
	DEPC	Diethyl pyrocarbonate
	DIO	Diet-induced obesity
	Dio2	Iodothyronine deiodinase 2
	DM	Diabetes mellitus
	DMEM	Dulbecco's Modified Eagle's Medium
	DMSO	Dimethyl sulfoxide
	DN	Double negative
	DP	Double positive
E	**E4bp4**	E4 promoter binding-protein 4
	ECM	Extracellular matrix
	Elovl3	Elongation of very long chain fatty acids 3
	ER	Endoplasmic reticulum
	ERRα	Estrogen-related receptor alpha
	ESR1	Estrogen receptor 1

F

Fam57b	TLC domain containing 3B
FASN	Acid synthase
FBS	Fetal Bovine Serum
FDG-PET	Fluorodeoxyglucose-positron emission tomography
FDR	False Discovery Rate
FFA	Free fatty acids
Fgf2	Fibroblast growth factor 2
FGF21	Fibroblast growth factor 21
FMO	Fluorescence minus one
FOXO1	Forkhead box protein O1
FOXP3	Forkhead box P3

G

G6Pase	Glucose 6-phosphatase
GATA3	GATA binding protein 3
Gck	Glucokinase
GDM	Gestational diabetes mellitus
Gpat3	Glycerol-3-Phosphate Acyltransferase 3
GLUT4	Glucose transporter type 4
GMCSF	Granulocyte-macrophage colony-stimulating factor
GM-CSF	Granulocyte-macrophage colony-stimulating factor
GSEA	Gene Set Enrichment Analysis
GTT	Glucose tolerance test
Gys2	Glycogen synthase 2

H

HDL	High-density lipoprotein
HFD	High fat diet
Hmgcr	3-hydroxy-3-methylglutaryl-CoA reductase
HNF4α	Hepatocyte nuclear factor 4 alpha

I

IBMX	3-Isobutyl-1-methylxanthine
Icos	Inducible T cell co-stimulator
Ifit2	Interferon-induced protein with tetratricopeptide repeats 2
IF	Intermittent fasting
Ifnar1	Interferon receptor 1
IFN	Interferon
IFN-β	Interferon β
IFN-γ	Interferon γ
IgG	Immunoglobulin G
Ikbke	Inhibitor of kappaB kinase epsilon [Mus musculus
IKKβ	Inhibitor of nuclear factor Kβ kinase
IL-10	Interleukin 10
IL-12	Interleukin 12

	IL-13	Interleukin 13
	IL-15	Interleukin 15
	IL-17	Interleukin 17
	IL-22	Interleukin 22
	IL-23r	Interleukin 23 receptor
	IL-4	Interleukin 4
	IL-5	Interleukin 5
	IL-6	Interleukin 6
	IL-8r1	C-X-C motif chemokine receptor 1
	IL-1β	Interleukin 1 β
	ILCs	Innate lymphoid cells
	iNKt	Invariant natural killer T
	Insig2a	Insulin induced gene 2a
	IR	Insulin resistance
	IRE-1α	Inositol requiring enzyme-1
	IRF3	Interferon regulatory factor 3
	IRF5	Interferon regulatory factor 5
	Irf7	Interferon regulatory factor 7
	IRS-1	Insulin receptor substrate 1
	ITGAL	Integrin Subunit Alpha L
	ITT	Insulin tolerance test
J	**JNK**	C-jun N-terminal kinase
K	**KO**	Knockout
L	**LBD**	Ligand-binding domain
	LDL	Low density lipoprotein
	LepR	Leptin receptor
	Lipc	Hepatic lipase C
	LPS	Lipopolysaccharide
	LTi	Lymphoid tissue inducer cells
M	**M1**	Classically activated macrophages
	M2	Alternatively activated macrophages
	MAMP	Microbe-associated molecular pattern
	MCP-1	Monocyte chemoattractant protein 1
	MHC	Major histocompatibility complex
	miRNA	MicroRNA
	MMP-3	Metalloproteinase 3
	MMP-9	Matrix metalloproteinase 9
	Mx1	Interferon-regulated resistance GTP-Binding Protein MxA

N

NAD^+	Nicotinamide adenine dinucleotide
NCoR1	Nuclear receptor co-repressor 1
NCS	Newborn Calf Serum
NFκB	Nuclear factor κB
Nos2	Nitric oxide synthase 2, inducible
NK	Natural killer
NKt	Natural killer T
NR	Nuclear receptor

O

Oas1	2'-5'-oligoadenylate synthetase 1
Oas2	2'-5'-oligoadenylate synthetase 2
OD	Optical density
OxPhos	Mitochondrial oxidative phosphorylation

P

P2X7R	Purinergic P2X7 receptors
p53	Tumor protein p53
PAI-1	Plasminogen activator inhibitor-1
PAMPs	Molecular patterns association with pathogens
PARPs	NAD+-depleting enzymes, like poly(ADP- ribose) polymerase
PCA	Principal component analysis
Pnpla3	Patatin-like phospholipase domain containing 3
PBS	Phosphate-buffered saline
PCR	Polymerase Chain Reaction
PDH	Pyruvate dehydrogenase
Pepck	Phosphoenolpyruvate carboxykinase
PERK	PKR-like ER kinase
PGC-1α/ Ppargc1a	Peroxisome proliferative activated receptor-γ co-activator 1-alpha
PGC-1β/ Ppargc1b	Peroxisome proliferative activated receptor-γ co-activator 1-beta
PI-3K	Phosphatidylinositol 3-kinase
PIP2	Phosphatidylinositol-4,5-bisphosphate
PK	Proteinase K
Pla2g2	Phospholipase A2
Plcd3	Phospholipase C, delta 3
PKC	Protein kinase C
PPARα	Proliferator activated receptor alpha
PRR	Pattern recognition receptors
PVDF	Polyvinyl difluoride

Q

qPCR	Real-time quantitative polymerase chain reaction

R

Rev-Erbα	Nuclear receptor subfamily 1 group D member 1
ROR	Retinol-related orphan receptors
ROREs	ROR response elements
RORα	Retinoid-related orphan receptor alpha
RORβ	Retinoid-related orphan receptor beta
RORγ	Retinoid-related orphan receptor gamma
RORγ-FAT-KO	Knockout mice for RORγ in adipose tissues

S

SDS-PAGE	Sodium dodecyl sulfate-polyacrylamide gel electrophoresis
Sell	Selectin, lymphocyte
Sg	Staggerer
SIRT	Sirtuin 1
siRNA	Small interfering RNA
Slc27a1	Solute carrier family 27 member 1
SMRT	Silencing mediator of retinoid and thyroid hormone receptor
SP	Single positive
Sqle	Squalene epoxidase
SREBP1	Sterol regulatory element-binding protein 1
SREBP1c	Sterol regulatory element binding transcription factor 1 c
STAT	Signal transducer and activator of transcription
SVF	Stromal vascular fraction

T

T1D	Type 1 diabetes
T2D	Type 2 diabetes
TAE	*Tris-Acetate-EDTA*
TAG	Triglycerides
T-bet	T-box expressed in T cells
Tc	T cytotoxic cells
Tcf7	Transcription factor 7, T cell specific
TCR	T cell receptor
TF	Tissue factor
TGF	Transforming growth factor
Th	T helper cells
Themis	Thymocyte selection associated
TLRs	Toll-like receptors
TNF-α	Tumor necrosis factor α
Tnfrsf26	Tumor necrosis factor receptor superfamily, member 26
TRAF2	Tumor-necrosis factor-receptor-associated factor 2
TRL7	Toll-like receptor 7
Treg	Regulatory T cells

U	**UCP1**	Uncoupling protein 1
	UPR	Unfolded protein response
V	**Vegfa**	Vascular endothelial growth factor A
W	**WAT**	White adipose tissue
	WHO	World Health Organization
	Wnt10b	MMTV integration site family, member 10B
	Wt	Wild type
X	**XBP-1**	X-box-binding protein-1
Z	**Zap70**	Zeta-chain (TCR) associated protein kinase

▼ ABSTRACT

White adipose tissue (WAT) acts as a crucial integrating element in the regulation of energy balance and glucose homeostasis. Hence, WAT dysfunction is associated with the development of metabolic diseases, such as obesity and *type 2 diabetes* (T2D), which have reached epidemic proportions worldwide. Interestingly, lifestyle interventions, such as *calorie restriction* (CR), have proven to be as effective as some of the currently available therapies for the treatment of T2D. However, the precise mechanisms by which CR improves metabolic diseases are still poorly defined. In a previous study of our laboratory, *Rorc* was identified as one of the top genes up-regulated in WAT in response to CR, leading us to hypothesize that RORγ1 could be a crucial mediator of the effects that CR has on WAT.

To decipher the role of RORγ1 in WAT, we generated an *in vitro* model in which *Rorc* was knocked down in 3T3-L1 adipocytes, as well as an *in vivo* model that lacks RORγ specifically in adipocytes (RORγ-FAT-KO mice). Gene expression profile analysis of both 3T3-L1 adipocytes knockdown for *Rorc* and WAT of RORγ-FAT-KO mice fed *ad libitum* (AL) with a *high fat diet* (HFD) revealed that RORγ1 regulates the expression of genes related to the immune function, particularly with type I interferon responses. In agreement with an immunomodulatory role of RORγ in response to nutritional cues, gene expression profiling of WAT from RORγ-FAT-KO mice subjected to CR also identified genes related to the immune function, particularly to the T cell recruitment and polarization, as main targets of RORγ1 in WAT in response to CR. The characterization of the resident immune cell populations in WAT by flow cytometry revealed that RORγ-FAT-KO mice display a more anti-inflammatory profile than their Wt littermates, particularly when subjected to CR, suggesting that RORγ acts as a pro-inflammatory mediator.

As RORγ is also highly expressed in *brown adipose tissue* (BAT) and our mouse model also lacks the expression of RORγ in brown adipocytes, we analyzed the potential role of RORγ in BAT thermogenesis. When exposed to low environment temperature, RORγ-FAT-KO mice, similarly to their Wt littermates, were able to maintain their body core temperature and induce the expression of BAT thermogenic genes, indicating that RORγ is not essential for non-shivering adaptive thermogenesis.

We also studied the role of RORγ1 in adipose tissues as a mediator of the beneficial effects that CR exerts on whole body energy homeostasis and insulin sensitivity. First, we found that lack of RORγ in adipocytes is not sufficient to induce obesity or impair glucose homeostasis in mice fed AL. Moreover, despite being highly induced in response to CR, we demonstrated that RORγ in adipose tissues is not required for the improvement of glucose homeostasis observed in response to CR.

Tacking together, our findings indicate that RORγ1 has an immunomodulatory function in WAT, particularly in response to CR. Still, lack of RORγ does not affect whole body energy and glucose homeostasis.

▼ RESUM

El *teixit adipós blanc* (WAT) és un element integrador crucial en la regulació del balanç energètic i l'homeòstasi de la glucosa. Així doncs, una disfunció del WAT està associada al desenvolupament de malalties metabòliques, com l'obesitat i la *diabetis tipus 2* (T2D), les quals han assolit proporcions epidèmiques a nivell mundial. Curiosament, intervencions en l'estil de vida, com la *restricció calòrica* (CR), han demostrat ser tant efectives pel tractament de la T2D com algunes de les teràpies farmacològiques actualment disponibles a la pràctica clínica. Malgrat tot, els mecanismes pels quals la CR millora les malalties metabòliques encara estan poc definits. En un estudi previ realitzat al nostre laboratori es va identificar *Rorc* entre els gens sobreexpressats en el WAT en resposta a la CR, fet que ens va fer hipotetitzar que RORγ1 podria ser un mediador crucial dels efectes de la CR en el WAT.

Per estudiar el paper de RORγ1 en el WAT, hem generat un model *in vitro* en el qual s'ha silenciat *Rorc* en adipòcits 3T3-L1 en cultiu, així com un model *in vivo* on hem generat ratolins mancats de *Rorc* específicament en els adipòcits (RORγ-FAT-KO). L'anàlisi d'expressió gènica tant dels adipòcits 3T3-L1 silenciats per *Rorc* com del WAT dels ratolins RORγ-FAT-KO alimentats *ad libitum* (AL) amb una *dieta rica en greixos* (HFD) van revelar que RORγ1 regula l'expressió de gens relacionats amb la funció immune, concretament amb la resposta a interferó de tipus I. En concordança amb el paper immunoregulador de RORγ en resposta a intervencions nutricionals, l'anàlisi d'expressió gènica del WAT de ratolins RORγ-FAT-KO sotmesos a CR també va identificar gens relacionats amb la funció immunitària, concretament amb el reclutament i polarització de les cèl·lules T, com a dianes principals de RORγ1 en el WAT en resposta a la CR. La caracterització de les poblacions de cèl·lules immunitàries residents en el WAT per citometria de flux va revelar que els ratolins RORγ-FAT-KO exhibeixen un perfil més antiinflamatori en comparació amb els Wt, sobretot quan estan sotmesos a CR, fet que suggereix que RORγ actua com a mediador pro-inflamatori.

Com que l'expressió de RORγ és també molt alta en el *teixit adipós marró* (BAT) i en el nostre model de ratolí l'expressió de RORγ també està noquejada en els adipòcits marrons, vam analitzar el paper potencial de RORγ en la termogènesis del BAT. En ser exposats a una temperatura ambiental freda, els ratolins RORγ-FAT-KO van ser capaços de mantenir la seva temperatura corporal i induir l'expressió de gens termogènics del BAT de la mateixa manera que els Wt, cosa que indica que RORγ no és essencial per la termogènesi adaptativa sense tremolor.

Vam estudiar també el paper de RORγ1 en els teixits adiposos com a mediador dels efectes beneficiosos que exerceix la CR en l'homeòstasi energètica i sensibilitat a la insulina a nivell sistèmic. En primer lloc, vam trobar que la manca de RORγ en els adipòcits no és suficient per induir obesitat o alterar a homeòstasi de la glucosa en els ratolins alimentats AL. A més a més, malgrat estar induït en resposta a la CR, vam demostrar que RORγ en els teixits adiposos no és necessari per a la millora de la homeòstasi de la glucosa observada en resposta a la CR.

En conjunt, els nostres resultats indiquen que RORγ1 té una funció immunoreguladora en el WAT, particularment en resposta a la CR. No obstant això, la manca de RORγ en els teixits adiposos no afecta a l'homeòstasi energètica i de la glucosa a nivell sistèmic.

INTRODUCTION

► 1.1 Epidemiology of obesity and type 2 diabetes

The *World Health Organization* (WHO) defines obesity as an abnormal or excessive fat accumulation that may impair health, which is diagnosed at a *Body Mass Index* (BMI) ≥ 30 kg/m^2. In the past 50 years, obesity and overweight have reached epidemic proportions worldwide. According to WHO, 39% of adults aged 18 and over were overweight in 2016. Of these, 13% were obese. Moreover, childhood obesity has become one of the most severe public health challenges of this century in developed countries, with 18% of children and adolescents between 5-19 years old being overweight or obese in 2016 (1).

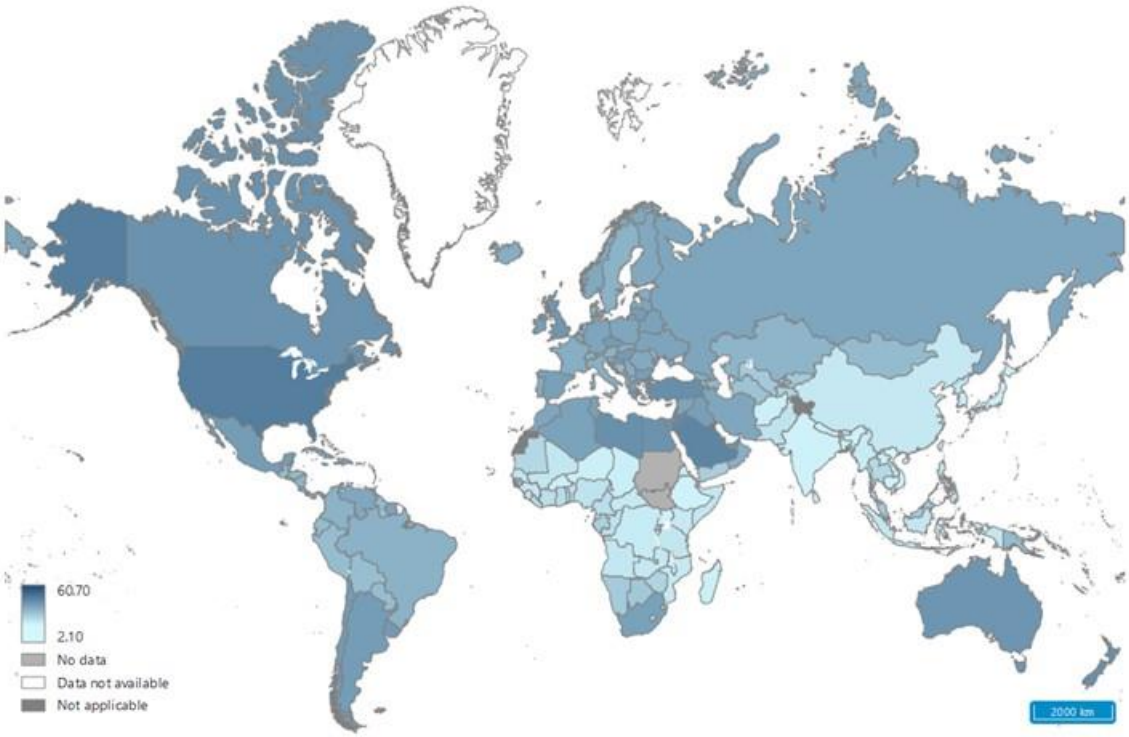

Figure 1.1. Illustrative map of obesity prevalence among adults over the world in 2016. Image extracted from (2).

Obesity represents a major health challenge because it is associated with a reduction of lifespan of between 5-20 years, depending on the severity of the condition and comorbid disorders (3,4). It is known that increased body mass is associated with an increase of the risk for numerous metabolic diseases, such as hypertension, coronary heart disease and *type 2 diabetes* (T2D). Then, it is not surprising to find out that, in parallel with the dramatic increase in obesity, T2D has become the most common metabolic disorder in the world, being recognized as one of the most deadly non-communicable diseases worldwide (5). Nowadays, it has been estimated that approximately 422 million people have diabetes, representing almost 10% of the world population (6). Although it is more common in adults, its prevalence is now alarmingly increasing in children and adolescents. In 2018, about 1 in 11 adults worldwide had diabetes, of which 90% had T2D. The prevalence of T2D is expected to double in the next 20 years, mainly because of the increase in obesity within population (7,8).

1.1.1 Insulin resistance in the pathogenesis of type 2 diabetes

Diabetes mellitus (DM) is a chronic metabolic disease characterized by high blood glucose level over prolonged period of time. Diabetes is linked to numerous complications, the most frequent

being coronary atherosclerosis, hypertension, diabetic retinopathy, peripheral neuropathy and nephropathy (9). DM is classified into three main types. ***Type 1 diabetes*** (T1D), once known as juvenile diabetes or insulin-dependent diabetes, is characterized by little or no insulin production by pancreas, and is mostly caused by the autoimmune destruction of pancreatic β-cells. **T2D**, or non-insulin-dependent diabetes**,** is caused by a combination of β-cell loss and dysfunction together with *insulin resistance* (IR) of target tissues. The third type of DM is ***gestational diabetes mellitus*** (GDM), which occurs in pregnant women. GDM usually disappears with delivery, but women affected and their children are at increased risk of developing T2D later in life (6,10).

IR is considered the primary cause of T2D. As defined by the *American Diabetes Association* (ADA), IR is a pathological state in which cells fail to respond to the normal actions of insulin, resulting in decreased glucose uptake, reduced glycogen synthesis and enhanced hepatic gluconeogenesis, leading to elevated blood glucose levels (11). Furthermore, in adipose tissue, IR produces an impaired inhibition of lipolysis, and consequently it results in elevated circulating levels of *free fatty acids* (FFA), which in turn contribute to worsen the insulin resistant state (12), as it will be further explained. Therefore, a defective insulin signaling results in an imbalanced metabolic function of the main insulin target tissues, and severely alters whole body glucose and lipid homeostasis (8).

Several evidences indicate that IR is a pathogenic factor for T2D (13,14). Indeed, different studies report that IR is present in almost all patients with T2D (15), as well as therapeutic interventions that improve insulin sensitivity prevent or delay the development of T2D (16). Additionally, IR precedes the formal establishment of T2D. In general, T2D develops when pancreatic β-cells fail to secrete sufficient amounts of insulin to meet the high metabolic demand caused by IR. At the beginning, pancreatic β-cells are able to compensate IR by hypersecretion of insulin and, therefore, there is a period of normal glycemia. At some point, however, this period of β-cell compensation is followed by β-cell failure, in which the pancreas fails to secrete sufficient insulin and diabetes ensues (17).

1.1.2 Mechanisms of insulin resistance

Some of the mechanisms that contribute to the onset of IR in insulin-responsive tissues have been identified. These include lipotoxicity, inflammation, *endoplasmic reticulum* (ER) stress and mitochondrial dysfunction (Figure 1.2), although novel factors, such as dysbiosis, has also been recently suggested to contribute to the development of IR (18).

Lipotoxicity is the result of an excess of circulating fatty acids, as a consequence of an excessive dietary intake of lipids, as well as the incapability of adipocytes to efficiently store fatty acids as *triglycerides* (TAG), as it occurs in obese individuals. This leads to an abnormal accumulation of TAG, fatty acids and other lipid intermediates, such as diacylglycerol and ceramides in tissues. Some of these lipid species have been reported to impair insulin signaling. Indeed, several studies have demonstrated that diacylglycerol accumulation activates *protein kinase C* (PKC) isoforms (13), which in turn phosphorylate and inhibit *insulin receptor substrate 1* (IRS-1), causing a reduction in the recruitment of *phosphatidylinositol 3-kinase* (PI-3K) and the inhibition of the insulin signaling pathway (19). Ceramides, which have also been found increased in tissues of obese patients (20), have been shown to induce IR through the activation of the atypical PKCζ isoform, which impairs insulin signaling by phosphorylating and inhibiting *protein kinase B* (AKT) (21).

Chronic low-grade inflammation, which is commonly found in obese patients, also plays an important role in the development of IR. Several types of immune cells reside in *white adipose tissue* (WAT), which, together with adipocytes and stromal vascular cells, constitute a cellular network that produces both pro- and anti-inflammatory cytokines. High circulating levels of pro-inflammatory cytokines, such as *tumor necrosis factor α* (TNF-α), *interleukin 1 β* (IL-1β) and *interleukin 6* (IL-6), are found in obese patients. These cytokines act by activating inflammatory pathways that involve diverse serine/threonine kinases, such as *c-jun N-terminal kinase* (JNK) or *inhibitor of nuclear factor Kβ kinase* (IKKβ). In insulin sensitive tissues, sustained activation of these kinases result in the inhibition of insulin signaling by specifically phosphorylating IRS-1 at inhibitory residue Ser307 (22). The inflammatory cytokines mentioned above are mainly secreted by pro-inflammatory macrophages residing in the WAT, but also by stressed adipocytes. In addition to directly inducing IR through the activation of JNK/IKK-dependent signaling pathways, these pro-inflammatory cytokines also increase lipolysis in WAT, an effect that will in turn contribute to IR through the accumulation of lipid intermediates in other insulin target tissues. Moreover, it has been demonstrated that circulating FFA can themselves act as inflammatory signals and activate the JNK pathway through the direct interaction with *Toll-like receptors 4* (TLR4), creating a synergistic relationship between lipotoxicity and inflammation (23). The role of different immune cells populations in obesity-linked IR and T2D will be further discussed in section 1.3.

ER stress is a relatively new mechanism proposed to be implicated in the origin of IR (24). ER is an organelle involved in protein synthesis and folding, lipid metabolism and calcium homeostasis. Certain environmental conditions, such as radiation and hypoxia, or endogenous conditions, such as accumulation of newly synthetized unfolded proteins in the ER lumen, can challenge ER function, causing stress. Then, this organelle produces an adaptive response to reduce this state, which is known as the *unfolded protein response* (UPR). Of note, intracellular FFA can also produce ER stress (25). In obesity, an induction of ER stress has been observed in close association with IR and T2D. Expression patterns of molecular indicators of ER stress are increased in dietary or genetic murine obesity models. Moreover, mice deficient in *X-box-binding protein-1* (XBP-1), which modulates the ER stress response, show an increased ER stress as well as impaired insulin signaling (26).The three axes of UPR signaling are *inositol requiring enzyme-1* (IRE-1α), *PKR-like ER kinase* (PERK) and *activating transcription factor-6* (ATF6), which under stress conditions activate and reduce unfolded proteins in the ER lumen (27). It has been reported that IRE-1 bind to *tumor-necrosis factor-receptor-associated factor 2* (TRAF2), which is an adaptor protein that promotes activation of JNK. Therefore, ER stress induces IR through the activation of JNK and IKKβ (28,29), which leads to phosphorylation of IRS and, consequently, inhibition of insulin signaling (Figure 1.2).

Numerous studies have also proposed a critical role of **reduced mitochondrial function** as a predisposing condition for IR. A wide range of studies in humans have found a tight correlation between mitochondrial dysfunction and IR and T2D. Indeed, it has been observed that impaired mitochondrial function occurs in obese people, as well as in the offspring of T2D patients (30). Additionally, T2D individuals present a reduction of β-oxidation (31), activity of *mitochondrial oxidative phosphorylation* (OxPhos) complexes and mitochondrial mass in skeletal muscle (32). Similarly to humans, adipose mitochondrial biogenesis is suppressed in genetic animal models of diabetes (db/db mice) as well as in *diet-induced obesity* (DIO) mice (33). On the contrary, treatment with thiazolidinediones, a family of antidiabetic insulin-sensitizing drugs, improves mitochondrial function by increasing mitochondrial biogenesis in adipose tissue (34).

All together, these data have led to suggest that impaired mitochondrial oxidative capacity could be one of the main underlying causes of IR and T2D, by promoting ectopic lipid accumulation and, therefore, lipotoxicity.

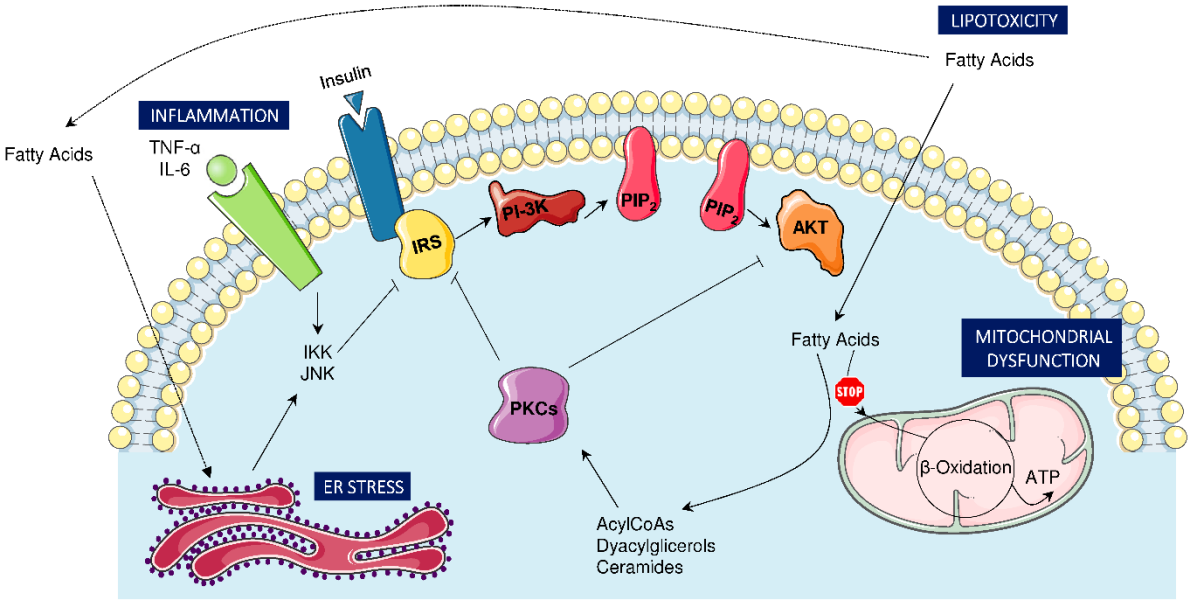

Figure 1.2. Scheme of the main mechanisms of IR. IRS, insulin receptor substrate; PI-3K, phosphatidylinositol 3-kinase; PIP_2, phosphatidylinositol-4,5-biphosphate; AKT, protein kinase B; PKC, protein kinase C; TNF-α, tumor necrosis factor α; IL-6, interleukin 6.Image adapted from (8).

► 1.2 Adipose tissue and control of glucose and energy homeostasis

Adipose tissue is considered as a crucial integrating element in the regulation of energy balance and glucose homeostasis. Adipose tissue is principally composed of adipocytes, considered as the functional unit of the tissue, and the *stromal vascular fraction* (SVF), which contains a variety of other cell types such as pre-adipocytes, macrophages, fibroblasts and endothelial cells (35). Two main types of adipose tissue are found in mammals, WAT and *brown adipose tissue* (BAT), both of them performing completely different functions, but still very important in the regulation of glucose homeostasis and energy balance.

1.2.1 White adipose tissue

WAT is characterized by its lipid storage and endocrine functions. Both in humans and in mice, females have a higher percentage of fat mass relative to males, representing 25-31% of women's and 18-24% of men's body weight in healthy conditions (36,37). At morphological level, white adipocytes appear as polyhedral cells of large diameter characterized by a single big lipid droplet that occupies most of their cytoplasm, and a low content of mitochondria and other organelles in their lateralized cytoplasm (35) (Figure 1.3).

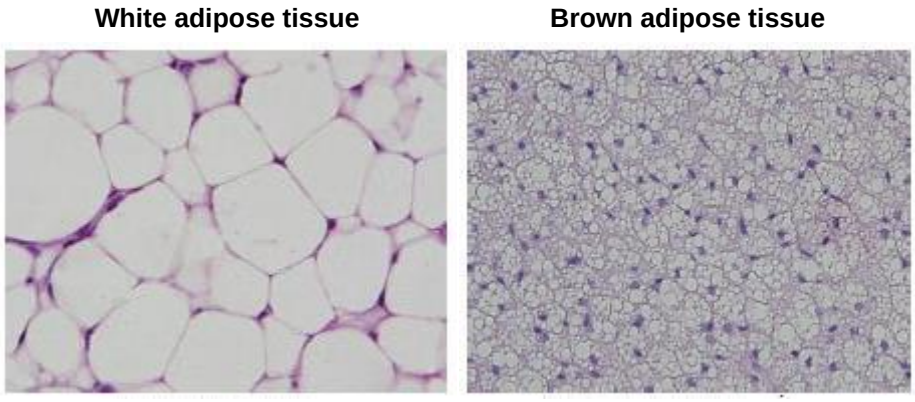

Figure 1.3. WAT and BAT cellular morphology. WAT adipocytes have a big lipid droplet with lateralized nucleus, while BAT adipocytes have a reddish aspect with more mitochondria and multiple small droplets. Images obtained from hematoxylin/eosin staining of mice adipose tissues done in the laboratory.

WAT accumulates in discrete locations, recognized as specific depots. According with the regional localization, in vertebrates, the most common classification distinguishes between subcutaneous, located under the skin and outside the peritoneal cavity, and visceral WAT, located in the thoracic and abdominal cavities (38). However, WAT can also be found around the mammary glands, between the muscle fibers or in the bone marrow.

Importantly, fat distribution varies considerably between species, thus many depots in humans do not precisely correlate with those in mice (Figure 1.4). **Visceral WAT** depots found in humans include mesenteric, omental, retroperitoneal, perirenal, epicardial and mediastinal. Similarly, in mice we find mesenteric, retroperitoneal, perirenal, mediastinal and perigonadal adipose tissues. Perigonadal or gonadal WAT, is only found surrounding reproductive organs in mice, but not in humans, and it is one of the most studied WAT depots due to its easy access in mice. However, the relevance of certain depots with regard to physiological and pathophysiological implications in mice and humans have been a matter of controversy (39).

In mice, **subcutaneous fat** is comprised of two main depots: the anterior subcutaneous depot, situated in the interscapular region, and the posterior subcutaneous depot (also called inguinal), which consists of a long strip of tissue located around the hind limbs and it is the most relevant subcutaneous depot. The distribution of subcutaneous fat in humans is pretty similar. Large depositions of subcutaneous fat are distributed in the posterior lumbar, epidural, buttock, gluteal and thigh regions. In obesity, these regions appear to join and form a continuous single depot of subcutaneous fat. However, humans present a subcutaneous abdominal adipose depot that is not found in mice. Both human and mice also present a subdermal fat layer (40).

Adipose depots are intrinsically different and display metabolic heterogeneity. It is known that intra-abdominal obesity is associated with risk of metabolic complications, such as IR, glucose intolerance and dyslipidemia, whereas some studies support subcutaneous adipose tissue as being metabolically beneficial (41). In rodents, an improvement in insulin action, glucose tolerance and longevity has been observed when visceral fat pads are surgically removed (42,43), whereas the removal of subcutaneous fat pads causes metabolic syndrome (44). In line with this, it has been observed that upper body fat distribution in humans, which is mainly composed by visceral WAT, is linked to a higher risk of metabolic dysfunction. On the other hand, lower body adiposity, principally formed by the subcutaneous gluteal and femoral regions, is associated with lower risk and could be protective (45).

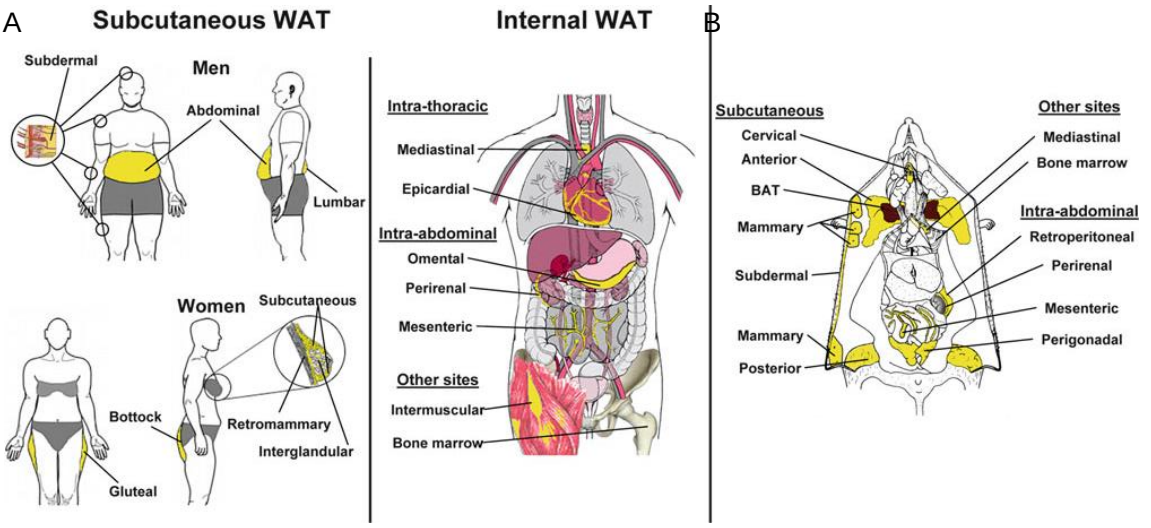

Figure 1.4. Distribution of major WAT depots in human (A) and mice (B). WAT is distributed throughout the body in both humans and mice. The two major compartments of WAT are subcutaneous and visceral WAT, although it can also be found in other regions. Although human and mice share most of their WAT depots, several differences exist between species. For instance, epicardial WAT is specific for humans, while the perigonadal WAT is only found in mice. Image obtained from (40).

The main function of WAT is to **store energy** under the form of TAG. When required, the stored energy is mobilized trough the hydrolysis of TAG by lipolysis, which delivers to the circulation FFA that will be used for other tissues. TAG can be synthesized through different processes: after uptake and metabolism of glucose (process termed *de novo* lipogenesis) and/or after uptake of fatty acids from blood and their esterification with glycerol. Both processes are regulated by the insulin pathway, the adrenergic pathway and the atrial natriuretic hormone pathways. Epinephrine and glucagon stimulate fatty acid release from TAG stored in adipocyte fat droplets, while insulin counteracts the actions of these hormones and induce fat storage. Additionally, insulin also controls *de novo* lipogenesis in adipocytes, stimulating glucose uptake through *glucose transporter type 4* (GLUT4) (46) and activating *pyruvate dehydrogenase* (PDH) (47) and indirectly increasing the expression of *fatty acid synthase* (FASN) and *acetyl-CoA carboxylase* (ACC) (48,49). WAT *de novo* lipogenesis in humans is considered to minimally contribute to the total body lipid storage, whereas in rodents generates an important amount of the TAG stored in WAT (50).

Another function of WAT, but not less important, is its **endocrine activity**. To date, more than one hundred factors are known to be produced and released by WAT, which are called adipokines. These products belong to different types and families of molecules, including exosomes, *microRNA* (miRNA), lipids, inflammatory cytokines and peptide hormones. Although some of the secreted adipokines by WAT are secreted by adipocytes, many others are synthesized and released by other cell types, such as the macrophages contained in the SVF (51,52).

Figure 1.5 gives an overview of the most important and best characterized adipose secreted products. Adipokines regulate multiple processes in the organism, such as glucose and lipid metabolism (resistin, adiponectin), inflammation (TNF-α, IL-1β), coagulation (*plasminogen activator inhibitor-1*, PAI-1), blood pressure (angiotensinogen and angiotensin II) and food intake (leptin). Many of these factors have a autocrine/paracrine effect while others act systematically and control the function of several organs and tissues, including liver, muscle, blood vessels and brain (53–55). Together, these hormones function to regulate food intake, the reproductive axis, insulin sensitivity and immune responses (54).

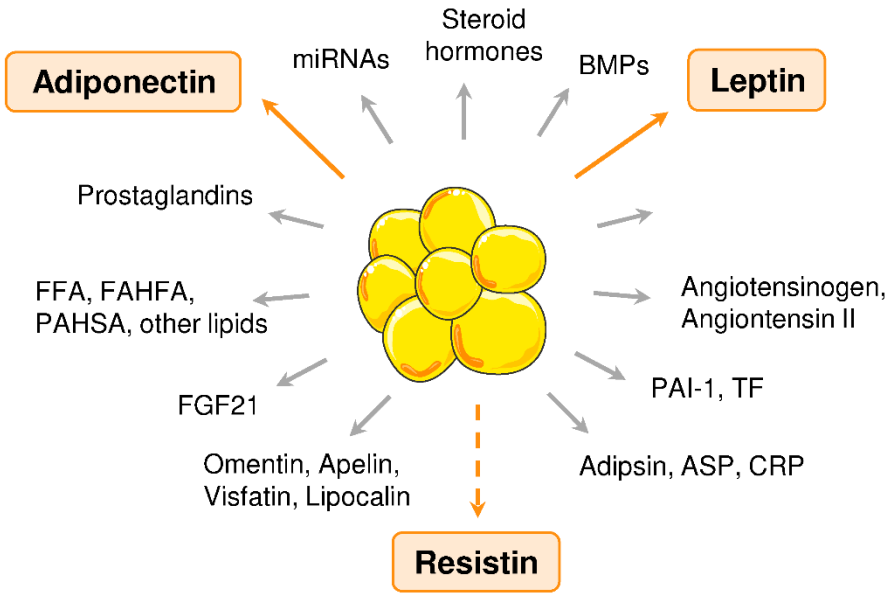

Figure 1.5. WAT as a secretory organ. Leptin, adiponectin and resistin are exclusively secreted from mouse adipocytes, although resistin is primarily produced by macrophages in humans. The other factors can also be secreted from other cell types within WAT. miRNA, microRNA; BMPs, bone morphogenetic proteins; PAI-1, plasminogen activator inhibitor 1, TF, tissue factor; ASP, acylation-stimulating protein; CRP, C reactive protein; FGF21, fibroblast growth factor 21; FFA, free fatty acid; FAHFA, fatty acid esters of hydroxyl fatty acids; PAHSA, palmitic acid hydroxy stearic acid. Figure adapted from (54,56,57).

One of the best characterized adipokines is **leptin**. It acts mainly via central mechanisms. Activation of leptin receptor in the hypothalamus leads to repression of orexigenic pathways and induction of anorexigeneic pathways, which leads to an appetite reduction (58). Leptin also mediates responses in peripheral tissues, including WAT, the endocrine pancreas and other insulin-sensitive tissues. Indeed, leptin suppresses insulin signaling in adipocytes and also antagonizes hepatic insulin signaling. In endocrine pancreas, leptin inhibits insulin and glucagon secretion from β-cells and α-cells, respectively. Insulin secretion from pancreatic β-cells promotes lipid storage and leptin synthesis in adipocytes, producing a bidirectional regulatory loop between β-cells and adipocytes (59).

Adiponectin is another important adipokine in the context of energy balance and insulin sensitivity (59). Adiponectin modulates insulin sensitivity by inhibiting hepatic glucose production, enhancing glucose uptake in muscle and increasing fatty acid oxidation in liver and muscle (60). Adiponectin also acts in the brain to increase body energy expenditure, which may promote weight loss.

Resistin is another small protein identified as an adipokine linking obesity to IR in rodents. Its expression is decreased in WAT in response to fasting in mice, while it is increased after refeeding or in DIO and genetic mice models of obesity (61,62). Noteworthy, although resistin induces IR and inflammation both in humans and mice, human resistin is predominantly secreted from macrophages, not adipocytes (63).

On the other hand, abdominal adipose tissue can produce large quantities of **IL-6**, **TNF-α** and **IL-1β**, which are known for their pro-inflammatory role. A positive correlation between the concentration of these cytokines in plasma with IR and increased risk of diabetes has been observed. Importantly, it has been suggested that IL-1β has a role in inflammatory pancreatic β-cell damage and apoptosis (64). Moreover, blocking IL-1β may be beneficial for preventing IR and inflammation of adipose tissue obese individuals (65). Likewise, it has been demonstrated that TNF-α impairs insulin sensitivity both *in vitro* and *in vivo* (66).

1.2.2 Brown adipose tissue

The primary function of BAT is to maintain body temperature through a process known as non-shivering adaptive thermogenesis. This process is regulated by the sympathetic nervous system and is activated by norepinephrine released under certain environmental stimuli, such as cold (67).

Unlike white adipocytes, brown adipocytes contain multiple small droplets homogenously distributed through their cytoplasm (Figure 1.3). The tissue is highly innervated and densely vascularized to ensure adequate supply of substrates and oxygen and efficient and rapid distribution of the heat produced by thermogenesis. Brown adipocytes are also rich in mitochondria, which confer its reddish color and a much greater oxidative power than the one of WAT.

BAT is also constituted of very specific depots. The major ones found in rodents, and in most mammals, include the interscapular, cervical and axillar BAT depots. Minor depots are located in the perirenal, intercostal and periaortic areas (Figure 1.6A) (68). The spatial distribution of BAT along the body allows temperature preservation of vital organs.

In humans, BAT was first thought to be present exclusively during the fetal and perinatal developmental stages and rapidly regressed afterwards. Nevertheless, recent studies using *fluorodeoxyglucose-positron emission tomography* (FDG-PET) in combination with *computed tomography* (CT) revealed that adult humans have identifiable and active BAT (69). Similar to mice, human BAT depots are mainly located in the cervical, interscapular, axillary, perirenal and periaortic regions (Figure 1.6B).

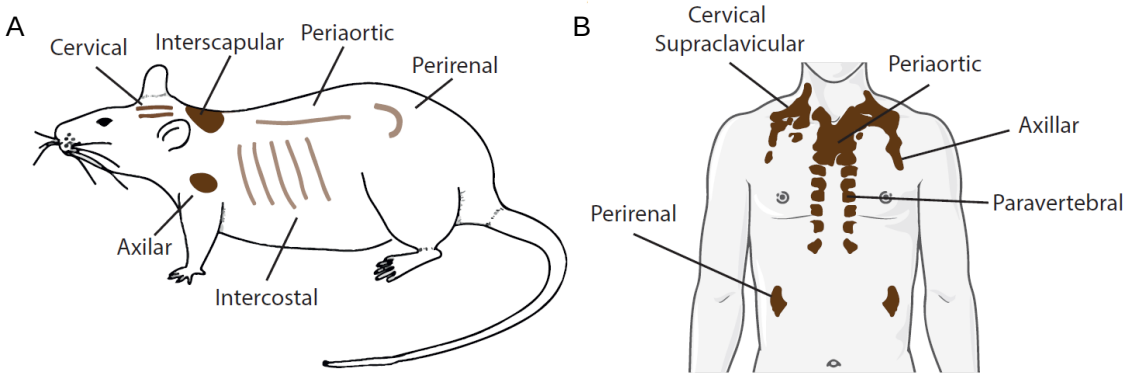

Figure 1.6. Distribution of major BAT depots in mice (A) and humans (B). Image extracted from (70).

At a molecular level, a unique defining feature of brown adipocytes is that they specifically express *uncoupling protein 1* (UCP1). The presence of UCP1 in the mitochondria of brown adipocytes is essential for thermogenesis. Located in the inner membrane of brown adipocytes' mitochondria, UCP1 acts as a proton channel that allows proton flux from the inter-membrane space to the mitochondrial matrix. Hence, it uncouples the oxidation of reducing equivalents from the synthesis of ATP, dissipating the proton gradient produced by the respiratory chain as heat (71,72).

Thermogenic adipocytes are not only found in the BAT depots mentioned above, but they can also appear distributed amongst white adipocytes from WAT under certain conditions. For example, prolonged cold exposure or treatment with β-adrenergic receptor agonists increase the appearance of brown adipocytes within WAT, a process called "browning" of WAT. To distinguish them from the classical brown adipocytes found in BAT depots, these UCP1-expressing adipocytes found in WAT are known as brite (brown in white) or beige adipocytes (70). These brite/beige adipocytes are also thermogenically competent (71).

BAT mass and activity have been linked to alterations in glucose and energy homeostasis. Obese individuals have lower amount of active BAT, which suggest that BAT activation or browning stimulation of WAT could contribute to reduce fat mass and improve metabolic health. Various studies performed in rodent models show that BAT transplantation increases fatty acid oxidation, which improves metabolic parameters, such as IR and liver steatosis (73). Moreover, it has been observed that there is an amelioration of obesity and IR when mice are treated with β_3-adrenergic receptor agonists, which activate BAT thermogenesis and promote the differentiation of precursor cells into brown adipocytes (74,75). These findings suggest that BAT could be a promising target to treat obesity and its comorbidities. However, despite the promising results obtained in mice, adrenergic stimulation in humans had considerable side effects on the cardiovascular system (76), precluding the use of β_3-adrenergic receptor agonists as therapeutic agents for the treatment of metabolic diseases. Also PPARγ agonists have been shown to increase brite adipocytes recruitment within WAT, which is associated with the insulin-sensitizing character (77,78). Recently, adrenergic-independent brown fat activators have been described, such as *fibroblast growth factor 21* (FGF21) or irisin. This opens an alternative way to activate BAT independently of the sympathetic nervous system by the use of specific drugs (79).

► 1.3 Adipose tissue and immune system interactions

Adipose tissue exerts metabolic control through various immunological mechanisms, which have prompted a new field of research termed immunometabolism (80). Adipose tissue resident immune cells have housekeeping functions, which include apoptotic cell clearance, *extracellular matrix* (ECM) remodeling and angiogenesis. Nevertheless, in obesity condition, metabolic signals from stressed adipocytes lead to a shift in immune-cell phenotypes and numbers that affect local and systemic metabolism and insulin sensitivity.

1.3.1 Biological function of immune infiltrate in adipose tissue

As mentioned above (see section 1.1), chronic inflammation plays an important role in obesity, contributing to the development of its associated metabolic complications. Although inflammatory signals primarily exert negative impact on metabolism, several authors propose that the metabolic response to inflammation, namely IR, is an adaptive mechanism that contributes to efficiently beat pathogenic invasions (81). For example, Th1 cells mainly develop following infections by intracellular bacteria and some viruses, in which immune cells require high levels of glucose to maintain the inflammatory phenotype and defeat the pathogens (82). Hence, transient generation of IR not only allows higher glucose availability for immune cells, but also increases the glucose storage mobilization. On the other hand, Th2 cells predominate in response to infestations by extracellular parasites (82). Th2 response stimulates insulin sensitivity and glucose uptake in peripheral tissues. Consequently, nutrient availability and use is guaranteed for host, whereas it is deprived for the parasite during infection (83,84).

Acute inflammatory response in WAT is therefore considered an adaptive mechanism that permits a proper expansion of the tissue to accommodate the excess of nutrients. In this regard, it has been demonstrated that mice lacking local WAT inflammatory response show increased DIO, ectopic lipid accumulation, glucose intolerance and systemic inflammation (81).

The first approximation of the mechanistic link between IR induced by obesity and adipose tissue inflammation showed that experimental models of obesity as well as obese patients have increased

levels of pro-inflammatory cytokines, like TNF-α, IL-1β, IL-6 or *C-reactive protein* (CRP) (85). The unequivocal role of inflammation in the development of IR has been demonstrated in studies in which neutralization of circulating TNF-α by the use of specific antibodies improved insulin sensitivity in insulin-resistant mice (86). In addition to elevated pro-inflammatory cytokine production, obesity is characterized by qualitative and quantitative changes in the different immune populations. The specific contribution of each of these cell populations to the obesity-associated inflammatory milieu and IR has just started to being deciphered. The knowledge accumulated to date regarding the contribution of each immune cell population to the progression of obesity-related inflammation and IR is discussed in the following paragraphs.

1.3.2 Innate immune cells in adipose tissue

Immune cells are categorized into innate and adaptive immune cells. The **innate immune system** relies on cells and soluble molecules that provide the first defense against infection. It consists of the less specific component of immunity and most of the components are present in the organism before the onset of infection. The two major players of innate immune system are neutrophils and macrophages, but also include eosinophils, basophils, mast cells, *natural killer* (NK) cells, *innate lymphoid cells* (ILCs) and *dendritic cells* (DCs). Innate immunity is mediated by a set of germline encoded non-clonal receptors which have mechanisms that can recognize conserved *molecular patterns association with pathogens* (PAMPs), such as *toll-like receptors* (TLRs) and *host-cell-derived danger-associated molecular patterns* (DAMPs). All of these receptors are referred as *pattern recognition receptors* (PRR). PRRs can signal the presence of pathogens and PAMP recognition can directly activate effector mechanisms of innate immunity, such as phagocytosis, induction of the synthesis of antimicrobial peptides and induction of nitric oxide synthase in macrophages. Moreover, PAMPs can also induce the expression of co-stimulatory molecules on *antigen presenting cells* (APCs), as well as the expression of inflammatory and effector cytokines and chemokines, which control the recruitment of leukocytes to the sites of infection and regulate the activation of appropriate effector mechanisms (87).

The persistant presence of antigenic stimulus leads to the activation of the **adaptive immune system**, constituted by T and B lymphocytes as well as *natural killer T* (NKt) cells. APCs engulf pathogens and digest antigens, which bind to *major histocompatibility complex* (MHC) molecules and are presented on the APC surface. Then, antigen/MHC complexes interact with the *T cell receptor* (TCR) on T cells or *B cell receptor* (BCR) on B cells, and induce the killing of pathogens by cytotoxic mechanisms or the production of antibodies, respectively (87,88).

Although the classical classification of immune cells categorizes them as belonging to innate or adaptive immune system, many cells play roles in both arms of immune system. These cells include NK cells, *invariant natural killer T* (iNKt) cells and ILCs. These cells not only produce cytokines that regulate innate immunity, but also help to shape the development of adaptive immunity (88).

In a situation of obesity, there are significant numerical, functional and relative changes in the cellular inflammatory mediators that will contribute to the development of obesity-induced inflammation and IR (see Figure 1.7 for an overview of the major immune cell populations).

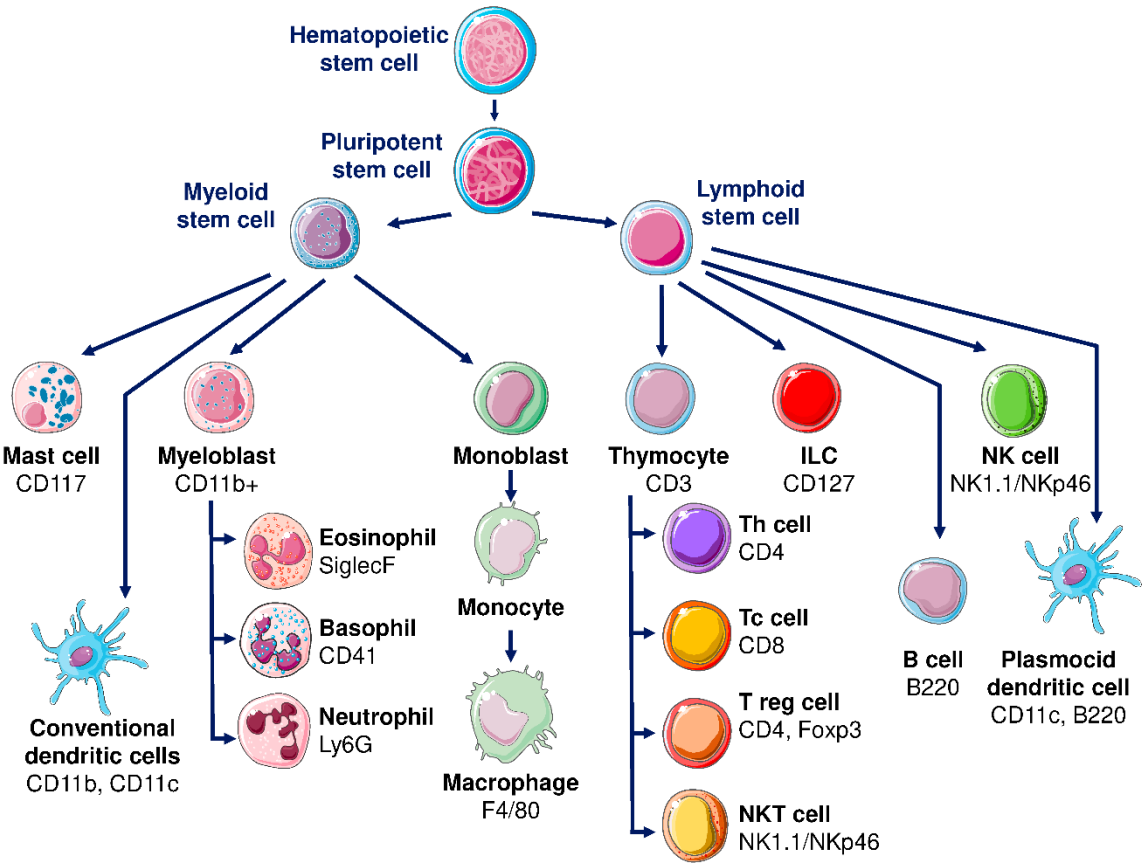

Figure 1.7. Lymphoid cells and myeloid cells maturation and some of their mouse immune cell markers of immune cell populations described to have a direct role on the development of IR.

1.3.2.1 Macrophages

Adipose tissue macrophages constitute the most abundant leukocyte population within WAT. Both in humans and mice, around 5% of the adipose tissue cells in the lean state are macrophages, and this percentage can increase up to 50% in conditions of obesity (89). Monocytes can differentiate into *classically activated macrophages* (M1) or *alternatively activated macrophages* (M2) upon stimulation. In lean state, macrophages display an M2 phenotype, characterized by the expression of high levels of arginase-1, *mannose receptor, C type 1* (CD206) and *C-type lectin domain family 10, member A* (CD301), and promote insulin sensitivity in adipocytes by secreting *interleukin 10* (IL-10). Anti-inflammatory Th2 cytokines such as *interleukin 4* (IL-4), IL-10 and *interleukin 13* (IL-13) stimulate the M2 polarization (90). M2 macrophages are important to help maintaining tissue homeostasis in steady lean state.

Conversely, the number of macrophages increases in obesity. *Interferon γ* (IFN-γ) and *lipopolysaccharide* (LPS) drive polarization toward M1 phenotype, promoting the production of pro-inflammatory cytokines such as IL-6, TNF-α, IL-1β, *interleukin 12* (IL-12) and *monocyte chemoattractant protein 1* (MCP-1, also known as *chemokine C-C motif ligand 2*; CCL2). A part from expressing surface specific macrophage markers such as F4/80 and CD11b, M1 macrophages specifically express CD11c proteins (90). The two types of macrophages also differ in their location, with M2 macrophages mostly found interstitially between the adipocytes, whereas M1 macrophages mostly localize in inflammatory foci known as *Crown-Like Structures* (CLS) (91).

It has been shown that impaired M2 macrophage activation in rodent models enhances predisposition to DIO and IR, whereas potentiation of M2 macrophage activation confers protection from obesity-associated metabolic dysfunction (92). In addition, it is proposed that M2 signaling and type 2 cytokine signaling can contribute to adipose tissue homeostasis acting on thermogenesis and beige adipogenesis, under lean or CR conditions (83,93–95). However, the pro-thermogenic function of M2 macrophages is still controversial (96). In contrast to M2 macrophages, accumulation of M1 macrophages in WAT directly contributes to local and systemic inflammation and IR. For instance, there is an improvement of insulin sensitivity and a decrease in inflammatory markers, both locally and systemically, when $CD11c^+$ cells are ablated (97).

1.3.2.2 Dendritic cells

DCs recognize and load foreign antigens onto MHC molecules and present them to T lymphocytes (98). The roles and presence of DCs in adipose tissue of lean and obese mice or humans has not been studied thoroughly, but several studies have reported that DCs are elevated in WAT in mouse and human obesity. It has been suggested a role for dendritic cells (DCs) in promoting adipose tissue macrophage infiltration (99). Aside from stimulating macrophage infiltration in adipose tissue and liver, DCs also regulate the differentiation of $CD4^+$ T cells into inflammatory Th17 cells (99,100). In accordance, a recent study using genetically-engineered mice deficient in DCs demonstrated that depletion of DCs is associated with protection from developing obesity and IR (101). Similar results have been observed in humans, where levels of DCs were higher in obese patients and correlated with BMI (100).

1.3.2.3 Neutrophils

Neutrophils are the most abundant white blood cells in the immune system. They are short-lived cells that are attracted by IL-8 and rapidly recruited to infected tissues. Subsequently, they are the primary effector cell type in acute inflammatory responses and facilitate the recruitment of macrophages, DCs and lymphocytes to the site of acute infection (102). The presence of neutrophils in WAT of lean animals is very low, representing less than 1% of the total immune cells (103).

Few reports in humans and mice show a systemic neutrophil activation and transient infiltration in WAT at the onset of obesity-induced WAT inflammation (104,105). Moreover, it has been reported that there is a recruitment of neutrophils to adipose tissue three days after initiation of *high fat diet* (HFD) feeding in mice (103,106). Interestingly, neutrophil elastase, a protein increased in obese WAT, is able to degrade IRS-1. In accordance with this, it has been found that both neutrophil elastase *knockout* (KO) mice and mice treated with an elastase inhibitor have reduced WAT inflammation and improved glucose tolerance (106,107). Based on these studies, it has been proposed that neutrophils are implicated in the modulation of adipose tissue inflammation and IR at early stages of the disease.

1.3.2.4 Natural killer cells

The main function of NK cells is to destroy infected or tumor cells without prior priming by releasing perforin and granzymes. However, another major function of NK cells is to secrete cytokines and chemokines, such as TNF-α, IFN-γ, *granulocyte-macrophage colony-stimulating factor* (GMCSF) and CCL2, and promote the recruitment and activation of other immune cells into the site of inflammation (108). Similar to neutrophils, the number of NK cells in WAT is triplicated in obese individuals and their activity is enhanced (109–112). Several studies in humans and rodents have

demonstrated that NK cells participate in the development of IR and T2D associated with obesity. Interestingly, the increase of NK cells is only observed in visceral WAT of obese mice. This could be explained because of the local increased expression of *interleukin 15* (IL-15) in the visceral depot, which promotes NK cell proliferation and activation (109,113,114). Moreover, NK cell numbers drop upon bariatric surgery or *calorie restriction* (CR) (110,115), two interventions known to improve glucose homeostasis. Also, the metabolic phenotype of HFD fed obese mice is improved when NK cells are depleted, improving the obesity-induced IR and adipose tissue inflammation (109,113).

IFN-γ is the classical signature of NK cells. Consequently, the increase in the proportion of IFN-γ and TNF-α expressing NK cells in visceral fat could explain the deleterious effect of NK cells on adipose tissue homeostasis by promoting M1 macrophage polarization and CCL2-dependent recruitment of monocytes and macrophages into the adipose tissue (109,113).

1.3.2.5 Eosinophils

Eosinophils are a type of granulocytes that play an important role in parasitic infections and mediate allergic response. Eosinophils circulate in the immature state and infiltrate and mature in specific tissues (116). Eosinophils have been demonstrated to be important regulators of adipose tissue homeostasis, preventing WAT inflammation and IR. Eosinophils are responsible for 90% of IL-4 expression in adipose tissue, which accelerate M2 macrophage polarization, contributing by this mean to the preservation of adipose tissue glucose homeostasis (83). Interestingly, the number of adipose tissue resident eosinophils is reduced in mice subjected to HFD. Besides, eosinophil-deficient mice display an increased fat mass and worsened glucose homeostasis.

In addition to WAT, HFD also reduces the abundance of eosinophils in the intestine. As eosinophils play a role in maintaining gastrointestinal homeostasis (i.e. maintaining IgA-producing plasma cells, DCs and T cells), depletion of intestinal eosinophils could lead to a state of relative immune deficiency and an increased intestinal permeability, which can contribute to the development of metabolic disease (117). Interestingly, eosinophils and M2 macrophages also appear to improve insulin sensitivity by promoting beige adipogenesis and thermogenesis. Indeed, it has been reported that meteorin-like, a myokine induced in the muscle after exercise and in adipose tissue upon cold exposure, improves glucose tolerance, stimulates the increase of eosinophil-dependent IL-4 expression and promotes M2 macrophage activation. Blocking meteorin-like action *in vivo* significantly attenuates chronic cold-exposure-induced alternative M2 macrophage activation and thermogenic gene responses. Conversely, an increase in circulating meteorin-like levels causes an improvement in glucose homeostasis in obese mice (94).

1.3.2.6 Innate lymphoid cells

ILCs are mainly found in mucosal tissues and participate in the immune response against infections and chronic inflammatory conditions. ILCs are lymphocytes lacking antigen recognition receptors that are activated in response to cytokines and through *microbe-associated molecular pattern* (MAMP). They represent the innate analogue of $CD4^+$ *T helper* (Th) cells (see section 1.3.3). ILCs are categorized into three subtypes namely ILC1, ILC2, ILC3, which have analogue functions to those of immune adaptive response lymphocytes Th1, Th2 and Th17. ILC1 express *T-box expressed in T cells* (T-bet) and secrete IFN-γ and TNF-α; ILC2 express *GATA binding protein* 3 (GATA3) and produce IL-4, IL-5 and IL-13; whereas ILC3 express *retinoid-related orphan receptor gamma 2* (RORγt) and release *interleukin 17*(IL-17) and *interleukin 22* (IL-22) (118,119). It has

been reported that ILC2 predominate in WAT of lean healthy individuals and contribute to adipose tissue homeostasis (120) by facilitating the maintenance of visceral adipose tissue eosinophils and M2 macrophages through the secretion of *interleukin 5* (IL-5) and IL-13. Accordingly, there is a reduction in the number of eosinophils and M2 macrophages in WAT of ILC2-depleted mice (121). Moreover, recent studies show that activated ILC2 positively regulate beige adipogenesis (93,122). Contrarily, ILC1 produce IFN-γ and consequently contribute to the polarization of M1 macrophages and promote IR (123).

1.3.3 Adaptive immune cells in adipose tissue

While innate immune cell responses are evoked by danger signals and play a key role in the initiation of inflammation, **adaptive immune cell** responses are activated in the chronic inflammatory state of obese adipose tissue (124).

1.3.3.1 T cells

T cells develop and mature in the thymus, and then migrate into peripheral tissues where they exert their function. T cells can be classified according to their TCR as αβT cells and γδT cells. The first ones have an important role in adaptive immunity, whereas the second ones mainly act in innate immunity (125). There are various subsets of T cells depending on the cell surface markers, including $CD4^+$ and $CD8^+$ T cells. T cells proliferate and differentiate into effector $CD4^+$ Th cells and CD8+ *cytotoxic T lymphocytes* (Tc) when they are activated by antigen stimulation. Naïve $CD4^+$ T cells differentiate into Th1, Th2, Th17 and *regulatory* (Treg) cells. Depending of the subtype, they express pro- and anti-inflammatory cytokines as shown in Figure 1.8 (126). The majority of the subtypes have been implicated in the regulation of adipose tissue inflammation in obesity.

Several studies suggest that **Th1 cells** are one of main cell types responsible for WAT inflammation and IR by secreting pro-inflammatory cytokines, such as IFN-γ. Th1 secreted IFN-γ, together with the IFN-γ produced by $CD8^+$ T cells, promote macrophage infiltration and their polarization to M1 type macrophages (127). In line with this, it has been reported that obese patients display an increased IFN-γ production (128). IFN-γ producing $CD4^+$ T cells are also increased in WAT of obese mice compared to lean controls (129). Supporting the notion that IFN-γ is a key mediator of obesity-induced inflammation, *ex vivo* treatment of WAT with IFN-γ results in an increase in pro-inflammatory markers, whereas IFN-γ KO mice fed with a HFD displayed a decrease in WAT inflammation and an improved glucose homeostasis (130). It has also been shown that, in obese mice, depletion of MHC II specifically in adipocytes or macrophages reduces $CD4^+$ T cell numbers and IFN-γ production in adipose tissue, leading to an improvement of insulin sensitivity (131,132).

Although **Th2 cells** are not very abundant compared with others $CD4^+$ T cells subtypes, several studies suggest that they have beneficial effects on glucose homeostasis by secreting IL-4 and IL-13 anti-inflammatory cytokines. Indeed, several clinical studies have shown that there is an inverse correlation between Th2 cells and systemic inflammation in human visceral WAT. In accordance, obese patients have lower levels of Th2 cells in visceral WAT (133,134). Moreover, mice subjected to HFD have less percentage of Th2 cells, although absolute numbers per weight of visceral WAT remains constant. Therefore, in obese mice there is an alteration of the Th1/Th2 cells balance that seems to lead to a pro-inflammatory environment (129).

Th17 cells are implicated in autoimmune disorders and are typically characterized by the production of IL-17 (135,136). Several studies reported that Th17 cells are dramatically increased in visceral WAT of obese patients, producing high amounts of IL-17, suggesting that Th17 cells can

directly participate in WAT inflammation and IR in obesity (100,137,138). In line with this, various studies reported that HFD-fed mice not only present higher levels of IL-17-expressing Th17 cells but also γδT cells, which can also produce IL-17 (100,139,140). IL-17 acts by activating JNK, which, as previously mentioned, induces IR by phosphorylating and inhibiting IRS1 (141). Accordingly, IL-17 deficient mice show enhanced glucose tolerance and insulin sensitivity. Moreover, IL-17 suppresses 3T3-L1 adipocyte differentiation and impairs glucose uptake in mature adipocytes (140).

On the other hand, **Treg cells** are known to play a suppressive role in inflammatory diseases, being required for the maintenance of an anti-inflammatory environment at a steady state. They secrete IL-10, which induces M2 macrophage polarization (142). In addition, adipocytes express IL-10 receptor, which produce an increase of insulin-stimulated glucose uptake and a reduction of CCL2 expression (90). These are key mechanisms for the reduction of adipose inflammation and improvement of glucose homeostasis upon stimulation by IL-10. Supporting this idea, it has been reported that lean mice in which Treg cell population has been depleted exhibit increased levels of insulin and pro-inflammatory cytokines, both in adipose tissue and circulation (127). Compared with spleen, lymph nodes and lung, Treg cells are highly enriched among $CD4^+$ T cells in WAT of lean mice. Importantly, obesity decreases the number of Treg cell population in abdominal WAT in obese mice models and human patients (127,142).

CD8+ T cells secrete pro-inflammatory cytokines, and immunomodulatory molecules to induce cytolysis of target cells. WAT of obese mice and humans have been shown to have elevated numbers of $CD8^+$ T cells (127,143). It has been also reported that mice show an increase of $CD8^+$ T cells in WAT as soon as two weeks after being fed a HFD, preceding macrophage recruitment, which is seen 6 weeks after HFD feeding. This suggests that, contrary to the previous dogma in the field, $CD8^+$ T cells recruitment and activation, but not macrophage infiltration, could be the initial trigger of adipose inflammation during obesity. Supporting this notion, depletion of $CD8^+$ T cells in HFD fed mice results in decreased number of macrophages, diminution of pro-inflammatory TNF-α and IL-6 levels and improved glucose homeostasis (127).

γδT cells are characterized for bridging innate and adaptive immune inflammatory responses and are found naturally activated in the periphery. Recently, two types of γδT cells have been described in WAT: IFN-γ-producing γδ T1 cells and IL-17-producing γδ T17 cells (136). So far, little is known about the function of γδT cells in WAT. Earlier investigations found γδT cells increased in HFD-induced obesity in WAT and suggested that γδT cells play a pro-inflammatory role in obesity-associated inflammation (144), contributing to macrophage accumulation, inflammation and IR. However, other studies reported that γδ T cells are decreased in the circulation of obese subjects and are negatively correlated with BMI (145). Interestingly, a recent study has shown that WAT resident γδT cells regulate Treg cells expansion and control core body temperature though the production of IL-33 (136). Additionally, γδT cells, though the production of IL-17, have been shown to negatively regulate adipogenesis and protect against obesity in mice (140). Therefore, although these studies demonstrate that γδT cells play an important role in shaping both pro- and anti-inflammatory T cell populations in WAT, the role of γδT cells in the development of metabolic syndrome is still a matter of controversy.

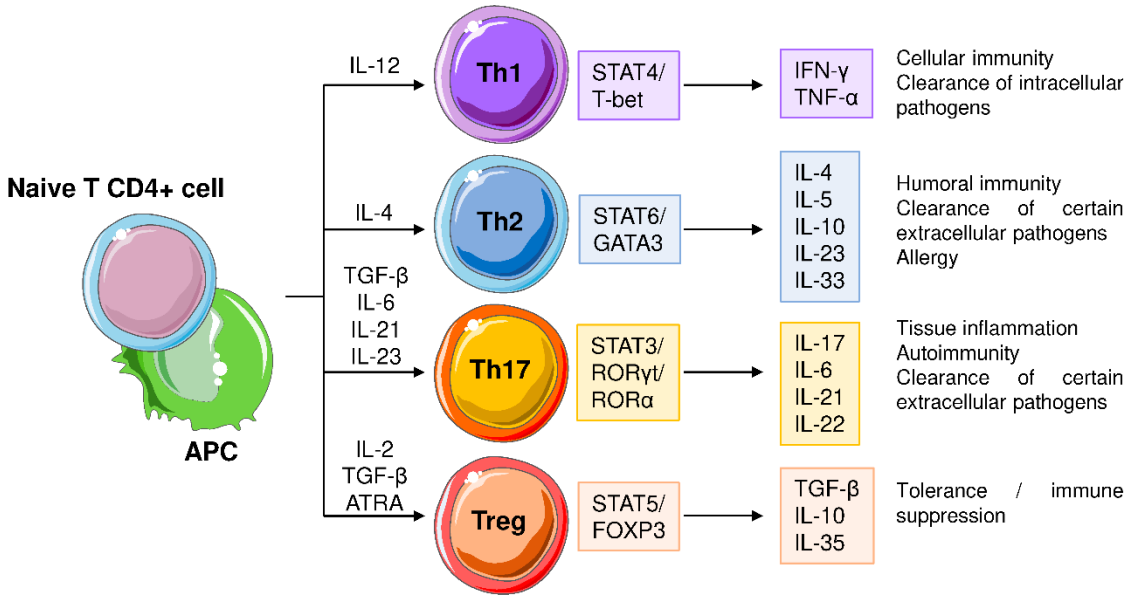

Figure 1.8. Naïve T cell differentiation into Th cell subpopulations. APC, antigen presenting cell; STAT, signal transducer and activator of transcription; Tbet, T-box expressed in T cells; GATA3, GATA binding protein 3; RORγ, RAR-related orphan receptor; FOXP3, forkhead box P3; IFN, interferon; TGF, transforming growth factor; Treg cell, regulatory T cell; TNF-α, tumour necrosis factor α. Adapted from (146,147).

1.3.3.2 Natural killer T cells

NKt cells are innate lymphocytes that bridge innate and adaptive immune responses. There are several subsets of NKt cells, being invariant iNKt the most prevalent (148). iNKt cells have a semi-invariant T cell receptor, which recognizes a variety of lipid antigens loaded on *cluster of differentiation 1d* (CD1d) molecules and do not recognize peptide antigens on MHC molecules (149,150). iNKt cells have the ability to rapidly produce both Th1 and Th2 cytokines when they are activated (149,151). Interestingly, human and mouse adipose tissues appear to be enriched for iNKt cells, but they are depleted in obesity (152). However, the role of iNKt cells in WAT inflammation is still a matter of controversy. Some studies suggest that the function of iNKt cells is not critical in adipose tissue inflammation, because CD1d KO mice do not present significantly changes in metabolic parameters and WAT inflammation when fed with a HFD (153). Conversely, other studies have demonstrated that both CD1d KO mice or Jα18-deficient mice (lacking iNKt cells) gain more weight and exhibit increased obesity-related inflammation and IR compared to *wild type* (Wt) counterparts (152,154).

1.3.3.3 B cells

B cells actively participate in both innate and adaptive immunity. They express certain TLRs for PAMP recognition, present antigens via MHC I or MHC II molecules and secrete antigen specific antibodies important for humoral immunity (155). During obesity, the total number of B cells increases in visceral WAT, where they appear to play a pathogenic role in inflammation and IR (156,157). In fact, it has been reported that *immunoglobulin G* (IgG) production and infiltration of IgG^+ B cells are increased in WAT in obesity. It has also been observed that mice lacking B cells are protected from metabolic disease despite weight gain when subjected to HFD feeding, but they develop IR when they are injected with serum IgG or MHC II expressing B cells (157). According to these studies, it appears that pathogenic antibody production by B cells directly activates macrophages, whereas MHC I and MHC II molecules on B cells promote activation of $CD8^+$ and $CD4^+$ T cells, respectively, contributing by this means to the inflammatory response observed in adipose tissue of obese mice (156).

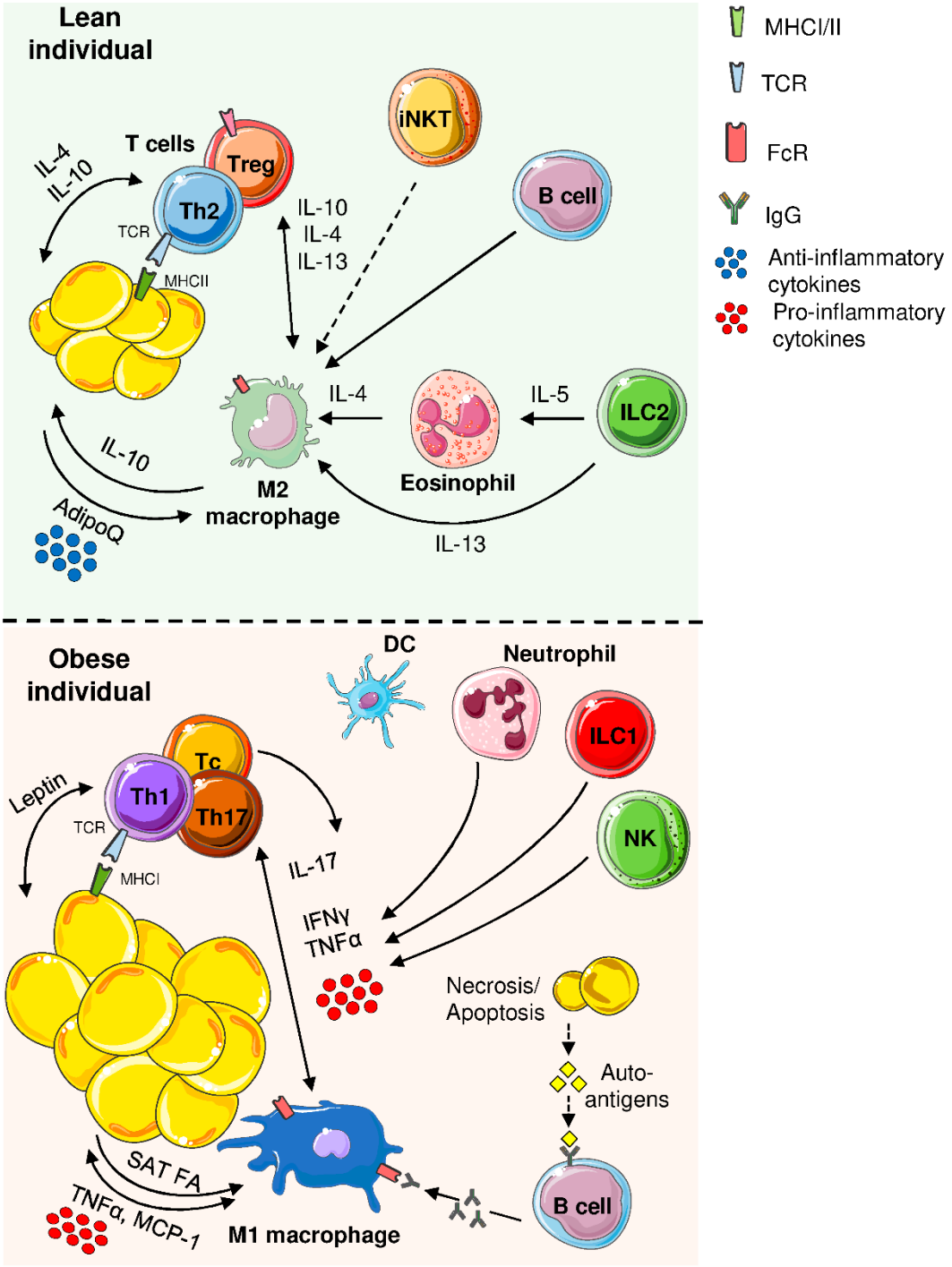

Figure 1.9. Changes in resident immune cell populations in a healthy adipose tissue and an obese adipose tissue. Lean WAT contains regulatory immune cells that suppress pro-inflammatory immune cells and sustain alternative activation of macrophages via Th2-associated cytokines. Conversely, obese WAT is infiltrated with pro-inflammatory immune cells that produce high amounts of inflammatory cytokines and chemokines. M1 macrophages accumulate in CLS around adipocytes. Adapted from (158–160).

In conclusion, multiple interactions between adipocytes and WAT-resident immune cells help to maintain an anti-inflammatory environment in lean individuals. On the other hand, obesity provides pathogen-like and metabolic danger signals that mimic bacterial infection. The disruption of the delicate balance between adipocytes and WAT-resident immune cells in obesity leads to the development of WAT inflammation and IR. Beyond the well stablished role of macrophages, many other WAT-resident immune cells are dysregulated in the context of obesity and T2D, but their precise role and mechanism of action are still not fully defined.

►1.4 Calorie restriction

Life style interventions, such as CR, are known to improve glucose homeostasis. Consequently, understanding the mechanisms of action involved in the effects of CR would be helpful for the treatment of metabolic diseases. CR is defined as a decrease of 30-50% of calorie intake compared to *ad libitum* (AL) fed individuals. CR is well known for being the only lifestyle intervention known to extend lifespan in a wide variety of species, from yeast to primates (161). The positive effects of CR on health are beyond weight loss and obesity. Thus, CR prevents or delays the onset of metabolic diseases and reduces risk factors of a wide variety of age-related diseases, including cancer, cardiovascular diseases, neurodegenerative diseases and T2D (161).

1.4.1 Effects of calorie restriction on glucose homeostasis

From an evolutionary point of view, organisms have to adapt to changes in food availability to survive. Thus, when food supply is abundant, metabolism and growth are activated, and the excess of energy is stored in form of glycogen and lipids. Contrarily, in periods of scarcity, when organisms are faced with an acute energy deficit, energy reserves are mobilized. Early studies on the effects that CR exerts on health and lifespan proposed that CR slows down metabolism and decreases oxidative stress, reducing cellular damage in all the body and improving overall health (161).

Although it is well known that CR improves whole-body insulin sensitivity and enhances insulin-dependent glucose uptake in skeletal muscle, liver and WAT, the precise mechanisms involved in the improvement of glucose homeostasis have not completely been defined yet (162). Several clinical studies show that long term energy restriction improves insulin sensitivity, a mechanism by which CR may act to extend lifespan (163–165). For instance, in a six-months study with 48 overweight volunteers demonstrated that there was a 40% improvement in insulin sensitivity in the CR group, although this did not reach statistical significance, as well as a decrease in the acute insulin response to glucose, indicating an improvement in β-cell responsiveness to glucose (166).

CR is suggested to prevent the development of a chronic and subacute pro-inflammatory state in WAT by regulating the secretion of cytokines and adipokines. It has been reported that CR modulates resident specific immune cells in adipose tissue, promoting the differentiation of anti-inflammatory immune cells, such as Th2, Treg cells, ILC3 and M2 macrophages (167–169). This results in a reduction of inflammatory cytokines production by immune cells and adipocytes. Moreover, a recent study reports that CR promotes the development of beige fat through the improvement of type 2 immune response and *sirtuin 1* (SIRT1) expression (170). It has also been demonstrated that CR alters resident immune system cells of HFD fed mice, increasing de $CD4^+/CD8^+$ cell ratio and promoting a macrophage reduction (169). However, more accurate studies are needed to characterize the precise immune response under CR.

In addition to changes in the inflammatory response, CR also positively regulates the secretion of adiponectin in adipocytes, while leptin levels are reduced (171,172). Consequently, insulin sensitivity, glucose uptake and fatty acids oxidation are improved in liver and muscle (173). In fact, adipocytes' metabolism is changed in response to CR, favoring fat mobilization and lipolysis, inhibiting adipogenesis in WAT and promoting browning of WAT (170,174).

Perhaps one of the most remarkable effects of CR is the increase in mitochondrial respiration rates (175,176). Increased mitochondrial mass and function in tissues, such as brain, heart and liver, are in parallel with the improvement in metabolic rates exerted by CR (177). In line with this notion,

several studies have reported that mitochondrial gene expression in response to CR is increased, as well as an improvement in the maintenance of healthy mitochondrial with high oxidative capacity, both in humans and rodents (177–180). Nevertheless, the induction of mitochondrial biogenesis by CR and its effects on glucose homeostasis is still a matter of controversy (181). In this regard, with the aim to study the role that increased mitochondrial biogenesis plays on glucose homeostasis following CR, our laboratory generated a mouse model simultaneously devoid specifically in adipocytes of *peroxisome proliferative activated receptor-γ coactivator 1-alpha* (PGC-1α) and *peroxisome proliferative activated receptor-γ coactivator 1-beta* (PGC-1β), which are major regulators of mitochondrial biogenesis. Despite having blunted mitochondrial respiratory function in response to CR, these mice normally respond to nutrient deprivation or CR by improving their glucose homeostasis to the same extent as Wt mice. These results strongly suggest that increased mitochondrial oxidative function in WAT is not required for the beneficial effects of CR on glucose homeostasis (182). In the same line, another study using muscle-specific PGC1-α KO model showed that PGC1-α is a major regulator of the mitochondrial response to CR but KO mice normally respond to CR by improving glucose homeostasis (183). Consequently, processes modulated by CR in WAT, other than mitochondrial biogenesis, could contribute to the improvement of health in response to CR.

1.4.2 Molecular mechanisms of calorie restriction on gene expression and metabolism

Recent studies indicate that metabolic and cellular processes altered in response to CR are highly regulated and require of regulatory proteins that are able to sense the energetic deficit and generate responses aimed at maintaining the energy status of the cell (8). A growing number of studies propose that **SIRT1**, a protein from the sirtuin family with *nicotinamide adenine dinucleotide* (NAD^+) dependent deacetylase activity, is one of the principal mediators of CR (Figure 1.10) (161).

Studies performed in rodent models have shown that CR induces expression and/or activity of SIRT1 in several tissues, such as muscle, heart, brain, liver and WAT. Transgenic mice that over-express SIRT1 exhibit similar phenotype than mice subjected to CR, being more resistant to the development of IR, T2D and hepatic steatosis (175,184). Conversely, adipose tissue-specific SIRT1 KO mice are more prone to develop IR, suggesting that SIRT1 is a key factor maintaining energy balance and insulin sensitivity (185).

CR increases SIRT1 activity in two different ways, either increasing its transcription or increasing the activity of the enzyme. At the genomic level, *estrogen-related receptor alpha* (ERRα), a nuclear receptor that controls mitochondrial function and PGC-1α expression, induces SIRT1 expression, (186). Some protein complexes, like *active regulator of SIRT1* (AROS), positively regulates SIRT1 expression, while *nuclear receptor co-repressor 1* (NCoR1) and *silencing mediator of retinoid and thyroid hormone receptor* (SMRT) are negative regulators of SIRT1 expression (187,188) (Figure 1.10). On the other hand, the two most important regulators of SIRT1 activity are NAD^+ and *AMP kinase* (AMPK), which in turn are sensors of the cell energy status (Figure 1.10). Modulation of **cofactor NAD^+** levels depend on the conversion to its reduced form NADH. NAD^+ levels increase during fasting, CR and exercise, while NAD^+ levels are reduced in situations in which glycolysis is very active or under HFD condition. NAD^+ is principally synthesized in liver and kidney from various precursors. Although *de novo* synthesis starts from the amino acid tryptophan, NAD^+ can also be synthesized from nicotinic acid or nicotinamide, both present in our diet as vitamin B3. Cellular NAD^+ levels can be also altered by manipulating the activities of *NAD^+-depleting enzymes, like*

poly(ADP- ribose) polymerase (PARPs),a family of nuclear enzymes involved in DNA repair that are considered the major NAD^+ degrading enzymes (186).

AMPK is another important player in the cellular and physiological responses elicited in response to CR. AMPK is a cellular energy sensor activated in response to an increase in the AMP/ATP ratio, as it occurs in a situation of high demand of energy. Conversely, AMPK activity is decreased when cells are full of energy, indicated by a lower AMP/ATP ratio (189). Hence, AMPK is activated under CR conditions. Once activated, AMPK increases oxidative pathways, which results in an increase of NAD^+/NADH ratio, ultimately leading to the activation of SIRT1 by NAD^+ (190). At a metabolic level, AMPK activation in cells prompts the activation of fatty acid oxidation, through ACC, and glucose oxidation, by activating glucose uptake and glycolysis. It also turns off many anabolic pathways, such as fatty acid synthesis. In an analogous manner, AMPK also exerts its control over energy homeostasis by activating lipolysis in adipocytes, regulating insulin secretion in pancreas, enhancing lipid usage in skeletal muscle and liver and reducing lipid synthesis and glycolysis in these organs, processes that will contribute to the improvement of insulin sensitivity (191). However, whether AMPK is the natural effector of the effects of CR is still a matter of controversy. While some studies reported that AMPK activity is not affected or reduced by CR (192,193), others indicated an increase in AMPK activity in heart and skeletal muscle (194,195). In fact, it has been reported that lack of AMPK in muscle impairs the improvement of glucose homeostasis induced by CR (196). These discrepancies could be attributed to the length of the period in which animals have been subjected to CR, as well as the age of the organism. The elucidation of these controversies requires future attention.

SIRT1 controls cellular metabolism in response to CR by producing changes in the **activity of key enzymes**, such as *phosphoenolpyruvate carboxykinase* (PEPCK) and *glucose 6-phosphatase* (G6Pase), but also by modulating **gene expression**. Consistent with a relevant role in the regulation of gene expression, SIRT1 is principally localized in the nucleus, where it deacetylates histones and other transcription factors that control the expression of genes implicated in different metabolic and cellular processes (186). So far, only a few effectors of SIRT1 have been uncovered. For example, SIRT1 deacetylases different histones, contributing by this means to genomic stability and cancer prevention, as well as it also blocks *tumor protein p53* (p53) activity to reduce apoptosis. In liver, *forkhead box protein O1* (FOXO1) activity is enhanced when it is deacetylated by SIRT1, leading to an increase in the expression of the genes involved in gluconeogenesis, which can be interpreted as an evolutionary mechanism intended to preserve glucose homeostasis in periods of restricted availability of nutrients and energy (197). SIRT1 also regulates hepatic PGC-1α, which acts as a major regulator of the gluconeogenic process by coactivating FOXO1, glucocorticoid receptors and *hepatocyte nuclear factor 4 alpha* (HNF4α). Also, in liver, SIRT1 deacetylates *sterol regulatory element-binding protein 1* (SREBP1) and targets the protein for destruction through the ubiquitin-proteasome system, resulting in the repression of lipid synthesis (198). Hence, SIRT1 play a protective role against hepatic steatosis and lipid-induced IR by reducing hepatic lipogenesis. Moreover, SIRT1 appears to inhibit *nuclear factor κB* (NFκB) signaling, reducing inflammation and therefore contributing to the beneficial effects of CR (186).

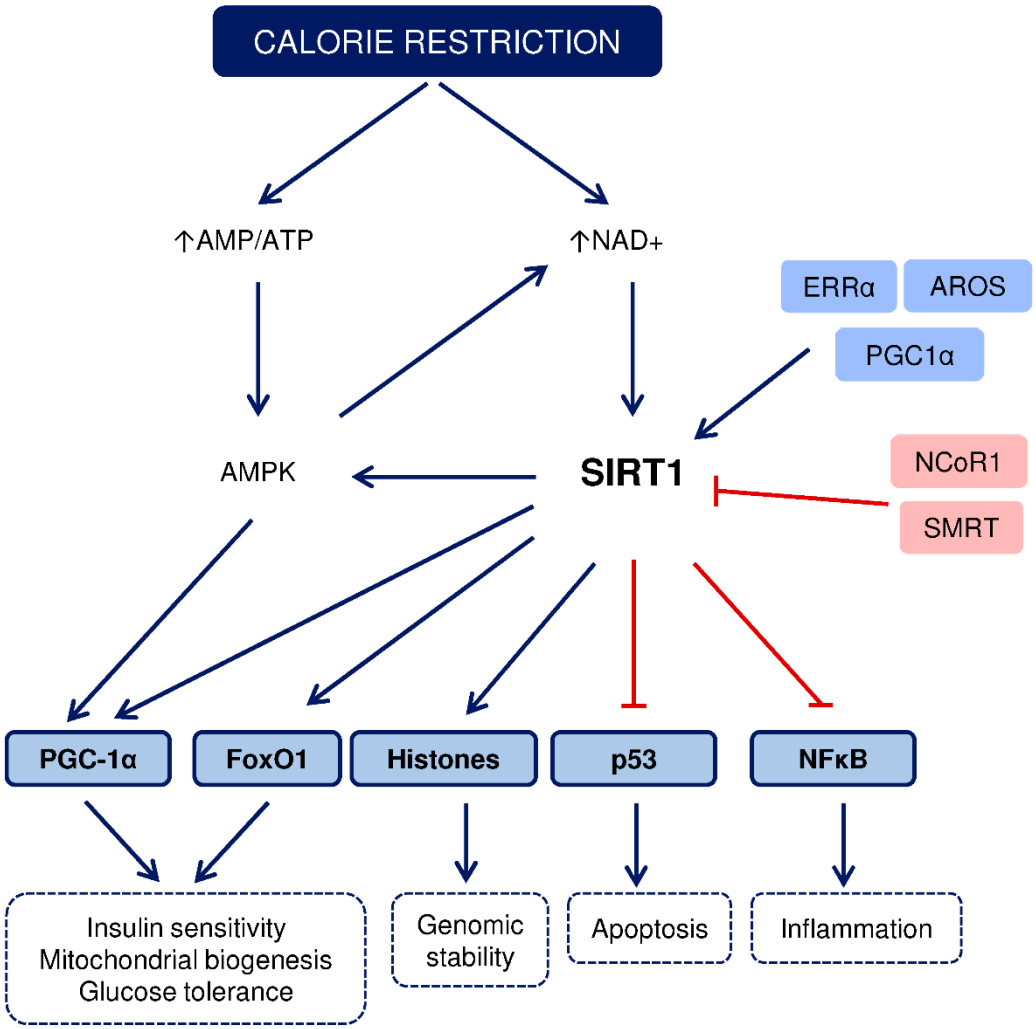

Figure 1.10. Mechanisms underlying the beneficial effects of CR. Under CR conditions, AMP/ATP ratio increased and activates AMPK. An increase in NAD^+ activates the NAD^+-dependent deacetylase SIRT1 that together with AMPK, activates PGC-1α. PGC-1α, together with FOXO1, improves insulin sensitivity and glucose tolerance and increases mitochondrial biogenesis. SIRT1 also deacetylases different histones generating genomic stability, while it inhibits p53 activity and NFκB signaling, reducing apoptosis and inflammation respectively. SIRT1, sirtuin 1; NAD^+, nicotinamide adenine dinucleotide; AMPK, AMP kinase; FOXO1, forkhead box protein O1; HNF4α, hepatocyte nuclear factor 4 alpha; p53, tumor protein p53; NFκB, nuclear factor κB; SREBP1, sterol regulatory element-binding protein 1; ERRα, estrogen-related receptor alpha; AROS, active regulator of SIRT1; NCoR1, nuclear receptor co-repressor 1; SMRT, silencing mediator of retinoid and thyroid hormone receptor. Adapted from (199)(200).

The identification of the molecular mediators involved in the beneficial effects of CR would be crucial to find potential targets and to develop new drugs that mimic CR. These SIRT1 mimetics could be used for the treatment of diabetes and other metabolic diseases, as well as cancer and neurodegenerative diseases. However, as mentioned, the mechanisms by which CR exerts its effects are still poorly defined (201). In this regard, as it will be further discussed along this dissertation, our laboratory has identified *Rorc* as a gene up-regulated in WAT in response to nutrient deprivation and, therefore, as a potential mediator of the effects of CR.

►1.5 Retinol-related orphan receptors

1.5.1 Structures and mechanisms of action

RORγ is a *nuclear receptor* (NR) that belongs to the subfamily of hormone nuclear *retinol-related orphan receptors* (ROR), which also includes *retinoid-related orphan receptor alpha* (RORα) and *retinoid-related orphan receptor beta* (RORβ). NRs are ligand-dependent transcription factors that regulate gene expression related to a wide variety of biological processes, such as metabolism, development and inflammation, among others (202). Almost half of the NRs have been characterized with their natural ligands. However, for the remaining receptors their cognate ligands have not been identified yet and, consequently, are classified as orphan nuclear receptors. This is the case of RORs (203,204).

As for the rest of nuclear receptors, the molecular structure of RORs consists of four functional domains. These domains include an N-terminal domain, which has been shown to play a critical role in conferring DNA binding specificity to the various ROR isoforms; a highly conserved *DNA-binding domain* (DBD) with two zinc fingers; *a ligand-binding domain* (LBD), which is multifunctional and facilitates co-activator and/or co-repressor binding to the receptor; and a hinge region that connects LBD and DBD domains (205) (Figure 1.11).

Each member of the ROR family is encoded by a different gene that generates different isoforms thanks to the use of alternative promoters and to differential splicing. The *Rora* gene generates four isoforms, RORα1-4, while RORβ and RORγ each generate two isoforms (Figure 1.11) (147). Most isoforms exhibit a distinct tissue-specific pattern of expression and regulate different biological processes and target genes. Still, the function of some of the mentioned isoforms has not been unraveled.

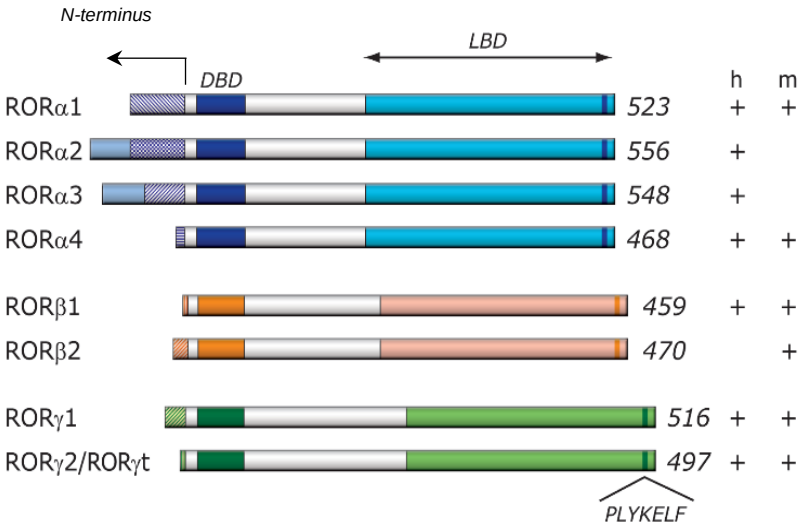

Figure 1.11. Schematic representation of the structure of ROR family members. As hormone nuclear receptors, ROR proteins contain a DNA binding domain (DBD), a ligand binding domain (LBD) and N-terminus. Different ROR isoforms in human and mice are shown on the right (h, human; m, mouse). Modified from (147).

RORs bind as monomers to specific DNA sequences, known as *ROR response elements* (ROREs), characterized by the RGGTCA consensus sequence. Although ROR members and their different isoforms recognize very similar ROREs, they do this with different affinities conferred by the N-terminus domain. In addition to RORE sequence and the amino terminus, the promoter context is also important to determine which ROR binds a specific RORE (147,206).

1.5.2 Retinol-related orphan receptors ligands

As a member of the hormone nuclear receptor family, RORγ possesses a ligand binding domain that could accommodate small lipophilic molecules. Therefore, its transcriptional activity is susceptible to be modulated by endogenous ligands or synthetic compounds. As all NRs, RORs ligand binding domain is multifunctional. Generally, ligands induce conformational changes in the receptor resulting in dissociation of co-repressors and recruitment of coactivators. Nevertheless, RORs appear to be constitutively active. This means that they are in an active conformation in the absence of ligand, suggesting that ligand binding may actually repress their activity (207) (Figure 1.12). Although identification of the endogenous ligands for RORs has been controversial, several studies have reported that natural oxysterols or intermediates of the cholesterol synthetic pathway are endogenous modulators that decrease ROR transcriptional activity. Actually, 7-oxygenated sterols bind to both RORα and RORγ isoforms and suppress their transactivation properties, acting as inverse agonists. Several other endogenous RORα and RORγ ligands have been described to be agonists, such as *25-hydroxycholesterol* (25-OHC), or inverse agonists, such as *24 S-hydroxycholesterol* (24*S*-OHC). However, whether or not these ligands are the endogenous ligand, the endogenous ligand is still a subject of debate (208).

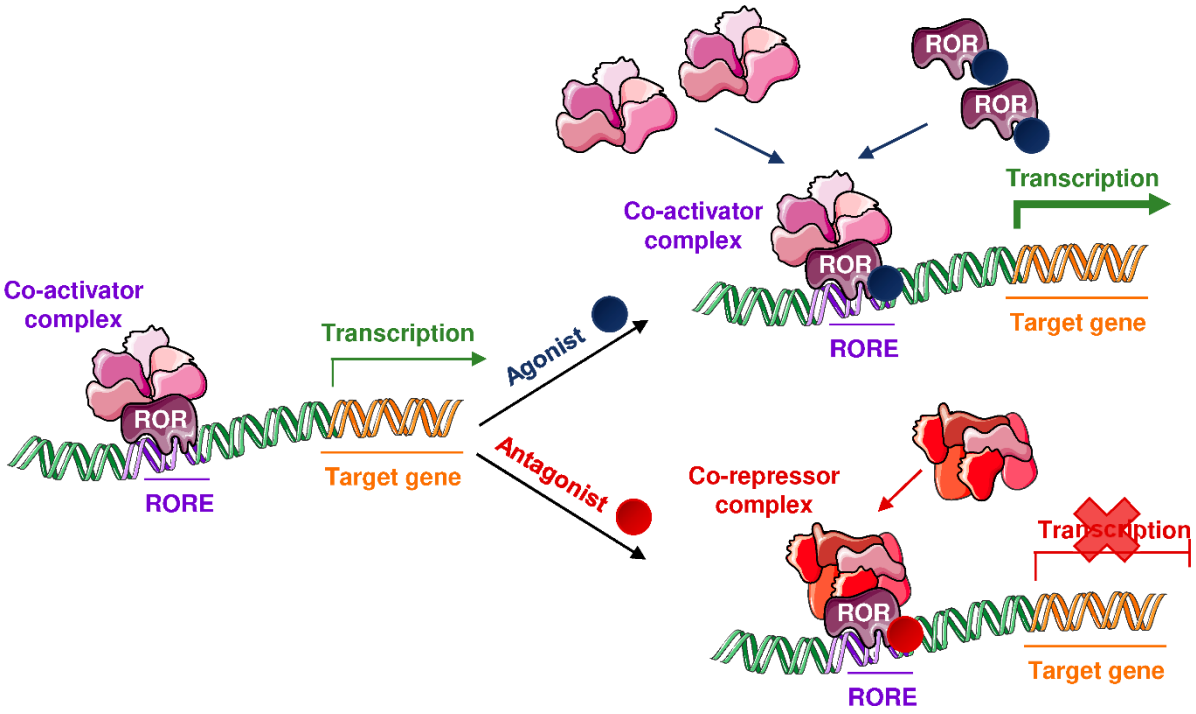

Figure 1.12. Regulation of ROR activity with agonist or inverse agonists. RORs are constitutively active and bind coactivators in the absence of ligands. A treatment with an agonist will recruit more coactivators, increasing ROR's transcriptional activity, whereas an inverse agonist binds to RORs LBD inducing a conformational change that dissociates coactivators proteins and recruits co-repressors, inhibiting ROR transcriptional activity. Adapted from (207).

In addition, some synthetic drugs with RORs agonist or inverse agonist activity have been described. The knowledge of RORγ crystal structure allowed to synthetize new synthetic ligands. A potent and effective RORγ inverse agonist described, which inhibits around 95% its activity, is SR2211 (1,1,1,3,3,3-hexafluoro-2- (2-fluoro-4'- ((4-(pyridin-4-ylmethyl) piperazin-1-yl) methyl)-[1,1'-biphenyl]-4-yl)propan-2-ol) (209,210). For instance, it has been reported that SR2211 diminishes inflammation in a collagen-induced arthritis mouse model (210). On the other hand,

SR1078 (N-[4-[2,2,2-trifluoro-1-hydroxy-1- (trifluoromethyl) ethyl] phenyl] -4-(trifluoromethyl)-benzamide) has been described as a RORγ agonist, although it is less specific because it also activates RORα (211,212).

As mice deficient in RORγt function have been shown to be protected against multiple autoimmune disease and several RORγt-dependent immune cells contribute to different degrees to the development and progression of autoimmune diseases, RORγ inverse agonists have been proposed to manage autoimmune diseases and advanced into clinical trials (213,214). For instance, GSK2981278 is the most advanced topically-dosed RORγt inverse agonist and has been reported to significantly reduce the levels of several pro-inflammatory cytokines, including IL-17 and IL-1β, in treated skin and reduce epidermal hyperplasia and skin thickness in psoriasis-like mouse model (215). However, the absence of improvement in psoriatic lesions following treatment with the drug were observed in a human randomized trial (216), probably due to an insufficient drug exposure at the target site, small treatment area and the need of systemic inhibition of RORγt.

Although identification of ligands for RORs has established these receptors as attractive new therapeutic targets, numerous highly active compounds with capacity to modulate RORγ activity have been interrupted for further development in the stages of preclinical studies or clinical trials due to off-target effects, toxicity and poor therapeutic efficacy (217,218).

1.5.3 Function of retinol-related orphan receptors α and β

RORα is expressed in a wide range of tissues, including testis, kidney, adipose tissues and liver, but its highest expression is found in brain, specifically in the cerebellum and thalamus (147). Although the role of RORα in the cerebellum remains to be defined, it has been observed that RORα modulates cell cycle and migration of Purkinje cells (219). RORα expression is also high in the retina, where some studies indicate that it plays a crucial role in cone development by directly regulating multiple cone-specific genes (220).

The relevant role of RORα in the nervous system is evidenced in the mutant mouse *staggerer* (sg), which carries a deletion within the *Rora* gene as a result of a 6.4 kb intragenic insertion that results in a premature stop codon. Sg/sg mice ($RORα^{sg/sg}$) show a phenotype characterized by tremor, body imbalance and hypotonia, as well as small size and premature death (221). RORα null mice, generated by targeted disruption of the RORα gene, display essentially an identical phenotype as homozygous staggerer mice (222,223). Indeed, RORα deficient mice suffer from ataxia and severe cerebellar atrophy with lower levels of Purkinje cells and loss of cerebellar granule cells (219,224).

Increasing evidence indicates that RORα also plays an important role in the regulation of different metabolic pathways, particularly of lipid and steroid metabolism (207,208,225). Mice with systemic loss of RORα have smaller adipocytes in WAT and BAT and show lower levels of hepatic TAG accumulation (147). They also exhibit lower levels of plasma cholesterol, *high- density lipoprotein* (HDL), *apoliprotein A1* (ApoA1) and circulating TAG compared to Wt. In this regard, mice lacking RORα are less susceptible to HFD-induced obesity and liver steatosis (226). The effects of RORα loss on TAG homeostasis has been attributed to changes in the expression of genes involved in the control of lipogenesis. Indeed, it has been reported that RORα positively increases the expression of *sterol regulatory element binding transcription factor 1 c* (SREBP1c), a critical regulator of lipogenesis in liver and muscle, and by this means RORα controls TAG homeostasis. This is consistent with the reduced serum lipids and dyslipemia observed sg/sg mice (227). RORα

is also involved in bone metabolism (147). Indeed, RORα deficient mice present different abnormalities, like thin long bones (219,224).

In addition to its role in regulating metabolism, RORα also participates in inflammatory processes. Several observations suggest that RORα may function as a negative regulator of inflammation. It has been observed that RORα-deficient mice are more susceptible to LPS-induced lung inflammation (228). Moreover, several studies indicate that RORα functions as a negative regulator of pro-inflammatory cytokines expression in certain immune cells, such as macrophages and mast cells (229,230). In line with this, over-expression of RORα suppresses inflammation and alleviates LPS-induced organ injury through the regulation of the SIRT1/NFκB pathway (231). In addition, other studies suggest that RORα could also have a role in thymopoiesis and lymphocyte development. Supporting this notion, RORα mRNA is expressed at low levels in $CD4^+CD8^+$ *double positive* (DP) thymocytes and at high levels in $CD4^+CD8^-$ *single positive* (SP) thymocytes, while it is decreased in mature $CD8^+$ and increased in mature $CD4^+$ T lymphocytes (230).

Contrary to RORα, **RORβ** expression is restricted to certain regions of the brain and the retina. Although there are few studies on RORβ, some evidences suggest that it has an important role in the maturation of photoreceptors, acting together with RORα (232). RORβ is also expressed in the olfactory nucleus posterior and sensory cortices, suggesting that it is involved in the processing of sensory information (147). Consistent with a relevant role on the nervous system, RORβ deficient mice show motor defects and impairment in some neurological reflexes. Moreover, they show behavioral changes, including increased exploratory activity and reduced anxiety behavior, olfactory deficits and delayed onset of male fertility (233).

1.5.4 RORγ: role of RORγ1 and RORγt isoforms

Rorc, the gene encoding by RORγ, generates two distinct proteins through alternative promoter usage and differential splicing. While RORγ2 (commonly referred as RORγt) is specifically expressed in immune system cells, RORγ1 is expressed in several peripheral tissues, including liver, kidney, muscle and adipose tissue (147). In the present dissertation, "RORγ" and "*Rorc*" will refer to RORγ protein and gene, respectively, without distinction between isoforms; "RORγ1" and "*Rorc1*" will refer to RORγ1 protein isoform and its encoding mRNA isoform, respectively; "RORγt" and "*Rorc2(t)*" to will refer to RORγ2 protein isoform and its encoding mRNA isoform, respectively.

RORγt plays a critical role in the regulation of immune system processes, including lymph node organogenesis, thymopoiesis and T cell lineage specification. It contributes to lymph nodes organogenesis and Peyer's patches development by promoting the survival of *lymphoid tissue inducer cells* (LTi) (226,234), but not to other lymphoid tissues, including bronchial- and nasal-associated lymphoid tissue (235). RORγt has also an important role in thymopoiesis, promoting survival of DP cells via *anti-apoptotic B-cell lymphoma-extra large* ($Bcl\text{-}X_L$) system (Figure 1.13). During the thymopoietic process, $CD4^-CD8^-$ T cell precursors differentiate through four stages to $CD4^+CD8^+$ DP T cells. After undergoing a selection process to eliminate nonfunctional or autoreactive thymocytes, DP cells mature into SP $CD4^+CD8^-$ helper and $CD4^-CD8^+$ cytotoxic T cells, which then colonize secondary lymphoid organs. RORγt expression is undetectable in *double negative* (DN) and SP, but very high in DP thymocytes.

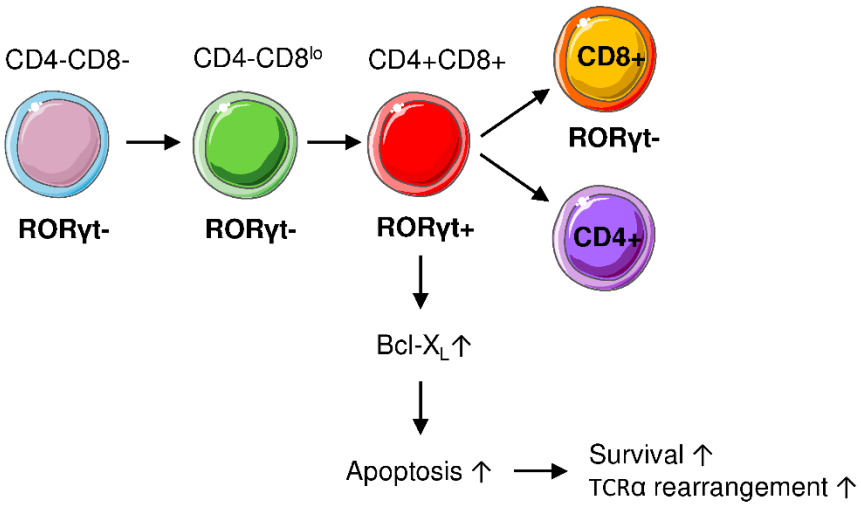

Figure 1.13. Role of RORγt in thymopoesis. $CD4^{-}CD8^{-}$ cells differentiate into immature SP cells ($CD4^{-}CD8^{lo}$). These cells subsequently differentiate into CD4+CD8+. RORγt and Bcl-X_L are induced during the transition from $CD4^{-}CD8^{lo}$ into $CD4^{+}CD8^{+}$, and down-regulated during the differentiation of $CD4^{+}CD8^{+}$ into $CD4^{+}$ and $CD8^{+}$ SP. RORγt promotes the differentiation of CD4-$CD8^{lo}$ to $CD4^{+}CD8^{+}$ and positively regulates the expression of the anti-apoptotic gene Bcl-X_L. Bcl-X_L, *anti-apoptotic B-cell lymphoma-extra large*; RORγ, RAR-related orphan receptor. Adapted from (147).

Together with *signal transducer and activator of transcription 3* (STAT3) and RORα, RORγt also participates in $CD4^{+}$ T cells differentiation into pro-inflammatory Th17 lineage by inducing genes like *Il17*, *Il22*, *chemokine (C-C motif) receptor 6* (*Ccr6*) and *interleukin 23 receptor* (*Il23r*) (Figure 1.8, section 1.3.3) (147). RORγt is also required for the differentiation of ILCs and γδ T cells (236,237).

The fact that RORα also functions as a positive regulator of Th17 differentiation suggests a degree of functional redundancy between RORγt and RORα. In addition to Th17 cells, γδT cells also express RORγt and produce IL-17 (238). RORγt is also expressed in ILC cells, specifically it is selectively expressed in ILC3 cells that produce IL-17A, IL-17F, IL-22, *granulocyte-macrophage colony-stimulating factor* (GM-CSF) and TNF-α. Additionally, it is also expressed in IL-22 producing NK cells (236,239) (Figure 1.14).

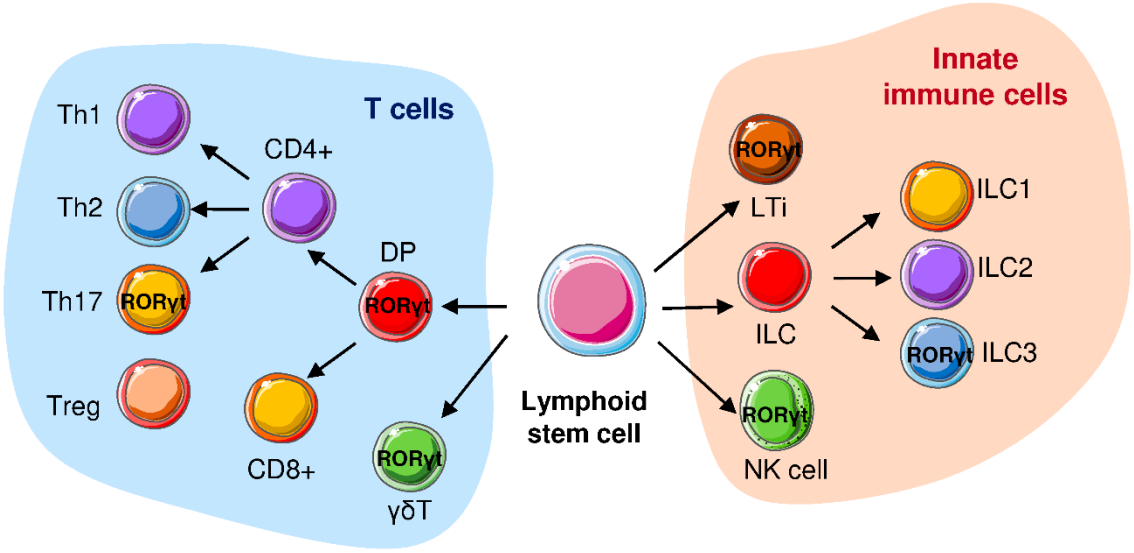

Figure 1.14. Development of T cells and ILCs depending on RORγt. Cells expressing RORγt are $CD4^{+}CD8^{+}DP\alpha\beta TCR^{+}T$ cells, γδTCR+T cells and $\alpha\beta TCR^{+}CD4^{+}$ Th17 cells, NK cells, Lti cells and ILC3. LTi, lymphoid tissue inducer; NK, natural killer; ILC, innate lymphoid cell; DP, double-positive; Th, T helper. Adapted from (240).

IL-17 induces the secretion of a variety of chemokines, cytokines, metalloproteinases and other pro-inflammatory mediators and promotes the recruitment of neutrophils (241,242). In fact, it has been reported that over-expression of RORγt has been implicated in autoimmune diseases and other inflammatory conditions, such as multiple sclerosis, rheumatoid arthritis, Crohn's disease and psoriasis. On the other hand, high RORγt activity can sometimes be beneficial and has been shown to enhance antitumor immunity by increasing IL-17 (243,244).

Interestingly, it has been reported that SIRT1 deacetylates RORγt and increases its transcriptional activity. Consequently, there is an increase of Th17 cell generation and function, which attributes a pro-inflammatory role for SIRT1 in the context of Th17 effector cell differentiation (237).

Contrary to RORγt, the physiological function of RORγ1 remains poorly defined. Several studies reported that RORγ1 regulates hepatic gens related to lipid metabolism, including *hepatic lipase C* (*Lipc*), *insulin induced gene 2a* (*Insig2a*), *cytochrome P450 family 8 subfamily B member 1* (*Cyp8b1*) or *elongation of very long chain fatty acids 3* (*Elovl3*). In this line, both liver-specific and systemic RORγ KO mice exhibit reduced levels of TAG, cholesterol, FFA, *low density lipoprotein* (LDL) and HDL. They also have a decrease of cholesterol and bile acids hepatic content (245). Moreover, RORγ1 also appears to positively regulate gluconeogenesis through the control of the expression of *G6Pase*, *Pepck*, *glucokinase* (*Gck*) and *glycogen synthase 2* (*Gys2*). Accordingly, systemic RORγ KO mice are more glucose tolerant than Wt, but with no differences in the response to insulin (246).

RORγ is associated with the circadian clock at different levels. Firstly, RORγ1 presents an oscillatory expression pattern in several tissues, such as liver, BAT, pancreatic β-cells and kidney, as a result of its regulation by components of the circadian clock (i. e. Clock/Bmal1 and Rev-Erb) but not in WAT (247). Secondly, RORγ1 is recruited to the promoters of different clock genes. Indeed, ROREs have been identified in clock genes, such as *cryptochrome 1* (*Cry1*), *brain and muscle ARNT-like* (*Bmal1*) and *nuclear receptor subfamily 1 group D member 1* (*Rev-Erbα*), which contain two putative ROREs, while the *repressor E4 promoter binding-protein 4* (*E4bp4*) and *circadian locomotor output cycles kaput* (*Clock*) genes contain one site. However, loss of RORγ1 has no major influence on the expression of clock genes and circadian rhythms (248), suggesting that RORγ1 is not a major driver of the expression of clock genes.

RORγ1 is also expressed in WAT. Clinical studies have associated RORγ1 with metabolic complications, including metabolic syndrome, IR and glucose intolerance. Interestingly, single nucleotide polymorphisms in the gene encoding for RORγ have been linked to obesity in mice and humans (249). In this regard, a study reported that individuals with obesity or IR have a significant increase in the expression of *Rorc* and its protein, especially in visceral depots compared to subcutaneous ones. This increment is positively correlated with TAG, insulin and leptin levels but negatively correlated with HDL and cholesterol (249). Therefore, the data provided by this study suggest that RORγ1 could be implicated in adipocyte hyperplasia and hypertrophy and that it is inversely correlated with insulin sensitivity and good health status. However, contradictory studies have emerged about the role of RORγ1 on adipocyte function using RORγ systemic KO mice. Thus, whereas one study reported the lack of any alterations in WAT mass or adipocyte size in RORγ KO mice (250), another showed that RORγ KO mice have increased number of adipocytes but, paradoxically, lower WAT mass and improved insulin sensitivity (251). This contradictory findings precludes any conclusion about the specific function of RORγ1 in adipose tissue and its potential implications in the development of metabolic pathologies, such as obesity or diabetes.

Moreover, it has been reported that RORγ1 over-expression in cultured 3T3-L1 cells partially impairs their differentiation into adipocytes by mechanisms that appears to require *metalloproteinase 3* (MMP3) (251). Although some studies report that mRNA and protein expression of RORγ is high in confluent 3T3-L1 preadipocytes (251), preliminary results in our laboratory found that *Rorc* expression was very low in preconfluent and confluent preadipocytes (Figure 1.15). However, consistent with other studies (251,252), we found that *Rorc* expression dramatically increases during differentiation of 3T3-L1 adipocytes (Figure 1.15), suggesting that mature adipocytes could be the major contributors to the levels of *Rorc* mRNA described in WAT.

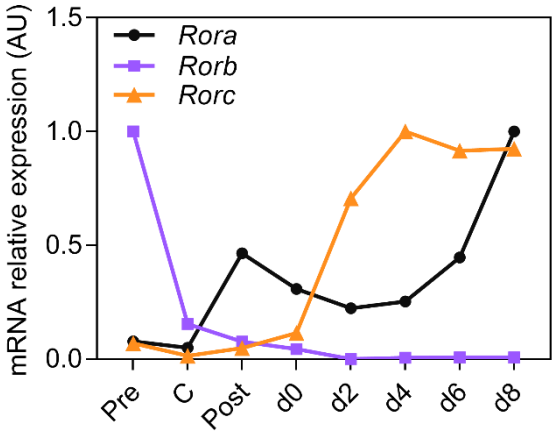

Figure 1.15. Gene expression analysis of ROR family members during 3T3-L1 cells adipogenesis. mRNA expression of *Rora*, *Rorb* and *Rorc* was assessed by real-time quantitative PCR. Pre, pre-confluent; C, confluent; Post, post-confluent; d, differentiation day. Results are expressed as mean ± SEM (n=3)

Indeed, evaluation of RORγ1 expression in the SVF and adipocyte fractions of mouse WAT showed that the expression of *Rorc* in WAT was mostly restricted to the adipocyte fraction, whereas its expression in the SVF was very low. This was in contrast with the expression of other RORs, whose mRNA levels were evenly distributed amongst the SVF and the adipocyte fractions (Figure 1.16).

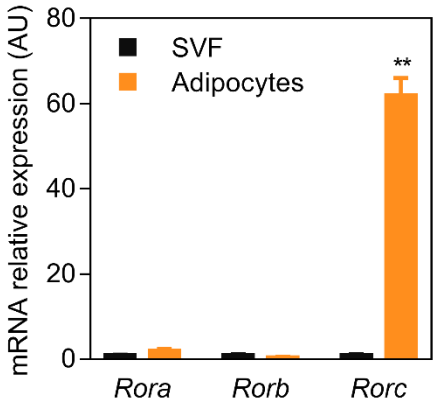

Figure 1.16. Gene expression analysis of ROR family members in WAT of mice fed with a standard diet. *Rorc*, but not *Rora* and *Rorb*, is specifically expressed in mouse adipocytes. mRNA expression levels of *Rora*, *Rorb* and *Rorc* were assessed by real-time quantitative PCR in white adipocytes and SVF isolated from inguinal WAT of mice fed with a standard diet and housed at 21ºC. Results are expressed as mean ± SEM (n=5 animals/group). * Indicates statistical significance between adipocytes and SVF. ** *P*≤0.01.

Moreover, in an attempt to uncover new gene networks and cellular processes regulated by CR in WAT that could be relevant for glucose homeostasis (182), we identified *Rorc* among the top genes up-regulated in WAT in response to nutrient deprivation (Figure 1.17), together with *peroxisome*

proliferator activated receptor alpha (*Ppara*), *Ppargc1a*, *Ppargc1b* and *estrogen receptor 1* (*Esr1*), suggesting a relevant role for RORγ in the adaptation of WAT to CR.

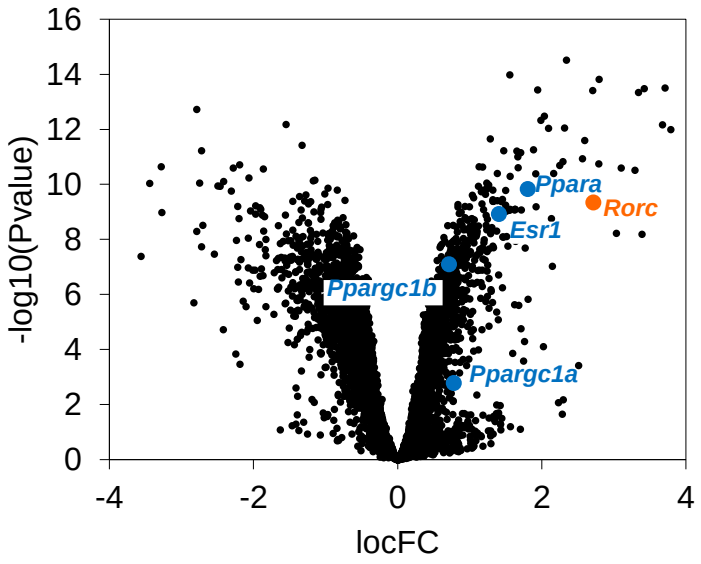

Figure 1.17. *Rorc* is highly induced by CR in WAT. A gene expression profiling analysis was conducted in mice subjected to 40% CR and their AL fed littermates. At the age of 8 weeks, individually caged Wt C57BL6/J mice started receiving a HFD, and 1 week later, they were randomly assigned to AL or CR groups. CR mice received 60% of the food eaten by AL animals for a period of 12 weeks. Volcano plot showing differentially expressed genes in WAT under CR. Orange spot labels *Rorc* gene.

HYPOTHESIS AND OBJECTIVES

► 2. Hypothesis and objectives

Given that i) RORγ1 is highly expressed in mature adipocytes and its expression is increased during adipocyte differentiation; ii) RORγ1 has been shown to be an important regulator of some genes related to lipid metabolism and iii) RORγ1 expression is induced in WAT in response to CR, **we hypothesize** that:

The nuclear receptor RORγ1 could play an essential role in WAT biology by controlling the expression of essential gene networks required for a correct adipocyte function. Furthermore, we propose that RORγ1 could be an important mediator of the metabolic changes exerted by CR in WAT that lead to an improvement of insulin sensitivity and a decrease of body mass.

Therefore, the **main objective** of the proposed study is to elucidate the function of the hormone nuclear receptor RORγ1 in WAT and its implication in the development of obesity and IR in response to different nutritional conditions. To prove our hypothesis, we proposed the following **specific aims**:

AIM 1. To identify the genetic programs regulated by RORγ1 in white adipocytes.

AIM 2. To study the role of RORγ1 as a regulator of the main metabolic and cellular process regulated by CR in adipose tissues using a new mouse model lacking RORγ specifically in adipocytes

AIM3. To determine to which extent the loss of RORγ1 in adipocytes affects the health benefits of CR on whole body energy homeostasis and insulin sensitivity.

MATERIALS AND METHODS

► 3.1 Animal studies

3.1.1 Generation of adipocyte-specific RORγ knockout mice

Systemic RORγ knockout have yielded conflicting results regarding the role of RORγ1 in WAT and its contribution to whole body energy balance and glucose homeostasis. Consequently, to avoid any confounding effects resulting from knocking out RORγ in non-adipose tissues, we have generated a new mouse model devoid of RORγ specifically in adipocytes.

For this, we used the *Cre/loxP* recombination system. This is a gene editing technique that consists in flanking a genetic locus of interest with two *loxP* motifs, a target nucleotide sequence consisting of 34 bp (ATAACTTCGTATANNNTANNNTATACGAAGTTAT). The *Cre* recombinase enzyme is also necessary because it deletes DNA fragments by targeting these specific *loxP* sites. To achieve adipocyte-specific recombination, *Cre* recombinase expression was driven by the promoter of *adiponectin* (*AdipoQ*) gene, which is exclusively expressed in adipocytes (253).

Mice with exons 3-6 of *Rorc* gene flanked by loxP sites (C57BL/6-Rorc^{tm1Litt}) were obtained from *The Jackson Laboratory* and crossed with transgenic mice that over-express *Cre* recombinase under the adipocyte-specific promoter of the *AdipoQ* gene (AdipoQ-Cre mice) (254), already available in the laboratory, to obtain adipose-specific RORγ KO mice (RORγ-FAT-KO mice).

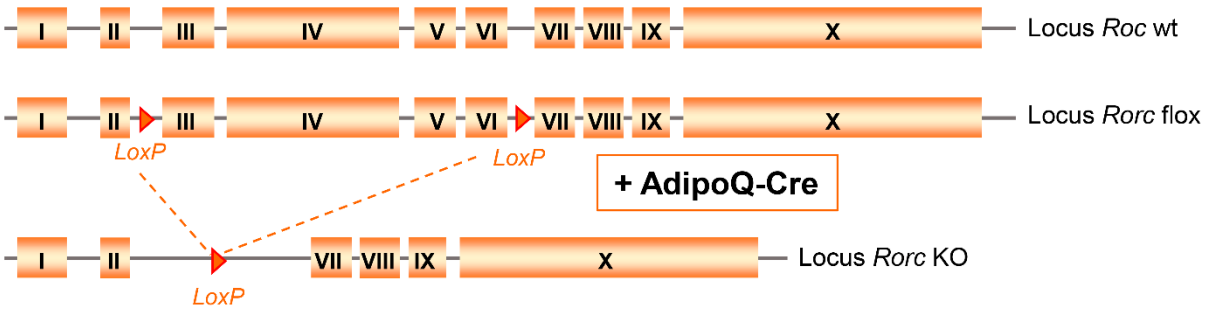

Figure 3.1. Scheme of RORγ-FAT-KO mice generation. Inactivation of Rorc was carried out by Cre recombinase, which recombines *loxP* sites flanking exons 3 and 6 of the *Rorc* gene resulting in their excision.

3.1.2 Mice genotyping

At 21 days of age, mice were weaned, marked with a numbered earring and genotyped to identify Wt and RORγ-FAT-KO mice. Mice genotyping was assessed by isolating total DNA from a small piece of the tail and next performing two independent *Polymerase Chain Reactions* (PCR) in order to identify mice with *Rorc* floxed alleles and those carrying the *AdipoQ-Cre* transgene. These procedures are explained in detail below.

3.1.2.1 DNA extraction

To isolate total DNA from the tail, we first performed a *Proteinase K* (PK) digestion, in order to disrupt tissue and cell integrity and, by this means, release DNA. For this, a small piece (1-2 mm) of tail was cut and digested overnight at 55ºC with constant shaking in 500 µL of PK digestion buffer (0.5% SDS, 0.1M NaCl, 0.05M Tris pH 8.3mM EDTA, 1U/mL PK). Then, DNA was extracted with chloroform followed by ethanol precipitation. For this, once tails were digested, 75 µL of potassium acetate 8 M and 500 µL of chloroform were added to each sample. After vigorous vortex, samples were stored for an hour at -80ºC. Under these conditions, potassium acetate helped in the precipitation of proteins, whereas chloroform contributed in DNA isolation from RNA and proteins.

Samples were then centrifuged 5 min at 13000 rpm at room temperature and the aqueous phase (containing DNA) was transferred to a new tube. Following this, 1 mL of 100% ethanol was added to precipitate de DNA and samples were again centrifuged at 13000 rpm for 5 min at 4ºC to pellet the DNA. DNA was washed with 500 µL of 70% ethanol, air-dried and re-suspended in miliQ water. To favor dissolution, samples were heated at 50ºC during 10 min with constant shaking. DNA concentration and purity were determined in a NanoDrop ND-2000 spectrophotometer.

3.1.2.2 PCR

To identify mice carrying *loxP* sites in the *Rorc* gene, specific primers flanking the *loxP* site located between exons 3 and 6 were used. The size of the amplicon of transgenic *Rorc*$^{flox/flox}$ mice is bigger than the one in Wt due to the presence of the *loxP* sequence. Moreover, the presence of the *AdipoQ-Cre* transgene was also determined.

To amplify target DNA, a master mix was prepared for several parallel reactions (volumes for a 25 µL reaction are given in Table 3.1).

Component	Volume	Final concentration
Water	17.15 µL	
10X PCR buffer	2.5 µL	2 mM $MgCl_2$
dNTP mix (10mM each)	0.5 µL	200 µM (of each dNTP)
Forward primer (10µM)	1.3 µL	0.52 µM
Reverse primer (10µM)	1.3 µL	0.52 µM
Taq DNA Polymerase (5U/µL)	0.25 µL	0.05 U/µL

Table 3.1. Master mix composition for PCR amplification. The volume of each reagent is indicated.

Two µL of DNA (60-120 ng) were used as a template. PCR reaction was carried out in a GenAmp PCR System 2400 (Perkin Elmer) thermocycler applying the conditions shown in Table 3.2A and 3.2B, and the specific primers shown in Table 3.3.

A) *Rorc* genotyping

Step	Temperature	Time	Cycles
Denaturation/Activation	95ºC	2 min	1
Denaturation	95ºC	20 sec	30
Annealing	60ºC	15 sec	
Extension	72ºC	30 sec	
Final extension	72ºC	2 min	1
Cooling	4ºC	∞	1

B) *Cre* genotyping

Step	Temperature	Time	Cycles
Denaturation/Activation	95ºC	2 min	1
Denaturation	95ºC	20 sec	30
Annealing	64ºC	15 sec	
Extension	72ºC	30 sec	
Final extension	72ºC	2 min	1
Cooling	4ºC	∞	1

Table 3.2. Thermal cycle conditions to genotype *Roca* (A) and *Cre* (B) PCR.

	SEQUENCE	FRAGMENT LENGTH
***Rorc* floxed allele**		
Forward primer	TTCCTTCCTTCTTCTTGAGCAGTC	Wt: 166 bp
Reverse primer	CAGAAGAAAAGTATATGTGGCTTGTTG	Tg: 226 bp
***Cre* transgene**		
Forward primer	GACGGAAATCCATCGCTCGACCAG	Tg: 596 bp
Reverse primer	GACATGTTCAGGGATCGC CAG GCG	

Table 3.3. Primers used for genotyping. Sequence of the primers to detect *Rorc* floxed allele and *Cre* transgene. The expected amplicon length is indicated.

3.1.2.3 Agarose gel electrophoresis

In order to separate DNA amplicons by size, an agarose gel electrophoresis in *Tris-Acetate-EDTA* (TAE) buffer (40 mM Tris, 20 mM acetic acid, 1 mM EDTA) was performed. Percentage of agarose was different for *Cre* (1%) and *Rorc* (2-2.5%) for an appropriate resolution of the amplified DNA products. During the preparation of the agarose gel, ethidium bromide was added to stain nucleic acids. Electrophoresis was performed at 80V for 25 min approximately and the resulting bands were seen in a U.V. transilluminator.

Mice genotype was assigned as follows depending on the bands observed (see an example in **Figure 3.2**):

- PCR for detection of *Rorc* floxed allele:
  - 226 bp band → $Rorc^{flox/flox}$ mouse
  - 226 and 166 bp band → $Rorc^{flox/+}$ mouse
  - 166 bp band → $Rorc^{+/+}$ mouse
- PCR for detection of *Cre* transgene:
  - 596 bp band → Cre^{+} mouse
  - No band → Cre^{-} mouse

We considered RORγ1-FAT-KO mice, the ones that were Cre^{+} and that had *Rorc* floxed alleles.

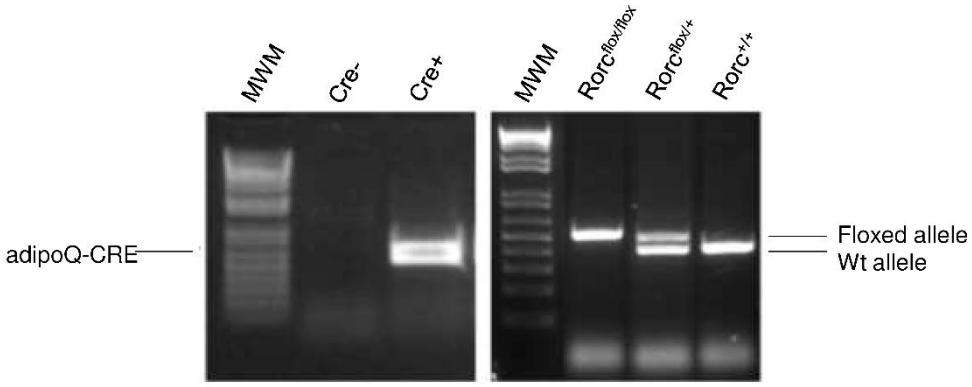

Figure 3.2. Example of gel electrophoresis genotypes. *Cre* genotype showing the presence of *Adiponectin-Cre* trangene (*left*) and *Rorc* genotype to identify *loxP* flanked *Rorc* alleles (*right*).

3.1.3 Mice housing conditions

Mice were bred and raised at 21ºC on a 12 h light/dark cycle in the standard clean area of Vall d'Hebron Research Institute (VHIR) animal facility.

For mouse breeding, adult $Rorc^{flox/flox}$/adipoQ-Cre^{-} (Wt) females were mated with adult $Rorc^{flox/flox}$/adipoQ-Cre^{+} (RORγ-FAT-KO) males. This breeding strategy results on a heterogeneous offspring of $Rorc^{flox/flox}$/adipoQ-Cre^{-} (Wt) and $Rorc^{flox/flox}$/adipoQ-Cre^{+} (RORγ-FAT-KO) mice.

Three weeks after birth, mice were weaned and separated in cages according to their sex. They were genotyped and distributed in cages containing 4-6 individuals/cage, placing similar number of Wt and RORγ-FAT-KO animals per cage, whenever possible. In accordance with the experiment, mice were given AL access to food and water, and fed a standard laboratory diet (Chow) (SAFE 150 Scientific Diets #19156; 21% calories from protein, 12.6% calories from fat, 66.4% calories from carbohydrates) or HFD (Research Diets #D-12492; 20% calories from protein, 60% calories from fat, 20% calories from carbohydrates). For the CR, at 8 weeks of age, mice were individually caged and started receiving a HFD. At the age of 9 weeks, mice were randomly assigned to AL or CR groups. During the following week, CR animals received 80% of the food eaten by their AL counterparts. Afterwards, CR mice started receiving 60% of the food eaten by AL animals. For this purpose, food consumption of AL fed mice was measured every day and 40% of as such amount of food was provided to the CR group the next evening. Mice were subjected to 40% CR for a period of 12 weeks.

All procedures involving animals were conducted according to the European Union Ethical Guidelines and approved by the Animal Experimentation and Ethics Committee of Vall d'Hebron Research Institute (ID 68/16 CEEA).

3.1.4 Assessment of glucose homeostasis

3.1.4.1 Basal glucose levels

Basal glucose levels from each animal were measured using a glucometer (Countour XT, Bayer) from tail vein blood after a 5-6 h of fasting.

3.1.4.2 Intraperitoneal glucose tolerance test

Glucose tolerance test (GTT) was performed on mice fasted for 5 h. Blood glucose levels were determined at 0, 15, 30, 60, 90 and 120 min after an intraperitoneal injection of sterile D-glucose (2g/kg dose, dissolved in saline solution). Glucose levels were determined from tail vein blood as described section 3.1.4.1.

3.1.4.3 Intraperitoneal insulin tolerance test

Insulin tolerance test (ITT) was performed on mice fasted for 5 h. Blood glucose levels were monitored after an insulin bolus (0.9 U/kg of insulin; specified in each experiment) administrated intraperitoneally. Glucose levels were measured at 0, 15, 30, 60, 90 and 120 min post-injection as described before. In this assay, we used Actrapid human insulin from Novo Nordisk®.

3.1.5 Serological analysis

Blood from Wt and RORγ-FAT-KO mice either fed AL or subjected to CR was first collected via tail cut in a Microvette capillary tube (Sarstedt) after a 5 h fast. To obtain serum, blood was centrifuged

at 3000 rpm during 5 min at 4ºC. Serum was collected and stored in aliquots at -20ºC for further use.

3.1.5.1 Triglycerides determination

TAG were determined using a commercial kit based on the Trinder colorimetric method (FAR diagnostics). The technique is relaying on TAG hydrolysis and quantification of products. TAG are first converted into glycerol and fatty acids by lipoprotein-lipase. Then, glycerol is transformed by glycerol kinase into glycerol-3-phosphate, which is oxidized by glycerol-phosphate-oxidase into de-hydroxyacetone phosphate, with hydrogen peroxide formation. In presence of peroxidase, hydrogen peroxide reacts with ethyl-sulphopropyl-toluidine and 4-aminophenazone to form a colored complex, whose color intensity is directly proportional to the concentration TAG in the sample. This colored product was measured colorimetrically at λ=550 nm using Spectra Max 340 spectrophotometer. A TAG solution (200 mg/dL) was used as a standard.

3.1.5.2 Non-esterified fatty acids (NEFA) determination

FFA were determined colorimetrically with the NEFA-HR kit (Wako Chemicals GmbH). This method is based in the action of Acyl-CoA oxidase and the usage of 3-Methyl-N-Ethyl-N-(β-Hydroxyethyl)-Aniline as a violet color agent. Firstly, NEFA are converted to Acyl-CoA, AMP and pyrophosphoric acid by Acyl-CoA synthetase, in the presence of coenzyme A and adenosine 5-triphosphate disodium salt. Then, Acyl-CoA is transformed to 2,3-trans-Enoyl-CoA and hydrogen peroxide by Acyl-CoA oxidase. In the presence of peroxidase, hydrogen peroxide helps in the oxidative condensation of 3-Methyl-N-Ethyl-N-(β-Hydroxyethyl)-Aniline with 4-aminoantipyrine, generating a pigment that can be measured at λ=550 nm. At this wave length, increasing absorbance is proportional to NEFA concentration. 1 mmol/L NEFA solution was used as a standard and absorbance was read with a Spectra Max 340 spectrophotometer.

3.1.5.3 Total cholesterol determination

Total cholesterol was measured by using a commercial kit based on the Trinder colorimetric method (FAR diagnostics). In this method, esterified cholesterol is hydrolyzed into free cholesterol and fatty acid by cholesterol esterase. Then, cholesterol oxidase oxidizes the free cholesterol into cholestene-3-one, forming hydrogen peroxide. When peroxidase is present, the hydrogen peroxide reacts with hydroxybenzoate and 4-aminoantipryine producing a colored complex. This color intensity, measured at λ=550 nm, is proportional to total cholesterol concentration. A cholesterol solution (200 mg/dL) was used as a standard and absorbance was read with a Spectra Max 340 spectrophotometer.

3.1.5.4 Insulin, leptin, adiponectin and resistin determination

Insulin was determined in serum by ELISA using an Ultra-Sensitive Mouse Insulin ELISA Kit (Crystal Chem). Leptin was assayed with Mouse Leptin ELISA Kit (Crystal Chem), adiponectin was measured using Mouse Adiponectin ELISA Kit (Crystal Chem) and resistin was determined with Mouse Resistin ELISA Kit (Thermo Scientific).

3.1.6 Histological analysis

A small fragment of inguinal WAT, gonadal WAT, liver and interscapular BAT was fixed during 24 hours with 4% paraformaldehyde. Then, tissue was dehydrated and embedded in paraffin for subsequent sectioning. Paraffin blocks were made by CIBER ICTS-NanBiosis platform (located at

VHIR). Tissue sections (5-8 µm) were obtained with a microtome and stained with hematoxylin/eosin. For this, Aqueous Harris haematoxylin (Química Clínica Aplicada) and 0.25% alcoholic Eosin (LEYCA) were used. Samples were first deparaffined with xylene and hydrated with decreasing concentrations of ethanol (two times of absolute ethanol, 96% ethanol, 70% ethanol, 50% ethanol and distilled water, 5 min each step). Then, samples were stained during 5 min with Harris Haematoxylin and washed with tap water. Samples were then dehydrated to be able to absorb eosin, which is hydrophobic. After dehydration in increasing concentrations of ethanol solutions (50% ethanol and 70% ethanol; 5 min each), samples were stained during 30 sec with eosin (0.25%) and later washed with 96% ethanol, two times of absolute ethanol and two times of xylol. Finally, wet slides were mounted with DPX (SIGMA).

Following staining and mounting, tissue sections were observed under a light field microscope (Model BX61, Olympus) and images of representative sections of the depots were captured for analysis.

To measure adipocyte size we used Image J software. For this, pictures of different randomly selected fields of tissue sections were taken from three animals of each experimental group. No less than 300 cells from each animal were measured from at least three independent tissue sections.

3.1.7 Acute cold exposure

For the acute cold exposure experiments, RORγ-FAT-KO and Wt mice were weaned at 21 days and kept at an environmental temperature of 21ºC. At the age of 4 weeks they were housed at thermoneutrality (30ºC) and fed a standard diet. After 8 weeks of acclimation at thermoneutrality, mice were individually caged, with free access to water but no food or bedding, and basal body temperature was determined with a rectal probe. Then, mice were immediately transferred to a room set at 4ºC. Body core temperature was monitored every hour for a period of 5h, as described above. A group of control Wt and RORγ-FAT-KO mice was maintained in parallel at thermoneutrality (30ºC) for the entire duration of the experiment. Afterwards, mice were weighed and euthanized by cervical dislocation to obtain different organs and tissues.

3.1.8 Tissue collection

Mice were sacrificed at the end of each experiment by cervical dislocation. Tissues and organs were collected, weighted and rapidly frozen in liquid nitrogen for RNA, DNA and protein analysis. For histological analysis, a piece of fresh tissue, approximately 0.5 cm^3, was fixed 24 hours with formalin for posterior processing, as described in section 3.1.7.

► 3.2 Isolation of mature adipocytes and stromal vascular fraction

Adipose tissue is a connective tissue that is mainly composed of two components: the SVF, which includes preadipocytes, fibroblasts, vascular endothelial cells and immune cells, and adipocytes. Cellular components of adipose tissue can be separated by collagenase digestion, an enzyme that breaks collagen peptide bonds which helps tissue disruption (Figure 3.3).

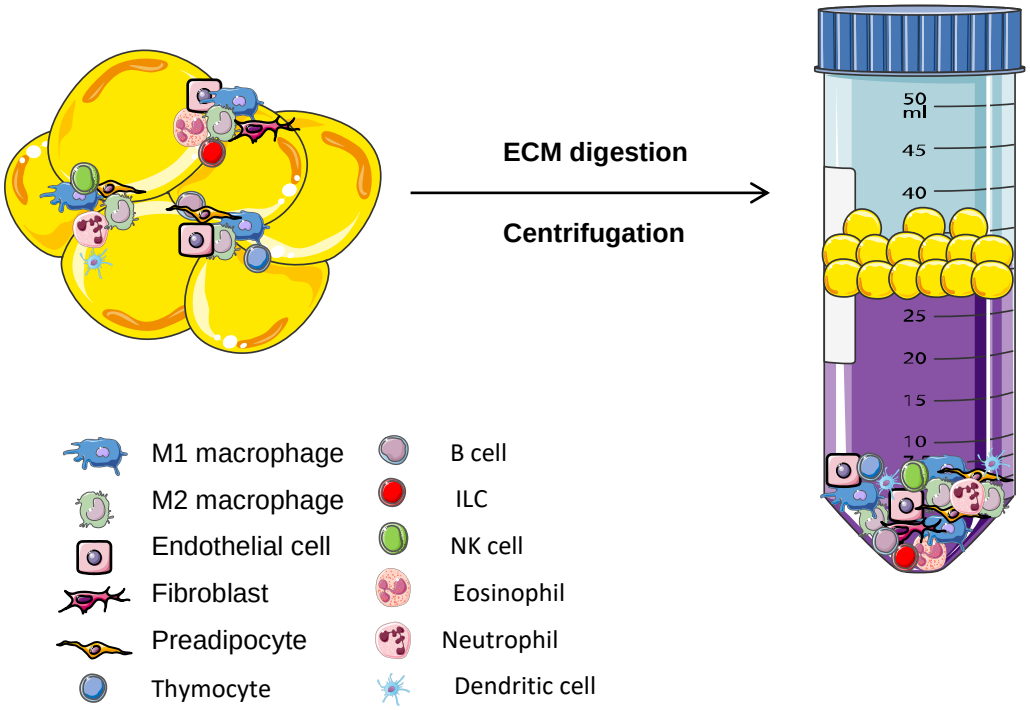

Figure 3.3. Separation of adipose tissue cellular components by collagenase digestion. SVF and adipocytes are separated after a digestion of the ECM followed with a centrifuge of the cellular mixture. Adipocytes will float and form a visible lipid layer at the top of the aqueous medium whereas SVF will be in the pellet. Adapted from (56).

Animals were sacrificed by cervical dislocation and inguinal and gonadal WAT depots were dissected and weighted. Then, fat pads were placed in a Petri Dish containing 10 mL of *Dulbecco's Modified Eagle's Medium* (DMEM) (4.5 g/L D-Glucose, GlutaMAX and 1.1 g/L sodium pyruvate), previously warmed. Samples were minced with scissors, placed in a tube containing 10 mL of warm digestion solution (Collagenase A 1 mg/mL, Hepes 100 mM pH 7.4, NaCl 123 mM, KCl 5 mM, $CaCl_2$ 1.3 mM, Glucose 5 mM, BSA 1.5%) and tubes were incubated for 30-35 min at 37ºC with soft shaking (120 rpm). Once most of the tissue was digested, 10 mL of DMEM high glucose supplemented with 10% *Fetal Bovine Serum* (FBS) was added to stop collagenase activity. Digested tissue was then filtered through a 100 µm cell strainer to retain undigested tissue pieces and then the filtered digestion solution was let stand for 20 min at room temperature to allow the flotation of adipocytes. Lower phase, containing the SVF, was collected with a syringe (20G needle) and transferred to a new tube. Afterwards, it was centrifuged at 700 g (2550 rpm) for 10 min at room temperature to pellet SVF cellular components.

For RNA isolation, 2 mL and 0.5 mL of TRIzol reagent (Invitrogen) were added to the adipocyte fraction and SVF, respectively. Samples were stored at -80ºC until required for RNA isolation and analysis.

For protein analysis by flow cytometry, cells from SVF were re-suspended in 10 mL of hemolysis solution (Tris 17 mM, NH_4Cl 0.75%) and incubated for 5 min at room temperature to lyse erythrocytes. The solution was then neutralized with 20 mL of DMEM with 10% FBS and centrifuged at 700 g (2550 rpm) for 10 min at room temperature. The SVF pellet was re-suspended with *Phosphate-buffered saline* (PBS). Cells were counted in a Neubauer Chamber and kept on ice for the following flow cytometry analysis (see section 3.6).

► 3.3 Spleen cells preparation

Splenocytes were used as positive and compensation controls for the antibodies used in the flow cytometry analysis. For the preparation of single-cell splenocytes, Wt mice were killed by cervical dislocation and spleens were collected in a 15 mL tube containing PBS. First, a 70 µm filter was placed above of 6 cm plate and pre-wet with 3 mL of DMEM media. Dissected spleen was placed on top of the pre-wet filter and smashed with the plunger of a 1 mL syringe mechanically disaggregating spleen by forcing cells through the filter mesh. Then, the filter was placed on a top a 50 mL tube to filter the medium containing splenocytes. The 6-cm-plate was rinsed with additional 3 mL of media, which were also filtered. The cell suspension was centrifuged 10 min at 1500 rpm to recover splenocytes, which were re-suspended in 1 mL of sterile water for 5 sec to lyse red blood cells. After that, 20 mL of DMEM supplemented with 10% FBS was added, and the content of the tube was filtrated again and centrifuged during 10 min at 1500 rpm. The pellet containing splenocytes was re-suspended in 1 mL of PBS. Finally, cells were counted in a Beckman Coulter counter and kept on ice for the following flow cytometry analysis (see section 3.6).

► 3.4 *In vitro* procedures

3.4.1 Cell culture of 3T3-L1 adipose cells

The 3T3-L1 cell line, obtained by clonal expansion of mouse embryonic fibroblasts, constitutes a model commonly used for adipose biology studies since, once differentiated, it exhibits all typical features of mature adipocytes, including storage of TAG and secretion of adipokines (255). 3T3-L1 cells used in this study were acquired from Tebu-Bio.

3.4.1.1 Thawing frozen 3T3-L1 cell stocks from liquid nitrogen

To thaw frozen 3T3-L1 preadipocytes, cryogenic vials were removed from liquid nitrogen and incubated in water bath at 37ºC with gentle shaking to rapidly thaw cells. Once thawed, the content of the cryogenic tube was transferred to a 6 cm dish containing 4mL of warm **proliferation medium** (DMEM supplemented with 10% *Newborn Calf Serum* (NCS) and 1X Antibiotic- Antimycotic (10000 units/mL of penicillin, 10000 µg/mL of streptomycin, and 25 µg/mL of amphotericin B)). After 6 h, once they were attached to the dish, cell medium was aspirated to remove dead cells and *dimethyl sulfoxide* (DMSO), and replaced by fresh proliferation medium.

3.4.1.2 Subculture of proliferating 3T3-L1 preadipocytes

3T3-L1 preadipocytes were maintained in proliferation medium, avoiding cells to reach confluence at any moment. Therefore, when preadipocytes reached 70-80% of confluence, they were passed to new dishes and seed at lower densitiy. To pass cells, proliferation medium was removed and cells were rinsed with PBS and 0.5 mL of trypsin (TrypLE Express) were added and distributed homogeneously. Cells were placed at 37ºC for 2-3 min at 37ºC. Once cells were detached, 10 mL of proliferation medium were added to neutralise the trypsin. Detached cells were collected, centrifuged at 500 g for 5 min and resuspended in proliferation medium. Cells were then counted using a Neubauer chamber and seeded in proliferation medium.

3.4.1.3 Differentiation of 3T3-L1 preadipocytes into adipocytes

To differentiate 3T3-L1 preadipocytes into adipocytes, cells were first grown in proliferation medium and allowed to reach confluence. Two days after cells have reached confluence, adipocyte differentiation was induced for 2 days with **induction medium** (DMEM supplemented with 10%

FBS, 1X Antibiotic-Antimycotic, 0.5 mM *3-Isobutyl-1-methylxanthine* (IBMX), 1 µM dexamethasone and 100 nM Insulin). After 2 days of induction (*day 0* of differentiation), cells were switched to **differentiation medium** (DMEM supplemented with 10% FBS, 1X Antibiotic-Antimycotic and 100 nM insulin) and allowed to differentiate for 6-8 days (Figure 3.4). Differentiation medium was replaced every two days. At day 6 of differentiation, cells already show an adipocyte-like morphology, characterized by a cytoplasm full of lipid droplets of various sizes.

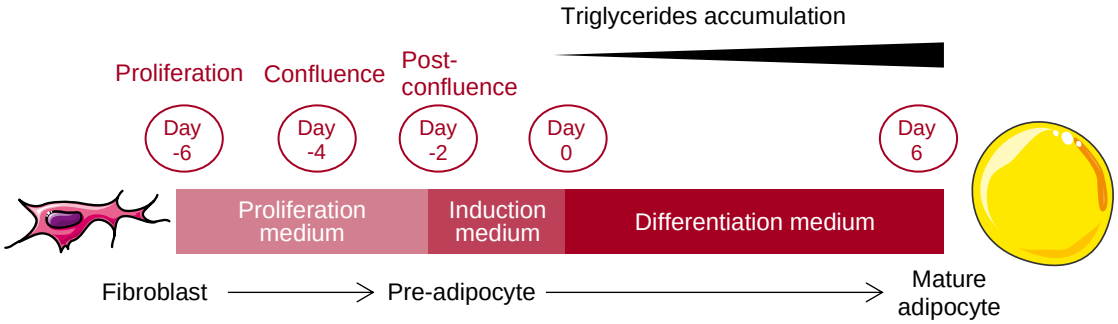

Figure 3.4. Representation of 3T3-L1 differentiation process protocol. Cells are maintained with proliferation medium until they spent two days at confluence and then they are induced for three days. After this, differentiation medium is used and at day 5-6 the experiment is performed. They start as fibroblast and end up the process as mature adipocytes with lip droplets and lateralized nucleus

3.4.1.4 Preparation of frozen stocks of 3T3-L1 preadipocytes

To prepare frozen stocks of 3T3-L1 cells, preadipocytes were collected when they reached 70-80% of confluence. At this point, cells were trypsinized and re-suspended in **freezing medium** (DMEM containing 20% NCS, 10% DMSO and 1X Antibiotic- Antimycotic). Cell concentration was adjusted approximately 300.000 cells/mL. Cell suspension was transferred to cryogenic tubes (1 mL/tube), placed in a polystyrene box to allow a slow freezing process and stored at -80ºC. Twenty-four hours later, vials were transferred to liquid nitrogen and stored until required.

► 3.5 Silencing *Rora* and *Rorc* genes in 3T3-L1 adipocytes with small interfering RNAs

In the present study, specific chemically synthetized *small interfering RNAs* (siRNAs) were used to silence *Rorc* and *Rora* in 3T3-L1 mature adipocytes.

For *Rora* and *Rorc* knowdown, adipocytes were transfected at day 6 of differentiation using DharmaFECT 4 reagent with 50 nM of ON-TARGETplus SMART pool siRNAs specifically targeting *Rora* (siRORa), *Rorc* (siRORc) or both simultaneously (siRORa/c). It consists in a pool of four different siRNA targeting *Rora* or *Rorc*, respectively, so that their specificity and potency are enhanced. ON-TARGETplus Non-Targeting siRNA#2 was used as negative control (siCont). Transfection was carried in suspension onto collagen-coated cell culture dished following the protocol described by Kilory *et al.* (256) with minor modifications.

Briefly, 50µg/mL collagen I were added in each well of a 12-well cell culture plate and incubated for 1 hour to create a surface where the adipocytes will efficiently attach during transfection. Then, 460.000/well 3T3-L1 adipocytes were added in each well of 12-well plate containing DMEM supplemented with 10% FBS, but no Antibiotic-Antimycotic.

Mixes with 50nM siRORa, siRORc and siCont were prepared as indicated in Table 3.4. Once mixes were prepared, they were incubated 5 min at RT. Then, the content of both tubes was mixed and 160µL/well of the mix were added to each well containing adipocytes in suspension. Following an overnight incubation, cells were cultured for additional 36 h in differentiation medium before being harvested to analyze gene expression.

		1.4 µL/cm² DharmaFECT		
		6-well dish	**12-well dish**	**24-well dish**
Tube 1	**DharmaFECT 4**	13.9 µL	5.6 µL	2.8 µL
	OptiMEM	184 µL	74.4 µL	37.2 µL
Tube 2	**siRNA 5µM**	24.8 µL	10 µL	5 µL
	OptiMEM	173.1 µL	70 µL	35 µL

Table 3.4. Content of each tube to prepare the transfection mix. In separate tubes, the siRNA (Tube 1) and DharmaFECT 4 transfection reagent (Tube 2) were diluted in OptiMEM medium. The volume of each reagent is indicated.

► 3.6 Flow cytometry

Single cell suspensions of SVF from WAT and spleenocytes were prepared as described (see sections 3.2 and 3.3).

Flow cytometry data was acquired on a three lasers cytometer (Cytoflex flow cytometer, Beckman Coulter), which allow up to 10 different antibody-fluorochrome combinations. Four multicolor immunofluorescence panels were designed and optimized to immunophenotype the SVF of mouse adipose tissues. Single-stained spleen cells were used as a compensation controls for each fluorochrome. *Fluorescence minus one* (FMO) and isotype control were used as negative controls to establish a positivity criterion of each antibody (Supplementary figure 1).

Cell subsets were analyzed using fluorochrome-conjugated monoclonal antibodies after discrimination of dead cells by FixableViability Stain (BD Pharmingen, BD Biosciences) and blocking Fc receptors with rat anti-mouse CD16/32 (BD Pharmingen, BD Biosciences). The antibody panels used in our study are described in Table 3.5.

	Antibody	Localization	Fluorochrom	Clone	Working dilution	Isotype
Panel 1 Main immune cells	B220	Extracellular	FITC	RA3-6B2	1/10	Rat IgG2a,k
	F4/80	Extracellular	PE	T45-2342	1/10	Rat IgG2a,k
	CD45	Extracellular	PC5	30-F11	1/100	Rat IgG2b,k
	CD11b	Extracellular	PE-Cy7	M1/70	1/500	Rat IgG2b,k
	CD25	Extracellular	eFluor450	PC61.5	1/5	Rat IgG1 K
	CD3	Extracellular	BV510	17A2	1/5	Rat IgG2b,k
	NK1.1	Extracellular	BV605	PK136	1/5	Mouse IgG2a,k
	Foxp3	Intracellular	APC	FJK-16s	1/10	Rat IgG2a,k
	CD4	Extracellular	APCH7	GK1.5	1/10	Rat IgG2a,k
Panel 2 T cell subsets	CD45	Extracellular	FITC	30F11	1/10	Rat IgG2b,k
	Gata3	Intracellular	PE	16E10A23	-	Mouse IgG2b,k
	Rorγt	Intracellular	PerCPeFluor710	B2D	-	Rat IgG1,k
	CD11b	Extracellular	PE-Cy7	M1/70	1/500	Rat IgG2b,k
	Tbet	Intracellular	BV421	4B10	-	Mouse IgG1,k

	CD3	Extracellular	BV510	17A2	1/5	Rat IgG2b,k
	CD8a	Extracellular	BV605	53-6.7	1/5	Rat IgG2a,k
	Foxp3	Intracellular	APC	FJK-16s	1/10	Rat IgG2a,k
	CD4	Extracellular	APCH7	GK1.5	1/10	Rat IgG2a,k
Panel 3 ILCs and NK cells subsets	CD45	Extracellular	FITC	30F11	1/10	Rat IgG2b,k
	Gata3	Intracellular	PE	16E10A23	-	Mouse IgG2b,k
	Rorγt	Intracellular	PerCPeFluor710	B2D	1/4	Rat IgG1,k
	CD11b	Extracellular	PE-Cy7	M1/70	1/500	Rat IgG2b,k
	Tbet	Intracellular	BV421	4B10	-	Mouse IgG1,k
	CD3	Extracellular	BV510	17A2	1/5	Rat IgG2b,k
	NK1.1	Extracellular	BV605	PK136	1/5	Mouse IgG2a,k
	CD127	Extracellular	APC	SB/199	1/10	Rat Ig2b,k
	B220	Extracellular	APC-eF780	RA3-6B2	1/10	IgG2a, kappa
Panel 4 Myeloid and γδ T cells	Ly6G	Extracellular	FITC	1A8	1/10	Rat IgG2a,k
	F4/80	Extracellular	PE	T45-2342	1/5	Rat IgG2a,k
	CD45	Extracellular	PC5	30-F11	1/100	Rat IgG2b,k
	CD11b	Extracellular	PE-Cy7	M1/70	1/500	Rat IgG2b,k
	SiglecF	Extracellular	BV421	E50-2440	1/10	Rat IgG 2a,k
	CD3	Extracellular	BV510	17A2	1/5	Rat IgG2b,k
	CD8a	Extracellular	BV605	53-6.7	1/5	Rat IgG2a,k
	TCRγ	Extracellular	APC	eBioGL3	1/10	A.hamster IgG
	CD4	Extracellular	APCH7	GK1.5	1/10	Rat IgG2a,k

Table 3.5. Antibody panels designed to immunophenotype SVF of mice adipose tissues.

Cells were first surface-stained with the indicated antibodies for 30 min at 4ºC. Then, for intracellular staining, cells were fixed and permeabilized using Foxp3/Transcription Factor Staining Buffer Set (Invitrogen), as described by the manufacturer. After that, cells were stained with the appropriate intracellular antibodies. Flow cytometry data was acquired on a Cytoflex flow cytometer and fluorescence was analyzed using CytExpert2.3 software (Beckman Coulter). 250.000 singlet events were recorded in SVF samples, whereas 50.000 events were recorded for the compensation controls.

The population of interest was first identified based on forward (FSC-H) and side scatter (SSC-H), where debris and other events that are not of interest were removed. FSC-A and FSC-H were then combined in a plot to remove doublets from the dataset. Next, a viability dye was used to eliminate dead cells from the analysis. Finally, immune infiltrate was selected using $CD45^+$ gate (Figure 3.5).

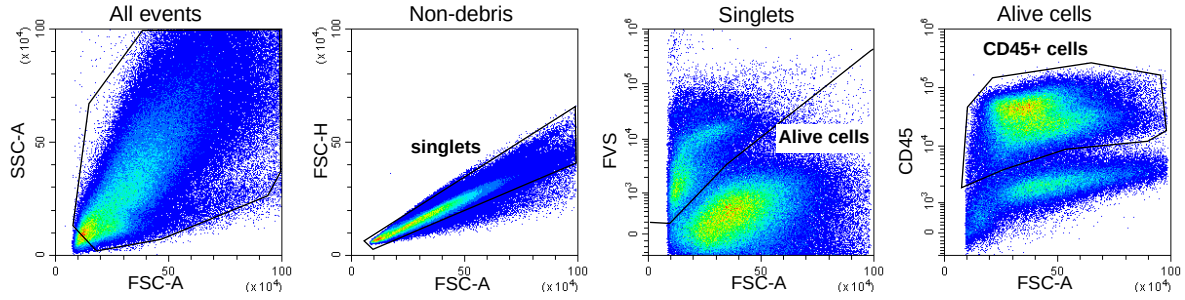

Figure 3.5. Flow cytometry gating strategy for immune infiltrate from SVF of mice adipose tissue. After excluding doublets and dead cells, $CD45^+$ cells were gated to select the immune infiltrate.

The frequency of each of the immune cell population identified was determined following the immunophenotyping described in Table 3.6 and Figure 3.6.

Cell population	Gating strategy
Myeloid cells	$CD45^+CD11b^+$
Eosinophils	$CD45^+CD11b^+F4/80^+SiglecF^+$
Macrophages	$CD45^+CD11b^+SiglecF^-F4/80^+$
Neutrophils	$CD45^+CD11b^+SiglecF^-F4/80^-Ly6G^+$
B cells	$CD45^+CD11b^-CD3^-B220^+$
NK cells	$CD45^+CD11b^-B220^-NK1.1^+$
NKt cells	$CD45^+CD11b^-B220^-NK1.1^+CD3^+$
ILCs	$CD45^+CD11b^-CD3^-B220^-CD127^+$
ILC1	$CD45^+CD11b^-CD3^-B220^-CD127^+Tbet^+$
ILC2	$CD45^+CD11b^-CD3^-B220^-CD127^+GATA3^+$
ILC3	$CD45^+CD11b^-CD3^-B220^-CD127^+RORγt^+$
T cells	$CD45^+CD11b^-CD3^+$
Th cells	$CD45^+CD11b^-CD3^+CD4^+CD8a^-$
Tc cells	$CD45^+CD11b^-CD3^+CD4^-CD8a^+$
γδT cells	$CD45^+CD11b^-CD3^+TCRγδ^+$
Th1 cells	$CD45^+CD11b^-CD3^+CD4^+CD8a^-Tbet^+$
Th2 cells	$CD45^+CD11b^-CD3^+CD4^+CD8a^-GATA3^+$
Th17 cells	$CD45^+CD11b^-CD3^+CD4^+CD8a^-RORγt^+$
Treg cells	$CD45^+CD11b^-CD3^+CD4^+CD8a^-Foxp3^+$

Table 3.6. Immunophenotyping strategy followed to characterize of immune populations studied.

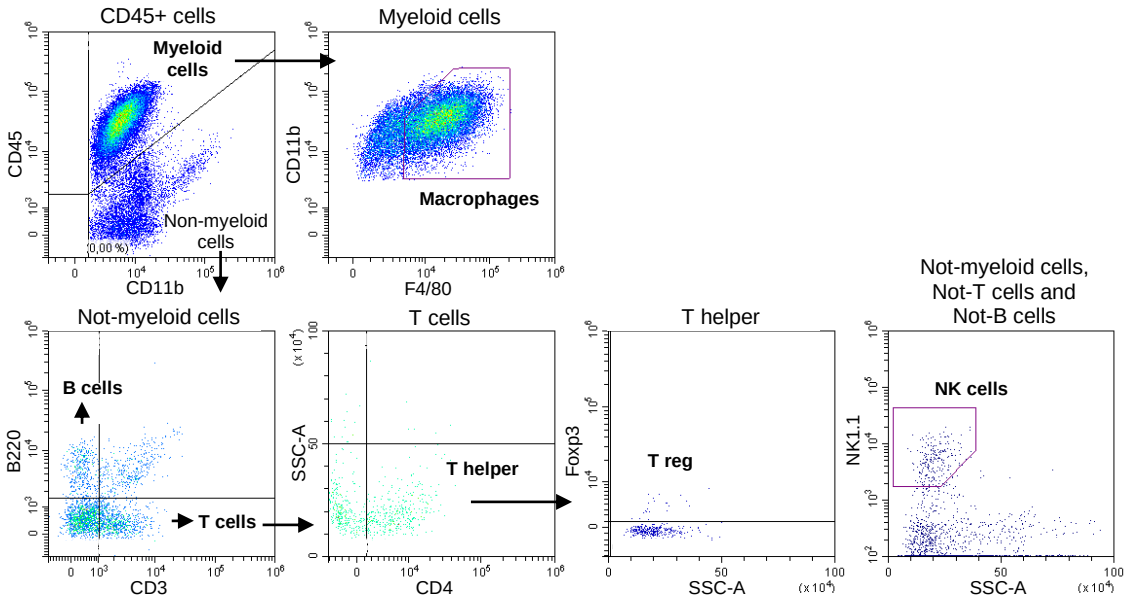

Figure 3.6. Flow cytometry gating strategy for panel 1 (main immune cell populations). Myeloid cells ($CD45^+CD11b^+$), macrophages ($CD45^+CD11b^+F4/80^+$), B cells ($CD45^+CD11b^-B220^+$), T cells ($CD45^+CD11b^-CD3^+$), T helper cells ($CD45^+CD11b^-CD3^+CD4^+$) and NK cells ($CD45^+CD11b^-NK1.1^+$).

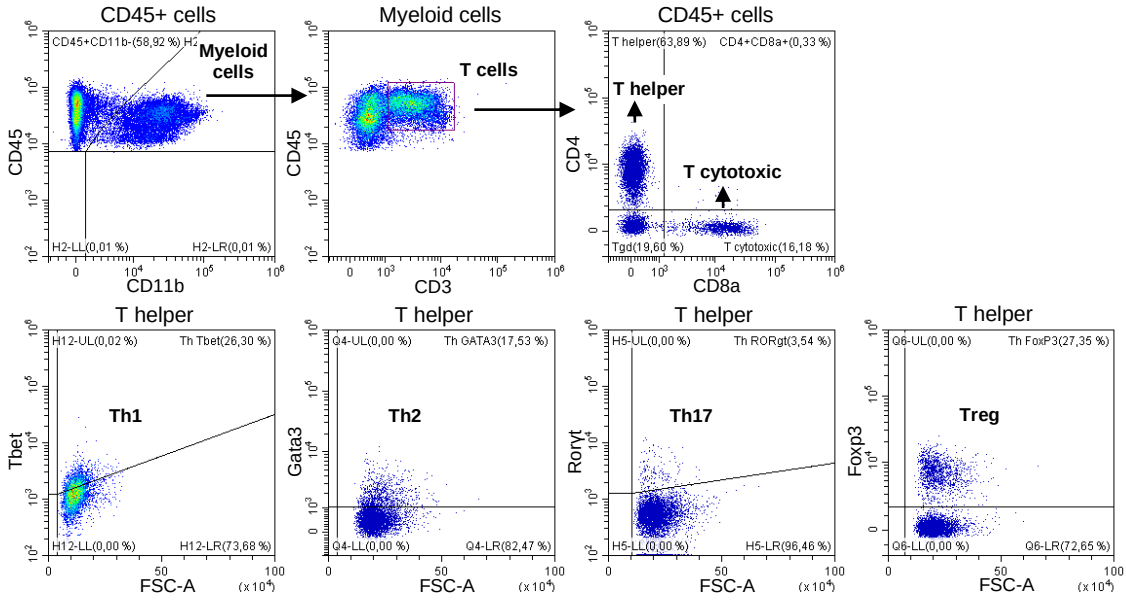

Figure 3.7. Flow cytometry gating strategy for panel 2 (T cell subsets). T cells ($CD45^+CD11b^-CD3^+$), T helper cells ($CD45^+CD11b^-CD3^+CD4^+CD8^-$), T cytotoxic cells ($CD45^+CD11b^-CD3^+CD4^-CD8a^+$), Th1 cells ($CD45^+CD11b^-CD3^+CD4^+CD8a^-Tbet^+$), Th2 cells ($CD45^+CD11b^-CD3^+CD4^+CD8a^-Gata3^+$), Th17 cells ($CD45^+CD11b^-CD3^+CD4^+CD8a^-Ror\gamma t^+$) and Treg cells ($CD45^+CD11b^-CD3^+CD4^+CD8a^-Foxp3^+$).

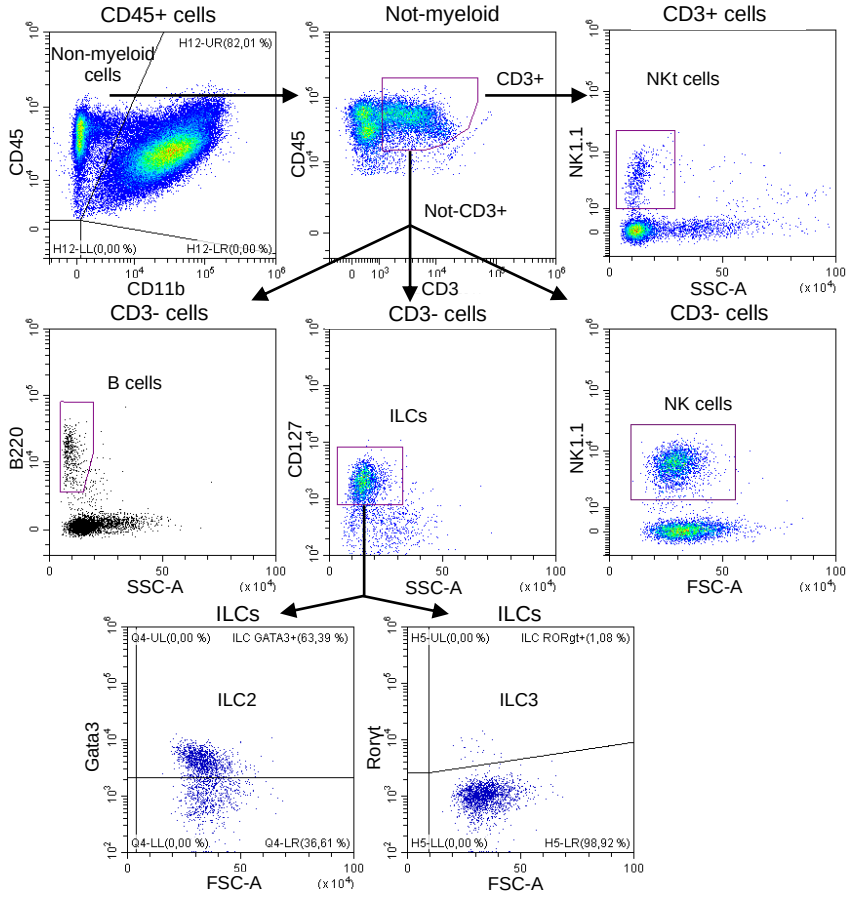

Figure 3.8. Flow cytometry gating strategy for panel 3 (ILCs and NK cells subsets). B cells ($CD45^+CD11b^-CD3^-B220^+$), ILCs ($CD45^+CD11b^-CD3^-B220^-CD127^+$), ILC2 ($CD45^+CD11b^-CD3^-B220^-CD127^+Gata3^+$), ILC3 ($CD45^+CD11b^-CD3^-B220^-CD127^+Ror\gamma t^+$), NK cells ($CD45^+CD11b^-B220^-CD3^-NK1.1^+$) and NKt cells ($CD45^+CD11b^-B220^-CD3^+NK1.1^+$).

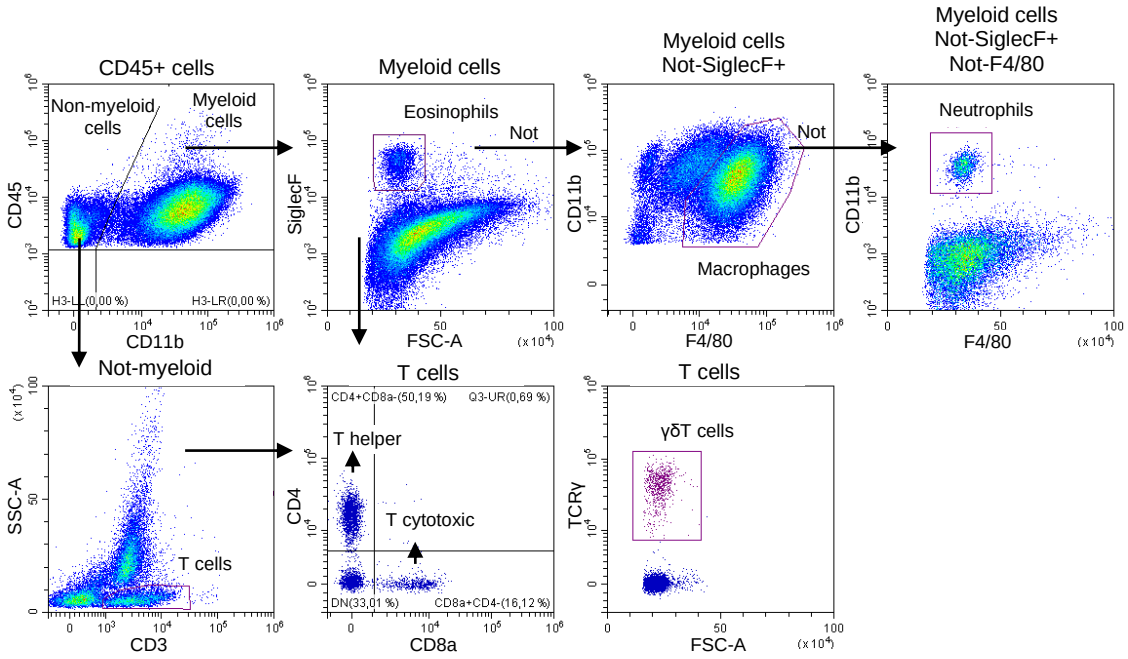

Figure 3.9. Flow cytometry gating strategy for panel 4 (myeloid cells and γδT cells). Myeloid cells ($CD45^+CD11b^+$), eosinophils ($CD45^+CD11b^+F4/80^+SiglecF^+$), macrophages ($CD45^+CD11b^+SiglecF^-F4/80^+$), neutrophils ($CD45^+CD11b^+SiglecF^-F4/80^-Ly6G^+$), T cells ($CD45^+CD11b^-CD3^+$), T helper cells ($CD45^+CD11b^-CD3^+CD4^+CD8a^-$), T cytotoxic cells ($CD45^+CD11b^-CD3^+CD4^-CD8a^+$) and γδ T cells ($CD45^+CD11b^-CD3^+TCR\gamma^+$).

► 3.7 Gene expression analysis

3.7.1 Total RNA isolation

Because RNA is easily degraded by RNases, we used RNAse-free solutions and materials to avoid RNA degradation and preserve its integrity. One of the most commonly used methods to inhibit RNases within water, buffers and other solutions is to treat them with 0.1% *Diethyl pyrocarbonate* (DEPC). DEPC irreversibly inactivates RNases by modifying -NH, -SH and -OH groups. Once treated, solutions are autoclaved to inactivate DEPC given its high toxicity and the fact that it can also react with RNA.

3.7.1.1. RNA isolation by isopropanol precipitation

To isolate RNA from cells and tissues, we used TRIzol (Invitrogen). It is a monophasic phenol and guanidine isothiocyanate solution, which is able to maintain RNA integrity because of its capacity of inhibition of RNase activity while disrupting cells and dissolving cell components during sample homogenization.

To isolate total RNA, first, 50-100 mg of frozen tissue samples were homogenized in 1 mL of TRIzol reagent using a rotor-stator homogenizer (Ultra-Turrax IKA T25). Afterwards, 200 µL of chloroform for each mL of TRIzol were added, followed by a centrifugation at 4ºC to separate the homogenate in three phases: an RNA-containing upper aqueous phase, an interphase composed by proteins and DNA, and a lower organic phase, composed by cell debris. The aqueous upper phase was transferred to a new tube and one volume of isopropanol was added to allow the precipitation of RNA. Samples were then centrifuged and the RNA pellet was washed with 75% ethanol. The RNA pellet was finally dissolved in RNase-free water and incubated 10 min at 55-60ºC with constant shacking to favor pellet dissolution. Samples were stored at -20ºC for further analysis.

3.7.1.2. RNA isolation from fatty tissues or cells Canvax Total RNA Purification Kit

Because WAT and 3T3-L1 adipocytes contain high amounts of lipids that can interfere in the subsequent analysis, total RNA from fatty tissues or cells was isolated using a silica gel column (GeneJET RNA Purification Kit, Thermofisher).

Samples from WAT and 3T3-L1 adipocytes were first harvested and homogenized in TRIzol. Samples were then centrifuged at 12000 rpm for 10 min at 4ºC in order to remove the excess of lipids, which appeared as top fatty layer. After this, 200 µL of chloroform were added to the TRIzol solution and samples were centrifuged at 4ºC to allow the separation of aqueous and organic phases, as described above. RNA contained in the aqueous upper phase was precipitated with isopropanol and then placed in RNesay columns from Canvax Total RNA Purification Kit. RNA purification was continued according to the manufacturers' instructions.

3.7.2 RNA quality control

After extraction, RNA concentration and purity were determined by spectrophotometry, in a NanoDrop ND-2000 spectrophotometer. The *Optical Density* (OD) at 260 nm determines RNA concentration in the solution, taking into account that A_{260} of 1.0 is equivalent to 40 µg/mL of RNA. To assess RNA purity, we looked at ratio of absorbance at 260 nm and 280 nm. In our study, samples with an A_{260}/A_{280} ratio ≥ 1.8 were accepted.

To assess RNA integrity, an aliquot of each sample (400ng) was run on a 1% agarose electrophoresis gel in TAE buffer. RNA was visualized by staining with ethidium bromide. If RNA's integrity is correct, three bands corresponding to the 5S rRNA, 18S rRNA and 28S rRNAs should be observed, although the band corresponding to 5S rRNA is lost when RNA extraction method is performed using silica gel columns.

3.7.3 Reverse transcription

RNA has to be reverse transcribed to *complementary DNA* (cDNA) in order to analyze mRNA expression by *real-time quantitative polymerase chain reaction* (qPCR). For this, a first mix was prepared with 400ng RNA, 500µL/mL Oligo(dT)$_{12\text{-}18}$ primers and DEPC water. Samples were heated at 65ºC for 10 min to break RNA secondary structure and then chilled at 4ºC to allow RNA annealing with Oligo(dT) primers. Then, Buffer 5X, 0.01 M DTT, 0.5 mM dNTPs mix and 50 U Super Script II RT were added and samples were incubated at 42ºC for 50 min to allow cDNA extension followed by an incubation at 70ºC for 15 min to inactivate RT.

3.7.4 Real-time quantitative PCR

qPCR was used to measure gene expression levels. In the most of cases, we used a **relative quantification method**, which measures the expression level of certain genes by comparing them with the expression of a reference gene. In this study, we used *Cyclophilin A* (*CypA*) as a reference gene, as we have previously determined that its expression is stable across the different experimental conditions used in this work.

qPCR was performed using the SYBR green fluorochrome and specific primers for each gene to be detected. Oligonucleotide primers were selected from PrimerBank database (http://pga.mgh.harvard.edu/primerbank/), or purchased predesigned primer pairs for quantifying gene expression (KiCqStart® Primers, Sigma).

To conduct qPCR, 1X SYBR green was mixed with Forward primer 0.5 µM, Reverse primer 0.5 µM, DEPC water and 2 µL of previously obtained cDNA. Each pair of primers was specific for each gene evaluated (Supplementary tamble 2). SDS 7000 detection system from Applied Biosystems was used with the conditions shown in Table 3.7. CT values were recorded and analyzed or the $2^{-\Delta\Delta CT}$ method using *CypA* as reference gene (257). A dissociation curve was produced following the real-time PCR to verify that the desired amplicon was detected, producing a single peak in the derivative plot.

On the other hand, **absolute quantification method** (258) was used when a reference gene was not available to compare expression levels of genes between different tissues. For that, a standard curve was done using the plasmid pcDNA3.1(-)mRorc, an expression vector that contains the coding sequence for *Rorc*. Standard curve dilutions were between 10^5 and 10^{11} molecules of pcDNA3.1(-)mRorc.

To obtain pcDNA3.1(-)mRorc vector, we first amplified *Rorc* cDNA from mouse gastrocnemius sample through RT-PCR using primers 5'-GATAGGCGGCCGCTAATGGACAGGGCCCCACAG-3' (forward) and 5'-GTATGAATTCTCACTTTGACAGCCCCTC-3' (reverse). The resulting fragment was inserted using ligase T4 into the NotI and EcoRI sites of the pCDNA3.1(-) vector. The ligation product was transformed in competent *E.coli* Dam+ cells, positive clones were selected and they were finally sequenced.

Step	Temperature	Time	Cycles
Initial activation	50ºC	2 min	1
DNA polymerase activation	95ºC	10 min	1
Denaturation	95ºC	20 sec	40
Annealing	60ºC	20 sec	
Extension	72ºC	34 sec	
Dissociation curve	95ºC	15 sec	1
	60ºC	1 min	
	ΔTº	+0.2º/second	
	95ºC	15 sec	
Cooling	4ºC	∞	1

Table 3.7. Thermal cycle conditions to determine gene expression by qPCR.

3.7.5 Gene expression profiling and bioinformatics analysis

For the identification of RORγ1 target genes, two different DNA microarray analyses were done. First, we compared the gene expression profile of control 3T3-L1 mature adipocytes (siControl) with that of 3T3-L1 adipocytes in which *Rorc*, *Rora* or both simultaneously had been knocked down by the use of specific siRNAs (siRORc, siRORa and siRORa/c, respectively). Second, we compared mRNA expression levels of inguinal WAT from Wt and RORγ-FAT-KO mice fed with a high fat diet either AL or subjected to CR.

For all experiments, we used *Mouse Clariom S Array (Affymetrix)*. Images from the array were processed with *Microarray Analysis Suite 5.0 software* and data obtained was analyzed using *Bioconductor* software (*http://www.bioconductor.org/*) to generate a list of genes differentially expressed in WAT of AL and CR RORγ-FAT-KO mice. Data analysis was performed by Unit of High Technology from Vall d'Hebron Research Institute (UAT). Raw expression values obtained

were preprocessed using the RMA method (259), which integrates background correction, normalization and summarization of probe values. Additionally, before performing any analysis, data was filtered and low signal genes and low variability genes were removed.

The analysis to select differentially expressed genes was based on adjusting a linear model with empirical Bayes moderation of the variance, which consists in a technique similar to *analysis of the variance* (ANOVA) specifically developed for microarray data analysis. To select differential expressed genes we considered a $P \leq 0.05$ in all the analysis performed. LogFC was also considered, but the criteria varies depending on the experiment and it is specified in each one. For each comparison, a list of genes sorted from most to least differentially expressed was produced, which is generically called “top table”.

Finally, a gene enrichment analysis was performed to identify the main biologic processes and gene networks regulated (both positively and negatively) by RORγ1. Two different analyses were performed in parallel, using the *Database for Annotation, Visualization and Integrated Discovery* (DAVID) Bioinformatics Database functional annotation tool (*https://david.ncifcrf.gov/tools.jsp*) (260), considering a $P \leq 0.05$, and the *Gene Set Enrichment Analysis* (GSEA) method (*https://www.gsea-msigdb.org/gsea/index.jsp*) (261), using a False Discovery Rate (FDR)<0.05.

► 3.8 Protein analysis by Western Blot

3.8.1 Total protein extraction and quantification

Protein extracts were obtained by homogenizing 50-150 mg of frozen tissue using a rotor-stator homogenizer (Ultra-Turrax IKA T25) in RIPA buffer (50mM Tris-HCl pH 8, 150mM NaCl, 1% Triton x-100, 0.5% sodium deoxycholate and 0.1% SDS, 10mM sodium glycerophosphate, 1mM sodium pyrophosphate, 1mM sodium orthovanadate, 1mM phenylmethanesulfonyl fluoride and commercial protease inhibitors (SIGMA). After homogenization, samples were centrifuged at 4ºC, 12000rpm for 30 min to remove non-soluble debris. After centrifugation, the supernatant containing solubilized proteins was transferred to a new tube.

Protein concentration was determined following *Bicinchoninic Acid* (BCA) Protein Assay Reagent (Pierce) instructions and using Spectra-max 340 plate reader. Once quantified, samples were stored at -20ºC.

3.8.2 SDS-polyacrylamide gel electrophoresis and Western Blot

Sodium dodecyl sulfate-polyacrylamide gel electrophoresis (SDS-PAGE) was used to separate complex mixtures of proteins depending on their size. Before running the gel electrophoresis, protein samples were mixed with 5X Laemmli’s loading buffer (312.5 mM Tris-HCl pH 6.8, 10% SDS, 50% Glycerol, 25% β-Mercaptoethanol, 0.04% Bromophenol Blue) and denatured by heating the samples at 95ºC for 10 min.

Two sequential gels are used in this system. The first one, the stacking gel (5% acrylamide mix, 125 mM Tris-HCl pH 6.8, 0.1% SDS, 0.1% Ammonium Persulfate, 6.6 mM TEMED), is slightly acidic and has a low acrylamide concentration allowing the proteins to concentrate in a sharply defined band at the beginning of resolving gel. The lower gel, or resolving gel (7-15% acrylamide mix, 375 mM Tris-Base pH 8.8, 0.1% SDS, 0.1% Ammonium Persulfate, 2.2 mM TEMED), is more basic and has a higher polyacrylamide content, which causes the gel to have narrower pores and allow protein separation based on their molecular weight.

Samples were run in a running buffer (25 mM Tris-Base, 192 mM Glycine, 0.1% SDS, pH=8,3). Once the samples were separated by SDS-PAGE, they were transferred electrophoretically using a transfer buffer (25 mM Tris-Base, 192 mM Glycine, 20 % methanol) to the surface of *a polyvinyl difluoride* (PVDF) membrane to become accessible for immunodetection. After transference, non-specific sites on the PVDF membranes were blocked by incubation for 1 hour or more in a solution of 5% skimmed milk in TBS-Tween (20 mM Tris–Base pH 7.4, 150 mM NaCl and 0.1% Tween 20), depending on the recommendations of each antibody datasheet. Afterwards, the primary antibody was applied to the blot and incubated with shacking in TBS-Tween + 5% skim milk or TBS-Tween + 5% BSA, depending on the antibody and the recommendations from the manufacturer. The antibodies and the dilutions are specified in Supplementary table 3. After washing the membranes in TBS-Tween, the membranes were incubated with the appropriate horseradish peroxidase (HRP)-conjugated secondary antibody in TBS-Tween + 5% skim milk.

Immunodetection of proteins was performed with the Enhanced chemiluminescence system. Western blot bands were quantified with ImageJ (NIH) software. Detection of vinculin or CypA proteins were used as a loading control.

3.8.3 Stripping of PVDF membranes

For stripping, PVDF membranes were incubated in a denaturizing buffer (62.5 mM Tris-HCl pH 6.8, 2% SDS, 0.075% β-mercaptoethanol) for 30 min at 50ºC with soft shaking. After the incubation, membranes were washed (4 x 15 min) in TBS-Tween and prepared for blocking and re-probing.

► 3.9 Statistical analysis

All results are expressed in figures and tables as mean ± SEM. When appropriate, unpaired *Student's t test* or ANOVA followed by post hoc analysis using Tukey's multiple comparison test were used to assess the significance of differences between experimental groups. Statistical analysis was performed using GraphPad Prism 7 software. Differences were considered significant when $P \leq 0.05$.

RESULTS

► 4.1 Effects of *Rora* and *Rorc* knockdown in cultured 3T3-L1 adipocytes

To unravel the function of RORγ1 in WAT, we first attempted to identify its target genes in cultured white adipocytes. For this, we set up an *in vitro* model to acutely knockdown *Rorc* in cultured 3T3-L1 white adipocytes, followed by the use of DNA microarrays to study the expression profile of adipocytes in which *Rorc* had been knocked down. As *Rora* is also expressed in mature 3T3-L1 adipocytes, *Rora* was also knocked down in order to discard any potential compensatory effects by this ROR isoform.

4.1.1 Optimization of the conditions for siRNA transfection and efficient gene expression knockdown in 3T3-L1 adipocytes

Fully differentiated 3T3-L1 adipocytes are among the most difficult cell types to transfect efficiently. The siRNA transfection protocol in the 3T3-L1 cell line is based on the use of a cationic lipid-based reagent called DharmaFECT 4 (Dharmacon, Thermofisher Scientific). The method consists in introducing siRNA into differentiated 3T3-L1 adipocytes using an approach based on forming the siRNA/DharmaFECT complex with the adipocytes in suspension rather than the classical transfection protocol in which cells are attached to the culture dish. This variation in the classic transfection protocol is based on a study by Kilroy *et al.* (256), who demonstrated a high efficiency of gene silencing using siRNAs in 3T3-L1 cells when transfection is performed in suspension, but not when cells are attached to the dish surface.

Still, some optimization of the transfection protocol was required. Firstly, with the purpose of improving the gene-silencing efficiency and siRNA uptake into the cells, differentiated 3T3-L1 adipocytes were transfected in suspension with three different concentrations of siGLO (25 nM, 50nM and 100 nM), a fluorescent oligonucleotide duplex that allows visual assessment of siRNA uptake into the cells. The maximal transfection efficiency was achieved using a siGLO concentration of 100 nM (Figure 4.1). However, we observed that 90% of cells were transfected by using a 50nM concentration. Thus, taking into account the relation between transfection efficiency and the amount of siRNA used, we considered 50nM as the optimal concentration.

Then, we verified that gene knockdown was efficiently achieved when fully differentiated 3T3-L1 adipocytes were transfected in suspension using a siRNA targeting *Rorc* (siRorc) with a concentration of 50 nM and compared it with the effects of siRNA transfection on attached cells. As seen in Figure 4.2, transfection in suspension resulted in a notable decrease of *Rorc* mRNA levels as compared to the negative control, while *Rora* mRNA levels were not changed. Contrarily, no significant silencing of the *Rorc* gene expression was achieved when attached cells were transfected with siRNAs.

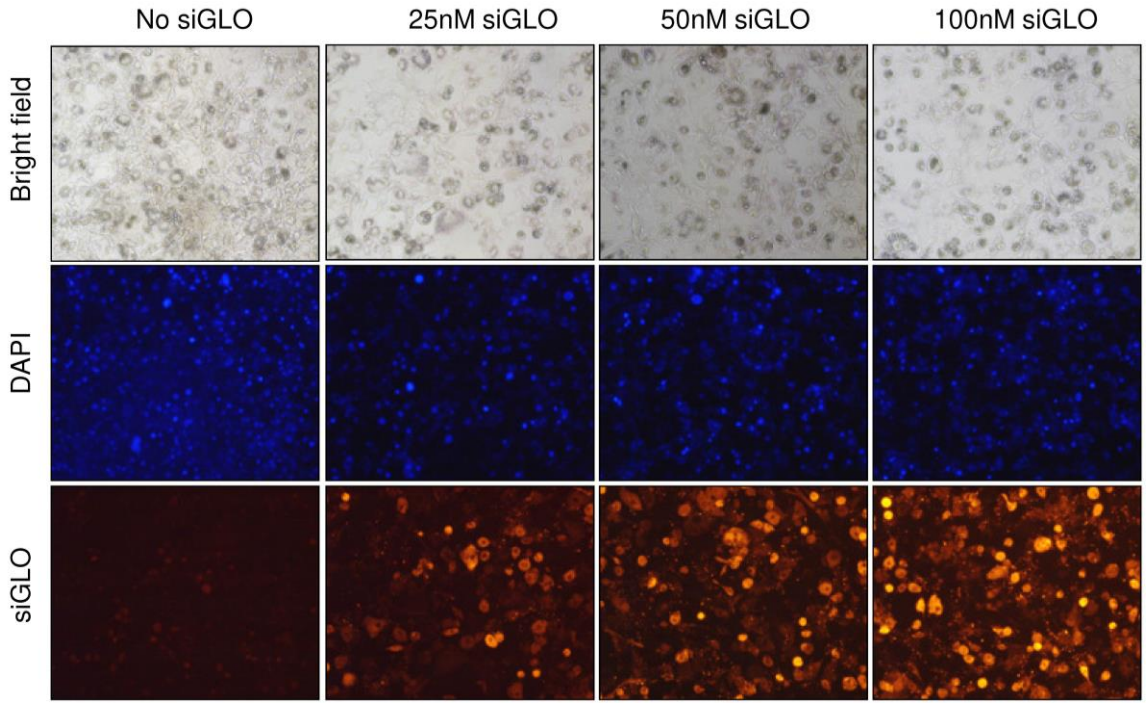

Figure 4.1. Assessment of optimal transfection conditions of 3T3-L1 adipocytes with siRNAs. Uptake of the fluorescent-labelled siGLO (red) was assayed 36h post transfection of 3T3-L1 adipocytes. Bright field and fluorescent images of adipocytes transfected with 1.4 µL/cm^2 of DharmaFECT 4 in combination with three concentrations of siGLO (25 nM, 50 nM and 100 nM) are shown. Nuclei were stained with DAPI.

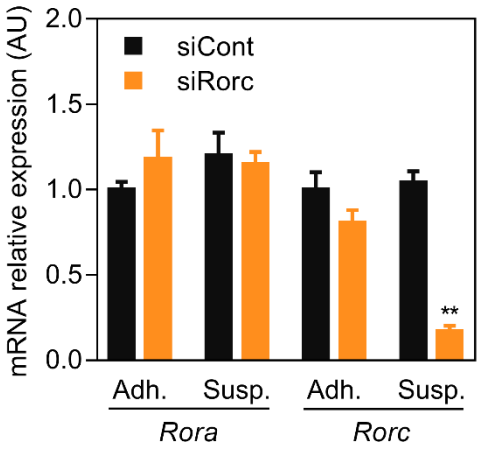

Figure 4.2. Evaluation of gene knockdown efficiency in 3T3-L1 cells transfected in suspension or adhered to the plate. 50 nM of non-targeting siRNA (siCont), 50 nM of siRNA targeted to *Rorc* (siRorc) and 1.4 µL/cm^2 of DharmaFECT 4 transfection reagent were used. Expression of *Rora* and *Rorc* genes was assayed by qPCR in triplicate. Adh., adherent; Susp., suspension. Results are expressed as mean ± SEM (n=3). ** $P \leq 0.01$.

4.1.2 Identification of target genes of RORγ and RORα in 3T3-L1 adipocytes

Once the conditions to transfect 3T3-L1 adipocytes were optimized, we proceeded to silence *Rorc in vitro* (siRorc). In order to discard any potential compensatory effects with other members of ROR family highly expressed in adipocytes (i. e. RORα), we performed parallel siRNA transfections to knockdown *Rora* or simultaneously *Rora* and *Rorc* in 3T3-L1 mature adipocytes (siRora and siRORa/c, respectively).

First, we verified the mRNA expression levels of *Rora* and *Rorc* genes in siRNA-treated 3T3-L1 adipocytes by qPCR (Figure 4.3). Gene targeting was achieved efficiently, obtaining a reduction of 77-93% in the expression of each of targeted genes.

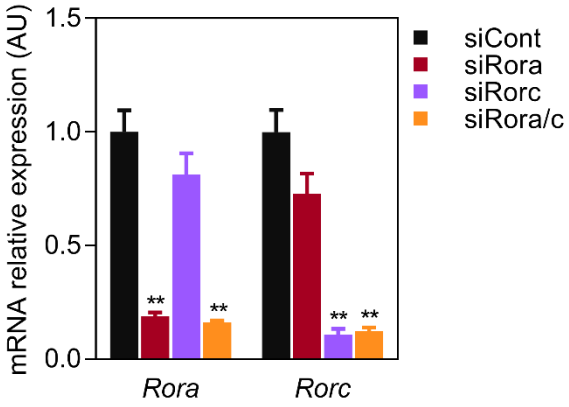

Figure 4.3. Assessment of efficient *Rora* and *Rorc* gene knockdown in 3T3-L1 cells transfected with siRNAs targeting *Rora*, *Rorc* or both simultaneously. mRNA levels of *Rora* and *Rorc* were assayed by qPCR in mature adipocytes in which the expression of *Rora*, *Rorc* or both was knocked down by the use of specific siRNAs (siRora, siRorc and siRora/c, respectively). Results are expressed as mean ± SEM of 3 experiments with triplicates. *Indicates statistical significance of the comparison between control adipocytes (siCont) and adipocytes in which any of the RORs has been knocked down. ***P*≤0.01.

Next, by using DNA microarrays, we compared the gene expression profile of mature control 3T3-L1 adipocytes (siCont) with 3T3-L1 adipocytes in which the expression of *Rora*, *Rorc* and both simultaneously had been acutely knocked down. After filtrating for non-annotated and redundant genes, we obtained 517 genes differentially regulated (*P*≤0.05) in siRorc 3T3-L1 adipocytes compared to control (Figure 4.4), of which 228 were up-regulated and 289 down-regulated. The first 50 genes up-regulated and the 50 first down-regulated genes are listed in Supplementary table 4.

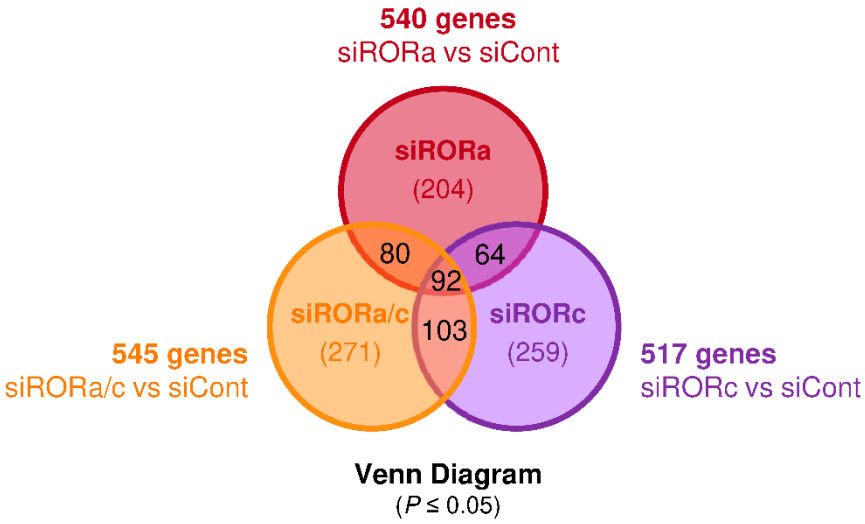

Figure 4.4. Venn diagram of genes dysregulated in 3T3-L1 adipocytes in which expression of *Rora* (red), *Rorc* (purple) and both genes (orange) was silenced. Non-annotated and redundant genes were filtrated. 517 genes were dysregulated in 3T3-L1 adipocytes knockdown by *Rorc* (siRorc), 540 genes were dysregulated in 3T3-L1 adipocytes knockdown by *Rora* (siRora) and 545 genes were dysregulated in 3T3-L1 adipocytes knockdown by *Rora* and *Rorc* (siRora/c) (*P*≤0.05). The number of common and uncommon genes differentially expressed in each condition are represented in the Venn diagram.

To gain insight into the biological function of RORγ1, we performed a gene enrichment analysis using the GSEA method. Using as a selection criteria a FDR <25%, we found no gene sets significantly enriched among the genes up-regulated in siRorc-treated 3T3-L1 adipocytes. Conversely, 7 gene sets were significantly enriched at FDR <25% in down-regulated genes.

We found that some of the genes down-regulated in adipocytes in which *Rorc* had been knocked down were related to the immune system and lipid metabolism. In particular, down-regulated genes

appeared enriched in genes related to type I IFN signaling and response to viral infections (Figure 4.5). These included some pro-inflammatory cytokines, such as *Tnfa*, *Il1b* and *Il6*, and interferon target genes, like *2'-5'-oligoadenylate synthetase 1* (*Oas1*), *2'-5'-oligoadenylate synthetase 2* (*Oas2*), *interferon regulatory factor 7* (*Irf7*) and *interferon-regulated resistance GTP-Binding Protein MxA* (*Mx1*), among others. Curiously, most of the genes included in the lipid metabolism gene set were not involved in conventional lipid metabolism related to fatty acid synthesis and accumulation, but were genes that encode for proteins with a relevant function in the immune system, such as *phospholipase A2* (*Pla2g2*), *anoctamin 6* (*Ano6*), *apolipoprotein L6* (*Apol6*) and *apolipoprotein 9b* (*Apol9b*). The last two genes mentioned are IFN-stimulated genes whose function is to promote the efflux of cholesterol from cells. On the other hand, *Pla2g2* may regulate the inflammatory response by releasing a precursor of prostaglandins and leukotrienes. Additionally, genes implicated in metabolism and biosynthesis of cholesterol were also found among the dysregulated genes, such as *squalene epoxidase* (*Sqle*), *cholesterol 24-hydroxylase* (*Cyp46*), *3-hydroxy-3-methylglutaryl-CoA reductase* (*Hmgcr*) and *solute carrier family 27 member 1* (*Slc27a1*). *Glycerol-3-Phosphate Acyltransferase 3* (*Gpat3*), which catalyses the conversion of glycerol-3-phosphate to lysophosphatidic acid in the synthesis of triacylglycerol, was also down-regulated in *Rorc* knockdown 3T3-L1 adipocytes.

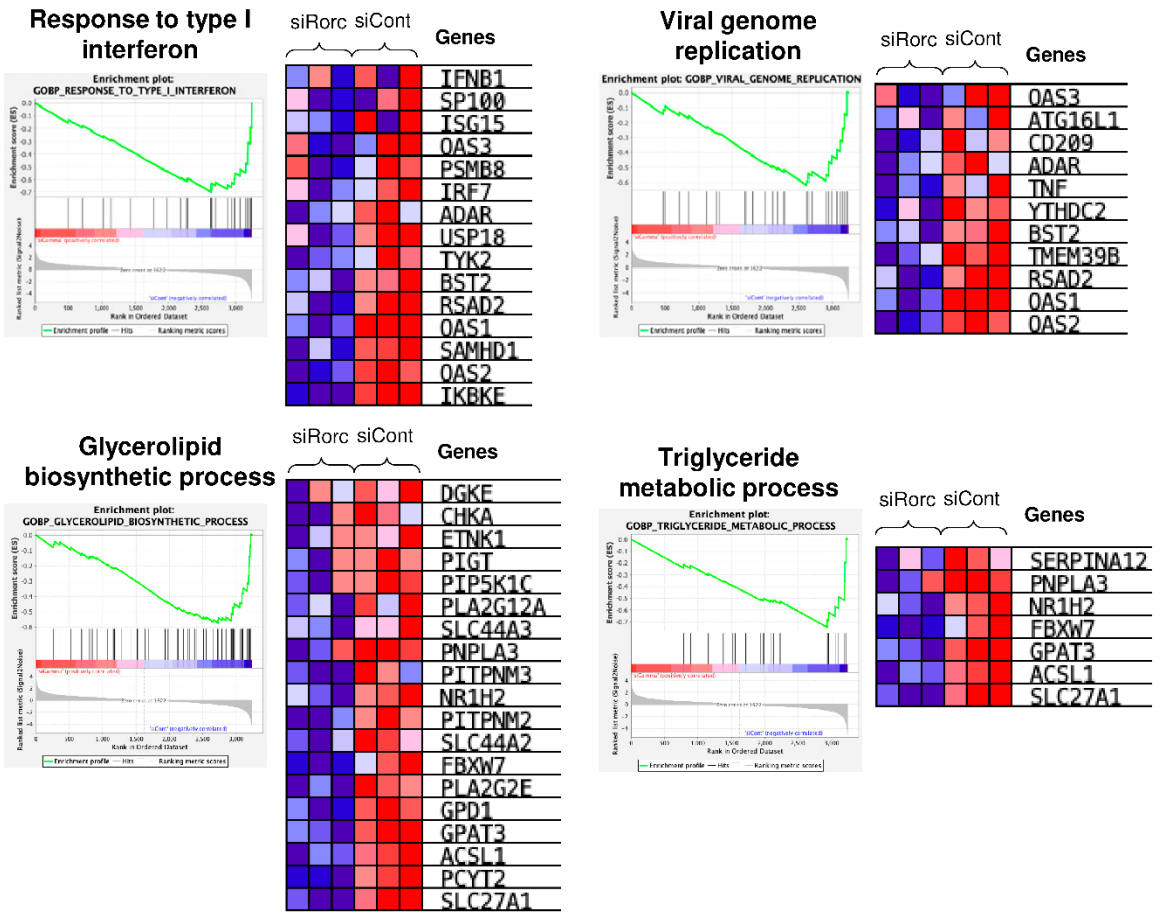

Figure 4.5. Gene-set enrichment analysis of dysregulated genes in *Rorc* knocked down 3T3-L1 adipocytes (siRorc) identified GO categories related to type I IFN and lipid homeostasis. The analysis was conducted using GSEA method. Statistical significant ($P \leq 0.05$ and FDR <25%) gene sets that provided relevant functional information. Next to the gene sets, heatmaps of statistically significant of differentially expressed genes with a positive core enrichment are shown.

We also analyzed the genes that were up-regulated and down-regulated ($P \leq 0.05$) using DAVID Bioinformatics Database functional annotation tool, which is less astringent than GSEA. Similar to the GSEA analysis, we found that up-regulated genes were grouped in a small number of GO functional categories, such as response to hypoxia, cellular response to necrosis factor and placenta development, although the number of the genes contained in these categories was very low (Supplementary table 5). On the other hand, similar to our findings using the GSEA method, down-regulated genes in adipocytes in which *Rorc* was knocked down were enriched in genes related with lipid metabolism and immune response to virus.

The analysis of the effects of knocking down *Rora* in mature adipocytes revealed the differential expression of 540 genes (Supplementary table 6), 156 of which were in common with those dysregulated in siRorc adipocytes (Figure 4.4). Similar to adipocytes in which *Rorc* was knocked down, GSEA method (Figure 4.6) and DAVID Bioinformatics tool (Supplementary table 7) revealed that the genes dysregulated in 3T3-L1 adipocytes by siRora were related to the immune system and lipid metabolism.

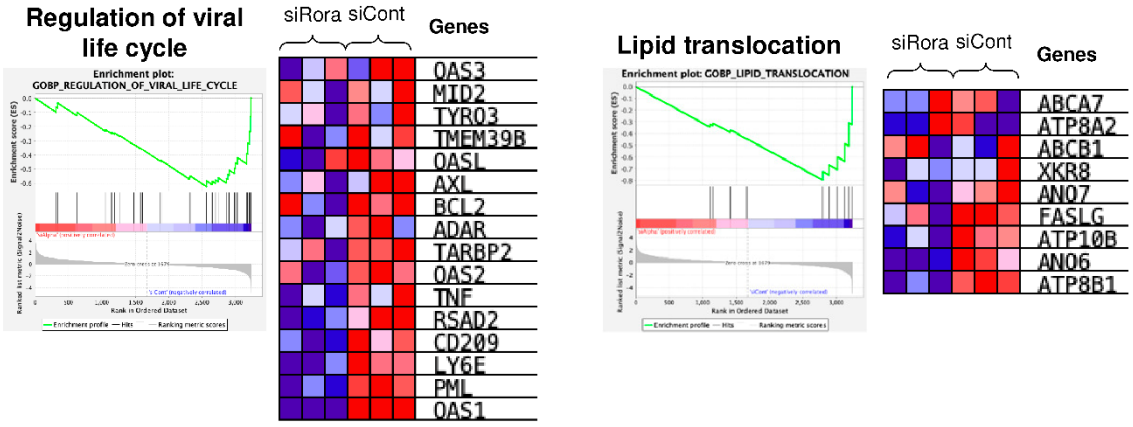

Figure 4.6. Gene-set enrichment analysis of dysregulated genes in *Rora* knocked down 3T3-L1 adipocytes (siRora). The analysis was conducted using GSEA method. Statistical significant ($P \leq 0.05$ and FDR <25%) gene sets that provided relevant functional information. Next to the gene sets, heatmaps of statistically significant of differentially expressed genes with a positive core enrichment are shown.

Additionally, 3T3-L1 adipocytes which had both *Rora* and *Rorc* silenced presented 545 dysregulated genes compared to control adipocytes, 195 of which were in common with siRorc adipocytes (Figure 4.4). The first 50 genes up-regulated and down-regulated in 3T3-L1 adipocytes treated with siRNAa/c are listed in Supplementary table 8. Interestingly, a significant number of dysregulated genes were in common between the genes differentially expressed in siRorc and those in siRora/c adipocytes. Gene enrichment analysis using GSEA method (Figure 4.7) and DAVID Bioinformatics Database functional tool (Supplementary table 9) showed that, similar to what we had previously described for siRora and siRorc, simultaneous knockdown of siRora/c led to a decrease in genes related to response to virus and to type I IFN signaling. This could be interpreted as a certain degree of functional redundancy between *Rora* and *Rorc*.

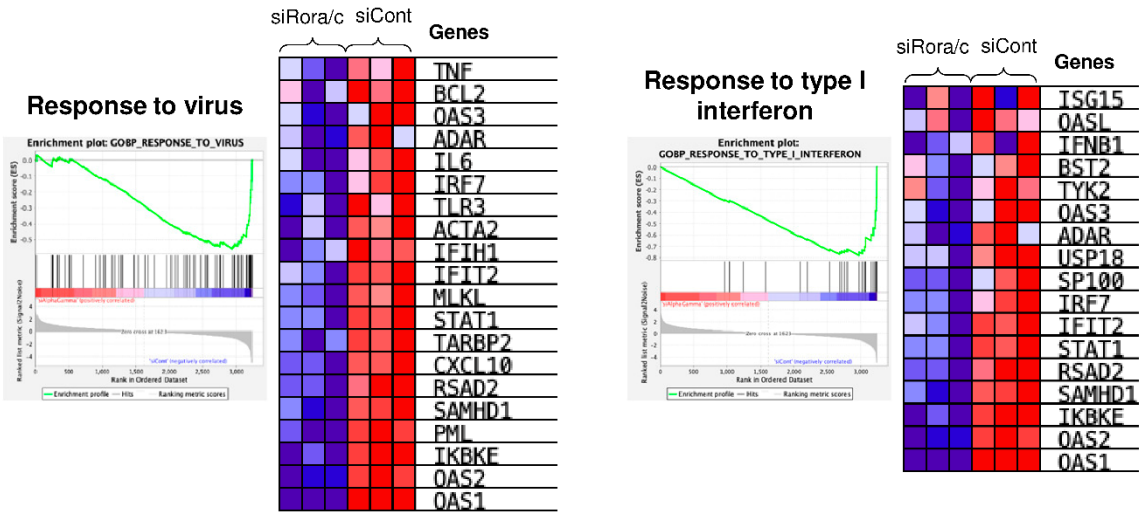

Figure 4.7. Gene-set enrichment analysis of dysregulated genes in simultaneously *Rora and Rorc* knocked down 3T3-L1 adipocytes (siRora/c). The analysis was conducted using GSEA method. Statistical significant (*P*≤0.05 and FDR <25%) gene sets that provided relevant functional information. Next to the gene sets, heatmaps of statistically significant of differentially expressed genes with a positive core enrichment are shown.

In summary, altogether, these results suggest that RORγ, but also RORα, could be regulating genes involved in the immune response modulation, more specifically in the response to pathogens mediated by *interferon beta* (IFN-β).

4.1.3 Quantification of the expression of RORγ target genes in 3T3-L1 adipocytes

Changes in the expression of genes identified as RORγ target genes in the gene expression profile study using DNA microarrays were independently validated by qPCR. Consistent with the results obtained in the microarray study, we found a mild reduction in mRNA levels of IFN response genes (i. e. *Oas2*, *Irf7* and *Mx1*), both in adipocytes in which *Rorc* was silenced, as well as those in which *Rora* was knocked down, although results did not always reached statistical significance (Figure 4.8). In the most cases, this effect was potentiated in double *Rora*/*Rorc*-knockdown 3T3-L1 adipocytes. On the other hand, we did not observe a statistically significant reduction of the expression of genes related to lipid metabolism when *Rorc* was knockdown, although some genes presented a significant reduction in siRora/c-treated adipocytes (Figure 4.9).

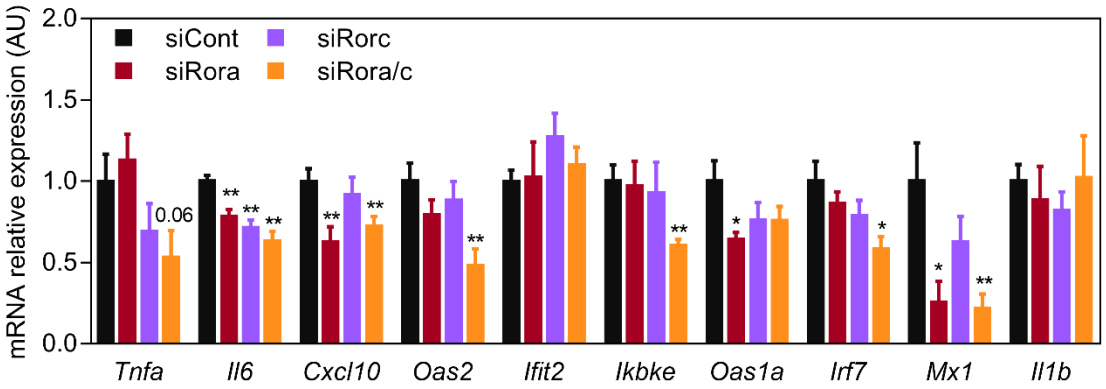

Figure 4.8. Gene expression analysis of genes related to IFN response in 3T3-L1 cells transfected with siRNAs targeting *Rora*, *Rorc* or both (siRora, siRorc or siRora/c, respectively) and control siRNA (siCont). mRNA levels were assayed by qPCR. Results are expressed as mean ± SEM of 3 experiments with triplicates. The complete name of genes is shown in the abbreviation section. * Indicates statistical significance of the comparison between control adipocytes and adipocytes in which any of the RORs have been knocked down. * *P*≤0.05; **P*≤0.01.

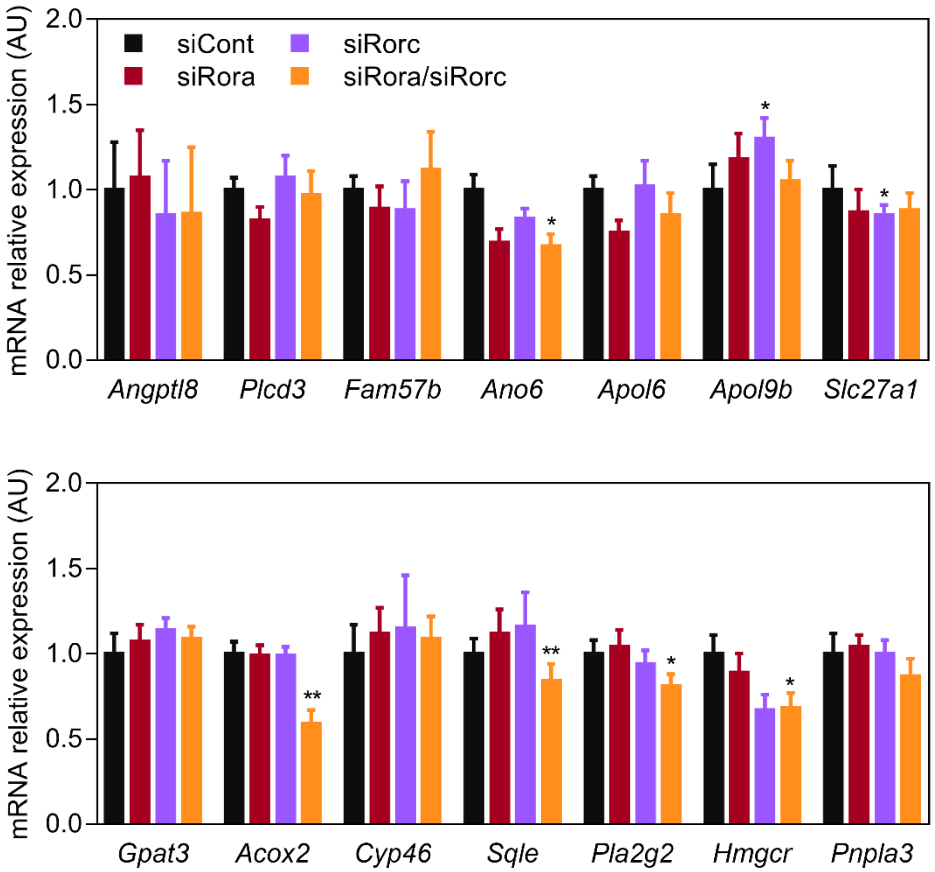

Figure 4.9. Gene expression analysis of genes related to lipid metabolism in 3T3-L1 cells transfected with siRNAs targeting *Rora*, *Rorc* or both (siRora, siRorc or siRora/c, respectively) and control siRNA (siCont). mRNA levels were assayed by qPCR. Results are expressed as mean ± SEM of 3 experiments with triplicates. The complete name of genes is shown in the abbreviation section. * Indicates statistical significance of the comparison between control adipocytes and adipocytes in which any of the RORs have been knocked down. * $P \leq 0.05$; *$P \leq 0.01$.

4.1.4 Assessing the role of RORγ as a mediator of IFN-β response in cultured adipocytes

Gene expression profiling studies *in vitro* using 3T3-L1 cells knocked down for *Rorc* gene showed that RORγ1 function is related to the control of the immune function, in particular to the response to IFN-β, which has immunomodulatory effects (262,263). Therefore, we aimed to study the potential role of RORγ1 as a mediator of the IFN-β response in adipocytes.

4.1.4.1 Optimization of IFN-β response in cultured 3T3-L1 adipocytes

We first optimized the dose of IFN-β that induces strong gene expression response without cellular toxicity. For this, we treated fully differentiated 3T3-L1 adipocytes with increasing doses of IFN-β, ranging from 0 to 100 U/mL, and determined the expression of genes that are well recognized to respond to IFN-β (i.e. *Irf7* and *Oas2*). We found that the expression of both *Irf7* and *Oas2* nicely increased in a dose-dependent manner, exhibiting the higher response to IFN-β at a dose of 100UI/mL (Figure 4.10). However, gene expression induction was higher than 100-fold for *Oas2* and 10-fold for *Irf7* at 30UI/mL, good enough to study gene expression and to avoid any potential cell toxicity due to excessive IFN-β.

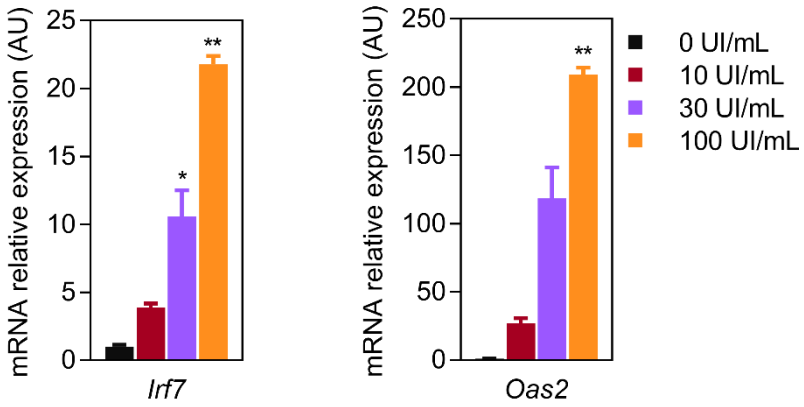

Figure 4.10. Expression levels of INF-β response genes in fully differentiated 3T3-L1 adipocytes. 3T3-L1 adipocytes were treated with increasing doses of IFN-β and harvested 24h later. Expression of IFN-β response genes was determined by qPCR. Results are expressed as mean ± SEM (n=6/condition). * Indicates statistical significance in the comparison between doses of IFN-β compared to untreated cells; * *P*≤0.05, ** *P*≤0.01.

4.1.4.2 Effects of RORγ silencing on the IFN-β response in 3T3-L1 adipocytes

To study the role of RORγ1 as a mediator of the IFN-β response, we first silenced *Rorc* in 3T3-L1 cells and, 36h after silencing *Rorc*, cells were treated with IFN-β or vehicle (PBS/BSA) for additional 24h. Then, the effects on the expression of *Rorc* target genes identified in the DNA microarray were evaluated.

Rorc silencing by specific siRNAs was highly effective and the treatment with IFN-β did not alter *Rorc* mRNA levels (Figure 4.11A). Although IFN-β target genes (*Irf7* and *Oas2*) increased their mRNA expression upon IFN-β treatment, their expression only increased approximately 2-fold in cells that had been transfected with siRNAs, but in any case the induction was not affected by the silencing of *Rorc* (Figure 4.11B). The induction of IFN-β target genes observed was very low compared with the response observed during the experimental setup to optimize the dose of IFN-β (Figure 4.10), where the induction observed ranged between 10- and 100-fold.

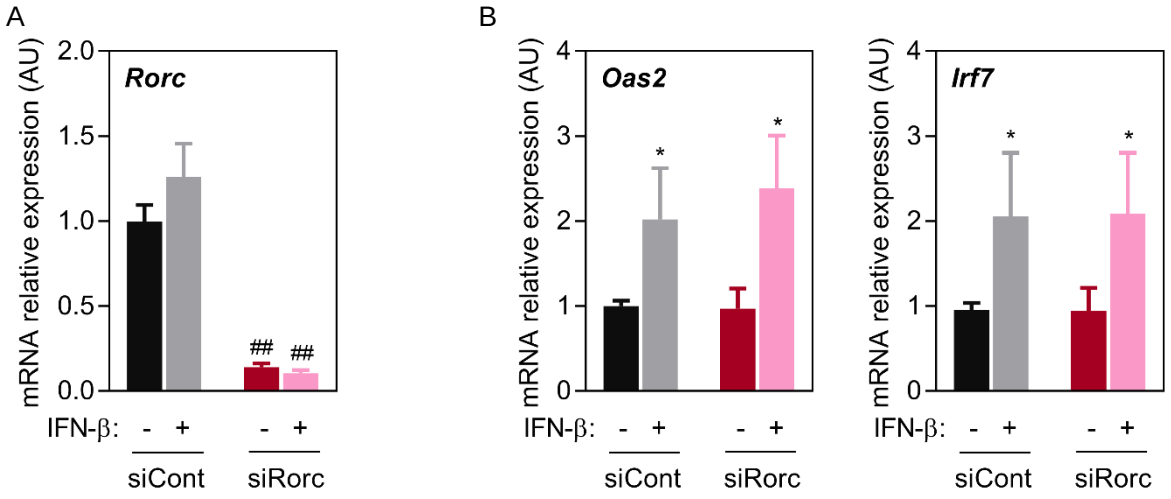

Figure 4.11. Expression levels of *Rorc* and IFN-β response genes in response to *Rorc* knockdown and IFN-β. Fully differentiated 3T3-L1 adipocytes were transfected with 50nM of non-targeting siRNA (siCont) or 50 nM of siRNA targeted to *Rorc* (siRorc). After transfection, they were treated with 30UI/mL IFN-β for 24h. *Rorc* levels of expression (A) and IFN-β response genes (B) were determined by qPCR. Results are expressed as mean ± SEM (n=6/condition). * Indicates statistical significance in the comparison between the presence or not of IFN-β; * *P*≤0.05, ** *P*≤0.01. # Indicates statistical significance in the comparison between siRorc and siControl; # *P*≤0.05, ## *P*≤0.01.

4.1.4.3 Assessment of the effects of siRNA transfection on the response to IFN-β in adipocytes

In order to discover which part of the process of siRNA transfection was negatively affecting the positive response to IFN-β, we performed an experiment using different controls of the key steps of the silencing protocol used.

To control whether detaching the cells in order to transfect them in suspension could hamper the response to IFN-β, we treated cells that were grown and differentiated in plates but never detached (control). Cells that were detached from the plate and then re-seeded onto collagen-treated plates (suspension), but not transfected with siRNAs, were also used as control. Finally, we also transfected cells with siRNAs using the protocol of transfection in suspension previously standardized in the laboratory (siControl and siRorc).

Compared to PBS/BSA-treated cells, IFN-β target genes (*Irf7* and *Oas2*) increased their expression in response to IFN-β by less than 3-fold when cells were transfected with siRNAs, either siControl or siRorc. Contrarily, 3T3-L1 cells that have not been transfected with siRNAs normally responded to IFN-β by strongly inducing the expression of *Irf7* and *Oas2*, independently of whether they were detached and re-seeded before treatment or not (Figure 4.12). Interestingly, cells treated with siRNAs (siControl and siRorc) showed a very high basal expression of IFN-β target genes compared to non-transfected cells in absence of IFN-β. This suggests that cells being transfected with siRNAs exhibit a strong IFNβ-like response, even in the absence of exogenous IFN-β. The poor specific response to IFN-β of cells treated with siRNAs precluded the use of this experimental model to properly assess the role of RORγ1 as a mediator of IFN-β in adipocytes.

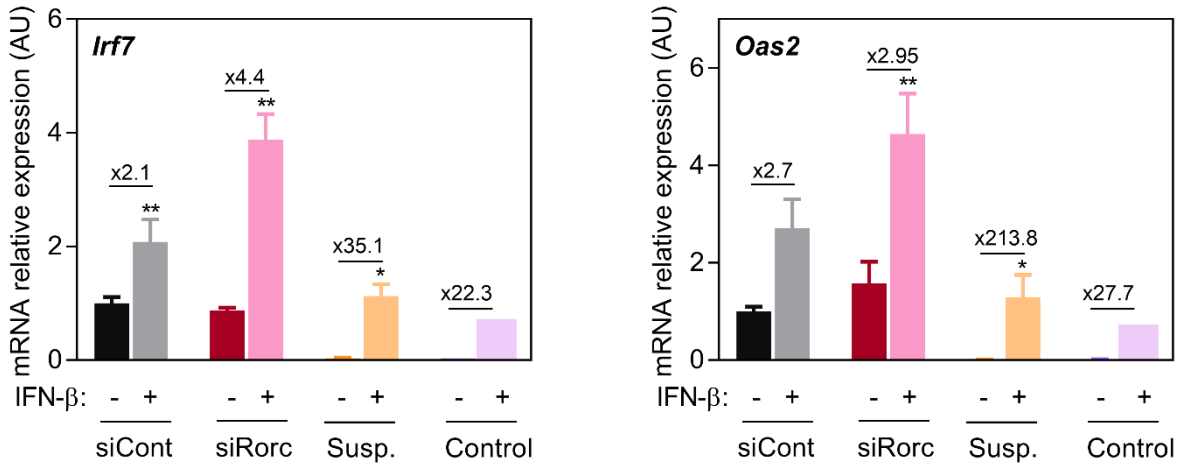

Figure 4.12. Levels of expression of RORγ target genes in response to siRNAs and IFN-β. Fully differentiated 3T3-L1 adipocytes were transfected with siRNA targeting *Rorc* (siRorc) or control (siCont), or they were not transfected and never detached from plates (control) or not transfected but detached from the plate and then re-seeded onto collagen-treated plates (susp.). Then, they were treated with 30UI/mL of IFN-β for 24h. Expression of *Irf7* and *Oas2* was determined by qPCR. Results are expressed as mean ± SEM (n=3/condition except control non detached cells, n=1). Numbers express induction folds when IFN-β is added compared to PBS/BSA (vehicle) treated cells. * Indicated statistical significance in the comparison between the presence or not of IFN-β;* $P \leq 0.05$, ** $P \leq 0.01$.

► 4.2 RORγ expression in white adipose tissue of calorie-restricted mice

As mentioned previously (see section 1.5.3), preliminary results showed that *Rorc*, but not other members of the ROR family, was highly induced in WAT in response to CR. First, we confirmed our previous observation by qPCR in a new cohort of animals. Indeed, we observed a dramatic induction in the expression of *Rorc* mRNA (Figure 4.13A) in inguinal WAT in response to CR. A similar increase was observed in gonadal WAT (Supplementary figure 2). The induction of *Rorc* mRNA appeared to be specific of WAT, since its expression did not change in response to CR in other tissues, like liver and skeletal muscle (Figure 4.13B). *Rorc* mRNA increase in response to CR correlated with elevated levels of RORγ protein (Figure 4.13C). Contrarly, RORα protein levels remained unaffected despite a mild increase in its mRNA in response to CR. Importantly, when using specific primers that allowed discrimination between the two isoforms of *Rorc*, we found that *Rorc1* isoform was the one over-expressed in response to nutrient deprivation in WAT, whereas *Rorc2(t)*, whose expression is restricted to immune cells, remained unchanged (Figure 4.13D).

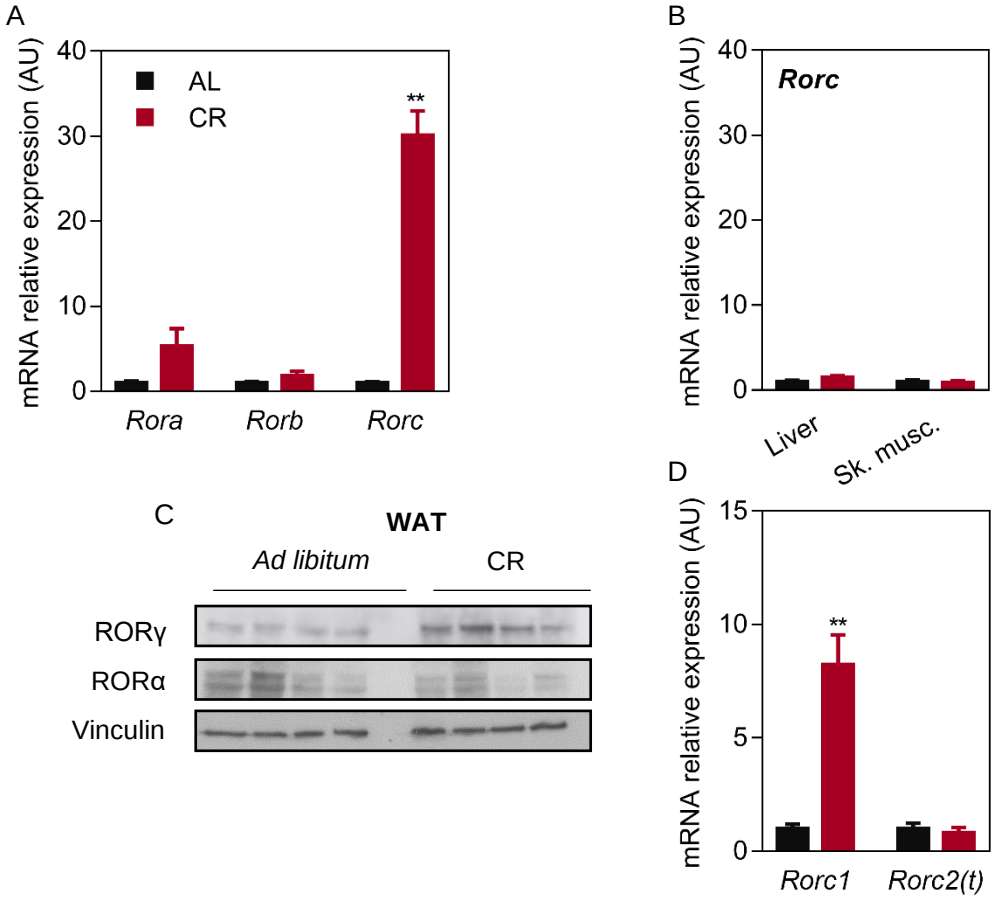

Figure 4.13. Effect of CR on *Rorc* mRNA and RORγ protein expression levels. A) mRNA expression levels of ROR family members in inguinal WAT of AL or CR mice. B) *Rorc* mRNA expression in liver and gastrocnemius muscle (sk. muscle) in AL or CR mice. C) Western blot analysis of RORγ and RORα protein levels in inguinal WAT of AL or CR mice fed with a HFD. Vinculin protein was used as a loading control. D) mRNA expression levels of *Rorc1* and *Rorc2(t)* isoforms in inguinal WAT of AL or CR mice. mRNA levels were determined by qPCR. Results are expressed as mean ± SEM (n=3-5 animals/group). AL, *ad libitum*; CR, calorie restriction. ** $P \leq 0.01$.

To determine which WAT cell fraction was responsible of the induction of *Rorc* expression in response to CR, adipocytes and SVF were isolated by collagenase digestion. We first verified the purity of both fractions by determining the expression of *MMTV integration site family, member 10B* (*Wnt10b*), a member of Wnt signaling pathway that is well-characterized as a preadipocyte marker (264,265), and *adipose triglyceride lipase* (*Atgl*), a gene that is exclusively expressed in mature

adipocytes (266) (Figure 4.14A). We observed that *Wnt10b* expression was significantly lower in the adipocyte fraction compared to SVF, which is in agreement with the highly abundance of preadipocytes in the SVF. Contrarily, *Atgl* expression was higher in the adipocyte fraction than in the SVF. These results indicate that the fractionation of WAT into adipocytes and non-adipose cells was correctly performed, and no significant cross-contamination between fractions occurred during the isolation process.

Similar to whole WAT, we observed that *Rorc* expression was dramatically increased upon CR in isolated adipocytes (Figure 4.14B). A mild increment in *Rorc* was also observed in the SVF in response to CR, suggesting that CR may also mildly up-regulate *Rorc* expression in other cells different from adipocytes, or it could be simply due to the presence of a small number of immature adipocytes present in the SVF. More specifically, CR induced the expression of the *Rorc1* isoform in adipocytes (Figure 4.14C). Although it did not reach statistical significance, we observed an induction of *Rorc2(t)* in the SVF, despite its expression in the adipocyte fraction was negligible (Figure 4.14C). Similar results were obtained in gonadal WAT (Supplementary figure 3).

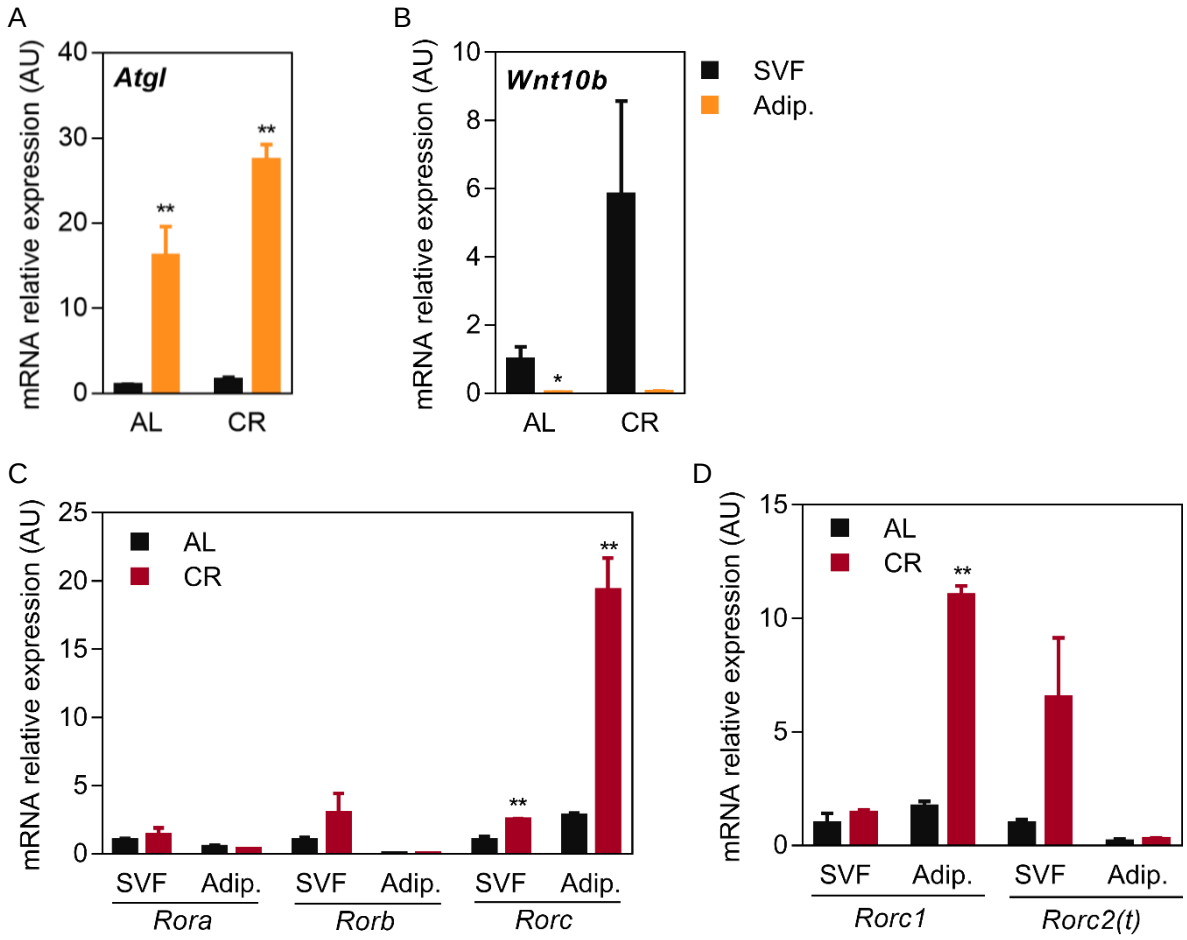

Figure 4.14. Expression of ROR family members in the adipocyte and SVF fractions from inguinal WAT of AL or CR mice. Adipocyte and SVF fractions were obtained by collagenase digestion. A) mRNA expression levels of mature adipocyte and preadipocyte makers *Atgl* and *Wnt10b*, respectively. B) mRNA expression levels of ROR family members in adipocyte and SVF fractions in response to CR. C) mRNA expression of *Rorc1* and *Rorc2(t)* isoforms in adipocyte and SVF fractions in response to CR. mRNA expression was assessed by qPCR. Results are expressed as mean ± SEM (n=3-5 animals/group). Adip., adipocytes; SVF, stromal vascular fraction; AL, *ad libitum*; CR, calorie restriction. * Indicates statistical significance between AL and CR or adipocytes and SVF. * $P \leq 0.05$; ** $P \leq 0.01$.

► 4.3 Generation of RORγ-FAT-KO mouse model to study the role of RORγ in adipose tissue

4.3.1 Generation of RORγ-FAT-KO mouse model

A conditional knockout mouse model lacking RORγ specifically in adipocytes (RORγ-FAT-KO) was generated to unravel the function of RORγ1 in adipose tissue and its contribution to glucose and energy homeostasis. In this model, the *Rorc* gene was disrupted by homologous recombination specifically in adipocytes using the *AdipoQ-Cre/loxP* technology.

Mice crossings gave rise to RORγ-FAT-KO and Wt mice at a Mendelian frequency at weaning (Wt=53%, KO=47%; n=741) and RORγ-FAT-KO mice appeared to develop normally without evident developmental, fertility or growth defects.

4.3.2 Effect of *Rorc* gene disruption

The effect of the disruption of *Rorc* gene on its mRNA expression was determined by qPCR in several tissues. Compared to their Wt littermates, RORγ-FAT-KO mice displayed a 70-88% decrease in *Rorc* mRNA expression in WAT, while BAT exhibited a reduction exceeding 98%. On the other hand, *Rorc* mRNA levels in non-adipose tissues remained unaltered (Figure 4.15).

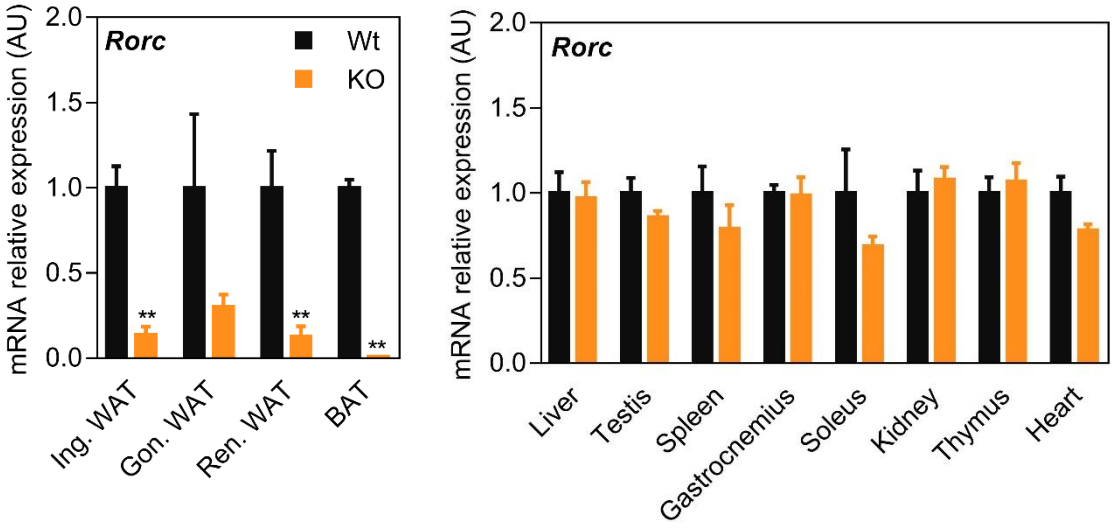

Figure 4.15. *Rorc* mRNA levels in tissues of male mice fed a chow diet and housed at 21ºC. The expression of *Rorc* mRNA in (A) adipose tissues and (B) non-adipose tissues of RORγ-FAT-KO mice and Wt littermates was assessed by qPCR. Results are expressed as mean ± SEM (n=5 animals/group). ** $P \leq 0.01$.

Additionally, we validated that *Rorc* was exclusively knocked out in the adipocytes. For this, the SVF and adipocyte fractions were isolated from inguinal WAT of RORγ-FAT-KO and Wt mice, and *Rorc* mRNA expression was determined by qPCR. As expected, a dramatic reduction of *Rorc* expression was observed in adipocytes of RORγ-FAT-KO mice (Figure 4.16). Similar results were obtained in gonadal WAT (Supplementary figure 4). A slight decrease of *Rorc* mRNA expression was also observed in SVF of WAT, which could be attributed to a mild contamination of this fraction by small adipocytes that could not be well separated by flotation from the SVF components. In fact, although we observed a substantial decrease of the adipocyte marker *Atgl* in the SVF compared to adipocyte fraction, we detected some expression of *Atgl* in the SVF that could reflect some adipocyte contamination.

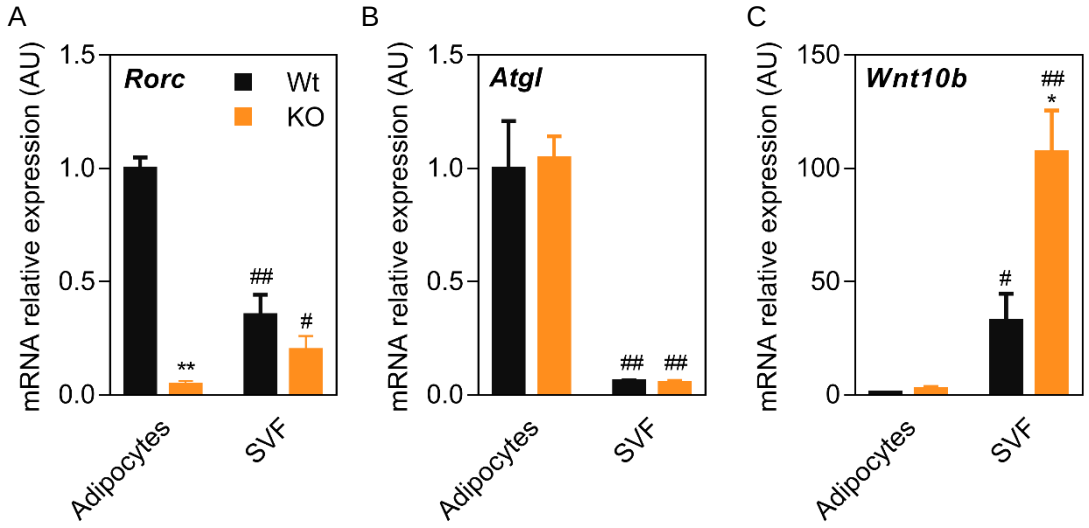

Figure 4.16. Gene expression analysis of mature adipocyte markers and *Rorc* in cell fractions of inguinal WAT. Expression of (A) *Rorc* (B) *Atgl* and (C) *Wnt10b* was assessed by qPCR in white adipocytes and SVF isolated from inguinal WAT of Wt and RORγ-FAT-KO mice. Results are expressed as mean ± SEM (n=4-5 animals/group). * Indicates statistical significance between Wt and RORγ-FAT-KO mice; # indicates statistical significance between adipocytes and SVF. *,# $P \leq 0.05$; **,## $P \leq 0.01$.

Because mRNA abundance does not always correlate with protein levels, we determined the effect of *Rorc* gene disruption in terms of protein levels. We first extracted protein from inguinal WAT, interscapular BAT, liver, skeletal muscle and thymus from Wt and RORγ-FAT-KO mice and then RORγ protein levels in each tissue were analyzed by western blot. We confirm that, compared to Wt mice, RORγ protein levels were almost absent in adipose tissues of RORγ-FAT-KO mice, while RORγ protein levels in other tissues remained unchanged. Moreover, we also examined RORα protein levels to discard any compensatory increase produced by the lack of RORγ (Figure 4.17). As shown in Figure 4.17, RORα protein levels were not increased in RORγ-FAT-KO mice and remained similar to those found in Wt mice.

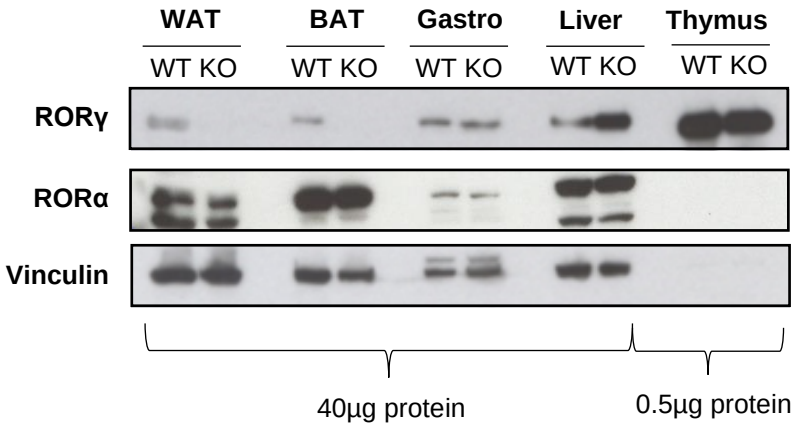

Figure 4.17. Western blot analysis of RORγ and RORα protein levels in WAT, BAT, liver and thymus of Wt and RORγ-FAT-KO mice. Detection of vinculin protein was used as loading control.

4.3.3 Physiological characterization of RORγ-FAT-KO mice

As WAT is a key regulator of whole body energy and glucose homeostasis and RORγ has been linked to obesity, we first characterized the impact that lack of RORγ has on body weight and adipose tissue mass in Wt and RORγ-FAT-KO male and female mice housed at 21ºC and fed a regular chow diet. No differences in body weight were observed between genotypes in both males (Figure 4.18A) and females (Figure 4.18C). Consistent with this, weight of major tissues, including BAT and main depots of WAT, was similar in both genotypes (Figure 4.18B and Figure 4.18D).

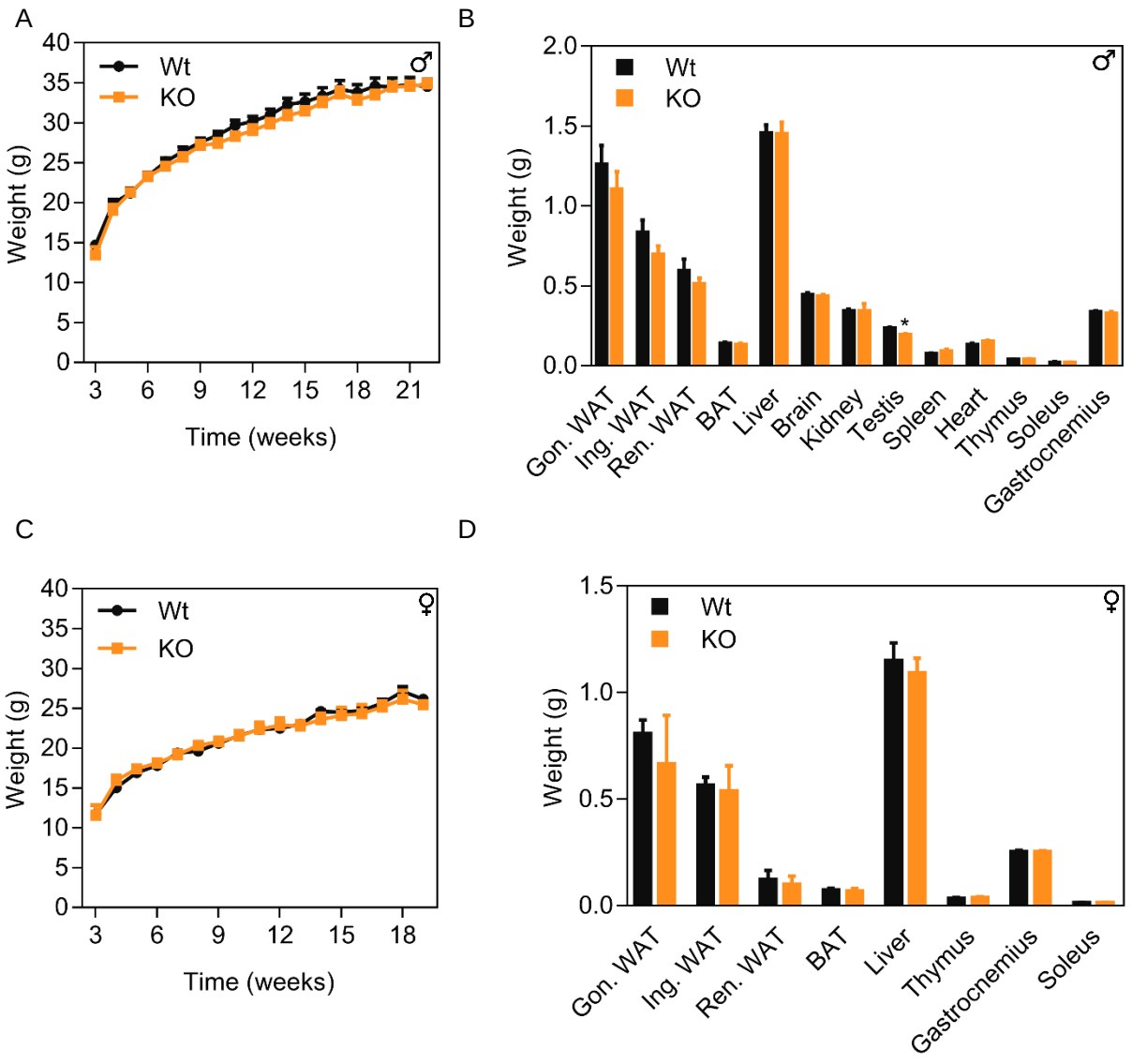

Figure 4.18. Analysis of body and tissue weight in Wt and RORγ-FAT-KO mice fed a chow diet and housed at 21ºC. (A) Body weight of male (A) and female (C) mice was measured weekly throughout the duration of the experiment. Tissue weights of male (B) and female (D) mice were measured when animals were euthanized at 22 weeks of age (males) and 19 weeks of age (females). Results are shown as mean ± SEM (n=5 animals/group). * Indicates statistical significance between Wt and RORγ-FAT-KO groups. * $P \leq 0.05$.

Furthermore, analysis of histological sections of inguinal WAT, gonadal WAT, interscapular BAT and liver did not reveal any gross abnormality between RORγ-FAT-KO mice and Wt littermates, in line with the lack of alterations found in body and tissue weight (Figure 4.19-21).

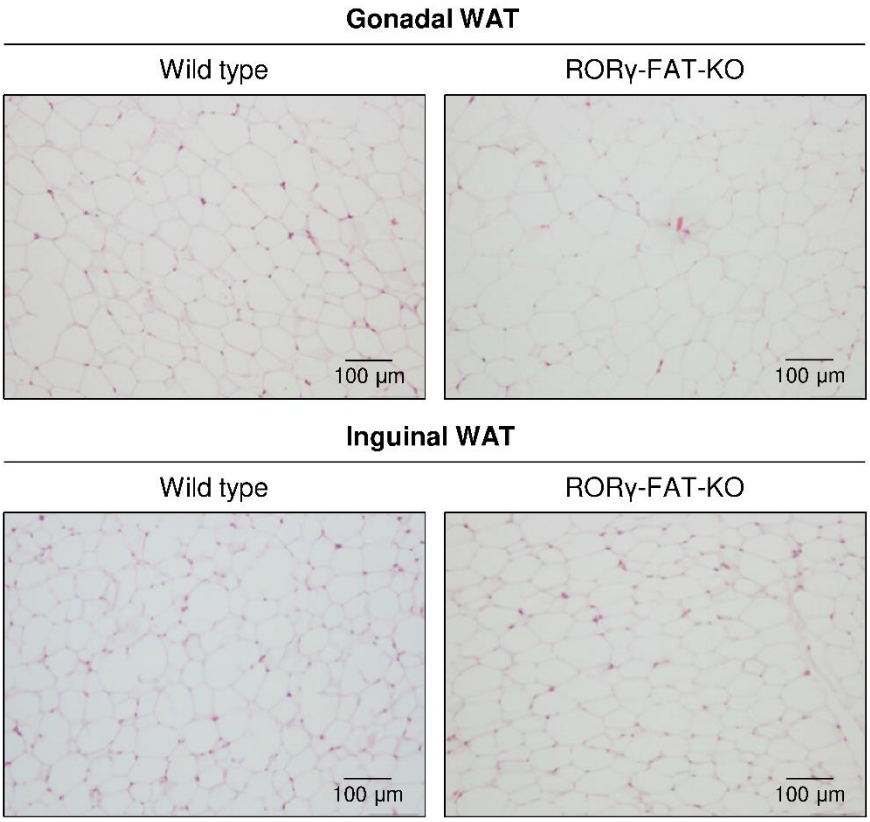

Figure 4.19. Histological sections of gonadal WAT and inguinal WAT from Wt and RORγ-FAT-KO mice. Histological sections from 22-week old male mice housed at 21ºC and fed a chow diet were stained with hematoxylin/eosin.

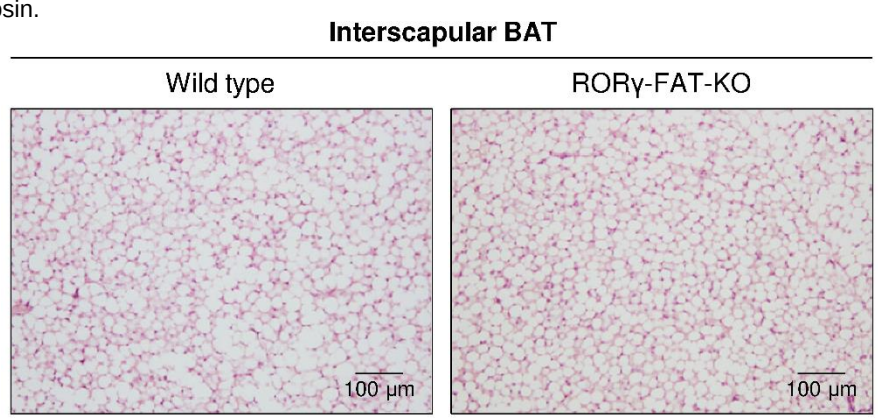

Figure 4.20. Histological sections of interscapular BAT from Wt and RORγ-FAT-KO mice. Histological sections from 22-week old male mice housed at 21ºC and fed a chow diet were stained with hematoxylin/eosin.

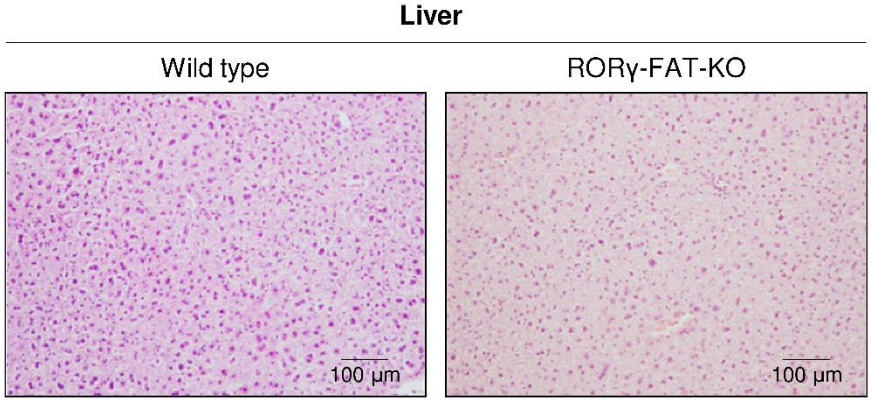

Figure 4.21. Histological sections of liver from Wt and RORγ-FAT-KO mice. Histological sections from 22-week old male mice housed at 21ºC and fed a chow diet were stained with hematoxylin/eosin.

To further characterize RORγ-FAT-KO mice, we also measured several biochemical parameters in serum of fasted mice (Table 4.1). We did not observe significant differences in any of the serum parameters analyzed between Wt and RORγ-FAT-KO mice, indicating that lack of RORγ in WAT does not lead to major metabolic alterations under basal conditions.

Parameter	Wt	RORγ-FAT-KO
Glucose, **mg/dL**	157.8 ± 7.6	154.4 ± 8.3
TAG, **mg/dL**	48.25 ± 3.00	44.93 ± 2.84
FFA, **mg/dL**	0.81 ± 0.13	0.63 ± 0.09
Cholesterol, **mg/dL**	168.13 ± 10.63	151.46 ± 17.37
Insulin, **ng/mL**	1.82 ± 0.22	1.63 ± 0.23
Leptin, **ng/mL**	14.09 ± 2.21	9.33 ± 2.06
Adiponectin, **µg/mL**	10.39 ± 0.57	8.11 ± 0.83
Resistin, **ng/mL**	48.67 ± 5.76	46.91 ± 2.47

Table 4.1. Analysis of serum metabolites and hormones of Wt and RORγ-FAT-KO male mice fed with a chow diet. Serum was collected via tail cut after 5-h of fasting. TAG and total cholesterol were determined using a commercial kit based on the Trinder colorimetric method. FFA were measured colorimetrically with the ACS-ACOD method. Insulin, leptin, adiponectin and resistin were determined in serum by ELISA. Results are expressed as mean ± SEM (n=5 animals/group).

► 4.4 Study of the cellular processes regulated by RORγ1 in white adipose tissue

4.4.1 Gene expression profile analysis of inguinal white adipose tissue from RORγ-FAT-KO mice subjected to calorie restriction

As RORγ was found induced by CR, we hypothesized that it may have relevant a role in regulating networks and cellular processes modulated by CR in WAT. Since the beneficial effects exerted by CR on mouse physiology, especially on glucose homeostasis, are more evident in a pathological context of obesity, all mice, either fed AL or submitted to CR, were fed with a HFD (60% of calories under the form of fat). This also provides a nutritional context that resembles that of modern human society, in which individuals are often exposed to hyper-caloric diets rich in fat and carbohydrates.

To gain insights into the genes and processes regulated by RORγ in WAT in response to CR, we performed a DNA microarray analysis to compare the gene expression profile of inguinal WAT from Wt and RORγ-FAT-KO mice fed AL or subjected to CR.

First, we confirmed that *Rorc* was over-expressed in Wt mice under CR, but that such induction was not seen in RORγ-FAT-KO mice (Figure 4.22). Moreover, neither *Rora* nor *Rorb* expression was significantly increased upon CR and was not significantly increased in WAT of RORγ-FAT-KO mice, suggesting that these genes do not compensate for the absence of *Rorc*.

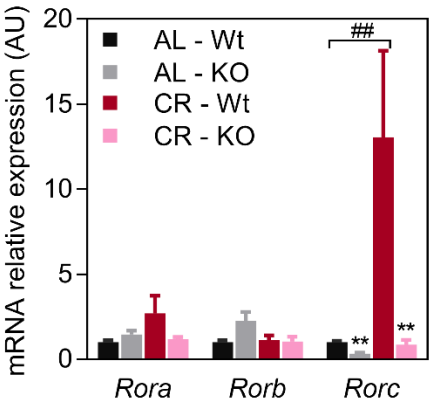

Figure 4.22. Analysis ROR family members expression in inguinal WAT of Wt and RORγ-FAT-KO mice fed AL or subjected to CR. mRNA expression levels of *Rora*, *Rorb* and *Rorc* was determined by qPCR. Results are expressed as mean ± SEM of 3-5 animals/group. * Indicates statistical differences between Wt and RORγ-FAT-KO mice. # Indicates statistical differences of the comparison between AL and CR group. AL, *ad libitum*; CR, calorie restriction. **## *P*≤0.01.

After filtrating for non-annotated and redundant genes, differentially regulated genes (*P*≤0.05) between all conditions were listed and plotted following the *Principal Component Analysis* (PCA). PC1 accounted for 27.2% of total variability whereas PC2 accounted for 18.5% (Figure 4.23). In this sense, bigger differences in gene expression were found between dietary interventions, represented by PC1. Interestingly, within the same diet, more differences were found between Wt and RORγ-FAT-KO mice subjected to CR, suggesting a major importance of the genotype under low-caloric conditions.

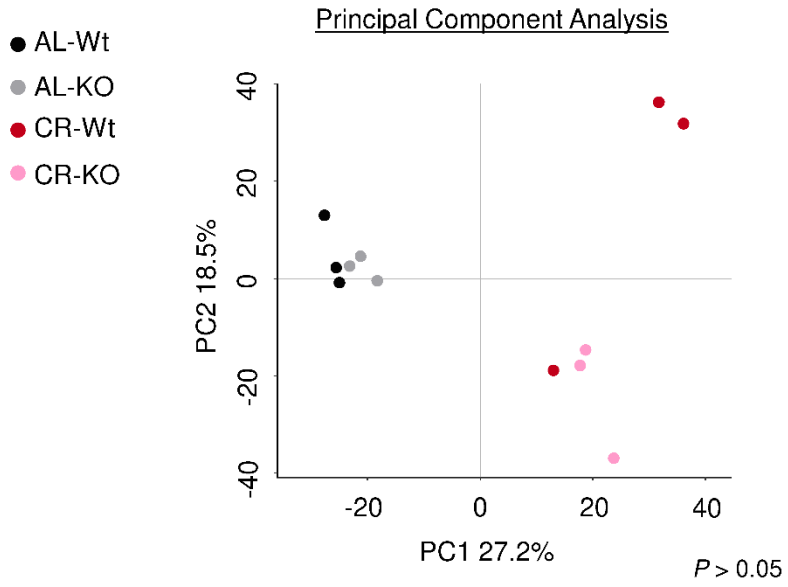

Figure 4.23. Principal Component Analysis from DNA microarray analysis. Each dot represents an animal subjected to one of the four conditions (AL-Wt, AL-KO, CR-Wt, CR-KO). Higher variability between groups is given by PC1, in this case separating AL and CR groups. PC2 shows variability amongst more related groups, in this case to Wt and RORγ-FAT-KO mice. AL, *ad libitum*; CR, calorie restriction.

As already indicated, we had previously conducted in our laboratory a gene-expression profiling study in inguinal WAT of AL and CR mice using DNA microarrays, in which we observed that gene networks related to mitochondria were among the most significantly increased in WAT in response to CR. On the other hand, GO categories related to ECM and immune system were also found over-represented among the genes down-regulated in WAT of CR treated mice (182).

In the present study, we found 1886 dysregulated genes in Wt mice subjected to CR compared to their AL counterparts, 580 up-regulated and 1306 down-regulated (Figure 4.24A). The list of first 50 up-regulated and down-regulated genes are shown in Supplementary table 10.

We performed GSEA analysis (FDR <25%) using a pre-ranked list of genes ($P \leq 0.05$). Consistent with our previous findings, GSEA analysis of our current study confirmed that gene networks related to mitochondria were also over-represented among the up-regulated genes in WAT of Wt by CR (Figure 4.24B), although they did not appear as one of the most statistically significant over-represented gene sets. Moreover, we also found GO categories related to ECM, specifically to cell adhesion, and to the immune system inflammatory response dysregulated in WAT of RORγ-FAT-KO mice (Figure 4.24). Interestingly, among the immune system categories, we found that gene sets related to adaptive immune cells were up-regulated by CR (Figure 4.24B), while gene sets related to innate immune cells were down-regulated (Figure 4.24C). These data were also analyzed using DAVID Bioinformatics Database functional annotation tool, which provided similar results (Supplementary table 11).

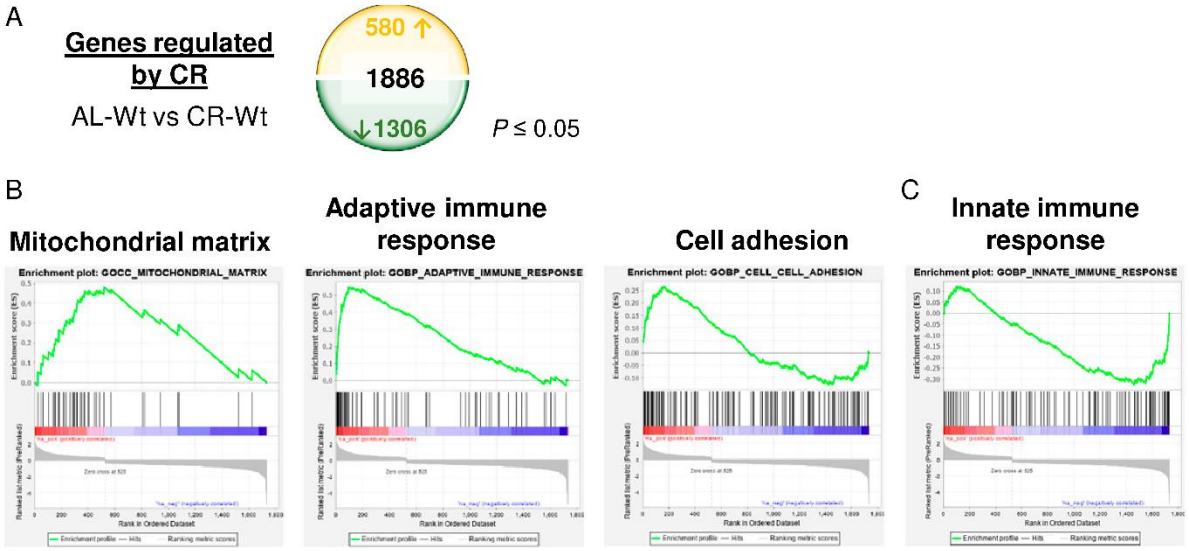

Figure 4.24. Analysis of genes dysregulated by CR in inguinal WAT. A) Diagram showing the number of genes dysregulated in inguinal WAT of Wt mice subjected to 40% CR compared with their AL counterparts ($P \leq 0.05$). The analysis was conducted using GSEA method. B) Statistical significant ($P \leq 0.05$ and FDR <25%) up regulated and C) down-regulated gene sets that provided relevant functional information.

With the aim of identifying RORγ target genes in WAT, we first analyzed differentially expressed genes under basal AL conditions. A reduced number of genes (344) emerged from the analysis with a $P \leq 0.05$, of which 166 genes were up-regulated and 178 down-regulated in WAT of RORγ-FAT-KO mice compared to Wt mice fed AL (Figure 4.25A and Supplementary table 12).

Using a FDR of <25%, the GSEA analysis revealed no gene sets enriched among up-regulated genes in WAT of RORγ-FAT-KO mice. Interestingly, of the few gene sets that appeared down-regulated in RORγ-FAT-KO mice, some of them were related to the immune response, specifically to type I IFN response or the regulation of pathogen infection. More specific, GO categories found had a low number of genes and a low P-value. Some of these categories were also related to the response to pathogens, such as pattern recognition signaling pathway, toll-like receptor signaling pathway or regulation of type I IFN (Figure 4.25B). We also found categories related to lipid metabolism, specifically to abnormal circulation of fatty acid concentration, although a very low number of genes were included in this category.

Additionally, up-regulated and down-regulated gene lists were analyzed separately using DAVID Bioinformatics Database functional annotation tool, in which similar results were obtained (Supplementary table 13).

The low number of gene sets differentially regulated in Wt and RORγ-FAT-KO mice is consistent with the similarity in the overall gene expression profiles exhibited by Wt and RORγ-FAT-KO mice fed AL, as shown in PCA (Figure 4.23). Together with the results obtained from our study in 3T3-L1 adipocytes in which the *Rorc* gene was silenced, these data suggest that the role of RORγ in WAT is related to the function of the cellular response to pathogens, although the low number of genes differentially expressed suggests that the functional implications of the loss of RORγ is minimal.

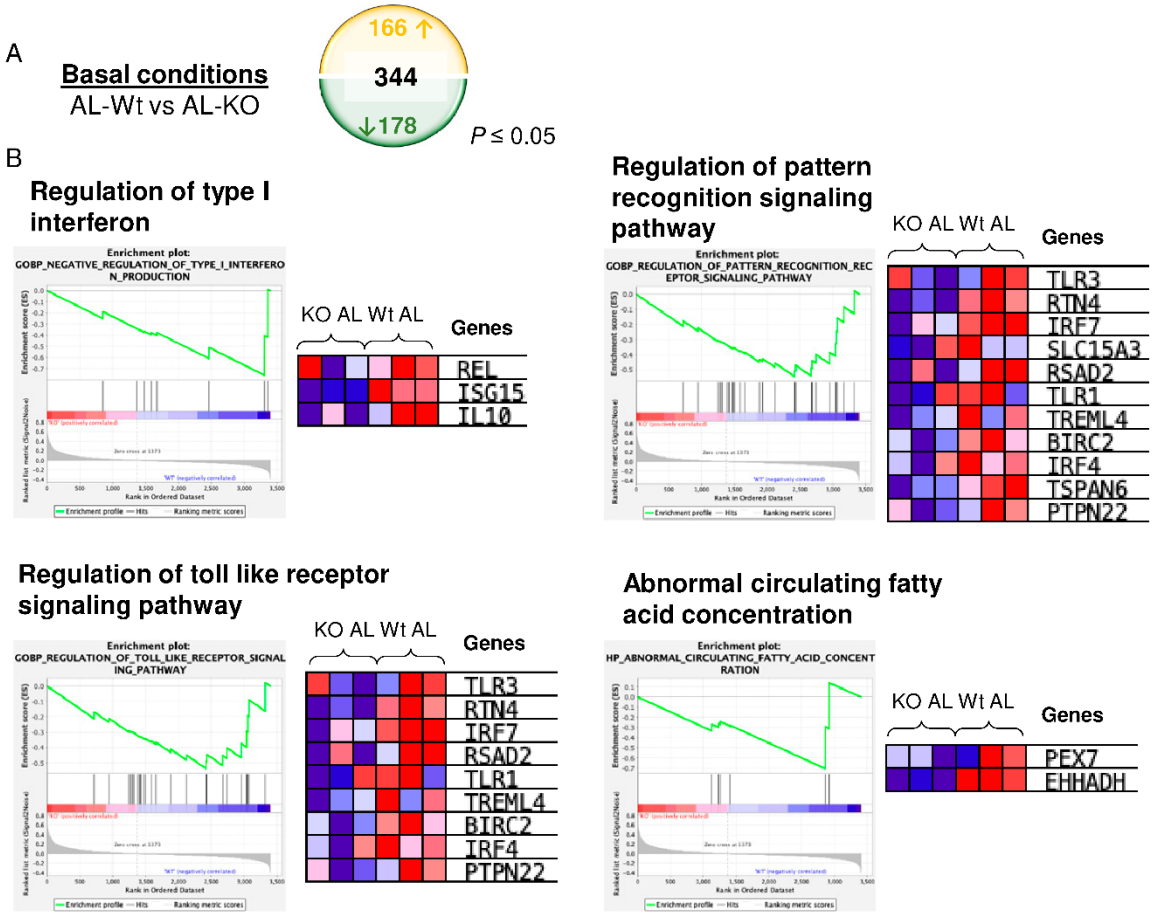

Figure 4.25. Analysis of RORγ target genes in AL HFD fed animals. A) Diagram showing the number of genes dysregulated in inguinal WAT of RORγ-FAT-KO mice fed AL with a HFD (*P*≤0.05). B) Gene-set enrichment analysis of differentially expressed genes in inguinal WAT of RORγ-FAT-KO mice fed AL using GSEA method. Statistical significant (*P*≤0.05 and FDR <25%) gene sets that provided relevant functional information are shown. Next to the gene sets, heatmaps of statistically significant of differentially expressed genes with a positive core enrichment are shown.

The next step was to unravel the genes regulated by RORγ in WAT in response to CR. Taking into account that RORγ is induced under CR and it is a transcriptional activator, we considered as potential RORγ target genes those genes that were up-regulated in response to CR in Wt mice but that did not respond to CR in RORγ-FAT-KO mice. As seen in Figure 4.26, 580 genes were significantly up-regulated by CR in Wt mice (*P*≤0.05), whereas 412 genes were down-regulated in RORγ-FAT-KO mice compared to Wt under CR (*P*≤0.05) (Figure 4.26). Of all these genes, 108 genes, representing 20% of the genes up-regulated by CR, met the criteria used to be considered

as RORγ target genes. The complete list of the 108 genes is shown in Supplementary table 14 in the annex section.

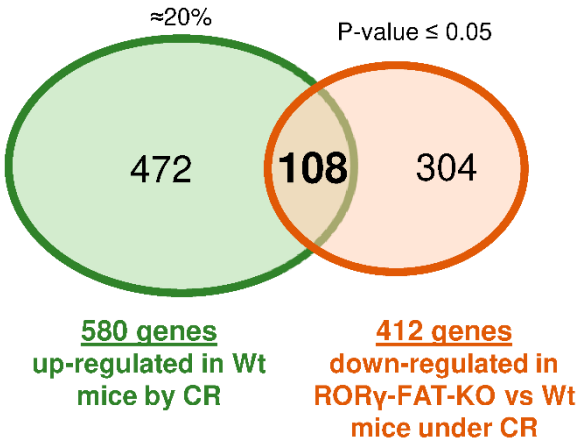

Figure 4.26. Venn's diagram showing genes up-regulated by CR in Wt mice (AL-Wt vs CR-Wt) and down-regulated in *Rorc* knockout mice compared to Wt mice under CR conditions (CR-Wt vs CR-KO).

To know the biological relevance of these 108 RORγ target genes, we performed a gene enrichment analysis using DAVID Bioinformatics tool, which allows the analysis of an unranked list of genes. Interestingly, most of the genes felt into GO categories of biological processes related to the immune system response, especially to T cell activation and differentiation, inflammation and cell adhesion (Table 4.2 and Supplementary table 15). Regarding cell compartment GO categories, most of the genes were located in cell membrane. However, no relevant information was provided by GO categories related to molecular function.

TABLE 4.2: Gene enrichment analysis of genes up-regulated by CR and down-regulated in RORγ-FAT-KO mice

Category	Term	Count	P-Value
GOTERM_BP	adaptive immune response	10	4.00E-08
GOTERM_BP	immune system process	14	7.90E-08
GOTERM_BP	positive regulation of T cell proliferation	7	9.30E-07
GOTERM_BP	immune response	11	1.40E-06
GOTERM_BP	T cell receptor signaling pathway	6	6.30E-06
GOTERM_BP	cell surface receptor signaling pathway	6	5.50E-03
GOTERM_BP	inflammatory response	7	8.70E-03
GOTERM_BP	cell differentiation	9	4.70E-02
GOTERM_BP	protein phosphorylation	7	7.60E-02
GOTERM_BP	phosphorylation	7	9.50E-02
GOTERM_CC	external side of plasma membrane	18	7.20E-13
GOTERM_CC	membrane	69	3.10E-10
GOTERM_CC	integral component of membrane	51	3.10E-03
GOTERM_CC	plasma membrane	39	4.10E-03

Table 4.2. Most significant GO terms obtained from gene enrichment analysis of RORγ target genes ($P \leq 0.05$) in WAT using DAVID bioinformatics source. (GOTERM_BP, biological process; GOTERM_CC, cellular component).

We also analyzed those genes that were down-regulated by CR in Wt mice and up-regulated in RORγ-FAT-KO mice, which would provide information about the genes potentially repressed by RORγ in response to CR. 1306 genes were downregulated by CR ($P \leq 0.05$) and 238 up-regulated in the RORγ-FAT-KO mice subjected to CR ($P \leq 0.05$). Of those, we just found 83 common genes

that fulfilled both conditions, representing approximately less than 6.5% of the genes down-regulated by CR (Figure 4.27 and Supplementary table 16). Gene enrichment analysis using DAVID bioinformatics tool did not give any valuable information related to the function or distribution of the proteins encoded by these genes, which were associated with very general biochemical pathways (Table 4.3 and Supplementary table 17).

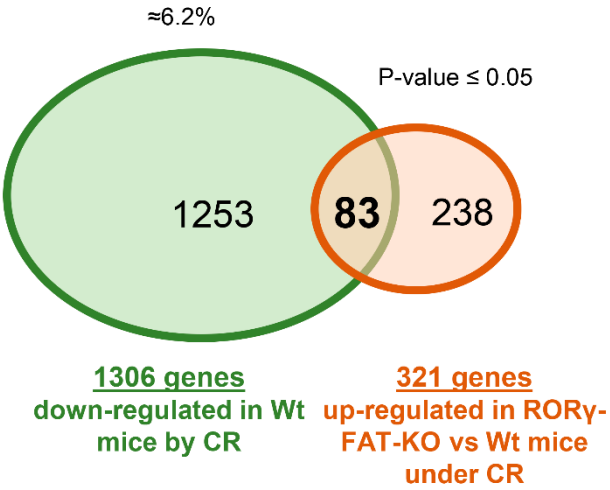

Figure 4.27. Venn's diagram showing genes down-regulated by CR in Wt mice (AL-Wt vs CR-Wt) and up-regulated in *Rorc* knockout mice compared to Wt mice under CR conditions (CR-Wt vs CR-KO).

TABLE 4.3: Gene enrichment analysis of genes down-regulated by CR and up-regulated in RORγ-FAT-KO mice

Category	Term	Count	P-Value
GOTERM_BP	negative regulation of signaling	12	1.10E-05
GOTERM_BP	oxidation-reduction process	12	1.30E-03
GOTERM_BP	negative regulation of signal transduction	12	2.90E-03
GOTERM_BP	negative regulation of cell communication	12	7.30E-03
GOTERM_CC	organelle membrane	24	1.10E-03
GOTERM_CC	whole membrane	14	1.10E-03
GOTERM_CC	cytoplasmic part	42	1.10E-03
GOTERM_MF	transition metal ion binding	13	9.00E-03

Table 4.3. Most significant GO terms obtained from gene enrichment analysis of RORγ target genes (*P*≤0.05) in WAT using DAVID bioinformatics source. (GOTERM_BP, biological process; GOTERM_CC, cellular component; GOTERM_MF, molecular function).

4.4.2 Validation of RORγ1 target genes in inguinal and gonadal white adipose tissue of RORγ-FAT-KO mice

Changes in gene expression found in the array were verified by qPCR. As mentioned above, according to DAVID gene enrichment analysis, most of the 108 RORγ target genes were grouped into immune system-related categories, especially regarding activation, trafficking and functioning of T lymphocytes. A representative group of 17 genes falling into these functional categories were validated in inguinal (Figure 4.28) and gonadal WAT (Figure 4.29).

Consistent with the results obtained in the arrays, most of the RORγ target genes validated in inguinal WAT significantly increased their expression in response to CR in Wt mice, but such induction was severely blunted in RORγ-FAT-KO mice. This is the case, for example, of genes

encoding for pro-inflammatory cytokines (*Ccl19*, *Ccl22*) and genes that participate in T-cell polarization or act as negative regulators of T-cell responses (*Icos*, *Btla1* and *Ctla4*) (Figure 4.28).

Major differences between Wt and RORγ-FAT-KO mice were found in inguinal WAT compared to gonadal WAT with regard to the response to CR. With few exceptions (*Il8r1* and *Lepr*), most of the genes validated did not respond to CR in gonadal WAT. However, similar to what we found in inguinal WAT, the expression of most of the genes identified as RORγ target genes was decreased in RORγ-FAT-KO mice subjected to CR, although the difference did not always reach statistical significance (Figure 4.29).

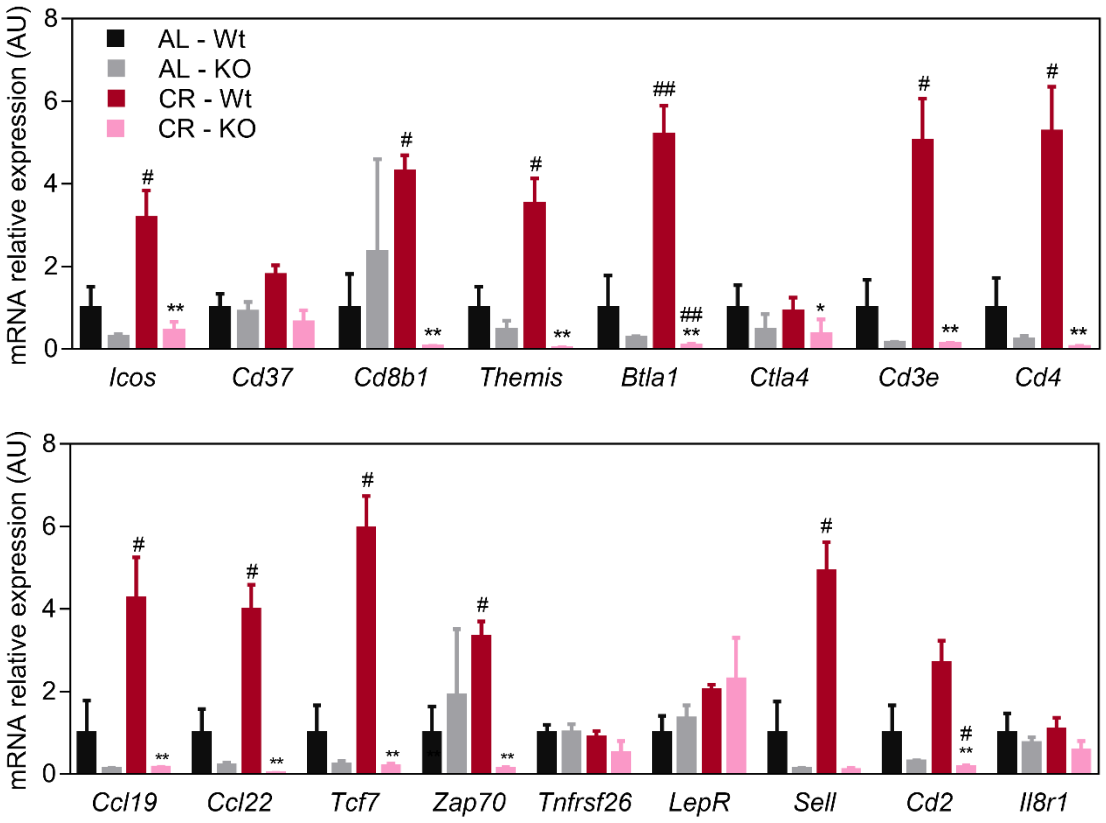

Figure 4.28. Expression analysis of potential RORγ target genes in inguinal WAT from Wt and RORγ-FAT-KO mice fed AL or subjected to CR. mRNA expression levels were determined by qPCR. The complete name of genes is shown in the abbreviation section. Results are expressed ad mean ± SEM (n=3-5 animals/group). * Indicates statistical differences between Wt and RORγ-FAT-KO mice. # Indicates statistical differences of the comparison between AL and CR group. AL, *ad libitum*; CR, calorie restriction. *# $P \leq 0.05$; **## $P \leq 0.01$.

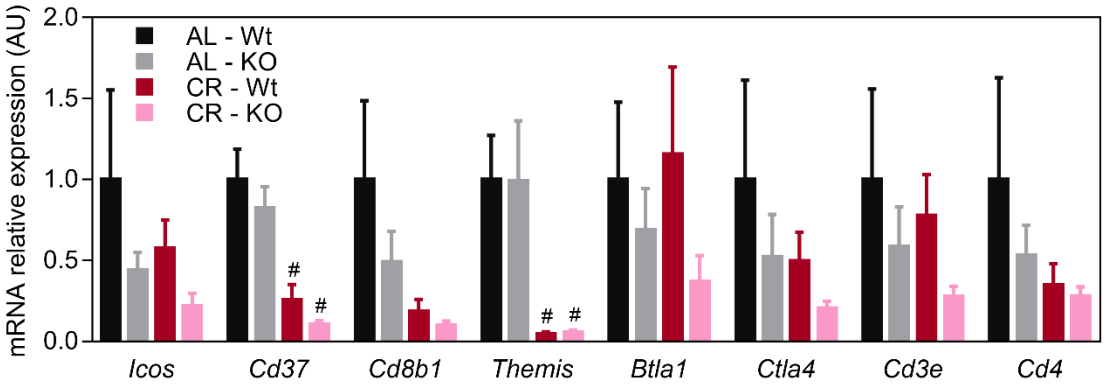

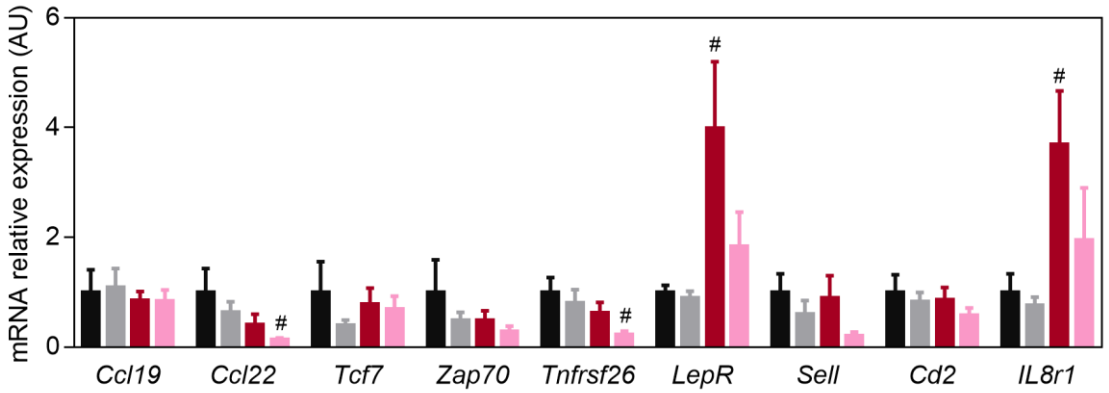

Figure 4.29. Expression analysis of potential RORγ target genes in gonadal WAT from Wt and RORγ-FAT-KO mice fed AL or subjected to CR. mRNA expression levels were determined by qPCR. The complete name of genes is shown in the abbreviation section. Results are expressed ad mean ± SEM (n=3-5 animals/group). * Indicates statistical differences between Wt and RORγ-FAT-KO mice. # Indicates statistical differences of the comparison between AL and CR group. AL, *ad libitum*; CR, calorie restriction. *# $P \leq 0.05$; **## $P \leq 0.01$.

► 4.5 Characterization of the immune cell populations in white adipose tissue of RORγ-FAT-KO mice subjected to calorie restriction

4.5.1 Calorie restriction reduces systemic inflammation induced by obesity in white adipose tissue

As mentioned, our gene expression profile revealed that CR altered the expression of genes related to the immune response, up-regulating the expression of genes related to the adaptive immune response and down-regulating the expression of genes related to innate response. In order to further evaluate the impact of CR on WAT inflammation, we quantified the content of different immune cell populations in the SVF of WAT by flow cytometry. First, we analyzed the percentage of $CD45^+$ cells of the SVF of inguinal and gonadal WAT of AL and CR mice, which provides an estimation of the total immune infiltrate in WAT. As expected, CR mice showed a significantly reduced number of immune cells compared to AL mice (Figure 4.30). Therefore, the increased immune infiltrate associated with obesity is rescued by CR.

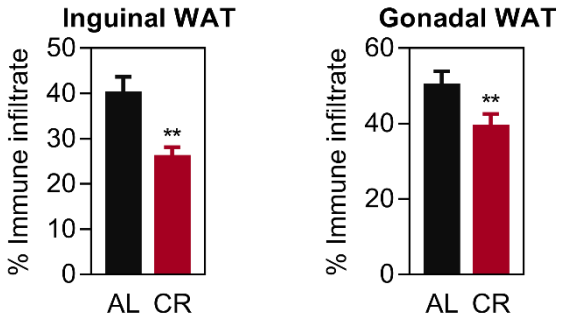

Figure 4.30. Evaluation of immune infiltrate in WAT of mice fed AL or subjected to CR. Percentage of immune infiltrate ($CD45^+$cells) of the SVF of inguinal and gonadal WAT from AL and CR mice analyzed by flow cytometry. Results are expressed as percentage of alive cells. Data are expressed as mean ± SEM (n=24-26 animals/group). * Indicates statistical differences of the comparison between AL and CR groups. AL, *ad libitum*; CR, calorie restriction. ** $P \leq 0.01$.

Then, we assessed the quality of the immune response in the white adipose tissues of AL and CR mice. For that, we immunophenotype the major immune cell populations by flow cytometry in both gonadal and inguinal WAT to perform a comprehensive characterization.

Compared to obese-insulin resistant mice fed AL with a HFD, CR mice, which were lean and showed improved insulin sensitivity, presented a reduction in macrophage cells populations. On the other hand, the proportion of neutrophils in CR mice was highly increased in both inguinal and gonadal WAT, while eosinophils were strongly increased just in gonadal WAT (Figure 4.31).

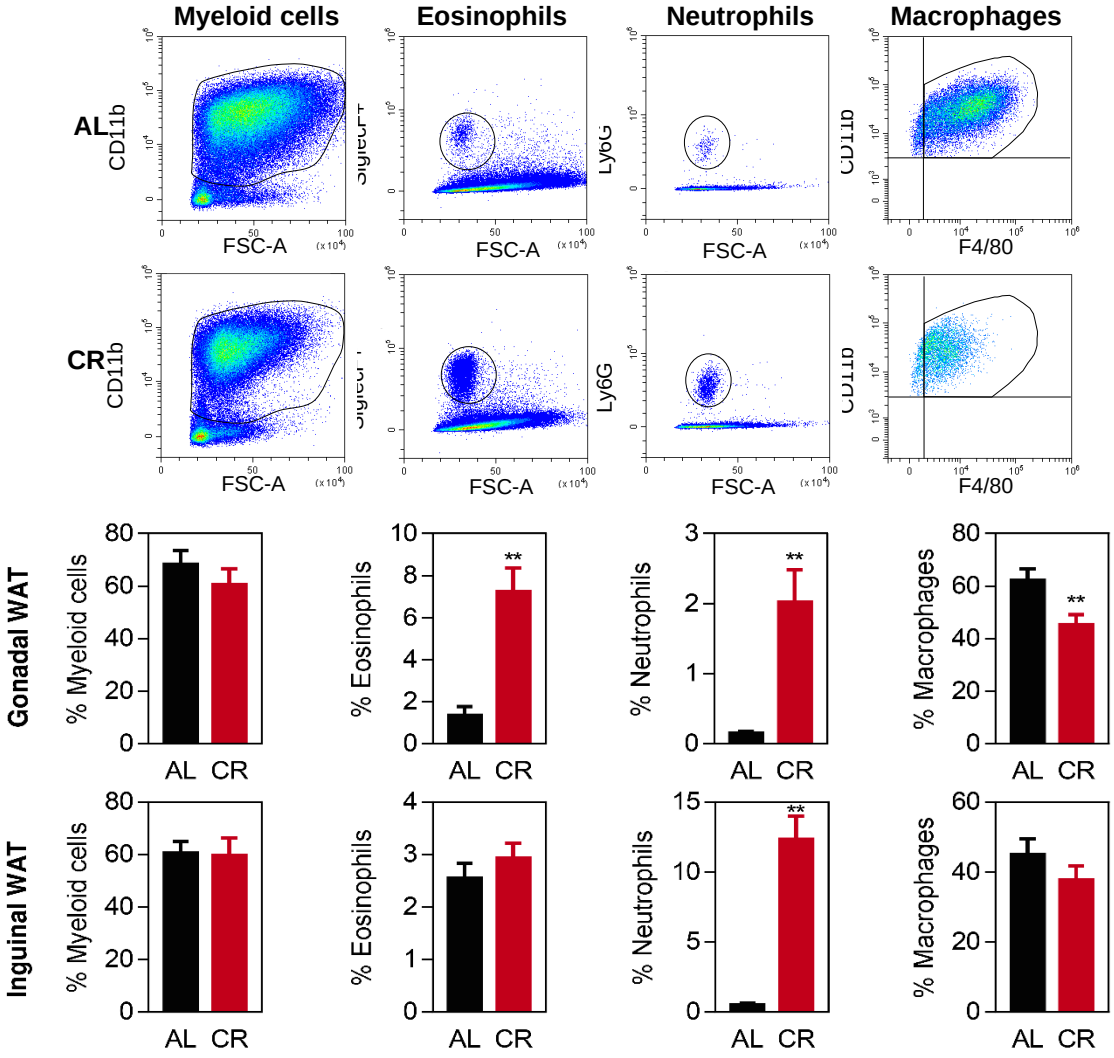

Figure 4.31. Flow cytometry analysis of myeloid cells from gonadal and inguinal WAT of AL and CR mice. Myeloid cells ($CD45^+CD11b^+$), eosinophils ($CD45^+CD11b^+F4/80^+SiglecF^+$), neutrophils ($CD45^+CD11b^+SiglecF^-F4/80^-Ly6G^+$) and macrophages ($CD45^+CD11b^+SiglecF^-F4/80^+$). Results are expressed as percentage of the parent population ($CD45^+$ for myeloid cells, and $CD45^+CD11b^+$ for de rest). Data are expressed as mean ± SEM of 6-14 animals/group. * Indicates statistical differences between Wt and RORγ-FAT-KO mice. # Indicates statistical differences of the comparison between AL and CR groups. AL, *ad libitum*; CR, calorie restriction. *# $P \leq 0.05$; **## $P \leq 0.01$.

We analyzed the expression of markers of pro-inflammatory (*Tnfa*, *Il1b*, *Il6*, *Ccl2, Ccl7*) and anti-inflammatory genes (*Il10*, *Il13*, *Il33*), as well as markers of inflammatory M1 macrophages (*Cd11c*, *Nos2*) and ant-inflammatory M2 macrophages (*Arg1*, *Cd206*, *Cd301*). Interestingly, in agreement with flow cytometry results, we found a general decrease in the mRNA expression of macrophage markers regardless of whether they are M1 pro-inflammatory or M2 anti-inflammatory (Figure 4.32).

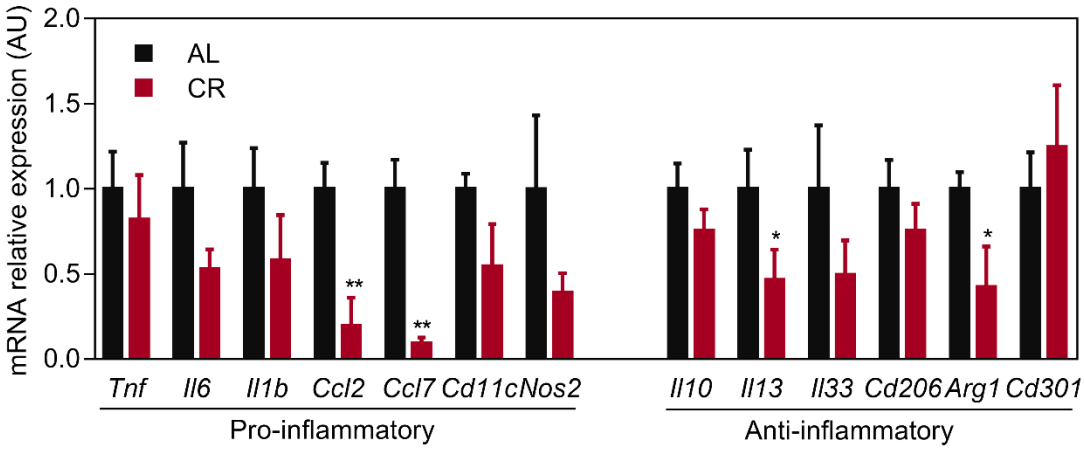

Figure 4.32. CR reduces the expression of genes related to inflammation. Expression analysis of genes related to inflammatory response in inguinal WAT of AL and CR mice. mRNA levels were determined by quantitative RT-PCR. The complete name of genes is shown in the abbreviation section. Data are expressed as mean ± SEM (n=5-6 animals/group). * Indicates statistical differences of the comparison between AL and CR groups. AL, *ad libitum*; CR, calorie restriction.* $P \leq 0.05$; ** $P \leq 0.01$.

The percentage of total T cells in the SVF of was not affected under a CR regime, although CR mice had a higher percentage of anti-inflammatory Th and Treg cells, and a reduced proportion of Tc cells in gonadal WAT, but not in inguinal WAT (Figure 4.33).

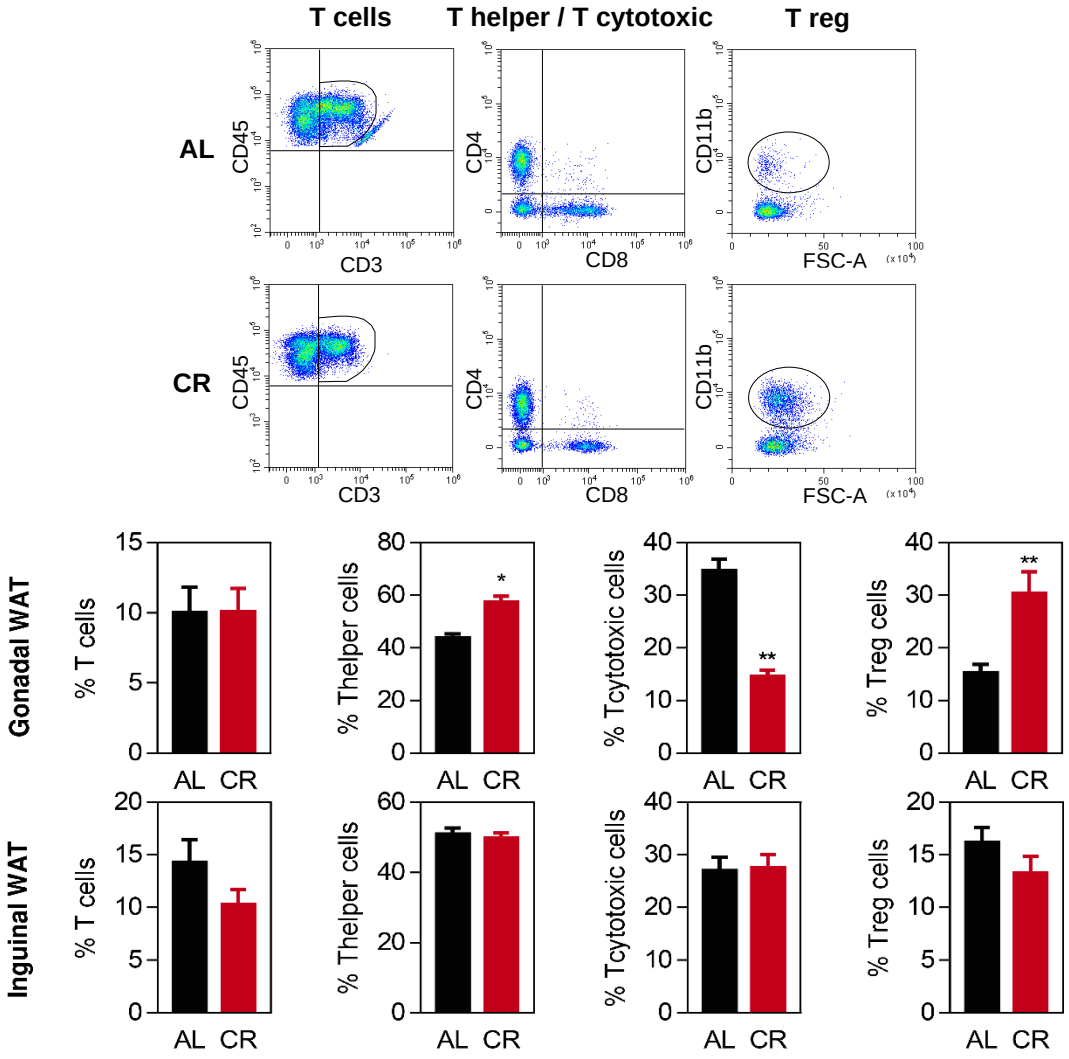

Figure 4.33. Flow cytometry analysis of T cells from gonadal and inguinal WAT of AL and CR mice. T cells ($CD45^+CD11b^-CD3^+$), T helper cells ($CD45^+CD11b^-CD3^+CD4^+CD8a^-$), T cytotoxic cells ($CD45^+CD11b^-CD3^+CD4^-CD8a^+$) and Treg cells ($CD45^+CD11b^-CD3^+CD4^+CD8a^-Foxp3^+$). Results are expressed as percentage of the parent population ($CD45^+CD11b^-$ for T cells, and $CD45^+CD11b^-CD3^+$ for Th, Tc and Treg cells). Data are expressed as mean ± SEM of 6-14 animals/group. * Indicates statistical differences between Wt and RORγ-FAT-KO mice. # Indicates statistical differences of the comparison between AL and CR groups. AL, *ad libitum*; CR, calorie restriction. *# $P \leq 0.05$; **## $P \leq 0.01$.

B cell population was mildly decreased in CR mice, although differences did not show statistical significance. Moreover, ILC cells were increased in mice subjected to CR, in both inguinal and gonadal WAT. NKt cells did not significantly change under CR, either in gonadal or in inguinal WAT, while NK cells were decreased in inguinal WAT (Figure 4.34).

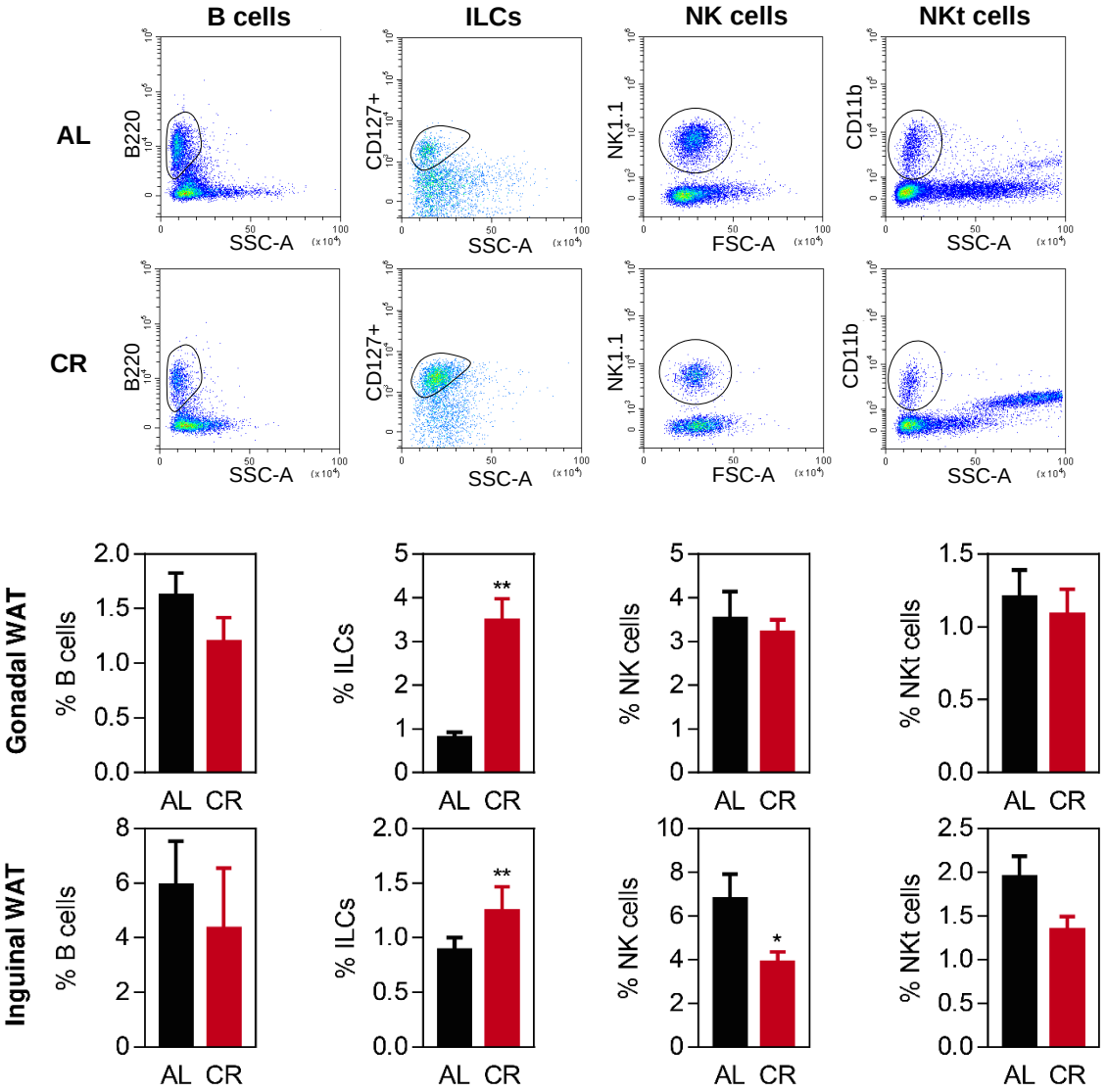

Figure 4.34. Flow cytometry analysis of B cells, ILCs, NK and NKt cells from gonadal and inguinal WAT of AL and CR mice. B cells ($CD45^+CD11b^-CD3^-B220^+$), ILC cells ($CD45^+CD11b^-CD3^-B220^-CD127^+$), NK cells ($CD45^+CD11b^-B220^-CD3^-NK1.1^+$) and NKt cells ($CD45^+CD11b^-B220^-CD3^+NK1.1^+$). Results are expressed as percentage of the parent population ($CD45^+CD11b^-CD3^-$ for B cells, ILCs and NK cells, and $CD45^+CD11b^-CD3^+$ for NKt cells). Data are expressed as mean ± SEM of 6-14 animals/group. * Indicates statistical differences between Wt and RORγ-FAT-KO mice. # Indicates statistical differences of the comparison between AL and CR groups. AL, *ad libitum*; CR, calorie restriction. *# $P \leq 0.05$; **## $P \leq 0.01$.

4.5.2 Immune cell characterization of RORγ-FAT-KO mice adipose tissues

Gene expression profiles indicated that RORγ could be modulating genes involved in the recruitment and activation of immune cells in WAT of mice submitted to CR. Hence, we analyzed the cellularity changes in the SVF fraction of RORγ-FAT-KO and Wt mice, either fed AL or subjected to CR.

Consistent with our previous results from WT mice fed AL or subjected to CR, total myeloid cell populations were neither changed between AL and CR mice, nor they were affected by the lack of RORγ. On the other hand, macrophages were diminished under CR conditions in inguinal and gonadal WAT, but the lack of RORγ did not have any effect on their abundance in WAT. Moreover, we found a dramatic increase of neutrophils and eosinophils upon CR. Interestingly, the increase in neutrophils in response to CR was mildly but consistently hampered in both inguinal and gonadal of RORγ-FAT-KO mice, although differences did not reach statistical significance (Figure 4.35).

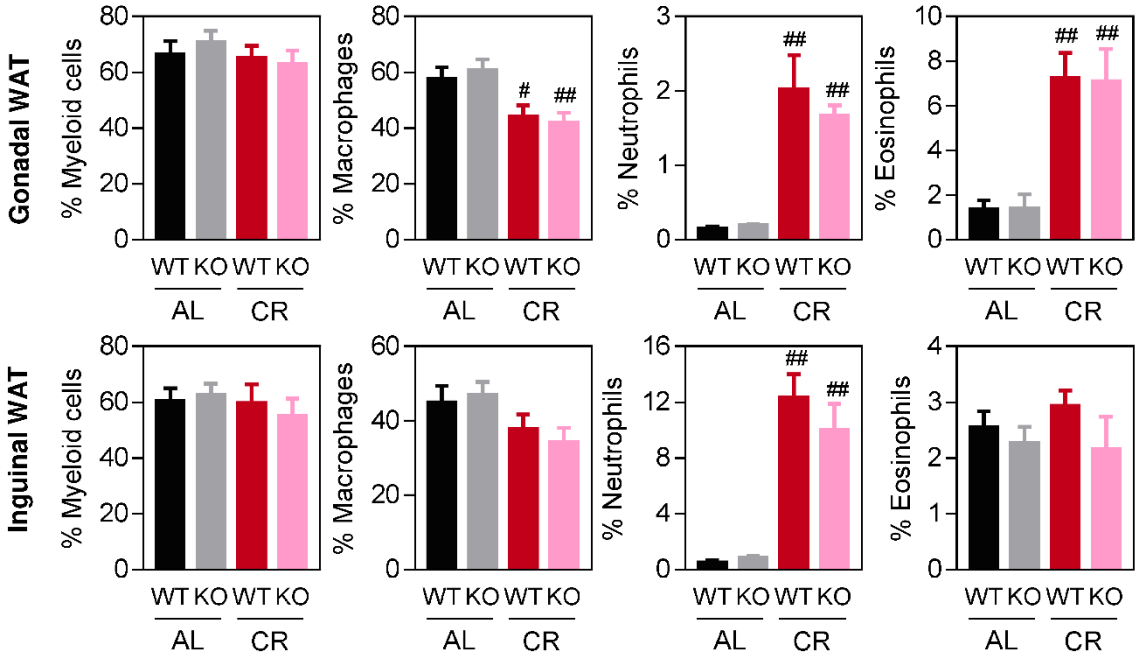

Figure 4.35. Flow cytometry analysis of myeloid cells, macrophages, neutrophils and eosinophils in gonadal and inguinal WAT of Wt and RORγ-FAT-KO mice fed AL or subjected to CR. Myeloid cells ($CD45^+CD11b^+$), macrophages ($CD45^+CD11b^+SiglecF^-F4/80^+$), neutrophils ($CD45^+CD11b^+SiglecF^-F4/80^-Ly6G^+$) and eosinophils ($CD45^+CD11b^+F4/80^+SiglecF^+$). Results are expressed as percentage of the parent population ($CD45^+$ for myeloid cells, and $CD45^+CD11b^+$ for macrophages, neutrophils and eosinophils). Data are expressed as mean ± SEM of 6-14 animals/group. * Indicates statistical differences between Wt and RORγ-FAT-KO mice. # Indicates statistical differences of the comparison between AL and CR groups. AL, *ad libitum*; CR, calorie restriction. *# $P \leq 0.05$; **## $P \leq 0.01$.

Results obtained from microarray analysis suggested that RORγ could interfere in the number and activation of immune T and B cell populations in WAT, as well as other innate immune cells. We found that B cells were decreased under CR conditions in Wt mice, especially in inguinal WAT. Interestingly, RORγ-FAT-KO mice failed to decrease B cells in response to CR, but this pattern was only observed in inguinal WAT (Figure 4.36).

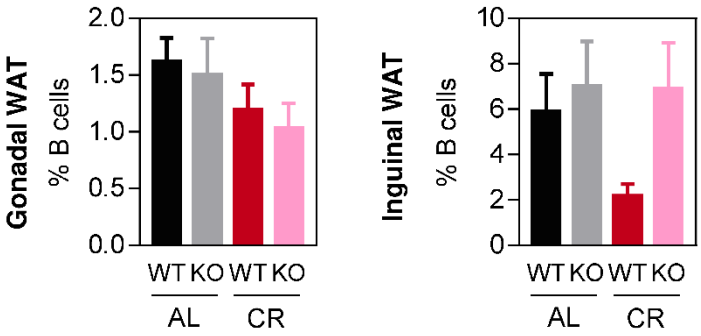

Figure 4.36. Flow cytometry analysis of B cells in gonadal and inguinal WAT of Wt and RORγ-FAT-KO mice fed AL or subjected to CR. B cells ($CD45^+CD11b^-CD3^-B220^+$. Results are expressed as percentage of the parent population ($CD45^+CD11b^-CD3^-$). Data are expressed as mean ± SEM of 6-14 animals/group. * Indicates statistical differences between Wt and RORγ-FAT-KO mice. # Indicates statistical differences of the comparison between AL and CR groups. AL, *ad libitum*; CR, calorie restriction. *# *P*≤0.05; **## *P*≤0.01.

The percentage of total T cells in the immune infiltrate of WAT was not altered by either the nutrient intervention or the genotype. However, when analyzing the specific T cell populations, we observed in gonadal WAT that Th populations were increased under CR, while Tc cells were decreased. These changes, although modest, were bigger in RORγ-FAT-KO mice compared to their Wt littermates. Somehow surprisingly, no major changes were observed in inguinal WAT, although a tendency towards an increase in the Th population in WAT of RORγ-FAT-KO mice in response to CR was observed. On the other hand, γδT cells, which play a pro-inflammatory role in obesity-associated inflammation, appeared increased in gonadal WAT upon CR, but they were not changed in inguinal WAT by the nutritional intervention. Curiously, γδT cells of mice lacking *Rorc* were significantly increased in mice fed AL (Figure 4.37).

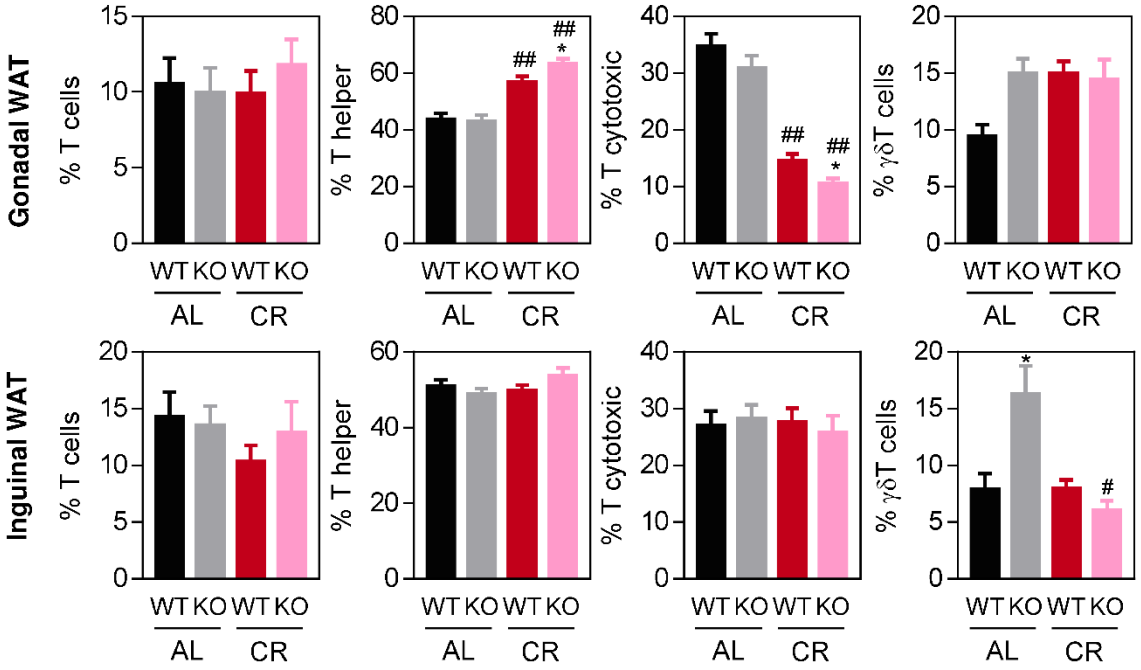

Figure 4.37. Flow cytometry analysis of T cells, T helper, T cytotoxic and γδT cells in gonadal and inguinal WAT of Wt and RORγ-FAT-KO mice fed AL or subjected to CR. T cells ($CD45^+CD11b^-CD3^+$), T helper cells ($CD45^+CD11b^-CD3^+CD4^+CD8a^-$), T cytotoxic cells ($CD45^+CD11b^-CD3^+CD4^-CD8a^+$), Treg cells ($CD45^+CD11b^-CD3^+CD4^+CD8a^-Foxp3^+$) and γδT cells ($CD45^+CD11b^-CD3^+TCR\gamma^+$). Results are expressed as percentage of the parent population ($CD45^+CD11b^-$ for T cells, and $CD45^+CD11b^-CD3^+$ for T helper, T cytotoxic and γδT cells). Data are expressed as mean ± SEM of 6-17 animals/group. * Indicates statistical differences between Wt and RORγ-FAT-KO mice. # Indicates statistical differences of the comparison between AL and CR groups. AL, *ad libitum*; CR, calorie restriction. *# *P*≤0.05; **## *P*≤0.01.

Next, we analyzed the proportion of the different Th subpopulations. We found that Th1 cells were reduced under CR, while Th2 and Treg cells were increased in gonadal WAT. Moreover, these changes were larger in RORγ-FAT-KO mice subjected to CR, exhibiting a reduction of pro-inflammatory Th1 cells and an increase of Th2 and Treg cells compared to their Wt counterparts. On the other hand, Th17 cells numbers were not changed, either mice fed AL or subjected to CR. Minor changes were observed in inguinal WAT. Still, although differences did not reach statistical significance, an increase of Th2 and Treg cells in RORγ-FAT-KO mice under CR was observed, compared to their Wt littermates also subjected to CR. Overall, these results show that lack of RORγ in adipocytes induced a switch towards an anti-inflammatory environment, especially in response to CR (Figure 4.38).

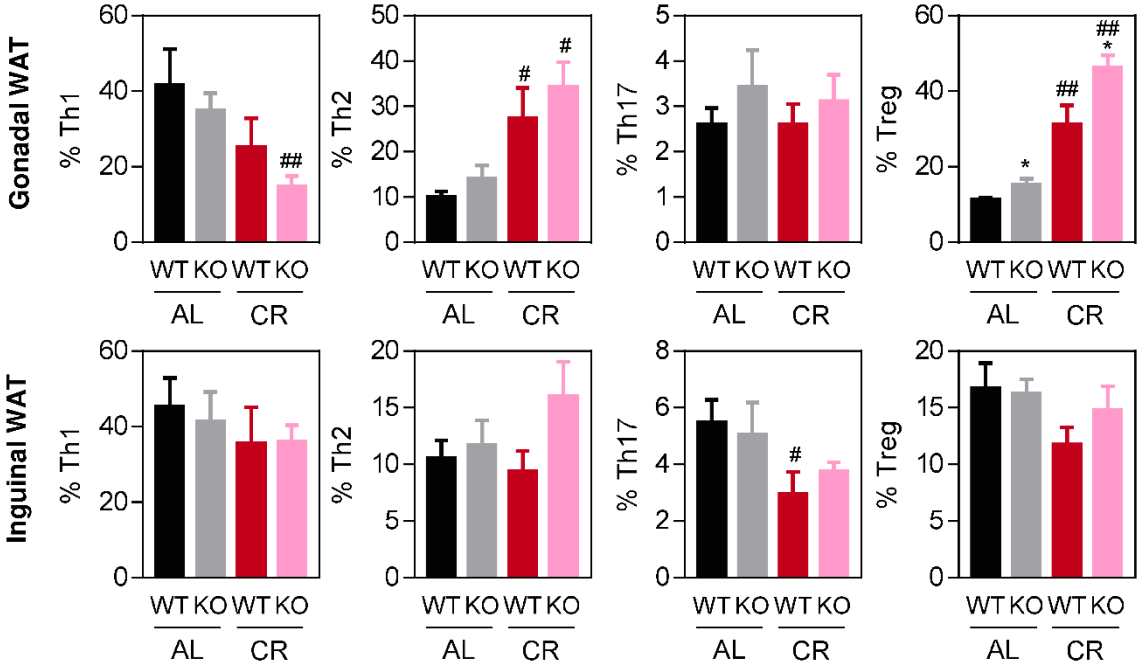

Figure 4.38. Flow cytometry analysis of Th1, Th2, Th17 and Treg cells in gonadal and inguinal WAT of Wt and RORγ-FAT-KO mice fed AL or subjected to CR. Th1 cells ($CD45^+CD11b^-CD3^+CD4^+CD8a^-Tbet^+$), Th2 cells ($CD45^+CD11b^-CD3^+CD4^+CD8a^-Gata3^+$), Th17 cells ($CD45^+CD11b^-CD3^+CD4^+CD8a^-Ror\gamma t^+$) and Treg cells ($CD45^+CD11b^-CD3^+CD4^+CD8a^-Foxp3^+$). Results are expressed as percentage of the parent population ($CD45^+CD11b^-CD3^+$). Data are expressed as mean ± SEM of 6-17 animals/group. * Indicates statistical differences between Wt and RORγ-FAT-KO mice. # Indicates statistical differences of the comparison between AL and CR groups. AL, *ad libitum*; CR, calorie restriction. *# $P \leq 0.05$; **## $P \leq 0.01$.

ILCs content in WAT was also determined. Under CR there was an increase of total ILC cells populations, both in inguinal and gonadal WAT, but no differences were found between Wt and RORγ-FAT-KO mice. When we analyzed the proportion of the different ILCs subpopulations, we found that ILC2 cells were the predominant subpopulation, constituting more than 60% of total ILCs. However, no differences were found between genotypes in either gonadal or inguinal WAT. ILC3 cells, which represented around 1-3% of total ILCs, were found dramatically diminished under CR conditions in gonadal WAT, and their abundance was mildly reduced in CR in inguinal WAT. On the other hand, ILC1 cells were not detected in WAT (Figure 4.39).

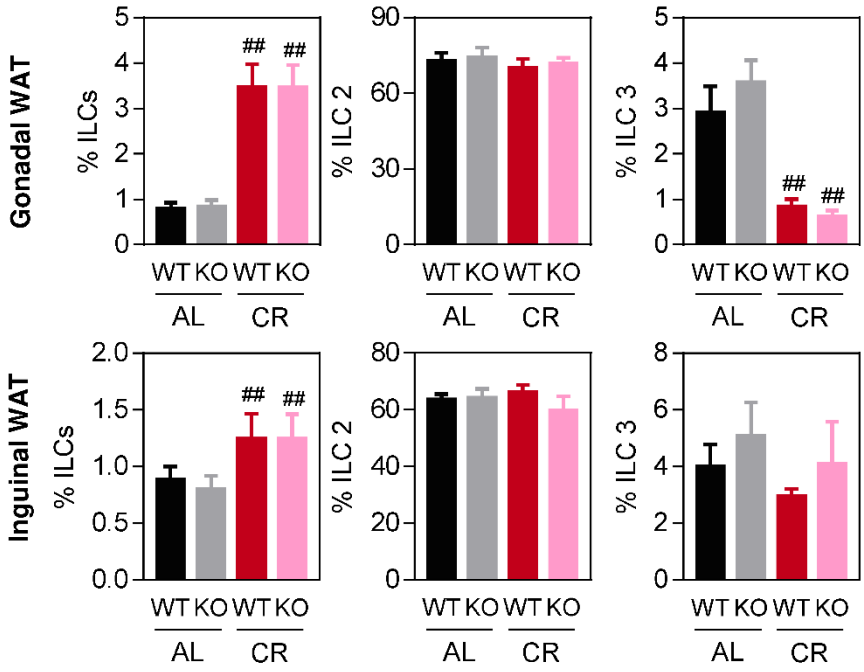

Figure 4.39. Flow cytometry analysis of ILCs, ILC2 and ILC3 in gonadal and inguinal WAT of Wt and RORγ-FAT-KO mice fed AL or subjected to CR. ILC cells ($CD45^+CD11b^-CD3^-B220^-CD127^+$), ILC2 cells ($CD45^+CD11b^-CD3^-B220^-CD127^+Gata3^+$) and ILC3 cells ($CD45^+CD11b^-CD3^-B220^-CD127^+Ror\gamma t^+$). Results are expressed as percentage of the parent population ($CD45^+CD11b^-CD3^-$ for ILCs and $CD45^+CD11b^-CD3^-CD127^+$ for ILC2 and ILC3). Data are expressed as mean ± SEM of 6 animals/group. * Indicates statistical differences between Wt and RORγ-FAT-KO mice. # Indicates statistical differences of the comparison between AL and CR groups. AL, *ad libitum*; CR, calorie restriction. *# $P \leq 0.05$; **## $P \leq 0.01$.

Finally, we also determined NK and NKt cells populations. In inguinal WAT, the percentage of NK cells was reduced upon nutrient deprivation, while a only mild reduction was observed in gonadal WAT. Interestingly, in both WAT depots, the percentage of NK cells in RORγ-FAT-KO mice fed AL was reduced, presenting similar numbers as mice subjected to CR.

On the other hand, in inguinal WAT, the percentage of NKt cells were decreased in response to CR, a change that was not observed in gonadal WAT. Interestingly, the levels of NKt cells of RORγ-FAT-KO mice fed AL were lower than Wt mice, both in gonadal and inguinal WAT, although differences did not reach statistical significance. Such decrease in RORγ-FAT-KO mice fed AL was reverted by CR (Figure 4.40).

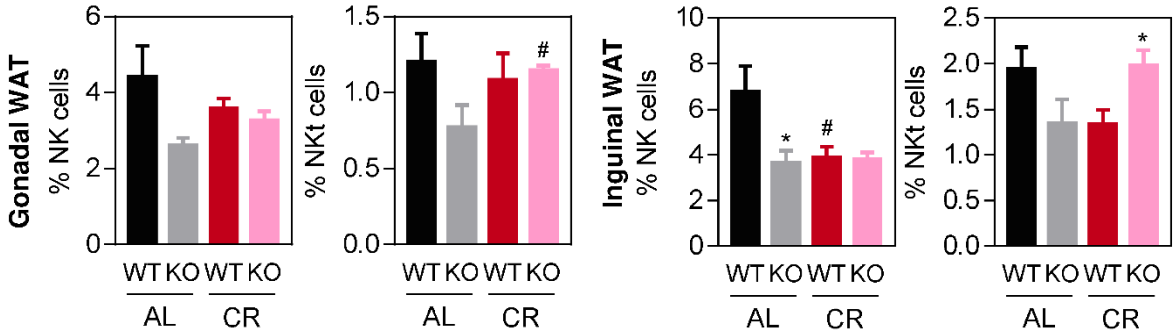

Figure 4.40. Flow cytometry analysis of NK and NKt cells in gonadal and inguinal WAT of Wt and RORγ-FAT-KO mice fed AL or subjected to CR. NK cells ($CD45^+CD11b^-B220^-CD3^-NK1.1^+$ and NKt cells ($CD45^+CD11b^-B220^-CD3^+NK1.1^+$). Results are expressed as percentage of the parent population ($CD45^+CD11b^-CD3^-$ for NK cells and $CD45^+CD11b^-CD3^+$ for NKt cells). Data are expressed as mean ± SEM of 6 animals/group. * Indicates statistical differences between Wt and RORγ-FAT-KO mice. # Indicates statistical differences of the comparison between AL and CR groups. AL, *ad libitum*; CR, calorie restriction. *# $P \leq 0.05$; **## $P \leq 0.01$.

To summarize, the immune cellular profile of mice lacking RORγ suggests that WAT of RORγ-FAT-KO mice show a more anti-inflammatory profile than their Wt littermates, especially in gonadal WAT that displays an increase of Th2 and Treg cells and a reduction of Tc and Th1 cells.

► 4.6 Role of RORγ in brown adipose tissue thermogenesis in response to cold

4.6.1 RORγ expression in brown adipose tissue

The RORγ-FAT-KO mouse model generated is adipose tissue specific and ensures the deletion of the *Rorc* gene not only in white adipocytes but also in brown adipocytes. Since the function of RORγ in BAT is unknown, we first quantified the expression of *Rorc* gene in BAT by absolute qPCR and compared them with the expression levels in WAT and other tissues. Although results did not reach statistical significance, we found that *Rorc* levels were 2 fold higher in BAT than in WAT (Figure 4.41). The high levels of *Rorc* mRNA suggest that it may play a relevant role in the function of BAT.

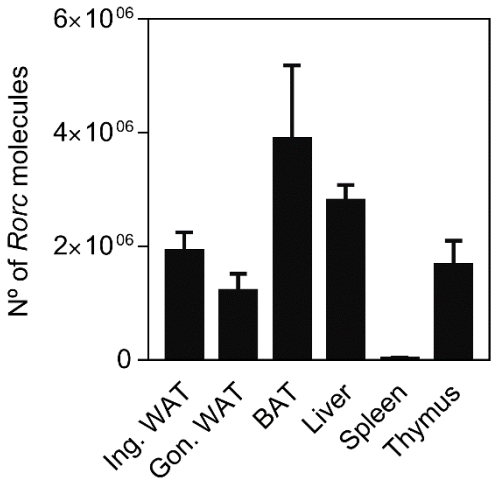

Figure 4.41. Absolute quantification of *Rorc* gene expression in inguinal WAT, gonadal WAT, BAT, liver, spleen and thymus. mRNA expression was assessed by absolute quantification qPCR using the plasmid pCDNA3.1(-)mRORγ, which contains the coding sequence for RORγ, as standard. Results are expressed as mean ± SEM (n=5 animals/group).

4.6.2 Effect of the lack of RORγ in brown adipose tissue thermogenesis in response to cold

Since RORγ is highly expressed in BAT, we aimed at studying the effects that lack of RORγ in brown adipocytes could have on BAT function. Given that BAT is specialized in the production of heat to maintain body temperature in response to cold through a process known as non-shivering adaptive thermogenesis (72), we first exposed RORγ-FAT-KO and Wt mice at 4ºC for 5h after being first acclimated at thermoneutrality (30ºC) for two weeks.

At thermoneutrality, and prior to being exposed to cold, Wt and RORγ-FAT-KO mice had the same body temperature (Figure 4.42A). However, when mice were exposed at 4ºC, both Wt and RORγ-FAT-KO mice were able to similarly maintain their body temperature (Figure 4.42B), suggesting that lack of RORγ in brown adipocytes does not significantly affect thermogenesis.

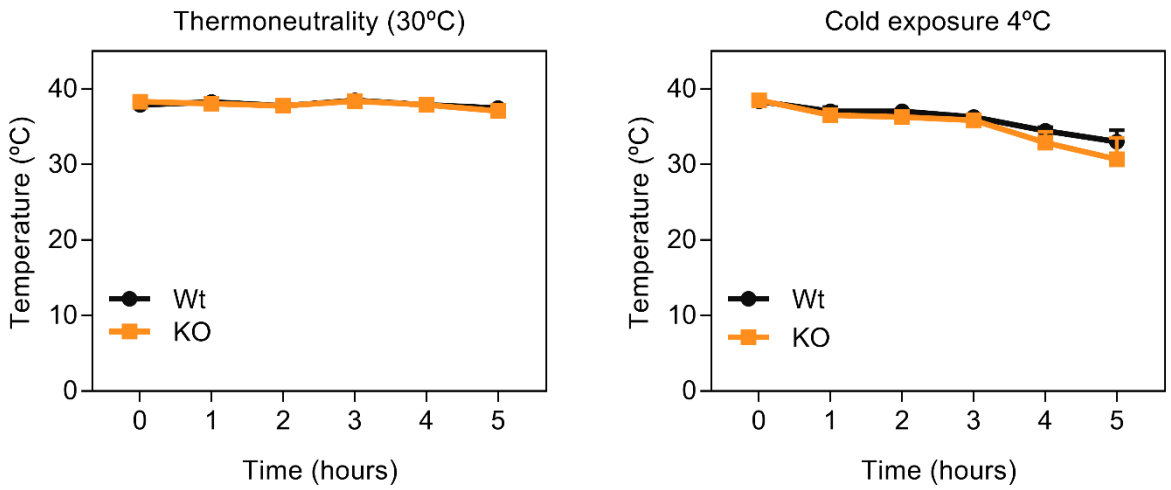

Figure 4.42. Body core temperature monitoring at 30ºC and 4ºC. A) Body temperature monitoring in RORγ1-FAT-KO and Wt mice at 30ºC and B) during cold exposure at 4ºC, after two weeks acclimatized at 30ºC. Mice were individually caged and exposed at 4ºC during 5h. Body temperature was measured every hour by using a digital thermometer with a rectal probe. Results are expressed as mean ± SEM (n=4-5 animals /group).

4.6.3 Tissue weight changes after cold exposure

After cold exposure, mice were weighted to determine possible effects of cold exposure on body weight (Figure 4.43). As expected, both Wt and RORγ-FAT-KO mice exposed at 4ºC had significant less weight compared to mice that had been kept at 30ºC, although no differences were found between genotypes.

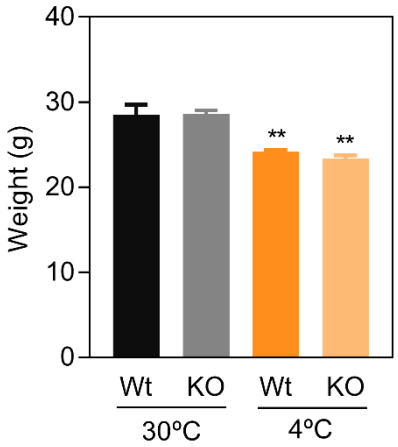

Figure 4.43. Body weight of RORγ-FAT-KO and Wt mice kept at thermoneutrality or after cold exposure. RORγ-FAT-KO and Wt mice were exposed at 4ºC for 5h after being first acclimated at thermoneutrality (30ºC) for two weeks. Results are expressed as mean ± SEM (n=4-5 animals/group). * Indicates statistical significance in the comparison between environmental temperatures. ** P≤0.01.

Consistent with the reduction in body weight, we observed a reduction in the weight of almost all tissues extracted in animals exposed to cold (Figure 4.44). The decrease was notably important in adipose tissues, both BAT and WAT, and a milder decrease was also observed in liver or muscle. This decrease in their weight, especially in adipose tissue, is consistent with the mobilization of TAG in these tissues to sustain thermogenesis by BAT. However, no differences in the weight of tissues were seen between genotypes, suggesting that the mobilization of lipids is not significantly altered by the lack of RORγ.

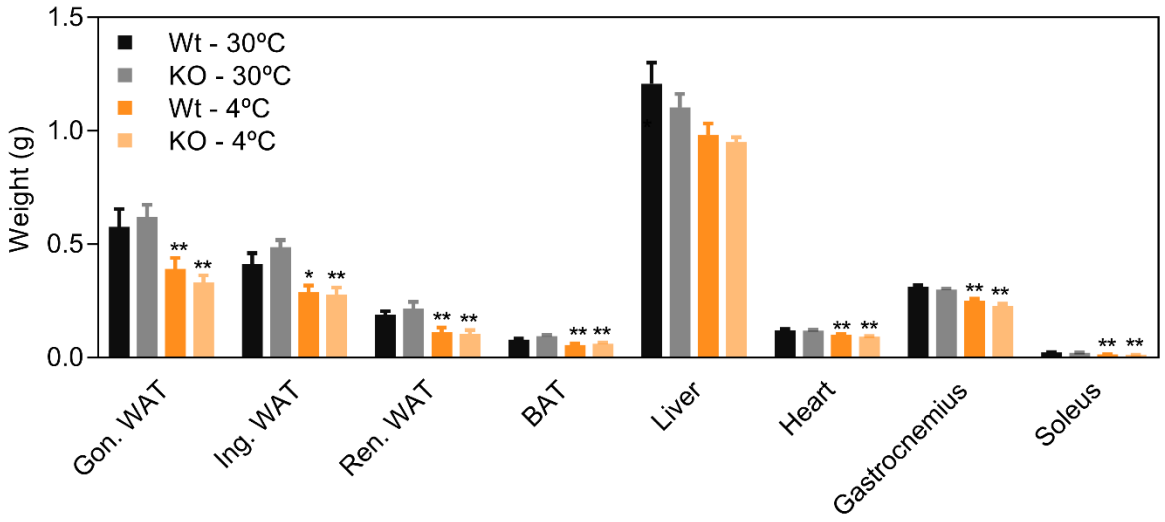

Figure 4.44. Tissue weight from RORγ-FAT-KO and Wt mice kept at 30ºC or after 5h at 4ºC. Results are expressed as mean ± SEM (n=4-5 animals/group). * Indicates statistical significance in the comparison between environmental temperatures. * P≤0.05; ** P≤0.01.

4.6.4 Histological changes in brown adipose tissue

We also examined histological sections of BAT. Brown adipocytes from both Wt and RORγ-FAT-KO mice kept at thermoneutrality (30ºC) similarly adopt a white adipocyte-like morphology and accumulate large amounts of TAG. On the other hand, mice exposed at 4ºC had less lipid content in brown adipocytes compared to the ones that stayed at 30ºC because TAG were mobilized to provide substrates for thermogenesis. However, we did not observe any differences in BAT morphology between genotypes in mice exposed to the same environmental temperature (Figure 4.45), indicating that, when exposed at 4ºC, RORγ-FAT-KO mice mobilized TAG accumulated within brown adipocytes as efficiently as their Wt littermates.

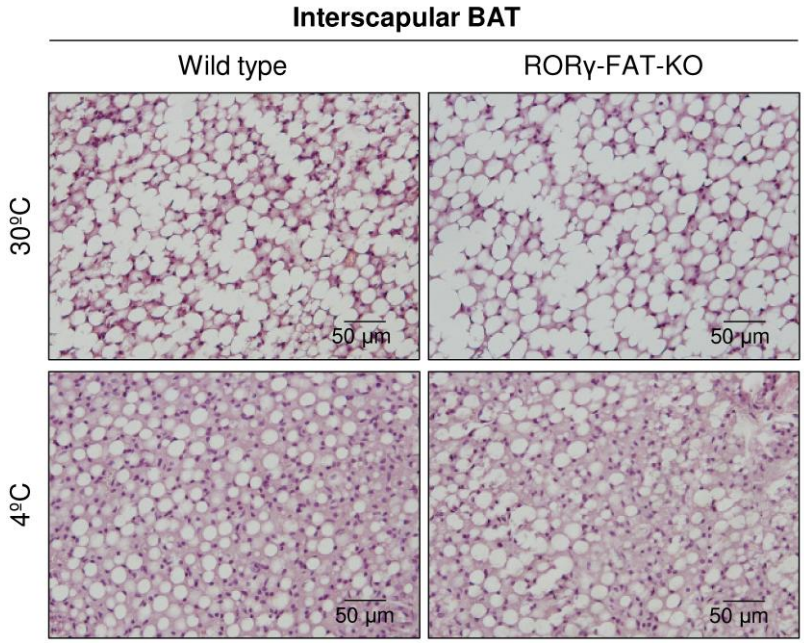

Figure 4.45. Histological changes in interscapular BAT in Wt and RORγ-FAT-KO mice stayed at 30ºC and 4ºC. Histological sections from 8-week old male mice fed a chow diet and housed at 30ºC or 4ºC were stained with hematoxylin/eosin.

4.6.5 Changes in gene expression in brown adipose tissue of RORγ-FAT-KO mice in response to cold

We first assessed *Rorc* mRNA levels by qPCR in Wt and RORγ-FAT-KO mice stayed at 30ºC and exposed to cold (4ºC). Wt mice exposed at 4ºC did not show a significant reduction of *Rorc* mRNA levels compared to 30ºC (Figure 4.46). On the other hand, as expected (Figure 4.15, section 4.3.2) RORγ-FAT-KO mice showed a very low levels of *Rorc* mRNA in BAT, which is consistent with an effective knockout of the *Rorc* gene in BAT.

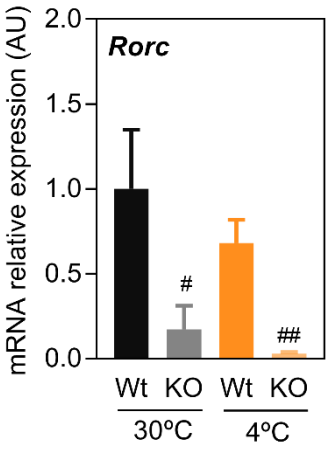

Figure 4.46. mRNA expression levels of *Rorc* expression in BAT of RORγ-FAT-KO and Wt mice kept at 30ºC or exposed for 5h at 4ºC. mRNA levels were determined by qPCR. Results are expressed as mean ± SEM (n=4-5 animals/group). * Indicates statistical significance in the comparison between environmental temperature; # indicates statistical significance between Wt and RORγ-FAT-KO. *,# P≤0.05; **,## P≤0.01.

Furthermore, we also studied the expression of genes that play a critical role in BAT thermogenesis (Figure 4.47A). mRNA levels of *Ucp1*, *Ppargc1a* and *iodothyronine deiodinase 2* (*Dio2*) dramatically increased when mice were exposed at 4ºC, although this induction was similar in Wt and RORγ-FAT-KO mice. Likewise, protein levels of UCP1 were mildly increased in Wt mice upon cold exposure, although, somehow surprisingly, the induction in RORγ-FAT-KO mice was higher (Figure 4.47B and Figure 4.47C).

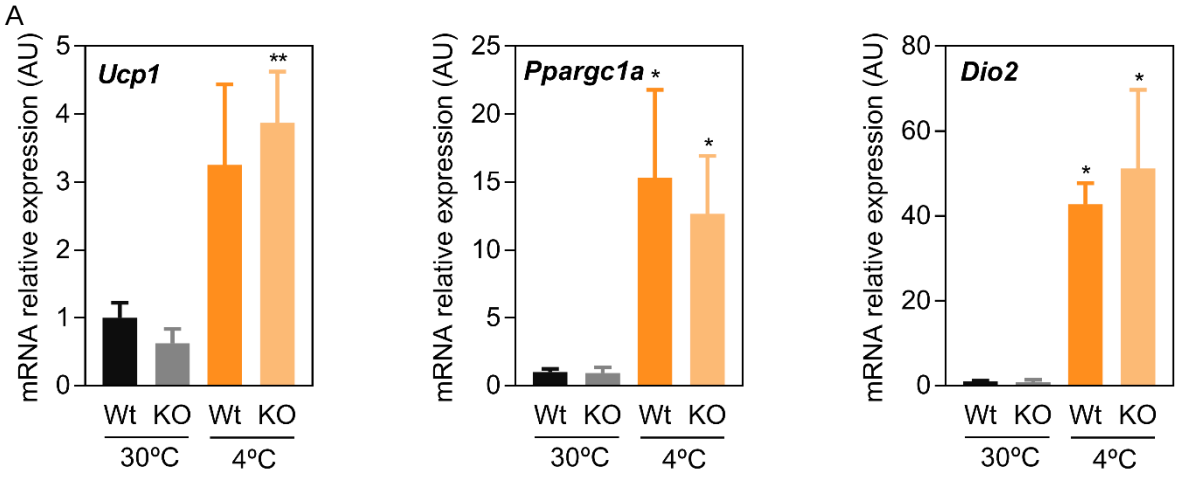

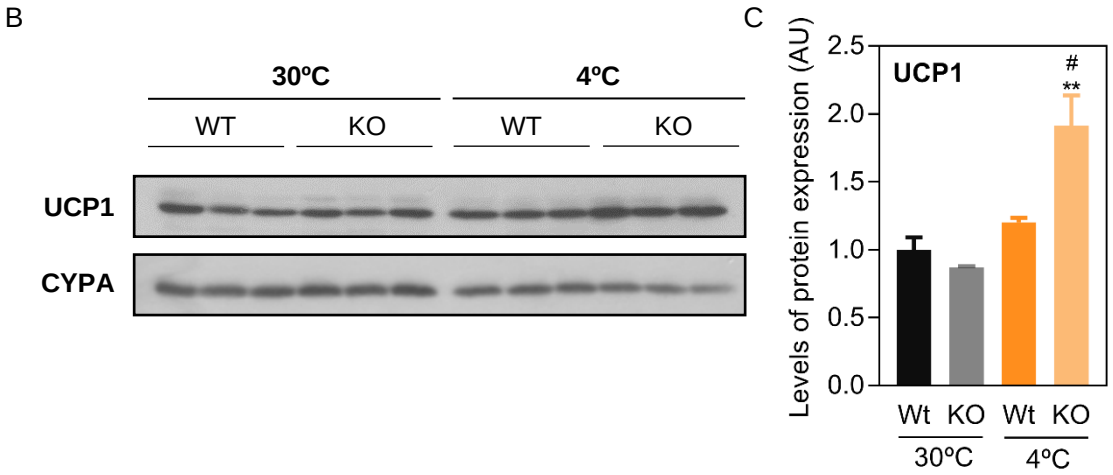

Figure 4.47. Expression of thermogenic genes in BAT of RORγ1-FAT-KO and Wt mice acclimated at 30ºC or exposed to 4ºC. A) mRNA expression levels of *Ucp1*, *Dio2* and *Ppargc1a* genes in BAT of Wt and RORγ-FAT-KO mice kept at 30ºC or exposed for 5h at 4ºC. mRNA levels were determined by qPCR. B) Western blot analysis of UCP1 protein expression in BAT of Wt and RORγ-FAT-KO mice kept at 30ºC or exposed for 5h at 4ºC. Detection of CYPA protein was used as a loading control. (C) Quantification UCP1 protein levels from western blot. Results are expressed as mean ± SEM (n=3-5 animals/group). * Indicates statistical significance in the comparison between environmental temperatures ; # indicates statistical significance between Wt and RORγ-FAT-KO * P≤0.05; ** P≤ 0.01.

► 4.7 Effect of calorie restriction and loss of RORγ on energy balance and glucose homeostasis

Since CR is known for having positive effects on glucose homeostasis, specifically improving whole-body glucose tolerance and insulin sensitivity, we aimed at studying how lack of RORγ in adipose tissues affected energy balance and glucose homeostasis in a context of DIO and CR.

4.7.1 Effects of lack of adipose RORγ on body weight and food intake

Regardless their genotype, daily ingestion of mice fed AL did not significantly change over the time, being stabilized at 3 grams/day/animal (Figure 4.48A). As expected, mice fed AL with a HFD rapidly gained weight and became obese, while their littermates fed with the same diet rich in fat but subjected to CR remained lean throughout the experimental period (Figure 4.48B). However, no differences were detected in body weight between genotypes.

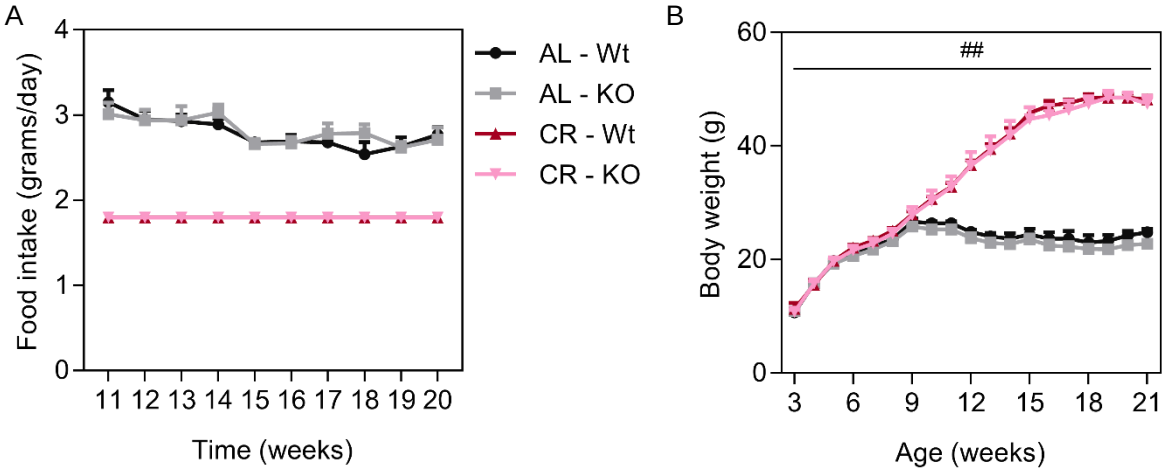

Figure 4.48. Body weight and food intake of mice fed AL or subjected to 40% CR. At the age of 7 weeks, individually-caged Wt and RORγ-FAT-KO mice started receiving a HFD and one week later they were randomly assigned to AL or CR groups. CR mice received 60% of the food eaten by AL animals for a period of 12 weeks. A)

Evolution of food intake of Wt and RORγ-FAT-KO mice fed AL or CR. B) Body weight of Wt and RORγ-FAT-KO mice was measured weekly thought the duration of the experiment. Results are expressed as mean ± SEM (n=5 animals/group). # Indicates statistical difference of the comparison between AL and CR groups. AL, *ad libitum*; CR, calorie restriction. ## $P \leq 0.01$.

Different tissues were obtained and weighed after euthanasia. Similar to previous observations, tissue weights of mice subjected to CR were lower than in AL fed mice, with adipose tissues and liver exhibiting a strong reduction, ranging from 17% to 30%. However, consistent with the absence of differences in body weight and food intake, RORγ-FAT-KO mice did not exhibit differences in the weight of major fat depots or liver compared to Wt littermates under both nutritional conditions (Figure 4.49). These results support the idea that CR reduces body weight and decreases fat mass, independently of adipose RORγ.

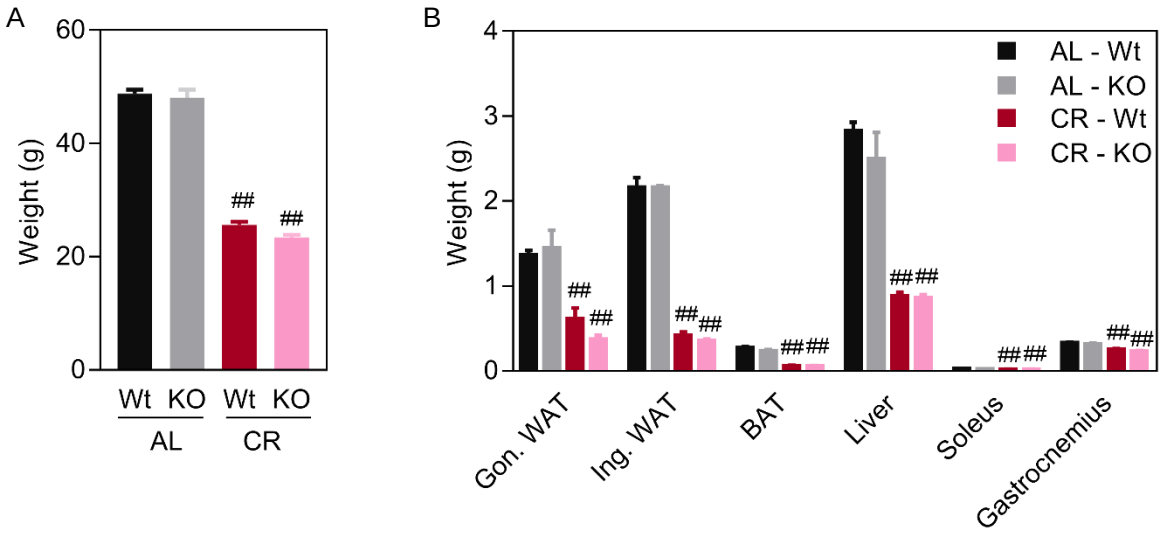

Figure 4.49. Body weight and tissue weight of mice fed AL or subjected to 40% CR. At the age of 7 weeks, individually-caged Wt and RORγ-FAT-KO mice started receiving a HFD and one week later they were randomly assigned to AL or CR groups. CR mice received 60% of the food eaten by AL animals for a period of 12 weeks. A) Mean of mice body weight after euthanasia at the age of 21 weeks. B) Tissue weight after euthanasia at the age of 21 weeks. Results are expressed as mean ± SEM (n=5 animals/group). # Indicates statistical difference of the comparison between AL and CR groups. AL, *ad libitum*; CR, calorie restriction. ## $P \leq 0.01$.

4.7.2 Morphological analysis of adipose tissues

To complete macroscopic analysis, histological microscopic analysis of gonadal WAT, inguinal WAT, liver and BAT was also performed. As expected, major differences were observed when comparing adipose tissues of AL fed mice or subjected to CR. Both inguinal and gonadal WAT from mice fed AL contained bigger adipocytes than WAT of mice subjected to CR (Figure 4.50). Remarkably, gonadal WAT showed greater inflammatory infiltrate that formed the typical CLS. On the other hand, histological analysis of WAT from CR mice revealed smaller adipocytes and a clear reduction in the number and size of CLS. However, WAT appearance was similar in Wt and RORγ-FAT-KO mice. Moreover, although it has recently been reported that CR induces browning in WAT depots (170), particularly in the inguinal WAT depot, we did not observe cells with the characteristic morphology of brown adipocytes in WAT of Wt or RORγ-FAT-KO mice subjected to CR.

Liver and BAT showed a similar pattern as WAT, exhibiting an excessive lipid accumulation in AL fed animals compared to CR. Nevertheless, no differences were observed between Wt and RORγ-FAT-KO mice (Figure 4.51 and Figure 4.52).

Hence, histological analysis supported the idea that CR had a strong effect in fat-related tissues, not only decreasing adiposity but also reducing adipocytes size. However, no differences were found between Wt and RORγ-FAT-KO mice.

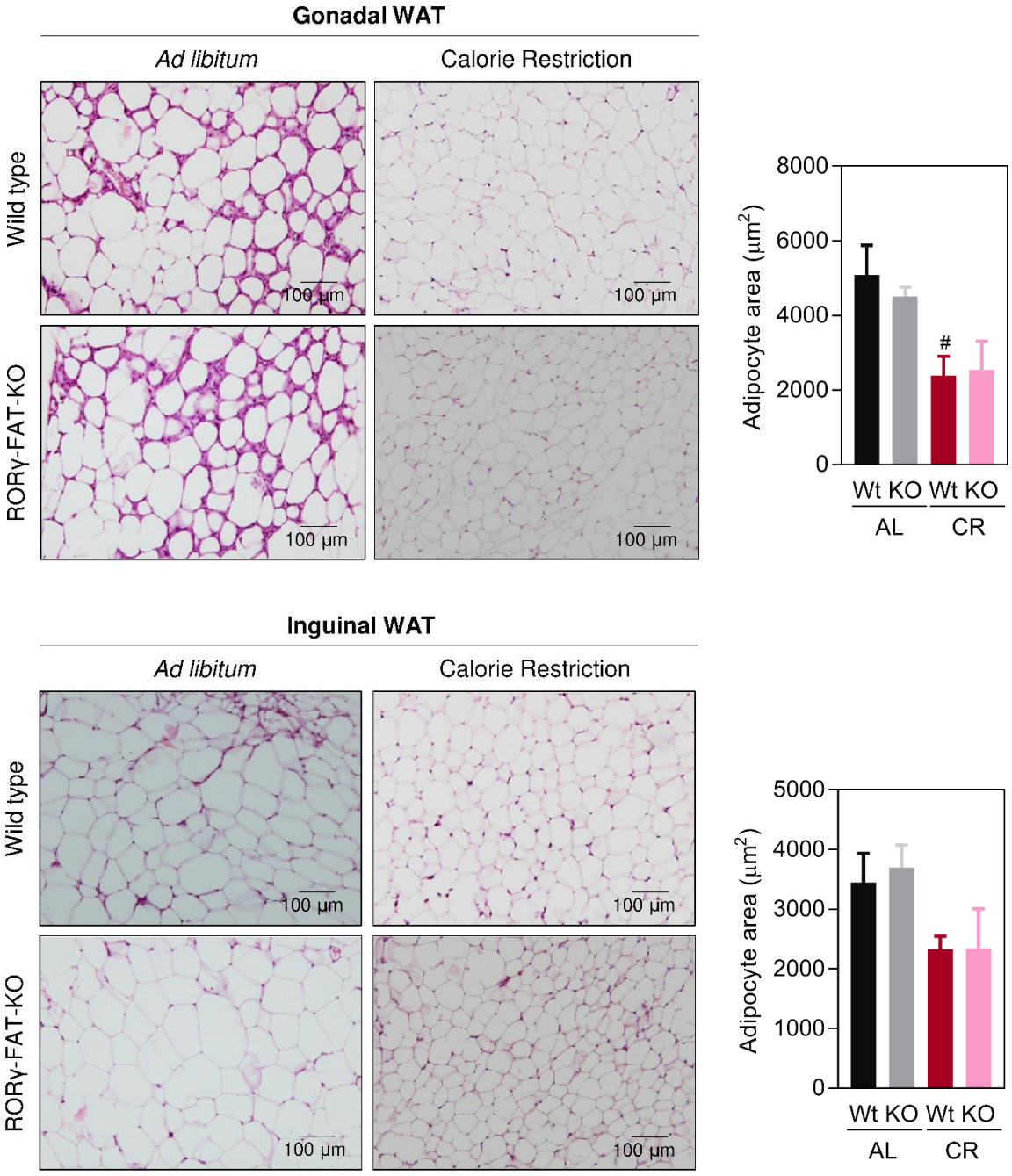

Figure 4.50. Histological analysis and adipocyte area quantification of gonadal WAT and inguinal WAT from Wt and RORγ-FAT-KO mice. Histological sections from 21-week old male mice fed AL or subjected to a CR with a HFD were stained with hematoxylin/eosin. Mean adipocyte area was measured using pictures of different randomly selected fields of tissue sections from three animals of each experimental group. # Indicates statistical difference of the comparison between AL and CR groups. AL, *ad libitum*; CR, calorie restriction. # $P \leq 0.05$.

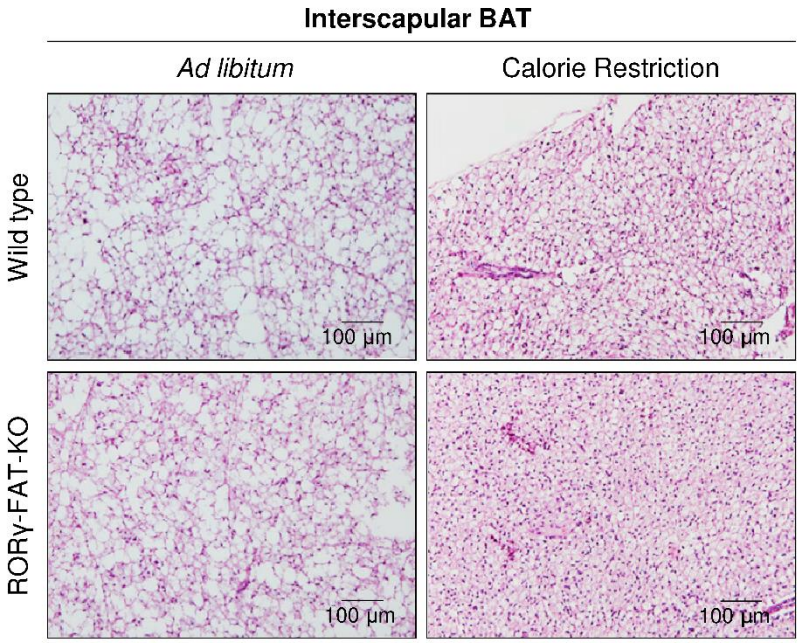

Figure 4.51. Histological analysis of interscapular BAT from Wt and RORγ-FAT-KO mice. Histological sections from 21-week old male mice fed AL or subjected to a CR with a HFD were stained with hematoxylin/eosin. AL, *ad libitum*; CR, calorie restriction.

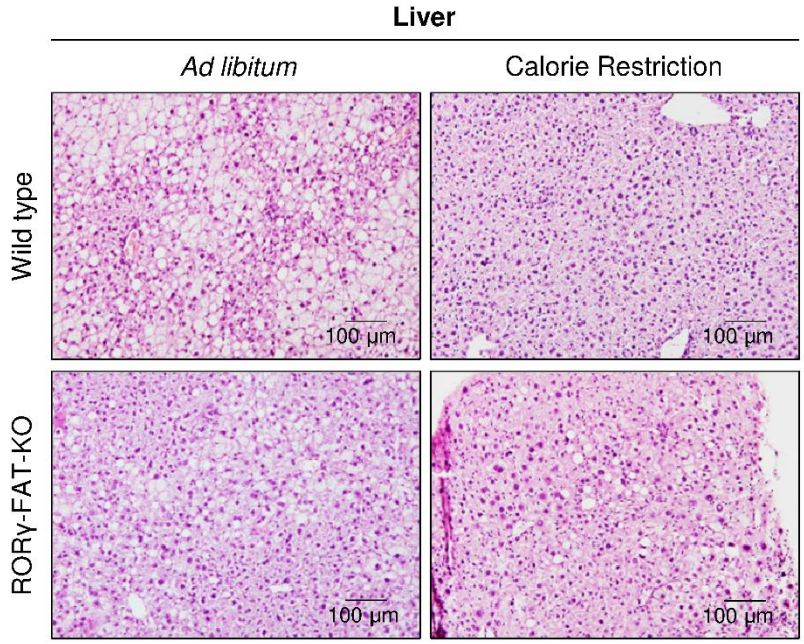

Figure 4.52. Histological analysis of liver from Wt and RORγ-FAT-KO mice. Histological sections from 21-week old male mice fed AL or subjected to a CR with a HFD were stained with hematoxylin/eosin. AL, *ad libitum*; CR, calorie restriction.

4.7.3 Evaluation of glucose homeostasis in RORγ-FAT-KO mice

As RORγ has been associated with altered glucose homeostasis and its expression is increased by CR, we aimed at determining how lack of RORγ in adipocytes affects glucose homeostasis in a model of DIO and its amelioration upon CR. As expected, the high glycemic levels observed in Wt mice fed AL with a HFD were ameliorated by CR. However, lack of RORγ did not affect basal glucose blood levels in each of the nutritional conditions. GTT and ITT were performed to test whole body glucose tolerance and insulin sensitivity, respectively (Figure 4.53). During the course of a GTT, an increment in glucose levels and more difficulties to return to normal levels was observed in AL mice, whereas CR group were able to clear glucose faster (Figure 4.53A), indicating that AL mice were more glucose intolerant that those subjected to CR. However, no differences were detected between genotypes. On the other hand, when injected with insulin, AL mice slowly decreased glucose levels, while CR mice rapidly clear glucose from circulation (Figure 4.53B). Again, no differences were observed between Wt and RORγ-FAT-KO mice. Overall, these results suggest that RORγ depletion in adipocytes does not have an overt effect in regulating whole body glucose homeostasis.

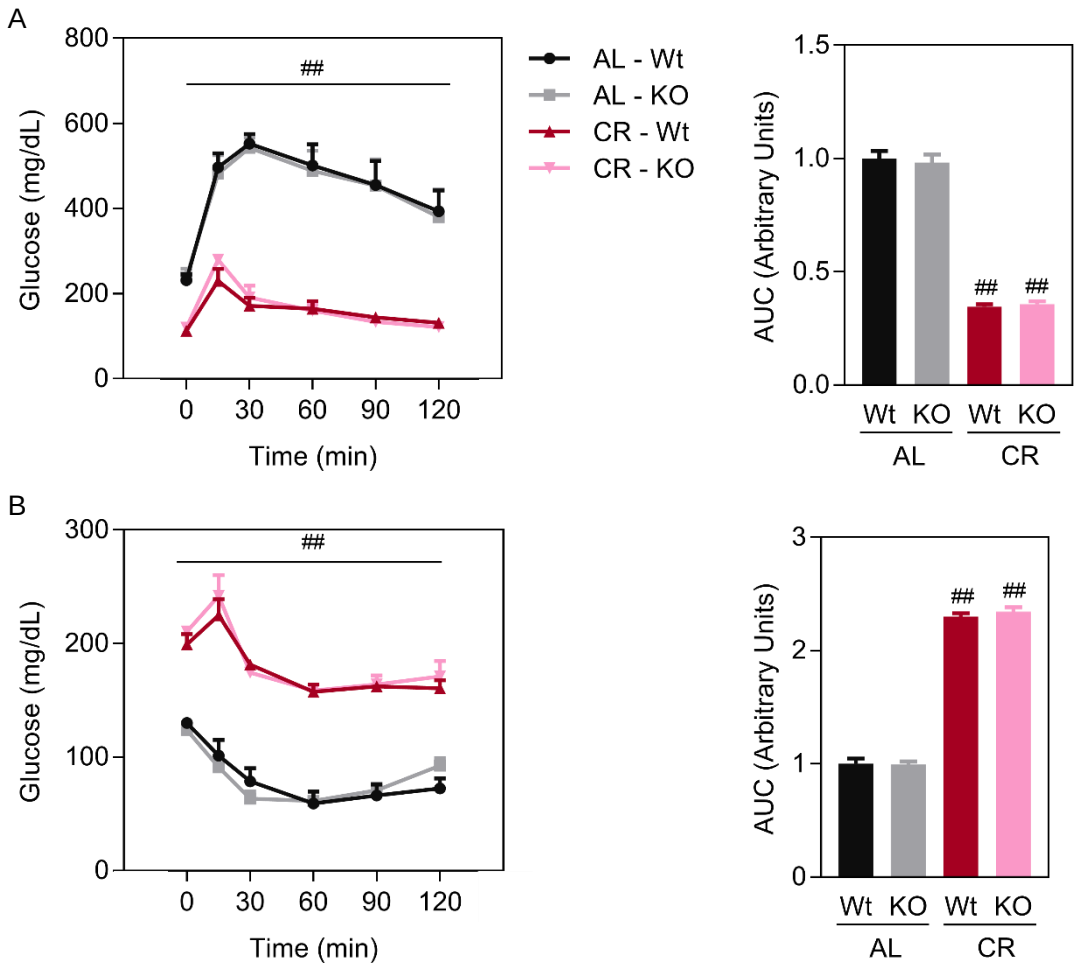

Figure 4.53. Analysis of whole body glucose homeostasis of Wt and RORγ-FAT-KO mice fed AL or subjected to CR. Glucose tolerance test (A) and insulin tolerance test (B) were performed after 6-h of fasting. Blood glucose levels were measured at 0, 15, 30, 60, 90 and 120 min after an intraperitoneal injection of glucose (2g/kg) or insulin (0.9 U/kg), respectively. Glucose tolerance and insulin sensitivity was estimated as the area under the curve (AUC) of the glucose excursion during GTT and ITT, respectively.Results are shown as mean ± SEM of 5 animals/group. # Indicates statistical differences of the comparison between AL and CR groups. AL, *ad libitum*; CR, calorie restriction. ## $P \leq 0.01$.

4.7.4 Evaluation of serum parameters

It has been reported that prolonged HFD feeding results in obesity associated with hyperlipidemia, hyperinsulinemia and glucose intolerance (267), which are improved by CR. Therefore, several biochemical parameters were determined to identify metabolic changes caused by CR or the loss of RORγ expression in adipocytes.

Consistent with previous data from ITT showing that mice subjected to CR were more sensitive to insulin, we found that basal serum insulin levels in both Wt and RORγ-FAT-KO mice were significantly lower in CR mice than in their AL fed counterparts, which show hyperinsulinemia. However, there were not any differences between genotypes. Similarly, cholesterol serum concentration was found decreased upon CR, whereas TAG and NEFA were not changed by diet or genotype. Leptin levels appeared dramatically decreased upon CR in both Wt and RORγ-FAT-KO mice, which is proportional to the amount of adipose tissue. However, adiponectin and resistin levels were not changed by the genotype or in response to CR, despite the dramatic changes observed in glucose homeostasis by this nutritional intervention (Table 4.4). Taking together, both Wt and RORγ-FAT-KO mice subjected to CR presented a healthier metabolic status, regardless their genotype.

	Ad libitum		**Calorie Restriction**	
Parameter	Wt	RORγ-FAT-KO	Wt	RORγ-FAT-KO
Glucose**, mg/dL**	231.8 ± 13.5	238.4 ± 20.5	112.8 ± 4.1	120.4 ± 3.8
TAG**, mg/dL**	57.87 ± 3.37	61.12 ± 1.70	52.71 ± 2.35	51.99 ± 1.38
FFA**, mg/dL**	0.39 ± 0.16	0.62 ± 0.05	0.75 ± 0.13	0.58 ± 0.02
Cholesterol**, mg/dL**	186.92 ± 10.89	163.72 ± 7.4	148.0 ± 9.48	142.93 ± 3.82
Insulin**, ng/mL**	4.48 ± 0.40	5.50 ± 1.20	0.37 ± 0.09$^{\#\#}$	0.41 ± 0.12$^{\#\#}$
Leptin**, ng/mL**	71.22 ± 5.07	65.73 ± 5.15	12.08 ± 1.70$^{\#\#}$	10.68 ± 1.24$^{\#\#}$
Adiponectin**, µg/mL**	12.03 ± 0.06	11.09 ± 0.53	11.83 ± 0.34	11.40 ± 0.37
Resistin**, ng/mL**	66.48 ± 73.87	78.40 ± 10.42	70.27 ± 31.74	66.73 ± 29.26

Table 4.4. Analysis of serum metabolites and hormones of mice fed AL with HFD or subjected to CR. Serum was collected via tail cut after 5-h of fasting. TAG and total cholesterol were determined using a commercial kit based on the Trinder colorimetric method. FFA were measured colorimetrically with the ACS-ACOD method. Insulin, leptin, adiponectin and resistin were determined in serum by immunoassay. Results are expressed as mean ± SEM (n=5 animals/group). # Indicates statistical differences of the comparison between AL and CR groups. ## $P \leq 0.01$.

DISCUSSION

► 5.1 Beneficial effects of calorie restriction in white adipose tissue

The incidence of obesity and its comorbidities is alarmingly increasing each year in the modern society, principally due to changes in lifestyle that impose increased calorie intake and reduced physical activity (268). Obesity is characterized by an altered function of WAT, which is one of the largest organs in the human body and plays a key role in the control of energy balance and glucose metabolism. Under a context of obesity, the functional alteration of WAT has been associated with dysregulated lipolysis, reduced mitochondrial mass and inflammation. Lipotoxicity that results from high levels of fatty acids, either from diet or TAG lipolysis, results in an increased production of pro-inflammatory cytokines by adipocytes, apoptosis and necrosis of these cells. This inflammatory situation, which persists in time, is considered to be a major contributing factor to the development of IR in WAT and other peripheral tissues through the activation of the JNK and NFκB pathways (8).

Despite intense research efforts, currently, there is not an optimal and effective pharmacological treatment for obesity and its comorbidities. In cases of extreme obesity, bariatric surgery is conducted on patients as the last option for the treatment of the disease. For these reasons, it is very important to find new pharmacological targets to treat obesity. In this regard, CR has been widely proved not only to improve obesity, but also to ameliorate IR, T2D and many other diseases like Alzheimer, Parkinson or cancer. Moreover, CR also increases lifespan in a wide range of organisms, including mammals (161,163–165,269). Given the positive effects of CR on health, it is important to understand how CR exerts its beneficial effects as a way to find novel therapeutic targets that mimic CR to treat metabolic disorders and other diseases. Hence, considering the key role of WAT in the control of energy balance and glucose homeostasis and the effects of CR on health, in this doctoral thesis we have focused on exploring the processes and the molecular mechanisms modulated by CR in WAT function.

CR is defined as 30-50% reduction in calorie intake. Numerous types and regimes of CR have been used in both animal and human studies. Classical or continuous CR requires consistent daily reduction in energy intake, between 30-50%. Food is provided once daily or in portions throughout the week. Although it has been well proved that continuous CR improves metabolic health associated with aging, many patients find difficult to adhere to prolonged CR (270) because food intake is continuously limited. Therefore, alternative feeding methods have been developed to provide similar benefits as continuous CR. Intermittent CR or *intermittent fasting* (IF) has gained attraction in the last years. IF is a periodic energy restriction which implies eating patterns in which fasting periods are followed by periods of AL feeding (271). There are different patterns of IF, the most common ones include alternate-day fasting, with 3 days of feeding interspaced with 4 days of fasting; 5:2 cycle, which consists of 5 days of feeding followed by 2 consecutive days of fasting; time-restricted feeding, where the feeding window is limited to 4 h or 8 h over a 24-h period; and the fasting mimicking diet, which is comprised of 4 days of low caloric intake followed by 10 days of AL feeding (272).

It is important to point out that studying CR in animal models has some limitations. When studying the impact of CR in rodents, it is intrinsically introduced a fasting time. Animals are routinely fed once a day. When the food is available, animals rapidly eat within 2h, despite 24h food availability (273). As the level of CR is higher, the faster the food is consumed and, consequently, a longer daily fasting time (16-20h) (273,274).

For the CR experiments conducted in this thesis, CR mice received 60% of the food eaten by AL animals during a 12 week period. The food was provided every evening. Hence, the CR regime used mimics a continuous CR, but with the intrinsic time-restricted feeding that implies. Anyway, both continuous and intermittent CR appear to affect similar cellular processes and to yield comparable results in terms of health (272).

Moreover, it is important to consider that CR can be applied to either healthy individuals or individuals that have some pathological condition. In already healthy individuals, although is possible to observe changes in some metabolic parameters, such as fat accumulation or body weight, a further improvement in health is not observed. However, in most of the organisms studied, long term CR does impact lifespan (175,176). In our studies, we used a pathological experimental context. To mimic the obesogenic nutritional context of modern society in humans, all experimental groups were fed with a diet rich in fat (60% Kcal from fat), which induces obesity and IR (275). It has been proved that feeding C57BL6/J mice with a HFD for a period of 3 weeks is sufficient to develop IR in skeletal muscle, WAT and liver (276). Consistent with this, we found mice fed with a HFD that have free access to diet become rapidly obese and glucose intolerant. Contrarily, we observed that although they are fed with a HFD, CR mice remain leaner and are protected from the deleterious effects of a HFD, remaining insulin sensitive and glucose tolerant. This is consistent with numerous studies that report that CR-fed mice exhibit a significant improvement in insulin sensitivity, independent of diet composition (274,277). Studies conducted on human and rodent models show that both intermittent CR and continuous CR improve glucose homeostasis (164,274,278).

As CR exerts positive effects, it is interesting to unravel the processes modulated by CR in WAT responsible for the improvement of health. In our case, we focused on the prevention of obesity and IR. On the view of the high number of genes (1886) differentially regulated by CR, it is evident that CR has a profound effect on WAT. The gene set enrichment study showed that CR in Wt mice alters the expression of genes related to three major cellular processes: mitochondrial function, ECM remodelling and immune function. As expected, these findings are similar to the ones found in a previous study performed in our laboratory, in which we also compared the gene expression profile in inguinal WAT from Wt animals fed AL with a HFD (45% Kcal from fat) or subjected to CR with the same diet (182). Indeed, the functional analysis of the dysregulated genes revealed a great similarity in the GO categories found in both studies, although subtle differences were observed.

We found that CR increases the expression of genes related to mitochondrial function and biogenesis (182). However, in the present study, the number of the genes included in mitochondrial-related GO categories, as well as the statistical power achieved, was not of the same degree as in the previous study performed (182). In fact, in the present study, GO categories related with mitochondria only appear as differentially regulated in WAT of CR mice when a gene enrichment analysis was performed with the less stringent DAVID Bioinformatics tool or GSEA using a pre-ranked list of genes. On the other hand, in both studies, gene-expression profiling analysis identified genes related to ECM remodeling and immune system inflammatory response among the gene networks dysregulated in WAT in response to CR. However, whereas in the study of Pardo *et al.* the GO categories related to ECM and immune system were over-represented only among the down-regulated genes in WAT of CR mice, meaning that CR reduced the accumulation of ECM proteins and alleviated inflammation (182), in the present study some of the genes included in the GO categories related to the immune function appeared up-regulated, while others were

down-regulated. Although this may appear contradictory, it is interesting to highlight that immune system-related GO categories dysregulated in response to CR followed a specific pattern, with GO categories related to adaptive immune cells being up-regulated by CR and those related to innate immune cells being down-regulated. This differential expression behavior of genes related to the immune function is consistent with the immunoregulatory effects exerted by CR, in which the number of anti-inflammatory Treg cells is increased in WAT, while the number of macrophages is reduced (169). This expression pattern and composition of the immune compartment in WAT is the opposite to the one observed in obesity, where there is an increase of macrophages as well as an alteration in the balance between pro-inflammatory and suppressive T cells responses in WAT, with Treg cells reducing their number and losing their phenotypic identity and function (279).

Although both microarray analysis have been performed in inguinal WAT of mice subjected to a 40% of CR for 12 weeks and fed with a HFD, the subtle differences in the gene expression profiles observed between the two studies could be attributed to some variations in their experimental set up. On the one hand, the diet used in first study contained 45% of calories from fat (182), while the one used in this study contained 60% of calories from fat. Despite all mice used were from C57BL/6 inbred strain, minor differences in the genetic background between mice of the two experiments could exist because they belong to different colonies. Additionally, animals were bred in different animal facilities and, consequently, the minor environmental changes associated with this could have also contributed to the differential outcome of the two studies.

Once identified the main cellular processes regulated by CR in WAT, the question is how relevant each of these processes is to the improvement of health mediated by CR? Increased mitochondrial mass and oxidative function have been proposed as main determinants of whole-body insulin sensitivity. This hypothesis is based on numerous studies showing that WAT, and also skeletal muscle, of obese insulin resistant mouse models or humans subjects have lower mitochondrial mass, oxidative capacity and/or expression of mitochondrial genes (reviewed in (8)). It has been postulated that the impaired fatty acid oxidation capacity of the tissues from obese individuals would favor the accumulation of multiple lipid species and induce lipotoxicty (18), a well-known trigger of IR. However, few studies argue against impaired mitochondrial biogenesis/function as a mechanism of IR. For example, multiple engineered mouse models with a deficiency in muscle or WAT mitochondrial biogenesis do not exhibit IR, even when fed a HFD (182,183,280). Still, an increase in mitochondrial biogenesis and oxidative capacity has been observed in response to CR. Therefore, it is possible to speculate that the increase in mitochondrial mass and oxidative capacity of WAT (or other tissues) is required for the improvement exerted by CR on glucose homeostasis. However, a previous work from our laboratory using a mouse model devoid of the coactivators PGC-1α and PGC-1β specifically in adipocytes demonstrated that the induction of mitochondrial mass and mitochondrial oxidative function in response to CR mostly depends on PGC-1s, but, more importantly, provided evidences that increased mitochondrial oxidative function in WAT is not required for the beneficial effects of CR on glucose homeostasis (182). In the same line, a study using muscle-specific PGC-1α KO mice presented a failure to increase mitochondrial mass, but these mice were able to respond to CR improving glucose tolerance and insulin sensitivity as their Wt counterparts (183). Hence, the increase of mitochondrial biogenesis observed could be interpreted as a metabolic adaptation to facilitate oxidation of fatty acids, which are the main substrate for oxidative phosphorylation under CR conditions.

As mentioned, our gene expression profiling in the present study also identified genes related to ECM remodeling as down regulated by CR in WAT. ECM remodeling seems to be required for a healthy WAT expansion and adaptation to changing nutritional conditions (281). Fibrosis, defined as an excess of deposition of ECM components such as collagens, elastin and fibronectin, is a tissue response to chronic inflammation. In fact, in obesity, the excessive lipid accumulation in adipocytes provokes fibrosis, among other effects (282). Conversely, is has been demonstrated that long-term CR ameliorates fibrosis in WAT (283). Of note, changes of ECM have been associated with metabolic diseases. For instance, it has been shown that increased expression in WAT of ECM genes, such as *Collagen Type VI Alpha 3 Chain* (*COL6A3*) and *matrix metalloproteinase 9* (*MMP-9*), associates with increased body mass and tissue inflammation in humans (284,285). In addition, studies *in vitro* have shown that preadipocytes in contact with inflammatory cells, such as macrophages, produce high levels of selective fibrotic molecules, including collagen (282,286). It has also been reported that mice over-expressing endotrophin, which is a cleavage product of COL6A3, specifically in adipocytes develop WAT fibrosis and inflammation during consumption of a HFD (287). Otherwise, obese COL6A3 KO mice show an improvement in insulin sensitivity (288). Taking into account that this fibrotic process in WAT may be related to metabolic complications such as systemic IR, we can suspect that CR may improve IR, at least in part, by downregulating the expression of genes encoding for ECM proteins and reducing fibrosis. This is an aspect that we have not addressed in our study but that would need to be considered for further studies.

Our study shows that there is an increase in the immune infiltrate of WAT in response to HFD, which was reversed by CR. The enrichment of immune system GO categories in WAT of mice subjected to CR is not surprising, since it is well known that both obesity and CR induce dramatic changes in WAT resident immune system cells. WAT contains a unique immunological compartment that is important for physiologic responses to fasting and feeding, regulation of body weight and thermogenesis. Recent studies show that WAT remodeling due to inflammation is a reversible phenomenon closely associated with insulin sensitivity and adiposity. It is well established that in WAT of obese individuals the chronic pro-inflammatory milieu causes IR, whereas the anti-inflammatory response elicited by CR is associated with a preservation of insulin sensitivity (167–169,289).

Consistent with the changes in resident immune cell populations within WAT, histological sections of the animals fed AL with a HFD not only contained bigger adipocytes in both inguinal and gonadal WAT than mice fed a chow diet or subjected to CR, but also they showed a dramatic increase in the immune infiltrate, particularly in the gonadal depot. Flow cytometry quantification of this immune infiltrate, in both inguinal and gonadal WAT depots, confirmed the histological observations and demonstrated that WAT of HFD mice contains a significantly high number of immune cells ($CD45^+$ cells) compared to animals subjected to CR. The increased recruitment of immune cells in WAT of obese mice, particularly of macrophages, is the result of the noxious effects that excessive calorie intake has on WAT mass and function. Certainly, an increased caloric intake results in hypertrophic and hyperplastic WAT expansion, which is an adaptation of WAT to the positive energy balance, increasing its storage capacity (290). Activation of hypertrophic adipocytes leads to the activation of stress signaling pathways, such as JNK/IKKβ pathway, which results in an increase of cell death and an inflammatory response in WAT. As a result, more immune cells are recruited leading to a chronic low-grade inflammation, characterized by an enhanced macrophage polarization toward M1 pro-inflammatory type and augmented secretion of inflammatory cytokines that contribute to

the impairment of insulin signaling (291,292). Contrary to what we observed in AL mice, flow cytometry quantification of immune cells ($CD45^+$ cells) in WAT of mice subjected to CR showed that both inguinal and gonadal depots exhibited a significant reduction of immune infiltrate. These data are in agreement with several studies in rodent and humans reporting that CR decreases the extent of WAT inflammation (283,289,293).

Most of the studies conducted by other authors coincide in describing an increase in macrophages, which not only greatly expand in number but also shift their phenotype to classically activated M1 macrophages in obesity. However, few seminal studies have shown that these changes in the immune infiltrate are not exclusively the result of changes in macrophages recruitment, but other relevant pro-inflammatory immune cells (like neutrophils, Th1 cells, B cells and Tc cells) also change their number in WAT in response to HFD and play a relevant role in the onset of IR and other comorbidities (294–296). By contrast, few studies reported that CR promotes the recruitment of anti-inflammatory immune cells to WAT, like M2 macrophages, eosinophils, Th2 and Treg cells, which secrete anti-inflammatory cytokines and maintain an active crosstalk with adipocytes in order to keep lipid homeostasis in normal states (167,169). Consistent with these reports, we found that CR mice exhibit an anti-inflammatory immune infiltrate profile. Indeed, myeloid cells and macrophages dramatically decreased under CR, especially in gonadal depot. The differences exhibited by the subcutaneous and visceral WAT depots with regard to resident macrophages are in agreement with the data published in other studies, which describe higher number of macrophages residing in visceral WAT compared to subcutaneous WAT, both in humans and rodents (297–299). Moreover, although it is well accepted that CR enhances polarization of M2 macrophages (170), gene expression results obtained in our study are against such switch, since markers of M1 and M2 macrophages are both similarly downregulated by CR in WAT. In fact, it has been proposed that the M1/M2 macrophage classification is an oversimplification. An emerging evidence revealed a wider and more dynamic spectrum of macrophage states, considering the M1/M2 binary classification a biased approach that only considers specific pro- and anti-inflammatory genes (300,301). Therefore, we suggest that part of the anti-inflammatory effects of CR are exerted through a reduction of total resident macrophages, regardless of their polarization status.

As mentioned above, not only WAT macrophages are important for the IR associated with obesity. Several studies have provided data supporting the notion that other immune cell populations in WAT can contribute to the inflammation and influence glucose homeostasis. We found an increase in the number of eosinophils and ILCs, specifically ILC2, in gonadal WAT upon CR. Our data are consistent with a recent study showing that obesity induced by HFD feeding reduces eosinophil content in WAT, whereas mice subjected to a dietary weight loss present a restoration of eosinophils and a reduction of pro-inflammatory macrophage levels in WAT (302). In this regard, it has been proposed that eosinophils in WAT improve insulin sensitivity by mediating M2 macrophage polarization (290). This role for eosinophils in glucose homeostasis is supported by data showing that eosinophil-deficient mice are more glucose intolerant and exhibit a decrease in M2 macrophage numbers when they are fed with a HFD (83). The increase of ILC2 upon CR was not surprising, as it has been reported that ILC2, through the secretion of IL-5 and IL-13, promote eosinophils and M2 macrophages preservation (303).

Consistent with other studies (169), although the total number of T cells remained unchanged between the dietary interventions in our study, we show that CR significantly increases the

proportions of Th cells and decreases Tc cells in gonadal WAT, which leads to a rise in the $CD4^+/CD8^+$ ratio. More specifically, in gonadal WAT we found that pro-inflammatory Th1 cells were reduced in mice subjected to CR, while anti-inflammatory Th2 and Treg cells were increased. These findings clearly indicate that, at least with regard to T cells, CR induced an anti-inflammatory response, reverting the inflammation of WAT characteristic of the obese state (142,304).

Somehow surprising, we found that neutrophils were markedly increased in mice subjected to CR, both in inguinal and gonadal WAT. However, neutrophils have been proposed to have a role during the early stages of obesity, being involved in the modulation of WAT and IR. Treatment of hepatocytes or adipocytes with neutrophil elastase, a protease secreted by neutrophils that promote inflammatory responses, has shown to promote cellular IR by causing IRS1 degradation and, consequently, lowering insulin signaling. Additionally, mice have been shown to have an increased number of neutrophils after 3 days of HFD (106). On the other hand, and contrary to our observations, several studies support that dietary restriction induces a significant reduction in local neutrophils (305,306). The reason for the unexpected increase in the number of neutrophils in response to CR in our study is unclear and deserves further investigation.

In contrast to the increase of B cells number under a situation of obesity (156,157), we found that B cells were decreased when mice were subjected to CR, which could be attributed to the anti-inflammatory state of CR. Indeed, it has been reported that fasting drastically reduces the levels of B cells in Peyer's patches and naïve B cells migrate to bone marrow during fasting and only go back upon refeeding (307). Certainly, B cells have been shown to have a role in the pathogenesis of inflammation and IR in obesity, due to their capacity to secret pro-inflammatory cytokines and promote pro-inflammatory T-cell function (156). Similar to B cells, NK cells and NKt cells were also reduced after CR intervention, especially in inguinal WAT. This result is consistent with the notion that NK cells regulate the development of obesity-induced IR and act as an upstream regulator of WAT macrophages in obesity (113). On the other hand, the role of NKt cells in DIO remains unknown.

Finally, although γδT cells act as guardians against pathogens at barrier sites, they are also highly enriched in WAT. Of interest, we found that γδT cells were increased in gonadal WAT upon CR, but they were not changed in inguinal WAT. Although the function of γδT cells is still unclear, the increase of γδT cells found in gonadal WAT in response to CR could be associated with the anti-inflammatory activity of CR. In support of this notion, a recent study has shown that WAT resident γδT cells regulate Treg cells expansion and control core body temperature though the production of IL-33 (136).

It is interesting to highlight the differences found between visceral and subcutaneous fat depots. The composition of the immune infiltrate of gonadal fat depot was dramatically changed upon CR, while changes in inguinal WAT went in the same direction but the magnitude of the change was lower. The regional differences observed are consistent with data provided by other studies reporting that gonadal and inguinal fat depots differ in immune cell composition (283,299,308).

Taking together, our data show that CR mice displays a shift towards an anti-inflammatory profile in the cellular composition of WAT, which could be crucial for the effects of CR in the prevention of the IR.

► 5.2 Mechanisms and cellular processes regulated by calorie restriction in white adipose tissue: role of RORγ1 in adipose tissue biology

The mechanisms by which CR regulates the cellular processes mentioned earlier (i.e. mitochondrial biogenesis, inflammation or ECM remodeling) and improves health are not well known. Numerous studies have identified SIRT1 as a major mediator of CR, and provided evidences that support a relevant role of SIRT1 in the control of at least some of the major processes modulated by CR (309,310). Consistent with a crucial role of SIRT1 in energy metabolism and health, WAT-specific SIRT1 KO mice under a HFD are glucose intolerant and insulin resistant. Additionally, several seminal studies have demonstrated that SIRT1 deacetylates and activates PGC-1α (as well as PGC-1β) in liver and muscle and, by this means, it would control mitochondrial biogenesis in response, for example, to CR (190,311–313). However, the role that SIRT1 plays in the regulation of mitochondrial biogenesis remains controversial. Thus, a recent study from our laboratory, in which the gene expression profiles of WAT from transgenic mice that overexpress SIRT1 or mice subjected to 40% CR were compared, demonstrated that, contrary to CR, SIRT1 over-expression does not lead to an increase in mitochondrial gene expression in WAT (314). This discrepancy with regard to the capacity of SIRT1 and CR to induce mitochondrial biogenesis has been confirmed by other authors using similar experimental approaches (315). Interestingly, despite the lack of any effect on mitochondrial biogenesis, SIRT1 transgenic mice fed AL with a HFD remain slightly leaner and have an improvement of HFD-induced glucose intolerance than control mice, although they have similar food intake than Wt mice (314). The prevention of obesity and IR by SIRT1 gain of function is consistent with other studies (175,316). These findings raise some doubt about the role of SIRT1 in the increase of mitochondrial biogenesis in response to CR, at least in WAT, and clearly supports the notion that increased mitochondrial biogenesis is not the mechanism by which SIRT1 and CR improve metabolic health in mice.

On the other hand, the fact that gene networks related to WAT inflammation appeared altered in both CR and SIRT1 transgenic mice, rather advocates for SIRT1 as a mediator of the effects of CR on WAT immune infiltrate. A central role of SIRT1 in alleviating obesity-associated WAT inflammation in response to CR is supported by other studies, which report that ablation of *Sirt1* specifically in adipocytes leads to WAT inflammation characterized by increased recruitment of macrophages and exacerbated production of pro-inflammatory cytokines (185,317,318). Interestingly, although we observed a massive reduction of immune cell infiltrate, including macrophages and T cells, in mice subjected to CR and a reduction in the expression of genes related to the immune system in SIRT1 transgenic mice, the mechanisms involved in the anti-inflammatory actions of CR and SIRT1 appear to be different. Indeed, it has been described that CR inactivates JNK, NFκB and STAT3 pathways in WAT, while recent work from our laboratory showed that SIRT1 transgenic mice, despite the improvement of the metabolic health, exhibit a sustained activity of these intracellular stress pathways in WAT. These findings suggest that SIRT1 reduces tissue inflammation by mechanisms that do not depend on reducing the phosphorylation-dependent activity of JNK and STAT3 pathways (314). Although it was found that phosphorylation levels of P65-NFκB in WAT of SIRT1 transgenic mice was similar to those found in HFD mice, it is well known that SIRT1 inhibit NFκB signaling by deacetylating P65-NFκB (319). Therefore, it is possible that both CR and SIRT1 act on NFκB to inhibit its activity and reduce inflammation, although the molecular mechanisms by which such inhibition is achieved is different. All of these data suggest that CR could modulate gene expression and exert at least some of the metabolic actions independently of SIRT1 and PGC-1s.

Our study has identified RORγ as new potential mediator of the effects that CR exerts in reshaping the immune landscape of WAT of obese mice. In WAT, the induction by CR of *Rorc* expression was mostly restricted to the adipocyte fraction (approximately 20 fold), although a minor increase in the expression of *Rorc* was also observed in the SVF. When analyzing the expression of the specific *Rorc* isoforms, we found a consistent induction of *Rorc1* by CR only in the adipocyte fraction. Somehow surprisingly, a non-negligible induction of the *Rorc2(t)* isoform was also observed in the SVF. Since *Rorc2(t)* does not appear to be significantly changed in the whole tissue, this induction in the SVF could be attributed to changes in the different immune cell populations within WAT. In any case, the contribution of the RORγt isoform to the global induction of RORγ in the whole WAT appears to be minimal.

Considering that RORγ1 is induced during adipocyte differentiation, its expression is mostly restricted in adipocytes and it is induced by CR in adipocytes, we initially hypothesized that RORγ1 could play a role in the regulation of genes needed to acquire the specific functions of mature adipocytes (i.e. lipid accumulation and endocrine function). To tackle this question, we used an *in vitro* model of cultured 3T3-L1 adipocytes, which are widely used for the study of adipocyte biology. We also generated a mouse model with targeted deletion of *Rorc* specifically in adipocytes. The choice of a tissue-specific KO model stems from the conflicting results obtained when using systemic RORγ KO mice. Indeed, while some studies reported that mice devoid of RORγ in all tissues exhibit no alterations in WAT mass or adipocyte size, others using similar models showed an increased number of adipocytes and improved insulin sensitivity (250,251). Therefore, to avoid any confounding effects on energy balance and glucose homeostasis resulting from knocking out RORγ in non-adipose tissues, we chose to generate a KO mouse model devoid of RORγ specifically in adipocytes (RORγ-FAT-KO). Two different *Cre* transgenes have been broadly used for this purpose, being the most common the one that uses the promoter of the *adipocyte fatty acid-binding protein 4* (*aP2*) gene to drive *Cre* expression. However, although this *Cre* line has been shown to induce recombination in adipose tissues, few studies reported that *aP2* is also expressed in other cell types, including macrophages and brain (320–322). Therefore, to avoid the possible side effects of gene deletion in cells other than adipocytes, when using aP2-Cre mouse line, in our studies we used adiponectin-Cre transgenic mice (AdipoQ-Cre mice). This mouse model has proven to exhibit adipocyte-specific deletion of the target gene, with no observable recombination in any other tissues examined (323). The assessment of RORγ expression in several tissues of our mouse model confirmed that, at mRNA and protein level, *Rorc* was exclusively knocked out in adipocytes. It is interesting to mention that RORγ1 presents an oscillatory expression pattern in several tissues, although it has not been observed in WAT (247). However, in order to minimize the possible effect of circadian rhythms in our studies, all mice were sacrificed at the same hour and during the time frame ensuring almost the highest expression of *Rorc*.

RORγ-FAT-KO mice were viable and, somehow surprisingly, they did not present any differences in body weight, as well as in the mass and morphology of the principal metabolic tissues compared to their Wt littermates, whether fed with a chow diet or HFD. The lack of any gross alteration in WAT mass is consistent with the minor changes in gene expression observed in KO mice, at least under basal AL conditions. Indeed, gene expression profiling showed that the expression profiles of Wt and RORγ-FAT-KO mice were very similar under basal AL conditions, and only few genes were found dysregulated. This would suggest that RORγ does not have an essential role under basal conditions, so that lack of RORγ does not have a great impact on gene expression or WAT development. Another possibility is that, under these conditions, the lack of RORγ was

compensated by other ROR isoforms, as it will be discussed later. These *in vivo* results are in accordance with *in vitro* results obtained from 3T3-L1 adipocytes, in which *Rorc* expression was knocked down. Indeed, reduced *Rorc* expression had a minor impact on gene expression, and certainly no effect on adipocyte morphology, indicating that RORγ does not significantly contribute to adipocyte differentiation or lipid accumulation.

Nevertheless, it is worth mentioning that, among the few genes found regulated by RORγ in 3T3-L1 adipocytes or WAT from AL RORγ-FAT-KO mice, we found genes associated to GO categories related with the immune system as well as lipid metabolism with a relevant function in the immune system. Specifically, the immune system categories found were related to IFN-β response, which has immunomodulatory effects (262,263). Several studies have reported a relation between type I IFN signaling and a protection against metabolic diseases. For instance, it has been reported that mice fed with a HFD and with adipose tissue-specific deletion of *interferon receptor 1* (*Ifnar1*) exhibit an increase in body weight, IR and an impaired glucose tolerance (324). Additionally, overexpression of IFN-β attenuates obesity-induced adipose tissue inflammation and helps to maintain glucose homeostasis (325). These data would support a role of RORγ in the improvement of glucose homeostasis, at least in the context of CR, by triggering a type I IFN response that will reshape the immune landscape of WAT towards an anti-inflammatory profile. However, the role of type I IFN on glucose and energy homeostasis remains controversial. Other studies have shown that, far from improving IR and decreasing body weight, type I IFN signaling promotes obesity and IR. For instance, Hannibal *et al.* reported that mice in which type I IFN signaling has been disrupted by systemically KO of *Ifnar1* are resistant to develop DIO and IR (101). Similarly, mice deficient in *Irf7*, an IFN response gene, are protected from DIO and IR (326). In this line, *interferon regulatory factor 3* (IRF3) has been reported to inhibit PPARγ expression and adipogenesis (327), while *interferon regulatory factor 5* (IRF5) has been implicated in polarizing macrophages towards an inflammatory phenotype (328).

Interestingly, tightly linked to changes in the IFN-β signaling pathway and the immune system gene networks, our gene profiling study found alteration in the expression of genes related to lipid metabolism. Some of the genes found (i.e. *Apol6* and *Apol9b*) are recognized as IFN-stimulated genes, whose function is to promote the efflux of cholesterol from cells. It has been reported that type I IFN also shift the balance of lipid metabolism by decreasing the synthesis and increasing the import of cholesterol and long fatty acids. Moreover, limiting the cholesterol biosynthetic flux spontaneously induces a type I IFN response in triple negative breast cancer cells (329,330). Remarkably, it has been reported that RORγ functions as an essential activator of the entire cholesterol-biosynthesis program (331). In line with this notion, both liver-specific and systemic RORγ KO mice have shown a reduction of cholesterol as well as a decrease in the hepatic cholesterol content (245). Moreover, in porcine liver organoids, time-restricted feeding has been shown to downregulate cholesterol biosynthesis genes and improve lipid metabolism through RORγ-mediated chromatin remodeling (332). Although these studies underline a potential role for RORγ in the regulation of cholesterol synthesis, and such role agrees with the changes in the expression of few genes related cholesterol metabolism observed in our profiling studies both *in vivo* and *in vitro*, the fact that changes in the expression genes related to cholesterol metabolism were not statistically significant when gene expression was verified by qPCR suggests that the impact of lack of RORγ on cholesterol metabolism in adipocytes could be minor.

Moreover, besides cholesterol synthesis, the genes included in the lipid metabolism categories corresponded to genes encoding for proteins involved in the synthesis of singular lipid species with a function in the immune response. For instance, *Gpat3* catalyses the conversion of glycerol-3-phosphate to lysophosphatidic acid in the synthesis of triacylglycerol. Interestingly, it has been reported that intracellular fatty acid content influences $CD4^+$ and $CD8^+$ T subsets, as these cells discriminate between both quantity and quality of fatty acids (333). Another example would be *Pla2g2*, which has been shown to regulate prostaglandins and, consequently, have a role in the progression of obesity regulating inflammation (334). Additionally, ANO6, which is an essential protein for the calcium-dependent exposure of phosphatidylserine on the cell surface, is also a crucial component of the immune defense by macrophages. It has been shown that ANO6 stimulates *purinergic P2X7 receptors* (P2X7R) and contributes to ATP-induced membrane blebbing and apoptosis, which support phagocytosis and subsequent killing of phagocytosed bacteria (335).

However, we realized that siRNAs treatment *per se* generates an IFN-like response in 3T3-L1 adipocytes, in which the levels of IFNβ-target genes in 3T3-L1 adipocytes transfected with siRNAs were higher than in cells that were not exposed to siRNAs. Consequently, treating transfected cells with IFN-β did not result, as we expected, in a strong induction of IFNβ-target genes, as they were already highly expressed as a result of IFN-like response turned on by cells exposed to siRNAs. This precluded us to study the role of RORγ1 as a mediator of IFN-β response in the *in vitro* model generated. The induction of IFN-β response by siRNAs is in accordance with the IFN-β and its targets functions. Cells can detect siRNAs as exogenous and trigger a cellular response though intracellular sensors that detect viral components in the cytoplasm and activate NFκB that, in turn, activates IFN-β gene expression and the resulting defense response (336). Indeed, this is consistent with the findings observed in other studies, which reported that long >23-bp siRNA can influence cell viability and induce a potent IFN response in a cell-type specific manner. Additionally, sequences containing GUCCUUCAAA are reported to induce IFN response through *toll-like receptor 7* (TRL7) (337,338). Hence, using siRNAs to knockdown *Rorc* in 3T3-L1 adipocytes to study the role of RORγ1 in mediating the effects of IFN-β in adipocytes is not suitable, simply because the use of siRNA already sets a very high basal IFN-β mediated response that makes tremendously difficult the observation of any further response to IFN-β treatment. Consequently, other options, such as using RORγ inverse agonists or the CRISPR/Cas9 editing system, must be considered in the future to study the role of RORγ in the regulation of gene expression in response to IFN-β. Still, as appropriate controls have been used, we think that the IFN-β related response observed in cells in which RORγ, but also RORα, have been silenced is not an experimental artifact and that RORγ is involved in the regulation of the expression of genes related to cell defense against pathogens. This notion is supported by our *in vivo* data in RORγ-FAT-KO mice, in which lack of RORγ also alters the expression of genes related to several aspects of the immune system function, including the response to IFN.

Given the relatively low number of genes whose expression was altered by the lack of RORγ, both *in vivo* (under basal AL conditions) and *in vitro*, as well as the fact that we found RORγ expression to be highly induced in response to CR, we speculated that the main role of RORγ was to act as a mediator of the response to CR. In this regard, our finding that some of the genes regulated by RORγ in response to CR are involved in the recruitment of immune cells in WAT suggests that RORγ is crucial for modulating the function of adipocytes as immune regulatory cells, stimulating conventional immune cells in response to changing nutritional conditions. For example, we found that chemokines *Ccl19* and *Ccl22* were modulated by RORγ upon CR conditions. Several studies

reported that the expression of the mentioned chemokines in WAT is induced in obesity, promoting the recruitment of pro-inflammatory macrophages and lymphocytes, and are associated with IR and metabolic inflammation (339–341). However, in line with our findings, other studies indicate that CR regulates the expression of these genes in WAT, contributing to the recruitment of immune cells, but in this case with anti-inflammatory effects (293,342).

We also found that in response to CR, RORγ could be up-regulating genes involved in lymphocyte differentiation, mainly related with T cells differentiation and development. In this sense, *Tcf7* was found increased in response to CR, an increase that was blunted in mice lacking RORγ. This gene is expressed predominantly in T-cells and plays a critical role in NK cells and innate lymphoid cells development (343,344). Protein receptors found on the T cells surface with in the signaling function were also altered, such as *Icos*, *Cd3e*, *Cd2* and *Zap70*. In this regard, ICOS is an inducible co-stimulatory receptor that can be expressed by anti-inflammatory T cells, such as Th2 and Treg cells, but also by pro-inflammatory T cells, like Th1 and Th17 cells (345).

Surprisingly, *Cd8b1* was also found increased by RORγ under CR. CD8B1 is a cell surface glycoprotein found on most Tc lymphocytes. Tc cells are significantly increased in WAT in obesity. The increase of WAT Tc cells appears to precede and contributes the accumulation of macrophages and metabolic dysfunctions in obesity (127). Besides their contribution to WAT inflammation, tissue Tc cells are known to function in restricting T cell expansion and activation in inflamed WAT through perforin (346). However, some studies support that CR and weight loss result in a significantly increase in proportions of Tc cells in liver and WAT, although their metabolic profile is improved (168,347). Remarkably, the induction of pro-inflammatory genes by CR observed in our gene expression profiling study results somehow paradoxical. However, other studies have described the induction of conventional pro-inflammatory genes in response to CR, even if the overall response observed is clearly anti-inflammatory (289,293,348). For instance, patients subjected to CR have pro-inflammatory genes, such as the *chemokine (C-C motif) ligand 17* (*Ccl17*) (293).

Other genes, such as, *Cd4*, *Btla1*, *Ctla4*, and *Ms4a4b*, with a more evident role in anti-inflammatory responses have their expression upregulated in response to CR in a RORγ-dependent manner. These genes encode for membrane proteins in T lymphocytes that mainly polarize T cells to an anti-inflammatory response. *Cd4* is a protein present in Th lymphocytes, which play a critical immune-regulatory role in WAT homeostasis (349). Moreover, T cells in obese WAT exhibit enrichment of genes characteristic of T cell exhaustion and increased expression of co-inhibitory receptors, such as *Ctla4* and *Btla*. They are involved in inhibiting the Th1 “pro-inflammatory” T-cell response (350), as well positively regulates Treg cells expression (351,352). In a similar way, *Ms4a4b* expression in tightly regulated in T cell development, being highly expressed in Th1 and Treg cells and mediating both pro- and anti-inflammatory effects (353,354).

Taking together, the gene expression profiles described suggest that up-regulation of RORγ by CR in inguinal WAT results in activation and recruitment of immune cells, particularly of T cells. However, the pro- or anti-inflammatory profile of recruited immune cells that accumulate in inguinal WAT is not evident based on the gene expression profile, since many of these molecules contribute to both pro- and anti-inflammatory activities. In any case, since these genes are expressed in immune cells, but not in adipocytes in which we knocked out RORγ, we consider that the changes in gene expression observed in the gene expression profiles rather reflect changes in the cell composition of WAT, especially in response to CR. Consequently, most of the genes identified in

our microarray study cannot be considered as direct targets of RORγ. Nevertheless, our results suggest that RORγ in adipocytes regulate the expression of genes that mediate the crosstalk between adipocytes and immune cells of the SVF, inducing changes in the immune cell populations residing in WAT, as it will be further discussed.

► 5.3 Changes in immune cell populations in RORγ-FAT-KO mice adipose tissue

Consistent with the gene expression profile, we observed substantial changes in the WAT residing immune cells populations in RORγ-FAT-KO mice, both when fed AL or in response to CR. Although dramatic changes in some immune cell populations (i.e. macrophages, ILCs and Treg cells) were observed in response to CR, the effect that lack of RORγ in adipocytes has on these populations was rather mild, and not always consistent along gonadal and inguinal WAT. RORγ-FAT-KO mice fed AL with a HFD presented an increase of Treg cell populations in gonadal WAT. At the same time, there was a tendency towards a reduction of Th1 cells as well as rise of Th2 cells, although without statistical significance. Additionally, in both gonadal and inguinal WAT, NK cells were severely diminished, while γδT cells were increased. Of interest, although γδT cells have traditionally been attributed a pro-inflammatory activity and function in the defense against pathogens, very recent reports indicate that adipose resident γδT cells are crucial in regulating Treg cells accumulation in WAT through the secretion of IL-17A (136). Overall, the cellular profile observed in WAT under basal AL conditions indicate that RORγ-FAT-KO mice have a switch of immune infiltrate towards a more anti-inflammatory profile, suggesting that RORγ acts as a pro-inflammatory mediator.

Under CR conditions, WAT displays a clear anti-inflammatory profile, more evident in the gonadal depot. Indeed, gonadal WAT of mice subjected to CR exhibits a clear reduction of Tc, Th1, macropahes and NK cells, and an increase in Th2, Treg, ILC2 cells and eosinophils. This anti-inflammatory profile in response to CR seems enhanced in RORγ-FAT-KO mice, supporting the notion that RORγ acts as a pro-inflammatory molecule. Indeed, under CR, gonadal WAT of RORγ-FAT-KO mice displayed an evident reduction of pro-inflammatory populations (i.e. Tc and Th1 cells), whereas anti-inflammatory populations (i.e. Th2 and Treg cells) were increased. On the other hand, minor changes were observed in inguinal WAT of RORγ-FAT-KO mice under CR, probably because it is a tissue that *per se* presents less inflammation, making more difficult to see the effects that lack of RORγ has on immune cell populations. Still, we observed an increase of Th2 cells, B cells and NKt cells.

On the basis of the overall changes observed in the immune cells populations within WAT, we propose that RORγ might have a pro-inflammatory role, so that in the absence of RORγ an anti-inflammatory immune response is exacerbated. The fact that RORγ is increased in WAT in response to CR conditions, which is associated with an overall reduction of WAT inflammation, appears to be contradictory with a pro-inflammatory function of RORγ. However, RORγ could be modulating the anti-inflammatory response, acting as a brake, to ensure that a certain pro-inflammatory response remains in the tissue so that it can combat potential pathogens. It is also possible to speculate that such pro-inflammatory response might be need to help in the profound remodeling that WAT is undergoing when animals are exposed to CR and that implies a reduction in the size and number of adipocytes and a re-structuration of the ECM of the tissue. Although inflammatory signals are known to have a negative impact on metabolism, pro-inflammatory signaling in adipocytes is also required to facilitate WAT remodeling (81). Thus, in agreement with

our findings, it has been described that decreased fat mass and improvement in glucose homeostasis in obese subjects undergoing a short term low caloric diet is not associated with a generalized decreased in pro-inflammatory markers, but some of such pro-inflammatory genes are increased, like *IL-12A*, *CCL-19*, *Fc Fragment Of IgG Receptor IIa* (*CD32*) or *Integrin Subunit Alpha L* (*ITGAL*) (289). Moreover, it has recently been reported that tissue remodeling factors, such as *Mmp9*, *vascular endothelial growth factor A* (*Vegfa*) and *fibroblast growth factor 2* (*Fgf2*), are increased 21 days after weigh loss (302), which suggests a dependence of WAT remodeling on changes in inflammation.

The pro-inflammatory role of RORγ is compatible with the results obtained in the gene expression profile, both in 3T3-L1 cells and *in vivo*, in which knocked down or knocked out of RORγ, respectively, leads to an expression pattern characterized by a reduction in the expression of genes related to the fight against pathogens through the activation of pathways related to pattern recognition receptor and type I IFN. Interestingly, the pro-inflammatory function of RORγ1 in adipocytes is in line with the pro-inflammatory role described for the Th17 cell-specific isoform RORγt, which only differ from RORγ1 in 21 amino acids of the amino-terminus. RORγt has been described to regulate the expression of the pro-inflammatory cytokine IL-17 in Th17 cells and, consequently, it has a role in inflammation. Remarkably, it has been recently reported that IL-17 plays a critical role in DIO and metabolic disorders in mice, as inhibition of IL-17A axis in adipocytes by inhibition of RORγt-mediated IL-17A production suppresses DIO and metabolic disorders in mice (355). However, the number of Th17 cells was not changed in RORγ-FAT-KO mice, neither in AL or CR mice. It is tempting to speculate that both, RORγ1 and RORγt, in agreement with their similar peptide sequence and structure, have an analogous pro-inflammatory role, though in different cellular and physiological contexts.

It is worth to remark that, although it has been previously found that adipocytes can produce immune mediators, such as IL-6 and TNF-α (356), their immune capacity might not be limited to directly producing immune mediators, but may include direct modulation of other immune cells (357). For instance, it has recently been suggested that adipocytes could act as antigen presenting cells to T cells in WAT to trigger an inflammatory response (358). Very recently, it has been also reported that adipocytes express cytokines, chemokines, multiple receptors, cell adhesion molecules and MHC class II family molecules and costimulatory signal molecules such as CD80 and CD86, which leads to T cell activation (131,359). Therefore, investigating the significance of adipocytes as antigen presenting cells in WAT would be critical to understand their precise role in modulating the residing immune cell populations in response to different stimuli, including nutritional cues.

► 5.4 Role of RORγ in BAT thermogenesis in response to cold

We found that *Rorc* is highly expressed in BAT, doubling the expression found in WAT. This, together with the fact that our AdipoQCre/loxP recombination system also deletes the *Rorc* gene in brown adipocytes, prompted us to study the role that RORγ could play in BAT. The main function of BAT is the production of heat to maintain body temperature in response to cold, being the principal effector organ of non-shivering thermogenesis. Considering the fact that RORγ-FAT-KO mice are able to maintain body temperature when acutely exposed to cold to the same extent as Wt littermates, we can conclude that RORγ does not have an essential role in BAT non-shivering thermogenesis. The lack of a role of RORγ on BAT adaptive thermogenesis not only is supported

by the absence of any effect on body temperature upon cold exposure, but also by the lack of changes in the expression of genes related to thermogenesis (i.e. *Ppargc1a and Ucp1*). Indeed, similar to Wt, RORγ-FAT-KO mice presented a significant induction of *Ucp1* and *Ppargc1a* mRNA levels after being exposed to 4ºC for 5 hours. This increase was also seen at protein evels, although it was mildy higher in RORγ-FAT-KO mice compared to their Wt littermates. However, whether this mild increase is attempted to compensate a real thermogenic defect is unlikely. These data discard any exacerbated expression of thermogenic genes that could be suggestive of a compensatory response aimed at maintaining BAT thermogenesis.

Similarly, no alterations in lipid accumulation, which is usually suggestive of impaired thermogenesis, were observed in RORγ-FAT-KO mice. TAG mobilization is a crucial step that provides substrates for thermogenesis. As a result of lipid mobilization and oxidation, we found that BAT of mice exposed to cold had less lipid droplets in brown adipocytes compared to mice that stayed at thermoneutrality (30ºC), which had inactivated BAT. However, no differences were observed between genotypes, which is again indicative that lack of RORγ does not influence BAT lipid mobilization. Anyway, BAT lipolysis is not as crucial for maintaining non-shivering thermogenesis. Thus, mice with defective lipolysis specifically in brown adipocytes do not present impaired cold-induced thermogenic capacity. The reason is that BAT mostly relies on fatty acids released by WAT for its thermogenic function (360). In this regard, we observed that both Wt and RORγ-FAT-KO mice showed lower total body weight after being exposed at 4ºC. In addition, the weight of BAT and WAT depots were similarly reduced upon cold exposure. These data suggest that lipid mobilization from adipose tissues to sustain thermogenesis is similar in Wt and RORγ-FAT-KO mice, and, therefore, that lack of RORγ does not affect, apparently, the lipolytic machinery.

It is possible to speculate that the function of RORγ in BAT non-shivering thermogenesis could be masked by the effect of other UCP1-independent thermogenic processes. For instance, UCP1 KO mice, despite having an impaired BAT non-shivering adaptive thermogenesis, are able to adapt to low temperatures by increasing shivering (361). In our experiment, although we did not determine it, the possibility that RORγ-FAT-KO mice have an increase in shivering thermogenesis should be considered and, therefore, it should be examined in detail. On the other hand, additional thermogenic processes besides UCP1-dependent classical non-shivering thermogenesis have been identified. These include UCP1-independent proton leak, calcium-dependent ATP hydrolysis and lipid cycling, consisting in a futile cycle of re-synthesis of TAG following lipolysis that generates heat. These thermogenic processes could be compensating possible deficiencies in BAT thermogenesis of RORγ1-FAT-KO due to the lack of RORγ (362). Importantly, RORα could also be compensating the lack of RORγ in brown adipocytes. Recent studies suggest that RORα is involved in the regulation of non-shivering thermogenesis by regulating the expression of genes involved in fatty acid oxidation, as well as *Ucp1* gene in subcutaneous WAT and BAT (363). In this regard, it has been recently demonstrated that pharmacological modulation of RORα controls fat browning and adaptive thermogenesis in mice (364).

Taking together, the results obtained suggest that RORγ does not have an essential role in BAT thermogenesis. Noteworthy, it would be interesting to investigate if long-term adaptation to mildly cold temperatures brings about a thermogenic defect in RORγ-FAT-KO mice, which was not observed under the temperature conditions used in the present study. Additionally, assessing the capacity of RORα and RORγ adipose specific double KO mice to maintain their body temperature in response to acute cold exposure would be interesting to determine if RORα exerts any

compensatory effects. Finally, since our findings in WAT indicate that RORγ could be modulating the resident immune cell populations both under basal and upon CR, it would be also interesting to characterize the immune infiltrate in brown adipocytes in our mouse model. Although BAT depots are less susceptible to develop local inflammation in response to obesity compared to WAT, several studies have proposed BAT as an insulin target tissue sensitive to inflammation. This condition directly impairs the thermogenic activity of BAT as well as the glucose uptake for its use as a fuel substrate. In line with this notion, a recent study has reported that BAT inflammation is reduced by SIRT1 overexpression in response to LPS-mediated inflammation (365).

► 5.5 Role of RORγ1 in glucose homeostasis

WAT is a key regulator of whole body energy and glucose homeostasis, and CR is well known for having positive effects on both body weight and fat mass, improving whole-body insulin sensitivity and enhancing insulin-dependent glucose uptake in muscle, liver and WAT (366,367). As we found that CR dramatically induces the expression of RORγ in WAT in association with the amelioration of whole body insulin sensitivity, we hypothesized that adipose RORγ1 could be an essential mediator of the positive effects that CR has on glucose homeostasis. However, based on the data obtained in our study, it does not seem that adipose RORγ plays a relevant role in regulating basal glucose homeostasis or in mediating the insulin sensitizing effects of CR. In fact, the role of RORγ on glucose homeostasis is still controversial, and some studies rather suggest that RORγ has a detrimental effect on glucose homeostasis. For instance, a study by Meissburger *et al.* using RORγ systemic KO mice show that lack of *Rorc* have lower WAT mass and an improvement of insulin sensitivity (251). Additionally, Takeda *et al.* reported that RORγ systemic KO mice exhibit reduced hepatic gluconeogenesis and, as a result, mice exhibit improved overall insulin sensitivity and glucose tolerance (246). These observations suggest that the loss or the inhibition of RORγ1 might instead protect against IR and T2D and, therefore, that RORγ plays a negative role on glucose homeostasis. In line with this notion, clinical studies reported that obese or insulin resistant individuals present an increase of *Rorc* expression in visceral WAT, suggesting that RORγ could be implicated in adipocyte hyperplasia and hypertrophy and consequently with an IR status (249). In spite of these data on human subjects, according to our results, RORγ does not seem to play a crucial role in the control of WAT mass. Although we found that CR dramatically reduced body weight, WAT weight and adipocyte size, WAT of Wt and RORγ-FAT-KO mice were almost identical regardless the dietary intervention. In line with this, leptin levels were similarly decreased by CR in Wt and RORγ-FAT-KO mice, indicating that the adiposity is similar in both (58,368). The absence of differences in body weight and WAT mass strongly suggests that RORγ does not play a relevant role in adipocyte terminal differentiation or lipid accumulation, contrary to what has been reported in total KO mice or in cultured 3T3-L1 cells. Indeed, the study by Meissburger *et al.* reported that RORγ over-expression partially impairs the differentiation of 3T3-L1 preadipocytes into adipocytes (251). However, an experiment performed in our laboratory using a specific RORγ antagonist over the course of 3T3-L1 preadipocytes differentiation showed that inhibition of RORγ activity does not affect adipocyte differentiation (unpublished results). Of note, the KO mouse model used in our study ensured the deletion of *Rorc* in mature adipocytes. Therefore, any potential effect of *Rorc* during the early phases of the differentiation of precursor cells that affected their capacity to give rise to adipocytes would have been difficult to be observed. Thus, with data arguing in favor and against a role of RORγ on adipocyte differentiation, this issue still remains to be clarified.

With regard to glucose homeostasis, results from GTT and ITT support the idea that adipose RORγ by itself does not have visible metabolic effects on mice, neither AL nor upon CR. Both tests indicated that CR improves glucose tolerance and insulin sensitivity, as mice fed AL responded worst to insulin and glucose than CR-treated mice, in agreement with numerous studies that have reported positive effects of CR on glucose homeostasis (163,369). Additionally, in line with GTT and ITT, blood insulin was diminished by CR, indicating an amelioration of insulin sensitivity, while no differences were seen between genotypes. Excessive local inflammation of WAT is related to systemic IR in rodents. In this sense, positive effects on glucose homeostasis induced by CR could be explained in part due to the reduction of inflammation in WAT, BAT and liver, as showed in histological analysis. This notion was also supported by flow cytometry analysis of inguinal and gonadal WAT immune populations that reveled a decrease in pro-inflammatory cells (i.e. Th1, Tc cells, macrophages and NK cells) and increase anti-inflammatory cells (i.e. eosinophils, Th2, Treg and ILC2 cells). On the other hand, RORγ-FAT-KO mice normally respond to CR by improving their glucose tolerance and insulin sensitivity to the same extent as Wt mice. Although our study has focused on the effects that CR and RORγ-FAT-KO have on WAT and how they impact whole body glucose homeostasis, the contribution of other tissues to glucose metabolism in response to CR cannot be neglected. Therefore, the fact that *Rorc* was specifically KO in WAT, leaving its expression unaltered in other target tissues involved in glucose homeostasis, such as liver and skeletal muscle, could explain the absence of changes in glucose homeostasis in adipose-specific RORγ KO mice. In fact, it has been reported that RORγ regulates the expression of genes associated with lipid and carbohydrate metabolism in skeletal muscle (370). Moreover, it has been proposed that RORγ belongs to the molecular cascade that regulates insulin secretion in pancreatic β-cells and inhibits insulin secretion in INS-1 cells (371). Collectively, these data suggest that physiologic effects on glucose tolerance, insulin sensitivity and lipid metabolism exerted by CR are not mediated by adipose RORγ expression. However, the effect in insulin sensitivity specifically in adipose tissues has not been directly assessed and, consequently, alterations in adipose insulin sensitivity as a result of the loss of RORγ cannot be discarded. Still, as lack of alterations has been found in whole body glucose homeostasis, an alteration in tissue-specific insulin signaling would not be sufficiently important to be noticed at the organic level.

In summary, ours findings suggest a pro-inflammatory role of RORγ1 in adipocytes, both under basal AL conditions and in response to CR. We speculate that RORγ in adipocytes regulates the expression of genes encoding for molecules (i.e. cytokines) or proteins involved in the synthesis of signaling molecules (i.e. lipids and metabolites) that participate in the crosstalk between adipocytes and immune cells. In this regard, further studies will be needed to uncover these signaling molecules produced by adipocytes in response to CR.

However, the interpretation of our results is hampered by the fact that the data regarding gene expression could reflect changes in the expression of RORγ target genes in adipocytes, as well as changes in the expression of genes associated with the alterations in the immune cell populations over the time. In fact, the use of a constitutive tissue-specific KO together with the long-term (3 months) nutritional interventions may have activated compensatory mechanisms to overcome the loss of RORγ that can be reflected as changes in gene expression, or even in cell composition, making difficult to identify the direct target and processes regulated by RORγ. In this regard, in future studies, it would need to be considered to use an inducible RORγ KO mouse to study the lack of RORγ in a specific time point. Moreover, the relatively mild phenotype observed in WAT and glucose homeostasis could have been due to the functional compensation by other RORs,

especially RORα. Although no changes in the mRNA or protein levels of RORα have been observed in WAT of RORγ-FAT-KO mice, an increase in the transcriptional activity of RORα to compensate for the lack of RORγ cannot be disregarded. The functional compensation is a plausible explanation for the mild phenotype observed, since it has been described that both RORs regulate similar functions and target genes (147). Therefore, the generation of a double KO of RORα and RORγ in WAT would help to unravel the role of RORs in WAT in response to diverse nutritional cues. Additionally, the unequivocal identification of RORγ target genes in adipocytes is required. We first suggest to perform a microarray analysis with adipocytes isolated from WAT of Wt and RORγ-FAT-KO mice subjected to CR, to identify genes differentially regulated by RORγ in this cellular fraction of WAT, avoiding any interference stemming from changes in the cellularity of the SVF. Although Affymetrix microarrays cartridges (Mouse Clariom S Array) provides an extensive coverage of all known well-annotated genes, other molecules such as non-coding RNAs or microRNA, which cannot be detectable in the DNA microarrays used, could be regulating the crosstalk between WAT and immune system. Therefore, other technologies that ensure a wider coverage of the transcriptome could be used, such as RNA-seq. Furthermore, especially considering the fact that among RORγ target genes identified in 3T3-L1 we found genes encoding for protein related to the metabolism of rare lipid species, it is possible to conceive that the crosstalk between adipocytes and the immune cells is mediated by signaling lipids. In this case, we foresee conduction a lipidomic study in our mouse or cellular model.

CONCLUSIONS

► 6 Conclusions

1. Gene-expression profiling identifies genes related to mitochondrial biogenesis and immune system among the most dysregulated gene networks by CR in WAT, in close association with a decreased body weight and improved glucose homeostasis.

2. Consistent with the dysregulation of genes related to the immune function in response to CR, we found that CR alters the immune cell populations residing in WAT of obese mice, especially in gonadal WAT, reducing the number of pro-inflammatory cells (i.e. macrophages, Tc cells, Th1 cells and NK cells) and increasing the number of cells with an anti-inflammatory function (i.e. eosinophils, Th2 cells, Treg cells and ILC2).

3. *Rorc1* expression, but not other members of ROR family, is specifically and highly induced in adipocytes in response to CR.

4. Knockdown of *Rorc*, but also *Rora* and *Rora/c*, in mature 3T3-L1 adipocytes decreases the expression of genes related to type I IFN responses and lipid metabolism.

5. Lack of RORγ expression specifically in adipocytes has a modest impact on the gene expression profile of WAT from mice fed AL with a HFD. Still, consistent with the data obtained in 3T3-L1 cells, genes related to type I IFN responses were found down-regulated in RORγ-FAT-KO mice.

6. Gene expression profiling in WAT of mice lacking RORγ in adipocytes identified genes related to the immune function, particularly to the T cell recruitment and polarization, as main targets of RORγ1 in WAT response to CR.

7. The characterization of the resident immune cells populations in WAT revealed that RORγ-FAT-KO mice display a more anti-inflammatory profile than their Wt littermates, particularly when subjected to CR, being characterized by an increase in Th2 and Treg cells and a decrease in Tc and Th1 cells in gonadal WAT.

8. Lack of RORγ in adipocytes is not sufficient to induce obesity or impair glucose homeostasis in mice fed AL. Moreover, the induction of RORγ in WAT is not required for the improvement of glucose homeostasis in response to CR.

9. RORγ1, despite being highly expressed in BAT, is not essential for non-shivering adaptive thermogenesis.

REFERENCES

► 7. References

1. WHO. WHO Overweight and obesity [Internet]. 2018. p. 1–2. Available from: https://www.who.int/news-room/fact-sheets/detail/obesity-and-overweight
2. WHO. Prevalence of obesity among adults [Internet]. WHO. 2016. Available from: https://www.who.int/data/gho/data/indicators/indicator-details/GHO/prevalence-of-obesity-among-adults-bmi-=-30-(crude-estimate)-(-)
3. Fontaine KR, Redden DT, Wang C, Westfall AO, Allison DB. Years of life lost due to obesity. J Am Med Assoc. 2003;289(2):187–93.
4. De Gonzalez AB, Hartge P, Cerhan JR, Flint AJ, Hannan L, MacInnis RJ, et al. Body-mass index and mortality among 1.46 million white adults. N Engl J Med. 2010;363(23):2211–9.
5. Danaei G, Finucane MM, Lu Y, Singh GM, Cowan MJ, Paciorek CJ, et al. National, regional, and global trends in fasting plasma glucose and diabetes prevalence since 1980: Systematic analysis of health examination surveys and epidemiological studies with 370 country-years and 2.7 million participants. Lancet. 2011;378(9785):31–40.
6. WHO. Diabetes [Internet]. WHO. 2020. Available from: https://www.who.int/news-room/facts-in-pictures/detail/diabetes
7. WHO. WHO | 10 facts on obesity [internet]. WHO. 2014. Available from: http://www.who.int/features/factfiles/obesity/en/
8. Zamora M, Villena JA. Targeting Mitochondrial Biogenesis to Treat Insulin Resistance. Curr Pharm Des. 2014;20(35):5527–57.
9. Struijs JN, Baan CA, Schellevis FG, Westert GP, Van Den Bos GAM. Comorbidity in patients with diabetes mellitus: Impact on medical health care utilization. BMC Health Serv Res. 2006;6(84).
10. Association AD. Diagnosis and classification of diabetes mellitus. Diabetes Care. 2014;37(SUPPL.1):81–90.
11. Kojta I, Chacińska M, Błachnio-Zabielska A. Obesity, bioactive lipids, and adipose tissue inflammation in insulin resistance. Nutrients. 2020;12(5):1305.
12. Reaven GM, Hollenbeck C, Jeng CY, Wu MS, Chen YDI. Measurement of plasma glucose, free fatty acid, lactate, and insulin for 24 h in patients with NIDDM. Diabetes. 1988;37(8):1020–4.
13. Itani SI, Ruderman NB, Schmieder F, Boden G. Lipid-induced insulin resistance in human muscle is associated with changes in diacylglycerol, protein kinase C, and IκB-α. Diabetes. 2002;51(7):2005–11.
14. Ginsberg HN. Insulin resistance and cardiovascular disease. J Clin Invest. 2000;106(4):453–8.
15. Factors OHR, Mokdad AH, Ford ES, Bowman BA, Dietz WH, Vinicor F, et al. Prevalence of Obesity, Diabetes, and Obesity-Related Health Risk Factors, 2001. J Am Med Assoc. 2013;289(1):76–9.
16. Warram JH, Martin BC, Krolewski AS, Soeldner JS, Kahn CR. Slow Glucose Removal Rate and Hyperinsulinemia Precede the Development of Type II Diabetes in the Offspring of Diabetic Parents. Ann Intern Med. 1990;113(12):909–15.
17. Kasuga M. Insulin resistance and pancreatic β cell failure. J Clin Invest. 2006;116(7):1756–60.
18. Johnson AMF, Olefsky JM. The origins and drivers of insulin resistance. Cell. 2013;152(4):673–84.

19. Yu C, Chen Y, Cline GW, Zhang D, Zong H, Wang Y, et al. Mechanism by which fatty acids inhibit insulin activation of insulin receptor substrate-1 (IRS-1)-associated phosphatidylinositol 3-kinase activity in muscle. J Biol Chem. 2002;277(52):50230–6.

20. Amati F, Dubé JJ, Alvarez-Carnero E, Edreira MM, Chomentowski P, Coen PM, et al. Skeletal muscle triglycerides, diacylglycerols, and ceramides in insulin resistance: Another paradox in endurance-trained athletes? Diabetes. 2011;60(10):2588–97.

21. Powell DJ, Hajduch E, Kular G, Hundal HS. Ceramide Disables 3-Phosphoinositide Binding to the Pleckstrin Homology Domain of Protein Kinase B (PKB)/Akt by a PKCζ-Dependent Mechanism. Mol Cell Biol. 2003;23(21):7794–808.

22. Zick Y. Role of Ser/Thr kinases in the uncoupling of insulin signaling. Int J Obes. 2003;27:S56–60.

23. Shi H, Kokoeva M V., Inouye K, Tzameli I, Yin H, Flier JS. TLR4 links innate immunity and fatty acid-induced insulin resistance. J Clin Invest. 2006;116(11):3015–25.

24. Hotamisligil GS. Endoplasmic Reticulum Stress and the Inflammatory Basis of Metabolic Disease. Cell. 2010;140(6):900–17.

25. Wang D, Wei Y, Pagliassotti MJ. Saturated fatty acids promote endoplasmic reticulum stress and liver injury in rats with hepatic steatosis. Endocrinology. 2006;147(2):943–51.

26. Özcan U, Cao Q, Yilmaz E, Lee A-H, Iwakoshi NN, Özdelen E, et al. Endoplasmic Reticulum Stress Links Obesity, Insulin Action, and Type 2 Diabetes. Science. 2004;306(5695):457–61.

27. Todd DJ, Lee AH, Glimcher LH. The endoplasmic reticulum stress response in immunity and autoimmunity. Nat Rev Immunol. 2008;8(9):663–74.

28. Urano F, Wang XZ, Bertolotti A, Zhang Y, Chung P, Harding HP, et al. Coupling of stress in the ER to activation of JNK protein kinases by transmembrane protein kinase IRE1. Science. 2000;287(5453):664–6.

29. Deng J, Lu PD, Zhang Y, Scheuner D, Kaufman RJ, Sonenberg N, et al. Translational Repression Mediates Activation of Nuclear Factor Kappa B by Phosphorylated Translation Initiation Factor 2. Mol Cell Biol. 2004;24(23):10161–8.

30. Petersen KF, Dufour S, Befroy D, Garcia R, Shulman GI. Impaired Mitochondrial Activity in the Insulin-Resistant Offspring of Patients with Type 2 Diabetes. N Engl J Med. 2004;350(7):664–71.

31. Blaak EE, Van Aggel-Leijssen DPC, Wagenmakers AJM, Saris WHM, Van Baak MA. Impaired oxidation of plasma-derived fatty acids in type 2 diabetic subjects during moderate-intensity exercise. Diabetes. 2000;49(12):2102–7.

32. Ritov VB, Menshikova E V, He J, Ferrell RE, Goodpaster BH, Kelley DE. Deficiency of Subsarcolemmal Mitochondria in Obesity and Type 2 Diabetes. Diabetes. 2005;54(1):8–14.

33. Lowell B, Shulman G. Mitochondrial dysfunction and type 2 diabetes. Science. 2005;5(3):177–83.

34. Rong JX, Qiu Y, Hansen MK, Zhu L, Zhang V, Xie M, et al. Adipose Mitochondrial Biogenesis Is Suppressed in db/db and High-Fat Diet–Fed Mice and Improved by Rosiglitazone. Diabetes. 2007;56:1751–60.

35. Rosen ED, Spiegelman BM. What we talk about when we talk about fat. Cell. 2014;156(1–2):20–44.

36. Sjöström L, Smith U, Krotkiewski M, Björntorp P. Cellularity in different regions of adipose tissue in young men and women. Metabolism. 1972;21(12):1143–53.

37. Macotela Y, Boucher J, Tran TT, Kahn CR. Sex and depot differences in adipocyte insulin sensitivity and glucose. Diabetes. 2009;58(4):803–12.

38. Lee MJ, Wu Y, Fried SK. Adipose tissue heterogeneity: Implication of depot differences in adipose tissue for obesity complications. Mol Aspects Med. 2013;34(1):1–11.

39. Harris RBS, Leibel RL. Location, Location, Location... Cell Metab. 2008;7(5):359–61.

40. Gest S, Kahn CR. White Adipose Tissue. In: Symonds ME, editor. Adipose tissue biology. 2012th ed. 2012. p. 71–123.

41. Pischon T, Boeing H, Hoffmann K, Bergmann M, Schulze MB, Overvad K, et al. General and Abdominal Adiposity and Risk of Death in Europe. N Engl J Med. 2008;359(20):2105–20.

42. Muzumdar R, Allison DB, Huffman DM, Ma X, Atzmon G, Einstein FH, et al. Visceral adipose tissue modulates mammalian longevity. Aging Cell. 2008;7(3):438–40.

43. Gabriely I, Ma XH, Yang XM, Atzmon G, Rajala MW, Berg AH, et al. Removal of visceral fat prevents insulin resistance and glucose intolerance of aging: An adipokine-mediated process? Diabetes. 2002;51(10):2951–8.

44. Weber R V., Buckley MC, Fried SK, Kral JG. Subcutaneous lipectomy causes a metabolic syndrome in hamsters. Am J Physiol - Regul Integr Comp Physiol. 2000;279(3):R936–43.

45. Karpe F, Pinnick KE. Biology of upper-body and lower-body adipose tissue - Link to whole-body phenotypes. Nat Rev Endocrinol. 2015;11(2):90–100.

46. James DE, Brown R, Navarro J, Pilch PF. Insulin-regulatable tissues express a unique insulin-sensitive glucose transport protein. Nature. 1988;333(6169):183–5.

47. Macaulay SL, Jarett L. Insulin mediator causes dephosphorylation of the α subunit of pyruvate dehydrogenase by stimulating phosphatase activity. Arch Biochem Biophys. 1985;237(1):142–50.

48. Shrago E, Woldegiorgis G. Regulation of the fatty acid synthase promoter by insulin. J Nutr. 2000;130(2 SUPPL.):315S–320S.

49. Foufelle F, Gouhot B, Pegorier JP, Perdereau D, Girard J, Ferre P. Glucose stimulation of lipogenic enzyme gene expression in cultured white adipose tissue: A role for glucose 6-phosphate. J Biol Chem. 1992;267(29):20543–6.

50. Hellerstein MK. De novo lipogenesis in humans: Metabolic and regulatory aspects. Eur J Clin Nutr. 1999;53:s53–65.

51. Fain JN, Madan AK, Hiler ML, Cheema P, Bahouth SW. Comparison of the release of adipokines by adipose tissue, adipose tissue matrix, and adipocytes from visceral and subcutaneous abdominal adipose tissues of obese humans. Endocrinology. 2004;145(5):2273–82.

52. Fain JN, Tichansky DS, Madan AK. Most of the interleukin 1 receptor antagonist, cathepsin S, macrophage migration inhibitory factor, nerve growth factor, and interleukin 18 release by explants of human adipose tissue is by the non-fat cells, not by the adipocytes. Metabolism. 2006;55(8):1113–21.

53. Turer AT, Scherer PE. Adiponectin: Mechanistic insights and clinical implications. Diabetologia. 2012;55(9):2319–26.

54. Fasshauer M, Blüher M. Adipokines in health and disease. Trends Pharmacol Sci. 2015;36(7):461–70.

55. Hajer GR, Van Haeften TW, Visseren FLJ. Adipose tissue dysfunction in obesity, diabetes, and vascular diseases. Eur Heart J. 2008;29(24):2959–71.

56. Richard AJ, White U, Elks CM, Stephens JM. Adipose Tissue: Physiology to Metabolic Dysfunction. South Dartmouth (MA): Endotext; 2020.

57. Hauner H. Secretory factors from human adipose tissue and their functional role. Proc Nutr Soc. 2005;64(2):163–9.

58. Mantzoros CS, Magkos F, Brinkoetter M, Sienkiewicz E, Dardeno TA, Kim SY, et al. Leptin in human physiology and pathophysiology. Am J Physiol - Endocrinol Metab. 2011;301(4).

59. Denroche HC, Huynh FK, Kieffer TJ. The role of leptin in glucose homeostasis. J Diabetes Investig. 2012;3(2):115–29.

60. Kadowaki T, Yamauchi T. Adiponectin and adiponectin receptors. Endocr Rev. 2005;26(3):439–51.

61. Kim KH, Lee K, Moon YS, Sul HS. A Cysteine-rich Adipose Tissue-specific Secretory Factor Inhibits Adipocyte Differentiation. J Biol Chem. 2001;276(14):11252–6.

62. Steppan CM, Bailey ST, Bhat S, Brown EJ, Banerjee RR, Wright CM, et al. The hormone resistin links obesity to diabetes. Nature. 2001;409(6818):307–12.

63. Curat CA, Wegner V, Sengenès C, Miranville A, Tonus C, Busse R, et al. Macrophages in human visceral adipose tissue: Increased accumulation in obesity and a source of resistin and visfatin. Diabetologia. 2006;49(4):744–7.

64. Larsen CM, Faulenbach M, Vaag A, Vølund A, Ehses JA, Seifert B, et al. Interleukin-1–Receptor Antagonist in Type 2 Diabetes Mellitus. N Engl J Med. 2007;356(15):1517–26.

65. Tack CJ, Stienstra R, Joosten LAB, Netea MG. Inflammation links excess fat to insulin resistance: The role of the interleukin-1 family. Immunol Rev. 2012;249(1):239–52.

66. Hotamisligil GS. The role of TNFα and TNF receptors in obesity and insulin resistance. J Intern Med. 1999;245(6):621–5.

67. Saely CH, Geiger K, Drexel H. Brown versus white adipose tissue: A mini-review. Gerontology. 2012;58(1):15–23.

68. Cinti S. The Adipose Organ. In: Fantuzzi G, Mazzone T, editors. Adipose Tissue and Adipokines in Health and Disease. Humana Press; 2007. p. 3–19.

69. Nedergaard J, Bengtsson T, Cannon B. Unexpected evidence for active brown adipose tissue in adult humans. Am J Physiol - Endocrinol Metab. 2007;293(2):444–52.

70. Villena JA. Brown Adipose Tissue and Control of Body Weight : a New Potential Target for the Treatment of Obesity. In: Press Ic, editor. Obesity epidemic. 1st editio. iConcept Press Ltd; 2008.

71. Shabalina IG, Petrovic N, deJong JMA, Kalinovich A V., Cannon B, Nedergaard J. UCP1 in Brite/Beige adipose tissue mitochondria is functionally thermogenic. Cell Rep. 2013;5(5):1196–203.

72. Cannon B, Nedergaard J. Brown Adipose Tissue: Function and Physiological Significance. Physiol Rev. 2004;84(1):277–359.

73. Liu X, Wang S, You Y, Meng M, Zheng Z, Dong M, et al. Brown adipose tissue transplantation reverses obesity in Ob/Ob mice. Endocrinology. 2015;156(7):2461–9.

74. Umekawa T, Yoshida T, Sakane N, Saito M, Kumamoto K, Kondo M. Anti-obesity and anti-diabetic effects of CL316,243, a highly specific β3-adrenoceptor agonist, in Otsuka Long-Evans Tokushima Fatty rats: Induction of uncoupling protein and activation of glucose transporter 4 in white fat. Eur J Endocrinol. 1997;136(4):429–37.

75. Kato H, Ohue M, Kato K, Nomura A, Toyosawa K, Furutani Y, et al. Mechanism of amelioration of insulin resistance by β3-adrenoceptor agonist AJ-9677 in the KK-Ay/Ta diabetic obese mouse model. Diabetes. 2001;50(1):113–22.

76. Cypess AM, Chen YC, Sze C, Wang K, English J, Chan O, et al. Cold but not sympathomimetics activates human brown adipose tissue in vivo. Proc Natl Acad Sci U S A. 2012;109(25):10001–5.

77. Sell H, Berger JP, Samson P, Castriota G, Lalonde J, Deshaies Y, et al. Peroxisome proliferator-activated receptor γ agonism increases the capacity for sympathetically mediated thermogenesis in lean and ob/ob mice. Endocrinology. 2004;145(8):3925–34.

78. Carmona MC, Louche K, Lefebvre B, Pilon A, Hennuyer N, Audinot-Bouchez V, et al. A new specific peroxisome proliferator-activated receptor γ modulator with potent antidiabetes and antiatherogenic effects. Diabetes. 2007;56(11):2797–808.

79. Villarroya F, Vidal-Puig A. Beyond the sympathetic tone: The new brown fat activators. Cell Metab. 2013;17(5):638–43.

80. Lugus JJ, Walsh K, Shoelson SE, Cantrell DA. Immunometabolism: an emerging frontier. Nat Publ Gr. 2011;11:81–3.

81. Asterholm IW, Tao C, Morley TS, Wang QA, Delgado-lopez F, Wang Z V, et al. Adipocyte inflammation is essential for healthy adipose tissue expansion and remodeling. Cell Metab. 2014;20(1):103–18.

82. Romagnani S. Th1/Th2 cells. Inflamm Bowel Dieseases. 1999;5(4):285–94.

83. Wu D, Molofsky AB, Liang H-E, Ricardo-Gonzalez RR, Jouihan HA, Bando JK, et al. Eosinophils sustain adipose alternatively activated macrophages associated with glucose homeostasis. Science. 2012;332(6026):243–7.

84. Kang YE, Kim HJ, Shong M. Regulation of Systemic Glucose Homeostasis by T Helper Type 2 Cytokines. Diabetes Metab J. 2019;43(5):549–59.

85. Cildir G, Akincilar SC, Tergaonkar V. Chronic adipose tissue inflammation: All immune cells on the stage. Trends Mol Med. 2013;19(8):487–500.

86. Hotamisligil GS, Atkinson RL, Spiegelman BM. Increased adipose tissue expression of tumor necrosis factor-alpha in human obesity and insulin resistance. J Clin Invest. 1995;95(5):2409–15.

87. Medzhitov R, Janeway CAJ. Innate immune recognition and control of adaptive immune responses. 1998;10(5):351–3.

88. Dal Santo B, Bonamichi F, Lee J. Unusual suspects in the development of obesity-induced inflammation and insulin resistance: NK cells, iNKT cells, and ILCs. Diabetes Metab J. 2017;41(4):229–50.

89. Weisberg SP, McCann D, Desai M, Rosenbaum M, Leibel RL, Ferrante AW. Obesity is associated with macrophage accumulation in adipose tissue. J Clin Invest. 2003;112(12):1796–808.

90. Lumeng CN, Bodzin JL, Saltiel AR. Obesity induces a phenotypic switch in adipose tissue macrophage polarization. J Clin Invest. 2007;117(1):175–84.

91. Lumeng CN, Delproposto JB, Westcott DJ, Saltiel AR. Phenotypic switching of adipose tissue macrophages with obesity is generated by spatiotemporal differences in macrophage subtypes. Diabetes. 2008;57(12):3239–46.

92. Odegaard JI, Ricardo-gonzalez RR, Goforth MH, Morel CR, Subramanian V, Mukundan L, et al. Macrophage-specific PPARgamma controls alternative activation and improves insulin resistance. Nature. 2007;447(7148):1116–20.

93. Lee M, Odegaard JI, Mukundan L, Qiu Y, Molofsky AB, Nussbaum JC, et al. Activated Type 2 Innate Lymphoid Cells Regulate Beige Fat Biogenesis. Cell. 2014;160(1–2):74–87.

94. Rao RR, Long JZ, White JP, Svensson KJ, Lou J, Lokurkar I, et al. Meteorin-like is a hormone that regulates immune-adipose interactions to increase beige fat thermogenesis. Cell. 2014;157(6):1279–91.

95. Hui X, Gu P, Zhang J, Wang Y, Lam KSL, Xu A, et al. Adiponectin Enhances Cold-Induced Browning of Subcutaneous Adipose Tissue via Promoting M2 Macrophage Proliferation. Cell Metab. 2015;22(2):279–90.

96. Fischer K, Ruiz HH, Jhun K, Finan B, Oberlin DJ, Heide V Van Der, et al. Alternatively activated macrophages do not synthesize catecholamines or contribute to adipose tissue adaptive thermogenesis. Nat Med. 2017;23(5):623–30.

97. Patsouris D, Li P, Thapar D, Chapman J, Olefsky JM, Neels JG. Ablation of CD11c-Positive Cells Normalizes Insulin Sensitivity in Obese Insulin Resistant Animals. Cell Metab. 2008;8(4):301–9.

98. Steinman RM. Dendritic cells: Versatile controllers of the immune system. Nat Med. 2007;13(10):1155–9.

99. Stefanovic-Racic M, Yang X, Turner MS, Mantell BS, Stolz DB, Sumpter TL, et al. Dendritic cells promote macrophage infiltration and comprise a substantial proportion of obesity-associated increases in CD11c+ cells in adipose tissue and liver. Diabetes. 2012;61(9):2330–9.

100. Bertola A, Ciucci T, Rousseau D, Bourlier V, Duffaut C, Bonnafous S, et al. Identification of adipose tissue dendritic cells correlated with obesity-associated insulin-resistance and inducing Th17 responses in mice and patients. Diabetes. 2012;61(9):2238–47.

101. Hannibal TD, Schmidt-Christensen A, Nilsson J, Fransén-Pettersson N, Hansen L, Holmberg D. Deficiency in plasmacytoid dendritic cells and type I interferon signalling prevents diet-induced obesity and insulin resistance in mice. Diabetologia. 2017;60(10):2033–41.

102. Borregaard N. Neutrophils, from Marrow to Microbes. Immunity. 2010;33(5):657–70.

103. Ferrante AW. The immune cells in adipose tissue. Diabetes, Obes Metab. 2013;15(S3):34–8.

104. Nijhuis J, Rensen SS, Slaats Y, Dielen FMH Van, Buurman WA, Greve JWM. Neutrophil Activation in Morbid Obesity, Chronic Activation of Acute Inflammation. Obesity. 2009;17(11):2014–8.

105. Elgazar-carmon V, Rudich A, Hadad N, Levy R. Neutrophils transiently infiltrate intra-abdominal fat early in the course of high-fat feeding. J Lipid Res. 2008;49(9):1894–903.

106. Talukdar S, Oh DY, Bandyopadhyay G, Li D, Mcnelis J, Lu M, et al. Neutrophils mediate insulin resistance in high fat diet fed mice via secreted elastase. Nat Med. 2012;18(9):1407–12.

107. Mansuy-Aubert V, Zhou QL, Xie X, Gong Z, Huang JY, Khan AR, et al. Imbalance between neutrophil elastase and its inhibitor α1-antitrypsin in obesity alters insulin sensitivity, inflammation, and energy expenditure. Cell Metab. 2013;17(4):534–48.

108. O'Sullivan TE, Sun JC, Lanier LL. Natural Killer Cell Memory. Immunity. 2015;43(4):634–45.

109. Wensveen FM, Jelenčić V, Valentić S, Šestan M, Wensveen TT, Theurich S, et al. NK cells link obesity-induced adipose stress to inflammation and insulin resistance. Nat Immunol. 2015;16(4):376–85.

110. Ballesteros-Pomar MD, Calleja S, Díez-Rodríguez R, Calleja-Fernández A, Vidal-Casariego A, Nuñez-Alonso A, et al. Inflammatory status is different in relationship to insulin resistance in severely obese people and changes after bariatric surgery or diet-induced weight loss. Exp Clin Endocrinol Diabetes. 2014;122(10):592–6.

111. O'Rourke RW, Metcalf MD, White AE, Madala A, Winters BR, Maizlin II, et al. Depot-specific differences in inflammatory mediators and a role for NK cells and IFN-γ in inflammation in human adipose tissue. Int J Obes. 2009;33(9):978–90.

112. Gua H, Xu B, Gao L, Sun X, Qu X, Li X, et al. High frequency of activated natural killer and natural killer T-cells in patients with new onset of type 2 diabetes mellitus. Exp Biol Med. 2012;237(5):556–62.

113. Lee B, Kim M, Pae M, Yamamoto Y, Eberlé D, Shimada T, et al. Adipose natural killer cells regulate adipose tissue macrophages to Promote Insulin Resistance in Obesity. Cell Metab. 2017;23(4):685–98.

114. O'Rourke RW, Meyer KA, Neeley CK, Gaston GD, Sekhri P, Szumowski M, et al. Systemic NK cell ablation attenuates intra-abdominal adipose tissue macrophage infiltration in murine obesity. Obesity. 2014;22(10):2109–14.

115. Kelley DS, Daudu PA, Branch LB, Johnson HL TP, B M. Energy restriction decreases number of circulating natural killer cells and serum levels of immunoglobulins in overweight women. Eur J Clin Nutr. 1994;48(1):9–18.

116. Rosenberg HF, Dyer KD, Foster PS. Eosinophils: Changing perspectives in health and disease. Nat Rev Immunol. 2013;13(1):9–22.

117. Johnson AMF, Costanzo A, Gareau MG, Armando AM, Quehenberger O, Jameson JM, et al. High fat diet causes depletion of intestinal eosinophils associated with intestinal permeability. PLoS One. 2015;10(4):e0122195.

118. Eberl G, Colonna M, Santo JP Di, Mckenzie ANJ. Innate Lymphoid Cells : a new paradigm in immunology. Science. 2015;348(6237).

119. Robinette M, Fuchs A, Cortez V, Lee J, Wang Y, Durum S, et al. Transcriptional Programs Define Molecular Characteristics of Innate Lymphoid Cell Classes and Subsets. Nat Immunol. 2015;16(3):306–17.

120. Moro K, Yamada T, Tanabe M, Takeuchi T, Ikawa T, Kawamoto H, et al. Innate production of T(H)2 cytokines by adipose tissue-associated c-Kit(+)Sca-1(+) lymphoid cells. Nature. 2010;463(7280):540–4.

121. Molofsky AB, Nussbaum JC, Liang H, Dyken SJ Van, Cheng LE, Mohapatra A, et al. Innate lymphoid type 2 cells sustain visceral adipose tissue eosinophils and alternatively activated macrophages. 2013;210(3):535–49.

122. Sonnenberg GF, Thome JJ, Farber DL, Seale P, Artis D. Group 2 innate lymphoid cells promote beiging of adipose and limit obesity. Nature. 2015;519(7542):242–6.

123. Sullivan TEO, Rapp M, Fan X, Walzer T, Dannenberg AJ, Sun JC, et al. Adipose-Resident Group 1 Innate Lymphoid Cells Promote Obesity-Associated Insulin Resistance Article Adipose-Resident Group 1 Innate Lymphoid Cells Promote Obesity-Associated Insulin Resistance. Immunity. 2016;45(2):428–41.

124. Boehm T. Design principles of adaptive immune systems. Nat Rev Immunol. 2011;11(5):307–17.

125. Abul Abbas, Andrew Lichtman SP. Cellular and Molecular Immunology. 8th ed. Philadelphia P: ES, editor. 2017.

126. Jäger A, Kuchroo VK. Effector and regulatory T-cell subsets in autoimmunity and tissue inflammation. Scand J Immunol. 2010;72(3):173–84.

127. Nishimura S, Manabe I, Nagasaki M, Eto K, Yamashita H, Ohsugi M, et al. CD8 + effector T cells contribute to macrophage recruitment and adipose tissue inflammation in obesity. Nat Med. 2009;15(8):914–20.

128. Pacifico L, Renzo L Di, Anania C, Osborn JF, Ippoliti F, Schiavo E, et al. Increased T-helper interferon-γ-secreting cells in obese children. Eur J Endocrinol. 2006;154(5):691–7.

129. Winer S, Chan Y, Paltser G, Truong D, Tsui H, Bahrami J, et al. Normalization of obesity-associated insulin resistance through immunotherapy. Nat Med. 2009;15(8):921–30.

130. Rocha VZ, Folco EJ, Sukhova G, Shimizu K, Gotsman I, Vernon AH, et al. Interferon-gamma, a Th1 cytokine, regulates fat inflammation: a role for adaptive immunity in obesity. Circ Res. 2008;103(5):467–76.

131. Deng T, Lyon CJ, Minze LJ, Lin J, Zou J, Liu JZ, et al. Class II major histocompatibility complex plays an essential role in obesity-induced adipose inflammation. Cell Metab. 2013;17(3):411–22.

132. Cho KW, Morris DL, delProposto JL, Geletka L, Zamarron B, Martinez-Santibanez G, et al. An MHC II-dependent activation loop between adipose tissue macrophages and CD4+ T cells controls obesity-induced inflammation. Cell Rep. 2014;9(2):605–17.

133. Mclaughlin T, Liu L, Lamendola C, Shen L, Morton J, Rivas H, et al. T-cell profile in adipose tissue is associated with insulin resistance and systemic inflammation in humans. 2014;34(12):2637–43.

134. Zeyda M, Huber J, Prager G, Stulnig TM. Inflammation correlates with markers of T-cell subsets including regulatory T cells in adipose tissue from obese patients. Obes (Silver Spring). 2009;19(4):743–8.

135. Sutton CE, Mielke LA, Mills KHG. IL-17-producing γδ T cells and innate lymphoid cells. Eur J Immunol. 2012;42(9):2221–31.

136. Kohlgruber AC, Gal-Oz ST, Lamarche NM, Shimazaki M, Duquette D, Koay H, et al. γδ T cells producing interleukin-17A regulate adipose regulatory T cell homeostasis and thermogenesis. Nat Immunol. 2018;19(5):464–74.

137. Jagannathan-bogdan M, Mcdonnell ME, Shin H, Rehman Q, Hasturk H, Caroline M, et al. Elevated Proinflammatory Cytokine Production by a Skewed T Cell Compartment Requires Monocytes and Promotes Inflammation in Type 2 Diabetes. J Immunol. 2021;186(2):1162–72.

138. Fabbrini E, Mohammed BS, Magkos F, Korenblat KM, Patterson BW KS. Alterations in adipose tissue and hepatic lipid kinetics in obese men and women with nonalcoholic fatty liver disease. Gastroenterology. 2008;134(2):424–31.

139. Winer S, Paltser G, Chan Y, Tsui H, Engleman E, Winer D, et al. Obesity predisposes to Th17 bias. Eur J Immunol. 2009;39(9):2629–35.

140. Zúñiga LA, Shen W, Joyce-shaikh B, Pyatnova EA, Richards AG, Thom C, et al. IL-17 Regulates Adipogenesis, Glucose Homeostasis, and Obesity. J Immunol. 2010;185(11):6947–59.

141. Zhu L, Wu Y, Wei H, Xing X, Zhan N, Xiong H, et al. IL-17R activation of human periodontal ligament fibroblasts induces IL-23 p19 production: Differential involvement of NF-κB versus JNK/AP-1 pathways. Mol Immunol. 2011;48(4):647–56.

142. Feuerer M, Herrero L, Cipolletta D, Naaz A, Wong J, Nayer A, et al. Lean, but not obese, fat is enriched for a unique population of regulatory T cells that affect metabolic parameters. Nat Med. 2009;15(8):930–9.

143. Rausch ME, Weisberg S, Vardhana P, Tortoriello D V. Obesity in C57BL/6J mice is characterized by adipose tissue hypoxia and cytotoxic T-cell infiltration. Int J Obes. 2008;32(3):451–63.

144. Mehta P, Nuotio-Antar AM, Smith CW. γδ T cells promote inflammation and insulin resistance during high fat diet-induced obesity in mice . J Leukoc Biol. 2015;97(1):121–34.

145. Costanzo AE, Taylor KR, Dutt S, Han PP, Fujioka K, Jameson JM. Obesity impairs γδ T cell homeostasis and antiviral function in humans. PLoS One. 2015;10(3):e0120918.

146. Meng X, Yang J, Dong M, Zhang K, Tu E, Gao Q, et al. Regulatory T cells in cardiovascular diseases. Nat Rev Cardiol. 2016;13(3):167–79.

147. Jetten AM. Retinoid-related orphan receptors (RORs): critical roles in development, immunity, circadian rhythm, and cellular metabolism. Nucl Recept Signal. 2009;7:e003.

148. Godfrey DI, MacDonald HR, Kronenberg M, Smyth MJ, Van Kaer L. NKT cells: What's in a name? Nat Rev Immunol. 2004;4(3):231–7.

149. Bendelac A, Savage PB, Teyton L. The biology of NKT cells. Annu Rev Immunol. 2007;25:297–336.

150. Borg NA, Wun KS, Kjer-Nielsen L, Wilce MCJ, Pellicci DG, Koh R, et al. CD1d-lipid-antigen recognition by the semi-invariant NKT T-cell receptor. Nature. 2007;448(7149):44–9.

151. Matsuda JL, Naidenko O V., Gapin L, Nakayama T, Taniguchi M, Wang CR, et al. Tracking the response of natural killer T cells to a glycolipid antigen using CD1d tetramers. J Exp Med. 2000;192(5):741–53.

152. Lynch L, Nowak M, Varghese B, Clark J, Hogan AE, Toxavidis V, et al. Adipose tissue invariant NKT cells protect against diet-induced obesity and metabolic disorder through regulatory cytokine production. Immunity. 2012;37(3):574–87.

153. Mantell BS, Stefanovic-Racic M, Yang X, Dedousis N, Sipula IJ, O'Doherty RM. Mice lacking NKT cells but with a complete complement of CD8+ T-Cells are not protected against the metabolic abnormalities of diet-induced obesity. PLoS One. 2011;6(6):e19831.

154. Wu L, Parekh V V., Gabriel CL, Bracy DP, Marks-Shulman PA, Tamboli RA, et al. Activation of invariant natural killer T cells by lipid excess promotes tissue inflammation, insulin resistance, and hepatic steatosis in obese mice. Proc Natl Acad Sci U S A. 2012;109(19):E1143-52.

155. Lebien TW, Tedder TF. B lymphocytes: How they develop and function. Blood. 2008;112(5):1570–80.

156. DeFuria J, Belkina AC, Jagannathan-Bogdan M, Snyder-Cappione J, Carr JD, Nersesova YR, et al. B cells promote inflammation in obesity and type 2 diabetes through regulation of T-cell function and an inflammatory cytokine profile. Proc Natl Acad Sci U S A. 2013;110(13):5133–8.

157. Winer DA, Winer S, Shen L, Wadia PP, Yantha J, Paltser G, et al. B cells promote insulin resistance through modulation of T cells and production of pathogenic IgG antibodies. Nat Med. 2011;17(5):610–7.

158. Han JM, Levings MK. Immune Regulation in Obesity-Associated Adipose Inflammation. J Immunol. 2013;191(2):527–32.

159. Catrysse L, van Loo G. Adipose tissue macrophages and their polarization in health and obesity. Cell Immunol. 2018;330:114–9.

160. Hruskova Z, Biswas SK. A new "immunological" role for adipocytes in obesity. Cell Metab. 2013;17(3):315–7.

161. Bordone L, Guarente L. Calorie restriction, SIRT1 and metabolism: understanding longevity. Nat Rev Mol Cell Biol. 2005;6(4):298–305.

162. Wetter TJ, Gazdag AC, Dean DJ, Cartee GD. Effect of calorie restriction on in vivo glucose metabolism by individual tissues in rats. Am J physioogy. 1999;276(4):E728-738.

163. Barnosky AR, Hoddy KK, Unterman TG, Varady KA. Intermittent fasting vs daily calorie restriction for type 2 diabetes prevention: A review of human findings. Transl Res. 2014;164(4):302–11.

164. Redman LM, Ravussin E. Caloric restriction in humans: impact on physiological, psychological, and behavioral outcomes. Antioxid Redox Signal. 2011;14(2):275–87.

165. Walford RL, Mock D, Verdery R, MacCallum T. Calorie restriction in biosphere 2: Alterations in physiologic, hematologic, hormonal, and biochemical parameters in humans restricted for a 2-year period. Journals Gerontol - Ser A Biol Sci Med Sci. 2002;57(6):B211–24.

166. Larson-Meyer DE, Heilbronn LK, Redman LM, Newcomer BR, Frisard MI, Anton S, et al. Effect of calorie restriction with or without exercise on insulin sensitivity, β-cell function, fat cell size, and ectopic lipid in overweight subjects. Diabetes Care. 2006;29(6):1337–44.

167. Jolly CA. Dietary restriction and immune function. J Nutr. 2004;134(8):1853–6.

168. White MJ, Beaver CM, Goodier MR, Bottomley C, Morgan J, Pearce DJ, et al. Calorie Restriction Attenuates Terminal Differentiation of Immune Cells. Front Immunol. 2017;7:667.

169. Wasinski F, Bacurau RFP, Moraes MR, Haro AS, Moraes-vieira PMM, Estrela GR, et al. Exercise and Caloric Restriction Alter the Immune System of Mice Submitted to a High-Fat Diet. Mediators Inflamm. 2013;2013:395672.

170. Fabbiano S, Sua N, Veyrat-durebex C, Dokic AS, Colin DJ, Veyrat-durebex C, et al. Caloric Restriction Leads to Browning of White Adipose Tissue through Type 2 Immune Signaling. Cell Metab. 2016;24(3):434–46.

171. Rogozina OP, Bonorden MJL, Seppanen CN, Grande JP, Cleary MP. Effect of chronic and intermittent calorie restriction on serum adiponectin and leptin and mammary tumorigenesis. Cancer Prev Res. 2011;4(4):568–82.

172. Hołowko J, Michalczyk MM, Zając A, Czerwińska-Rogowska M, Ryterska K, Banaszczak M, et al. Six Weeks of Calorie Restriction Improves Body Composition and Lipid Profile in Obese and Overweight Former Athletes. Nutrients. 2019;11(7):1461.

173. Stern JH, Rutkowski JM, Scherer PE. Adiponectin, Leptin, and Fatty Acids in the Maintenance of Metabolic Homeostasis Through Adipose Tissue Crosstalk. Cell Metab. 2016;23(5):770–84.

174. Most J, Maree Redman L. Impact of calorie restriction on energy metabolism in humans. Exp Gerontol. 2020;133:110875.

175. Pfluger PT, Herranz D, Velasco-Miguel S, Serrano M, Tschöp MH. Sirt1 protects against high-fat diet-induced metabolic damage. Proc Natl Acad Sci U S A. 2008;105(28):9793–8.

176. Lagouge M, Argmann C, Gerhart-Hines Z, Meziane H, Lerin C, Daussin F, et al. Resveratrol Improves Mitochondrial Function and Protects against Metabolic Disease by Activating SIRT1 and PGC-1α. Cell. 2006;127(6):1109–22.

177. Nisoli E, Tonello C, Cardile A, Cozzi V, Bracale R, Tedesco L, et al. Calorie restriction promotes mitochondrial biogenesis by inducing the expression of eNOS. Science. 2005;310(5746):314–7.

178. Higami Y, Pugh TD, Page GP, Allison DB, Prolla TA, Weindruch R. Adipose tissue energy metabolism: altered gene expression profile of mice subjected to long-term caloric restriction. FASEB J. 2004;18(2):415–7.

179. Civitarese AE, Carling S, Heilbronn LK, Hulver MH, Ukropcova B, Deutsch WA, et al. Calorie restriction increases muscle mitochondrial biogenesis in healthy humans. PLoS Med. 2007;4(3):e76.

180. Vann JM, Cray NL, Barger JL, Pugh TD, Mastaloudis A, Hester SN, et al. Identification of tissue-specific transcriptional markers of caloric restriction in the mouse and their use to evaluate caloric restriction mimetics. Aging Cell. 2017;16(4):750–60.

181. Hancock CR, Han D, Higashida K, Kim SH, Holloszy JO. Does calorie restriction induce mitochondrial biogenesis? A reevaluation. FASEB J. 2011;25(2):785–91.

182. Pardo R, Vilà M, Cervela L, De Marco M, Gama-Pérez P, González-Franquesa A, et al. Calorie restriction prevents diet-induced insulin resistance independently of PGC-1-driven mitochondrial biogenesis in white adipose tissue. FASEB J. 2019;33(2):2343–2358.

183. Finley LWS, Lee J, Souza A, Desquiret-Dumas V, Bullock K, Rowe GC, et al. Skeletal muscle transcriptional coactivator PGC-1α mediates mitochondrial, but not metabolic, changes during calorie restriction. Proc Natl Acad Sci U S A. 2012;109(8):2931–6.

184. Bordone L, Cohen D, Robinson A, Motta MC, Veen E Van, Czopik A, et al. SIRT1 transgenic mice show phenotypes resembling calorie restriction. Aging Cell. 2007;6(6):759–67.

185. Chalkiadaki A, Guarente L. High-fat diet triggers inflammation-induced cleavage of SIRT1 in adipose tissue to promote metabolic dysfunction. Cell Metab. 2012;16(2):180–8.

186. Houtkooper RH, Pirinen E, Auwerx J. Sirtuins as regulators of metabolism and healthspan. Nat Rev Mol Cell Biol. 2012;13(4):225–38.

187. Kim EJ, Kho JH, Kang MR, Um SJ. Active Regulator of SIRT1 Cooperates with SIRT1 and Facilitates Suppression of p53 Activity. Mol Cell. 2007;28(2):277–90.

188. Picard F, Kurtev M, Chung N, Topark-Ngarm A, Senawong T, Oliveira RM De, et al. Sirt1 promotes fat mobilization in white adipocytes by repressing PPAR-gamma. Nature. 2004;429(6993):771–6.

189. Hardie DG. Sensing of energy and nutrients by AMP-activated protein kinase. Am J Clin Nutr. 2011;93(4):891S-6S.

190. Cantó C, Gerhart-hines Z, Feige JN, Lagouge M, Milne JC, Elliott PJ, et al. AMPK regulates energy expenditure by modulating NAD+ metabolism and SIRT1 activity. Nature. 2009;458(7241):1056–60.

191. Kadowaki T, Yamauchi T, Kubota N, Hara K, Ueki K, Tobe K. Adiponectin and adiponectin receptors in insulin resistance, diabetes, and the metabolic syndrome. J Clin Invest. 2006;116(7):1784–92.

192. To K, Yamaza H, Komatsu T, Hayashida T, Hayashi H, Toyama H, et al. Down-regulation of AMP-activated protein kinase by calorie restriction in rat liver. Exp Gerontol. 2007;42(11):1063–71.

193. Gonzalez AA, Kumar R, Mulligan JD, Davis AJ, Weindruch R, Saupe KW. Metabolic adaptations to fasting and chronic caloric restriction in heart, muscle, and liver do not include changes in AMPK activity. Am J Physiol - Endocrinol Metab. 2004;287(5):1032–7.

194. Jäer S, Handschin C, St-Pierre J, Spiegelman BM. AMP-activated protein kinase (AMPK) action in skeletal muscle via direct phosphorylation of PGC-1α. Proc Natl Acad Sci U S A. 2007;104(29):12017–22.

195. Miller BF, Robinson MM, Bruss MD, Hellerstein M, Hamilton KL. A comprehensive assessment of mitochondrial protein synthesis and cellular proliferation with age and caloric restriction. Aging Cell. 2012;11(1):150–61.

196. Silvestre MFP, Viollet B, Caton PW, Leclerc J, Sakakibara I, Foretz M, et al. The AMPK-SIRT signaling network regulates glucose tolerance under calorie restriction conditions. Life Sci. 2014;100(1):55–60.

197. Frescas D, Valenti L, Accili D. Nuclear trapping of the forkhead transcription factor FoxO1 via sirt-dependent deacetylation promotes expression of glucogenetic genes. J Biol Chem. 2005;280(21):20589–95.

198. Walker AK, Yang F, Jiang K, Ji JY, Watts JL, Purushotham A, et al. Conserved role of SIRT1 orthologs in fasting-dependent inhibition of the lipid/cholesterol regulator SREBP. Genes Dev. 2010;24(13):1403–17.

199. Haigis MC, Sinclair DA. Mammalian Sirtuins: Biological Insights and Disease Relevance. Annu Rev Pathol. 2010;5:253–95.

200. Duan W. Sirtuins : from metabolic regulation to brain aging. Front Aging Neurosci. 2013;5:1–36.

201. Sinclair DA. Toward a unified theory of caloric restriction and longevity regulation. Mech Ageing Dev. 2005;126(9):987–1002.

202. Beaven SW, Tontonoz P. Nuclear receptors in lipid metabolism: Targeting the heart of dyslipidemia. Annu Rev Med. 2006;57(5):313–29.

203. Hummasti S, Tontonoz P. Adopting new orphans into the family of metabolic regulators. Mol Endocrinol. 2008;22(8):1743–53.

204. Zhang Y, Luo XY, Wu DH, Xu Y. ROR nuclear receptors: Structures, related diseases, and drug discovery. Acta Pharmacol Sin. 2015;36(1):71–87.

205. Solt LA, Griffin PR, Burris TP. Ligand regulation of retinoic acid receptor-related orphan receptors: implications for development of novel therapeutics. Curr Opin lipidiology. 2010;21(3):204–11.

206. Jetten AM, Kurebayashi S, Ueda E. The ROR nuclear orphan receptor subfamily: Critical regulators of multiple biological processes. Prog Nucleic Acid Res Mol Biol. 2001;69:205–47.

207. Solt LA, Burris TP. Action of RORs and their ligands in (patho)physiology. Trends Endocrinol Metab. 2012;23(12):619–627.

208. Kojetin DJ, Burris TP. REV-ERB and ROR nuclear receptors as drug targets. Physiol Behav. 2014;13(3):197–216.

209. Kumar N, Lyda B, Chang MR, Lauer JL, Solt LA, Burris TP, et al. Identification of SR2211: a potent synthetic RORγ-selective modulator. ACS Chem Biol. 2012;7(4):672–7.

210. Chang MR, Lyda B, Kamenecka TM, Griffin PR. Pharmacologic repression of retinoic acid receptor-related orphan nuclear receptor γ is therapeutic in the collagen-induced arthritis experimental model. Arthritis Rheumatol. 2014;66(3):579–88.

211. Liu Y, Chen Y, Zhang J, Liu Y, Zhang Y, Su Z. Retinoic acid receptor-related orphan receptor α stimulates adipose tissue inflammation by modulating endoplasmic reticulum stress. J Biol Chem. 2017;292(34):13959–69.

212. Wang Y, Kumar N, Nuhant P, Cameron MD, Istrate MA, Roush WR, et al. Identification of SR1078, a synthetic agonist for the orphan nuclear receptors RORα and RORγ. ACS Chem Biol. 2010;5(11):1029–34.

213. Xiao S, Yosef N, Yang J, Wang Y, Zhou L, Zhu C, et al. Small-molecule RORγt antagonists inhibit T helper 17 cell transcriptional network by divergent mechanisms. Immunity. 2014;40(4):477–89.

214. Santori FR, Huang P, Pavert SA Van De, Jr EFD, Leaver DJ, Haubrich BA, et al. Identification of Natural RORγ Ligands that Regulate the Development of Lymphoid Cells. Cell Metab. 2015;21(2):286–97.

215. Smith SH, Peredo CE, Takeda Y, Bui T, Neil J, Rickard D, et al. Development of a topical treatment for psoriasis targeting RORγ: From bench to skin. PLoS One. 2016;11(2):e0147979.

216. Kang EG, Wu S, Gupta A, von Mackensen YL, Siemetzki H, Freudenberg JM, et al. A phase I randomized controlled trial to evaluate safety and clinical effect of topically applied GSK2981278 ointment in a psoriasis plaque test. Br J Dermatol. 2018;178(6):1427–9.

217. Sun N, Guo H, Wang Y. Retinoic acid receptor-related orphan receptor gamma-t (RORγt) inhibitors in clinical development for the treatment of autoimmune diseases: a patent review (2016-present). Expert Opin Ther Pat. 2019;29(9):663–74.

218. Fauber BP, René O, De Leon Boenig G, Burton B, Deng Y, Eidenschenk C, et al. Reduction in lipophilicity improved the solubility, plasma-protein binding, and permeability of tertiary sulfonamide RORc inverse agonists. Bioorganic Med Chem Lett. 2014;24(16):3891–7.

219. Gold DA, Gent PM, Hamilton BA. RORα in genetic control of cerebellum development: 50 staggering years. Brain Res. 2007;1140(1):19–25.

220. Fujieda H, Bremner R, Mears AJ, Sasaki H. Retinoic acid receptor-related orphan receptor α regulates a subset of cone genes during mouse retinal development. J Neurochem. 2009;108(1):91–101.

221. Herrup K, Mullen RJ. Staggerer chimeras: Intrinsic nature of purkinje cell defects and implications for normal cerebellar development. Brain Res. 1979;178(2–3):443–57.

222. Hamilton BA, Frankel WN, Kerrebrock AW, Hawkins TL, FitzHugh W, Kusumi K, et al. Disruption of the nuclear hormone receptor RORα in staggerer mice. Vol. 379, Nature. 1996. p. 736–9.

223. Dussault I, Fawcett D, Matthyssen A, Bader JA, Giguère V. Orphan nuclear receptor RORα-deficient mice display the cerebellar defects of staggerer. Mech Dev. 1998;70(1–2):147–53.

224. Meyer T, Kneissel M, Mariani J, Fournier B. In vitro and in vivo evidence for orphan nuclear receptor RORα function in bone metabolism. Proc Natl Acad Sci U S A. 2000;97(16):9197–202.

225. Kadiri S, Monnier C, Ganbold M, Ledent T, Capeau J, Antoine B. The nuclear retinoid-related orphan receptor-α regulates adipose tissue glyceroneogenesis in addition to hepatic gluconeogenesis. Am J Physiol - Endocrinol Metab. 2015;309(2):E105–14.

226. Jetten AM, Joo JH. Retinoid-related orphan receptors (RORs): Roles in cellular differentiation and development. Adv Dev Biol. 2006;16:313–55.

227. Lau P, Fitzsimmons RL, Raichur S, Wang SCM, Lechtken A, Muscat GEO. The orphan nuclear receptor, RORα, regulates gene expression that controls lipid metabolism: Staggerer (sg/sg) mice are resistant to diet-induced obesity. J Biol Chem. 2008;283(26):18411–21.

228. Stapleton CM, Jaradat M, Dixon D, Kang HS, Kim SC, Liao G, et al. Enhanced susceptibility of staggerer (RORαsg/sg) mice to lipopolysaccharide-induced lung inflammation. Am J Physiol - Lung Cell Mol Physiol. 2005;289(1):L144–52.

229. Kopmels B, Mariani J, Delhaye-Bouchaud N, Audibert F, Fradelizi D, Wollman EE. Evidence for a Hyperexcitability State of Staggerer Mutant Mice Macrophages. J Neurochem. 1992;58(1):192–9.

230. Dzhagalov I, Giguère V, He Y-W. Lymphocyte Development and Function in the Absence of Retinoic Acid-Related Orphan Receptor α. J Immunol. 2004;173(5):2952–9.

231. Han S, Li Z, Han F, Jia Y, Qi L, Wu G, et al. ROR alpha protects against LPS-induced inflammation by down-regulating SIRT1/NF-kappa B pathway. Arch Biochem Biophys. 2019;668:1–8.

232. Srinivas M, Ng L, Liu H, Jia L, Forrest D. Activation of the blue opsin gene in cone photoreceptor development by retinoid-related orphan receptor β. Mol Endocrinol. 2006;20(8):1728–41.

233. Masana MI, Sumaya IC, Becker-Andre M, Dubocovich ML. Behavioral characterization and modulation of circadian rhythms by light and melatonin in C3H/HeN mice homozygous for the RORβ knockout. Am J Physiol - Regul Integr Comp Physiol. 2007;292(6):2357–67.

234. Eberl G, Marmon S, Sunshine MJ, Rennert PD, Choi Y, Littmann DR. An essential function for the nuclear receptor RORγt in the generation of fetal lymphoid tissue inducer cells. Nat Immunol. 2004;5(1):64–73.

235. Harmsen A, Kusser K, Hartson L, Tighe M, Sunshine MJ, Sedgwick JD, et al. Cutting Edge: Organogenesis of Nasal-Associated Lymphoid Tissue (NALT) Occurs Independently of Lymphotoxin-α (LTα) and Retinoic Acid Receptor-Related Orphan Receptor-γ, but the Organization of NALT Is LTα Dependent. J Immunol. 2002;168(3):986–90.

236. Sawa S, Cherrier M, Lochner M, Satoh-Takayama N, Fehling HJ, Langa F, et al. Lineage relationship analysis of RORγt+ innate lymphoid cells. Science. 2010;330(6004):665–9.

237. Venken K, Jacques P, Mortier C, Labadia ME, Decruy T, Coudenys J, et al. RORγt inhibition selectively targets IL-17 producing iNKT and γδ-T cells enriched in Spondyloarthritis patients. Nat Commun. 2019;10(1):9.

238. Sutton CE, Lalor SJ, Sweeney CM, Brereton CF, Lavelle EC, Mills KHG. Interleukin-1 and IL-23 Induce Innate IL-17 Production from γδ T Cells, Amplifying Th17 Responses and Autoimmunity. Immunity. 2009;31(2):331–41.

239. Aparicio-Domingo P, Cupedo T. Rorγt+ innate lymphoid cells in intestinal homeostasis and immunity. J Innate Immun. 2011;3(6):577–84.

240. Jetten AM, Cook DN. (Inverse) Agonists of Retinoic Acid–Related Orphan Receptor γ: Regulation of Immune Responses, Inflammation, and Autoimmune Disease. Annu Rev Pharmacol Toxicol. 2020;60(1):371–90.

241. Dong C. TH17 cells in development: An updated view of their molecular identity and genetic programming. Nat Rev Immunol. 2008;8(5):337–48.

242. Furuzawa-Carballeda J, Vargas-Rojas MI, Cabral AR. Autoimmune inflammation from the Th17 perspective. Autoimmun Rev. 2007;6(3):169–75.

243. Hu X, Majchrzak K, Liu X, Wyatt MM, Spooner CJ, Moisan J, et al. In vitro priming of adoptively transferred T Cells with a RORγ agonist confers durablememory and stemness in vivo. Cancer Res. 2018;78(14):3888–98.

244. Hu X, Liu X, Moisan J, Wang Y, Lesch CA, Spooner C, et al. Synthetic RORγ agonists regulate multiple pathways to enhance antitumor immunity. Oncoimmunology. 2016;5(12):1–13.

245. Takeda Y, Kang HS, Lih FB, Jiang H, Blaner WS, Jetten AM. Retinoid acid-related orphan receptor γ, RORγ, participates in diurnal transcriptional regulation of lipid metabolic genes. Nucleic Acids Res. 2014;42(16):19–22.

246. Takeda Y, Kang HS, Freudenberg J, Degraff LM, Jothi R, Jetten AM. Retinoic Acid-Related Orphan Receptor γ (RORγ): A Novel Participant in the Diurnal Regulation of Hepatic Gluconeogenesis and Insulin Sensitivity. PLoS Genet. 2014;10(5):e1004331.

247. Yang X, Downes M, Yu RT, Bookout AL, He W, Straume M, et al. Nuclear Receptor Expression Links the Circadian Clock to Metabolism. Cell. 2006;126(4):801–10.

248. Takeda Y, Jothi R, Birault V, Jetten AM. RORγ directly regulates the circadian expression of clock genes and downstream targets in vivo. Nucleic Acids Res. 2012;40(17):8519–35.

249. Tinahones FJ, Moreno-santos I, Vendrell J, Chacon MR, Garrido-sanchez L, García-fuentes E, et al. The Retinoic Acid Receptor-Related Orphan Nuclear Receptor γ1 (ROR γ1): A Novel Player Determinant of Insulin Sensitivity in Morbid Obesity. Obes (Silver Spring). 2012;20(3):488–97.

250. Kang HS, Okamoto K, Takeda Y, Beak JY, Gerrish K, Bortner CD, et al. Transcriptional profiling reveals a role for RORα in regulating gene expression in obesity-associated inflammation and hepatic steatosis. Physiol Genomics. 2011;43(13):818–28.

251. Meissburger B, Ukropec J, Roeder E, Beaton N, Geiger M, Teupser D, et al. Adipogenesis and insulin sensitivity in obesity are regulated by retinoid-related orphan receptor gamma. EMBO Mol Med. 2011;3(11):637–51.

252. Austin S, Medvedev A, Van ZH, Adachi H, Hirose T, Jetten AM. Induction of the nuclear orphan receptor RORγ during adipocyte differentiation of D1 and 3T3-L1 cells. Cell Growth Differ. 1998;9(3):267–76.

253. Mclellan MA, Rosenthal NA, Pinto AR. Cre- lox P-Mediated Recombination : General Principles and Experimental Considerations. 2017;7(March):1–12.

254. Eguchi J, Wang X, Yu S, Kershaw EE, Chiu PC, Estall JL, et al. Transcriptional control of adipose lipid handling by IRF4. Cell Metab. 2012;13(3):249–59.

255. Green H, Kehinde O. An established preadipose cell line and its differentiation in culture II. Factors affecting the adipose conversion. Cell. 1975;5(1):19–27.

256. Kilroy G, Burk DH, Floyd ZE. High efficiency lipid-based siRNA transfection of adipocytes in suspension. PLoS One. 2009;4(9):1–8.

257. Livak KJ, Schmittgen TD. Analysis of relative gene expression data using real-time quantitative PCR and the 2-ΔΔCT method. Methods. 2001;25(4):402–8.

258. Heid CA, Stevens J, Livak KJ, Williams P. Real time quantitative PCR. Genome Res. 1996;6(10):986–94.

259. Irizarry RA, Hobbs B, Collin F, Beazer-Barclay YD, Antonellis KJ, Scherf U, et al. Exploration, normalization, and summaries of high density oligonucleotide array probe level data. Biostatistics. 2003;4(2):249–64.

260. Huang DW, Sherman BT, Lempicki RA. Systematic and integrative analysis of large gene lists using DAVID bioinformatics resources. Nat Protoc. 2009;4(1):44–57.

261. Mootha VK, Lindgren CM, Eriksson KF, Subramanian A, Sihag S, Lehar J, et al. PGC-1α-responsive genes involved in oxidative phosphorylation are coordinately downregulated in human diabetes. Nat Genet. 2003;34(3):267–73.

262. Kasper LH, Reder AT. Immunomodulatory activity of interferon-beta. Ann Clin Transl Neurol. 2014;1(8):622–31.

263. Haji Abdolvahab M, Mofrad MRK, Schellekens H. Interferon Beta: From Molecular Level to Therapeutic Effects. Vol. 326, International Review of Cell and Molecular Biology. Elsevier Inc.; 2016. 343–372.

264. Bennett CN, Ross SE, Longo KA, Bajnok L, Hemati N, Johnson KW, et al. Regulation of Wnt signaling during adipogenesis. J Biol Chem. 2002;277(34):30998–1004.

265. Christodoulides C, Lagathu C, Sethi JK, Vidal- A. Adipogenesis and WNT signalling. Trends Endocrinol Metab. 2009;20(1):16–24.

266. Villena JA, Roy S, Sarkadi-Nagy E, Kim KH, Hei SS. Desnutrin, an adipocyte gene encoding a novel patatin domain-containing protein, is induced by fasting and glucocorticoids: Ectopic expression of desnutrin increases triglyceride hydrolysis. J Biol Chem. 2004;279(45):47066–75.

267. Akiyama T, Tachibana I, Shirohara H, Watanabe N, Otsuki M. High-fat hypercaloric diet induces obesity, glucose intolerance and hyperlipidemia in normal adult male Wistar rat. Diabetes Res Clin Pract. 1996;31(1–3):27–35.

268. Chooi YC, Ding C, Magkos F. The epidemiology of obesity. Metabolism. 2019;92:6–10.

269. Wilding JPH. The importance of weight management in type 2 diabetes mellitus. Int J Clin Pract. 2014;68(6):682–91.

270. Anastasiou CA, Karfopoulou E, Yannakoulia M. Weight regaining: From statistics and behaviors to physiology and metabolism. Metabolism. 2015;64(11):1395–407.

271. De Cabo R, Mattson MP. Effects of Intermittent Fasting on Health, Aging, and Disease. N Engl J Med. 2019;381(26):2541–51.

272. Di Francesco A, Di Germanio C, Bernier M, De Cabo R. A time to fast. 2018;775(November):770–5.

273. Acosta-Rodríguez VA, de Groot MHM, Rijo-Ferreira F, Green CB, Takahashi JS. Mice under Caloric Restriction Self-Impose a Temporal Restriction of Food Intake as Revealed by an Automated Feeder System. Cell Metab. 2017;26(1):267-277.e2.

274. Mitchell SJ, Bernier M, Mattison JA, Aon MA, Kaiser TA, Anson RM, et al. Daily Fasting Improves Health and Survival in Male Mice Independent of Diet Composition and Calories. Cell Metab. 2019;29(1):221-228.e3.

275. Pardo R, Enguix N, Lasheras J, Feliu JE, Kralli A, Villena JA. Rosiglitazone-induced mitochondrial biogenesis in white adipose tissue is independent of peroxisome proliferator-activated receptor γ coactivator-1α. PLoS One. 2011;6(11):e26989.

276. Park S-YY, Cho Y-RR, Kim HJ, Higashimori T, Danton C, Lee MK, et al. Unraveling the Temporal Pattern of Diet-Induced Insulin in C57BL/6 Mice. Diabetes. 2005;54:3530–40.

277. Solon-Biet SM, Mitchell SJ, Coogan SCP, Cogger VC, Gokarn R, McMahon AC, et al. Dietary Protein to Carbohydrate Ratio and Caloric Restriction: Comparing Metabolic Outcomes in Mice. Cell Rep. 2015;11(10):1529–34.

278. Aksungar FB, Sarikaya M, Coskun A, Serteser M, Unsal I. Comparison of intermittent fasting versus caloric restriction in obese subjects: A two year follow-up. J Nutr Heal Aging. 2017;21(6):681–5.

279. Cipolletta D, Cohen P, Spiegelman BM, Benoist C, Mathis D. Appearance and disappearance of the mRNA signature characteristic of Treg cells in visceral adipose tissue: Age, diet, and PPARγ effects. Proc Natl Acad Sci U S A. 2015;112(2):482–7.

280. Castillo A, Vilà M, Pedriza I, Pardo R, Cámara Y, Martín E, et al. Adipocyte MTERF4 regulates non-shivering adaptive thermogenesis and sympathetic-dependent glucose homeostasis. Biochim Biophys Acta - Mol Basis Dis. 2019;1865(6):1298–312.

281. Ruiz-Ojeda FJ, Méndez-Gutiérrez A, Aguilera CM, Plaza-Díaz J. Extracellular matrix remodeling of adipose tissue in obesity and metabolic diseases. Int J Mol Sci. 2019;20(19):4888.

282. Sun K, Tordjman J, Clément K, Scherer PE. Fibrosis and adipose tissue dysfunction. Cell Metab. 2013;18(4):470–7.

283. Corrales P, Vivas Y, Izquierdo-Lahuerta A, Horrillo D, Seoane-Collazo P, Velasco I, et al. Long-term caloric restriction ameliorates deleterious effects of aging on white and brown adipose tissue plasticity. Aging Cell. 2019;18(3):1–16.

284. Pasarica M, Gowronska-Kozak B, Burk D, Remedios I, Hymel D, Gimble J, et al. Adipose tissue collagen VI in obesity. J Clin Endocrinol Metab. 2009;94(12):5155–62.

285. Henegar C, Tordjman J, Achard V, Lacasa D, Cremer I, Guerre-Millo M, et al. Adipose tissue transcriptomic signature highlights the pathological relevance of extracellular matrix in human obesity. Genome Biol. 2008;9(1):1–32.

286. Keophiphath M, Achard V, Henegar C, Rouault C, Clément K, Lacasa D Le. Macrophage-secreted factors promote a profibrotic phenotype in human preadipocytes. Mol Endocrinol. 2009;23(1):11–24.

287. Sun K, Park J, Gupta OT, Holland WL, Auerbach P, Zhang N, et al. Endotrophin triggers adipose tissue fibrosis and metabolic dysfunction. Nat Commun. 2014;5:3485.

288. Khan T, Muise ES, Iyengar P, Wang Z V., Chandalia M, Abate N, et al. Metabolic Dysregulation and Adipose Tissue Fibrosis: Role of Collagen VI. Mol Cell Biol. 2009;29(6):1575–91.

289. Clément K, Viguerie N, Poitou C, Carette C, Pelloux Vé, Curat CA, et al. Weight loss regulates inflammation-related genes in white adipose tissue of obese subjects. FASEB J. 2004;18(14):1657–69.

290. Choe SS, Huh JY, Hwang IJ, Kim JI, Kim JB. Adipose tissue remodeling: Its role in energy metabolism and metabolic disorders. Front Endocrinol (Lausanne). 2016;7:1–16.

291. Chawla A, Nguyen KD, Goh YPS. Macrophage-mediated inflammation in metabolic disease. Nat Rev Immunol. 2011;11(11):738–49.

292. Wellen KE, Hotamisligil GS. Inflammation, stress, and diabetes. J Clin Invest. 2005;115(5):1111–9.

293. Mraz M, Lacinova Z, Drapalova J, Haluzikova D, Horinek A, Matoulek M, et al. The effect of very-low-calorie diet on mRNA expression of inflammation-related genes in subcutaneous adipose tissue and peripheral monocytes of obese patients with type 2 diabetes mellitus. J Clin Endocrinol Metab. 2011;96(4):606–13.

294. Wensveen FM, Valentić S, Šestan M, Turk Wensveen T, Polić B. Interactions between adipose tissue and the immune system in health and malnutrition. Semin Immunol. 2015;27(5):322–33.

295. Patel PS, Buras ED, Balasubramanyam A. The role of the immune system in obesity and insulin resistance. J Obes. 2013;2013.

296. Mraz M, Haluzik M. The role of adipose tissue immune cells in obesity and low-grade inflammation. J Endocrinol. 2014;222(3):113–27.

297. Kolak M, Westerbacka J, Velagapudi VR, Wågsäter D, Yetukuri L, Makkonen J, et al. Adipose tissue inflammation and increased ceramide content characterize subjects with high liver fat content independent of obesity. Diabetes. 2007;56(8):1960–8.

298. Altintas MM, Azad A, Nayer B, Contreras G, Zaias J, Faul C, et al. Mast cells, macrophages, and crown-like structures distinguish subcutaneous from visceral fat in mice. J Lipid Res. 2011;52(3):480–8.

299. Cancello R, Tordjman J, Poitou C, Guilhem G, Bouillot JL, Hugol D, et al. Increased infiltration of macrophages in omental adipose tissue is associated with marked hepatic lesions in morbid human obesity. Diabetes. 2006;55(6):1554–61.

300. Kratz M, Coats BR, Hisert KB, Hagman D, Mutskov V, Peris E, et al. Metabolic Dysfunction Drives a Mechanistically Distinct Proinflammatory Phenotype in Adipose Tissue Macrophages. Cell Metab. 2014;20(4):614–25.

301. Kraakman MJ, Murphy AJ, Jandeleit-dahm K, Kammoun HL. Macrophage polarization in obesity and type 2 diabetes : weighing down our understanding of macrophage function? Front Immunol. 2014;5:470.

302. Bolus WR, Kennedy AJ, Hasty AH. Obesity-induced reduction of adipose eosinophils is reversed with low-calorie dietary intervention. Physiol Rep. 2018;6(22).

303. Panduro M, Benoist C, Mathis D. Tissue Tregs. Annu Rev Immunol. 2016;34:609–33.

304. Cipolletta D, Kolodin D, Benoist C, Mathis D. Tissular Tregs: A unique population of adipose-tissue-resident Foxp3+CD4+ T cells that impacts organismal metabolism. Semin Immunol. 2011;23(6):431–7.

305. Ikeda S, Saito H, Fukatsu K, Inoue T, Han I, Furukawa S, et al. Dietary restriction impairs neutrophil exudation by reducing CD11b/CD18 expression and chemokine production. Arch Surg. 2001;136(3):297–304.

306. Meydani SN, Das SK, Pieper CF, Lewis MR, Klein S, Dixit VD, et al. Long-term moderate calorie restriction inhibits inflammation without impairing cell-mediated immunity: A randomized controlled trial in non-obese humans. Aging (Albany NY). 2016;8(7):1416–31.

307. Nagai M, Noguchi R, Takahashi D, Morikawa T, Koshida K, Komiyama S, et al. Fasting-Refeeding Impacts Immune Cell Dynamics and Mucosal Immune Responses. Cell. 2019;178(5):1072–87.

308. Gastaldelli A, Miyazaki Y, Pettiti M, Matsuda M, Mahankali S, Santini E, et al. Metabolic effects of visceral fat accumulation in type 2 diabetes. J Clin Endocrinol Metab. 2002;87(11):5098–103.

309. Boutant M, Canto C. SIRT1 metabolic actions: Integrating recent advances from mouse models. Mol Metab. 2013;3(1):5–18.

310. Cao Y, Jiang X, Ma H, Wang Y, Xue P, Liu Y. SIRT1 and insulin resistance. J Diabetes Complications. 2016;30(1):178–83.

311. Rodgers JT, Lerin C, Haas W, Gygi SP, Spiegelman BM, Puigserver P. Nutrient control of glucose homeostasis through a complex of PGC-1α and SIRT1. Nature. 2005;434(7029):113–8.

312. Gerhart-Hines Z, Rodgers JT, Bare O, Lerin C, Kim SH, Mostoslavsky R, et al. Metabolic control of muscle mitochondrial function and fatty acid oxidation through SIRT1/PGC-1α. EMBO J. 2007;26(7):1913–23.

313. Gerhart-Hines Z, Dominy JE, Blättler SM, Jedrychowski MP, Banks AS, Lim JH, et al. The cAMP/PKA Pathway Rapidly Activates SIRT1 to Promote Fatty Acid Oxidation Independently of Changes in NAD +. Mol Cell. 2011;44(6):851–63.

314. Pardo R, Velilla M, Herrero L, Cervela L, Ribeiro ML, Simó R, et al. Calorie Restriction and SIRT1 Overexpression Induce Different Gene Expression Profiles in White Adipose Tissue in Association with Metabolic Improvement. Mol Nutr Food Res. 2021;65(9):e2000672.

315. Boutant M, Kulkarni SS, Joffraud M, Raymond F, Métairon S, Descombes P, et al. SIRT1 Gain of Function Does Not Mimic or Enhance the Adaptations to Intermittent Fasting. Cell Rep. 2016;14(9):2068–75.

316. Banks AS, Kon N, Knight C, Matsumoto M, Gutiérrez-Juárez R, Rossetti L, et al. SirT1 Gain of Function Increases Energy Efficiency and Prevents Diabetes in Mice. Cell Metab. 2008;8(4):333–41.

317. Gillum MP, Kotas ME, Erion DM, Kursawe R, Chatterjee P, Nead KT, et al. SirT1 regulates adipose tissue inflammation. Diabetes. 2011;60(12):3235–45.

318. Yoshizaki T, Schenk S, Imamura T, Babendure JL, Sonoda N, Bae EJ, et al. SIRT1 inhibits inflammatory pathways in macrophages and modulates insulin sensitivity. Am J Physiol - Endocrinol Metab. 2010;298(3):419–28.

319. Yeung F, Hoberg JE, Ramsey CS, Keller MD, Jones DR, Frye RA, et al. Modulation of NF-κB-dependent transcription and cell survival by the SIRT1 deacetylase. EMBO J. 2004;23(12):2369–80.

320. Makowski L, Boord JB, Maeda K, Babaev VR, Uysal KT, Morgan MA, et al. Lack of macrophage fatty-acid-binding protein aP2 protects mice deficient in apolipoprotein E against atherosclerosis. Nat Med. 2001;7(6):699–705.

321. Elmasri H, Karaaslan C, Teper Y, Ghelfi E, Weng M, Ince TA, et al. Fatty acid binding protein 4 is a target of VEGF and a regulator of cell proliferation in endothelial cells. FASEB J. 2009;23(11):3865–73.

322. Fu Y, Luo N, Lopes-Virella MF. Oxidized LDL induces the expression of ALBP/aP2 mRNA and protein in human THP-1 macrophages. J Lipid Res. 2000;41(12):2017–23.

323. Lee KY, Russell SJ, Ussar S, Boucher J, Vernochet C, Mori MA, et al. Lessons on conditional gene targeting in mouse adipose tissue. Diabetes. 2013;62(3):864–74.

324. Wieser V, Adolph TE, Grander C, Grabherr F, Enrich B, Moser P, et al. Adipose type I interferon signalling protects against metabolic dysfunction. Gut. 2018;67(1):157–65.

325. Alsaggar M, Mills M, Liu D. Interferon beta overexpression attenuates adipose tissue inflammation and high-fat diet-induced obesity and maintains glucose homeostasis. Gene Ther. 2017;24(1):60–6.

326. Wang XA, Zhang R, Zhang S, Deng S, Jiang D, Zhong J, et al. Interferon regulatory factor 7 deficiency prevents diet-induced obesity and insulin resistance. Am J Physiol - Endocrinol Metab. 2013;305(4):485–95.

327. Tang P, Virtue S, Goie JYG, Png CW, Guo J, Li Y, et al. Regulation of adipogenic differentiation and adipose tissue inflammation by interferon regulatory factor 3. Cell Death Differ. 2021.

328. Dalmas E, Toubal A, Alzaid F, Blazek K, Eames HL, Lebozec K, et al. Irf5 deficiency in macrophages promotes beneficial adipose tissue expansion and insulin sensitivity during obesity. Nat Med. 2015;21(6):610–8.

329. York AG, Williams KJ, Argus JP, Zhou QD, Brar G, Vergnes L, et al. Limiting Cholesterol Biosynthetic Flux Spontaneously Engages Type I IFN Signaling. Cell. 2015;163(7):1716–29.

330. Wu D, Sanin DE, Everts B, Chen Q, Qiu J, Michael D, et al. Type 1 interferons induce changes in core metabolism that are critical for immune function. Immunity. 2016;44(6):1325–36.

331. Cai D, Wang J, Gao B, Li J, Wu F, Zou JX, et al. RORγ is a targetable master regulator of cholesterol biosynthesis in a cancer subtype. Nat Commun. 2019;10(1).

332. Zhang K, Li H, Xin Z, Li Y, Wang X, Hu Y, et al. Time-restricted feeding downregulates cholesterol biosynthesis program via RORγ-mediated chromatin modification in porcine liver organoids. J Anim Sci Biotechnol. 2020;11(1):1–13.

333. Howie D, Bokum A Ten, Necula AS, Cobbold SP, Waldmann H. The role of lipid metabolism in T lymphocyte differentiation and survival. Front Immunol. 2018;8.

334. Abbott MJ, Tang T, Sul HS. The Role of Phospholipase A2 -derived Mediators in Obesity. Drug Discov Today Dis Mech. 2010;7(3–4):e213–8.

335. Ousingsawat J, Wanitchakool P, Kmit A, Romao AM, Jantarajit W, Schreiber R, et al. Anoctamin 6 mediates effects essential for innate immunity downstream of P2X7 receptors in macrophages. Nat Commun. 2015;6:1–10.

336. Haller O, Kochs G, Weber F. The interferon response circuit: Induction and suppression by pathogenic viruses. Virology. 2006;344(1):119–30.

337. Hornung V, Guenthner-Biller M, Bourquin C, Ablasser A, Schlee M, Uematsu S, et al. Sequence-specific potent induction of IFN-α by short interfering RNA in plasmacytoid dendritic cells through TLR7. Nat Med. 2005;11(3):263–70.

338. Reynolds A, Anderson EM, Vermeulen A, Fedorov Y, Robinson K, Leake D, et al. Induction of the interferon response by siRNA is cell type- and duplex length-dependent. RNA. 2006;12(6):988–93.

339. Kochumon S, Al-Rashed F, Abu-Farha M, Devarajan S, Tuomilehto J, Ahmad R. Adipose tissue expression of CCL19 chemokine is positively associated with insulin resistance. Diabetes Metab Res Rev. 2019;35(2):1–7.

340. Sano T, Iwashita M, Nagayasu S, Yamashita A, Shinjo T, Hashikata A, et al. Protection from diet-induced obesity and insulin resistance in mice lacking CCL19-CCR7 signaling. Obesity. 2015;23(7):1460–71.

341. Xuan W, Qu Q, Zheng B, Xiong S, Fan G-H. The chemotaxis of M1 and M2 macrophages is regulated by different chemokines. J Leukoc Biol. 2015;97(1):61–9.

342. Montastier E, Villa-Vialaneix N, Caspar-Bauguil S, Hlavaty P, Tvrzicka E, Gonzalez I, et al. System Model Network for Adipose Tissue Signatures Related to Weight Changes in Response to Calorie Restriction and Subsequent Weight Maintenance. PLoS Comput Biol. 2015;11(1):1–22.

343. Verma M, Loh NY, Vasan SK, van Dam AD, Todorčević M, Neville MJ, et al. TCF7L2 plays a complex role in human adipose progenitor biology which may contribute to genetic susceptibility to type 2 diabetes. bioRxiv. 2019;8(5):55.

344. Nguyen-Tu MS, Martinez-Sanchez A, Leclerc I, Rutter GA, da Silva Xavier G. Adipocyte-specific deletion of Tcf7l2 induces dysregulated lipid metabolism and impairs glucose tolerance in mice. Diabetologia. 2021;64(1):129–41.

345. Wang Q, Wu H. T Cells in Adipose Tissue: Critical Players in Immunometabolism. Front Immunol. 2018;9:2509.

346. Lykens JE, Terrell CE, Zoller EE, Risma K, Jordan MB. Perforin is a critical physiologic regulator of T-cell activation. Blood. 2011;118(3):618–26.

347. Surendar J, Karunakaran I, Frohberger SJ, Koschel M, Hoerauf A, Hübner MP. Macrophages Mediate Increased CD8 T Cell Inflammation During Weight Loss in Formerly Obese Mice. Front Endocrinol (Lausanne). 2020;11(April):1–9.

348. Liu B, Hutchison AT, Thompson CH, Lange K, Heilbronn LK. Markers of adipose tissue inflammation are transiently elevated during intermittent fasting in women who are overweight or obese. Obes Res Clin Pract. 2019;13(4):408–15.

349. AlZaim I, Hammoud SH, Al-Koussa H, Ghazi A, Eid AH, El-Yazbi AF. Adipose Tissue Immunomodulation: A Novel Therapeutic Approach in Cardiovascular and Metabolic Diseases. Front Cardiovasc Med. 2020;17(7):1–40.

350. Watanabe N, Gavrieli M, Sedy JR, Yang J, Fallarino F, Loftin SK, et al. BTLA is a lymphocyte inhibitory receptor with similarities to CTLA-4 and PD-1. Nat Immunol. 2003;4(7):670–9.

351. Pilat N, Mahr B, Gattringer M, Baranyi U, Wekerle T. CTLA4Ig improves murine iTreg induction via TGFβ and suppressor function in vitro. J Immunol Res. 2018;2018:2484825.

352. Zhang HX, Zhu B, Fu XX, Zeng JC, Zhang JA, Wang WD, et al. BTLA associates with increased Foxp3 expression in CD4+ T cells in dextran sulfate sodium-induced colitis. Int J Clin Exp Pathol. 2015;8(2):1259–69.

353. Howie D, Nolan KF, Daley S, Butterfield E, Adams E, Garcia-Rueda H, et al. MS4A4B Is a GITR-Associated Membrane Adapter, Expressed by Regulatory T Cells, Which Modulates T Cell Activation. J Immunol. 2009;183(7):4197–204.

354. Xu H, Williams MS, Spain LM. Patterns of expression, membrane localization, and effects of ectopic expression suggest a function for MS4a4B, a CD20 homolog in Th1 T cells. Blood. 2006;107(6):2400–8.

355. Teijeiro A, Garrido A, Ferre A, Perna C, Djouder N. Inhibition of the IL-17A axis in adipocytes suppresses diet-induced obesity and metabolic disorders in mice. Nat Metab. 2021;3(4):496–512.

356. Faber DR, Kalkhoven E, Westerink J, Bouwman JJ, Monajemi HM, Visseren FLJ. Conditioned media from (pre)adipocytes stimulate fibrinogen and PAI-1 production by HepG2 hepatoma cells. Nutr Diabetes. 2012;2:e52-8.

357. Vielma SA, Klein RL, Levingston CA, Young MRI. Adipocytes as immune regulatory cells. Int Immunopharmacol. 2013;16(2):224–31.

358. Huh JY, Park YJ, Ham M, Kim JB. Crosstalk between adipocytes and immune cells in adipose tissue inflammation and metabolic dysregulation in obesity. Mol Cells. 2014;37(5):365–71.

359. Meijer K, de Vries M, Al-Lahham S, Bruinenberg M, Weening D, Dijkstra M, et al. Human primary adipocytes exhibit immune cell function: Adipocytes prime inflammation independent of macrophages. PLoS One. 2011;6(3).

360. Shin H, Ma Y, Chanturiya T, Cao Q, Wang Y, Kadegowda AKG, et al. Lipolysis in Brown Adipocytes Is Not Essential for Cold-Induced Thermogenesis in Mice. Cell Metab. 2017;26(5):764-777.e5.

361. Golozoubova V, Hohtola E, Matthias A, Jacobsson A, Cannon B, Nedergaard J. Only UCP1 can mediate adaptive nonshivering thermogenesis in the cold. FASEB J. 2001;15(11):2048–50.

362. Chouchani ET, Kazak L, Spiegelman BM. New Advances in Adaptive Thermogenesis: UCP1 and Beyond. Cell Metab. 2019;29(1):27–37.

363. Lau P, Tuong ZK, Wang SC, Fitzsimmons RL, Goode JM, Thomas GP, et al. Rorα deficiency and decreased adiposity are associated with induction of thermogenic gene expression in subcutaneous white adipose and brown adipose tissue. Am J Physiol - Endocrinol Metab. 2015;308(2):E159–71.

364. Auclair M, Roblot N, Capel E, Fève B, Antoine B. Pharmacological modulation of RORa controls fat browning, adaptive thermogenesis, and body weight in mice. Am J Physiol - Endocrinol Metab. 2021;320(2):E219–33.

365. Escalona-Garrido C, Vázquez P, Mera P, Zagmutt S, García-Casarrubios E, Montero-Pedrazuela A, et al. Moderate SIRT1 overexpression protects against brown adipose tissue inflammation. Mol Metab. 2020;42(October):101097.

366. Wetter TJ, Gazdag AC, Dean DJ, Cartee GD. Effect of calorie restriction on in vivo glucose metabolism by individual tissues in rats. Am J Physiol - Endocrinol Metab. 1999;276(4):E728–38.

367. Reaven E, Wright D, Mondon C, Solomon R, Ho H, Reaven G. Effect of age and diet on insulin secretion and insulin action in the rat. Diabetes. 1983;32(2):175–80.

368. Considine R V., Sinha MK, Heiman ML, Kriauciunas A, Stephens TW, Nyce MR, et al. Serum Immunoreactive-Leptin Concentrations in Normal-Weight and Obese Humans. N Engl J Med. 1996;6(4):349.

369. Park CY, Park S, Kim MS, Kim HK, Han SN. Effects of mild calorie restriction on lipid metabolism and inflammation in liver and adipose tissue. Biochem Biophys Res Commun. 2017;490(3):636–42.

370. Raichur S, Lau P, Staels B, Muscat GEO. Retinoid-related orphan receptor γ regulates several genes that control metabolism in skeletal muscle cells: Links to modulation of reactive oxygen species production. J Mol Endocrinol. 2007;39(1–2):29–44.

371. Taneera J, Mohammed AK, Dhaiban S, Hamad M, Prasad RB, Sulaiman N, et al. RORB and RORC associate with human islet dysfunction and inhibit insulin secretion in INS-1 cells. Islets. 2019;11(1):10–20.

ANNEX

► 8.1 Supplementary figures

SUPPLEMENTARY FIGURE 1

Myeloid cells

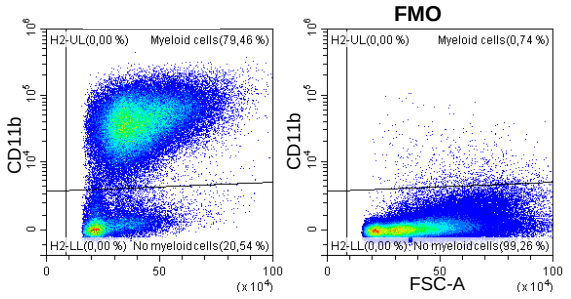

Macrophages

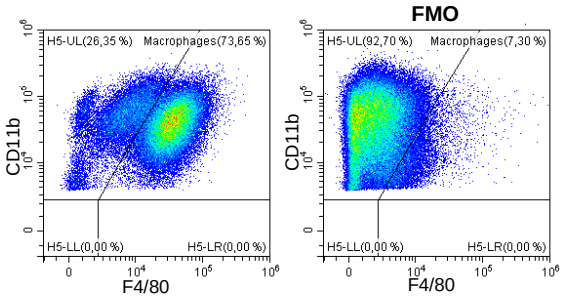

Neutrophils

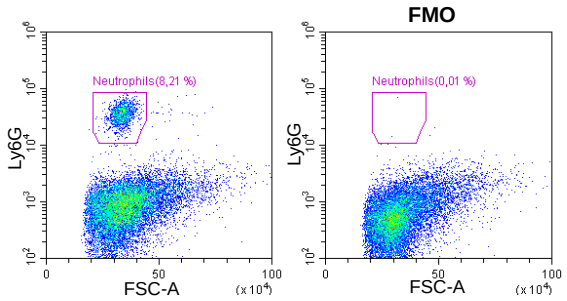

Eosinophils

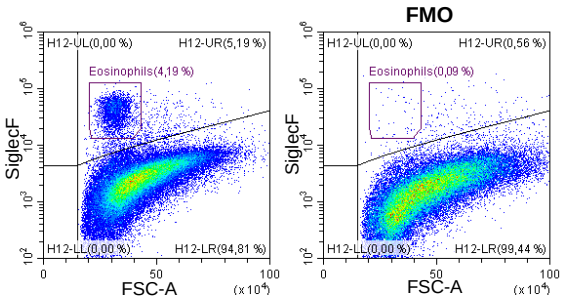

NK cells

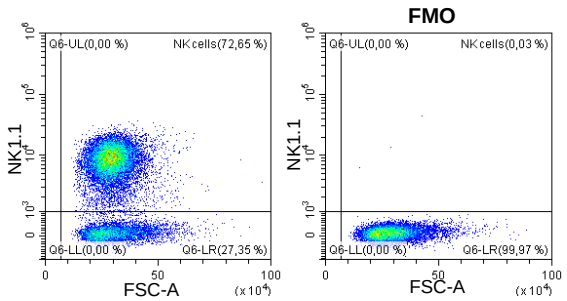

NKt cells

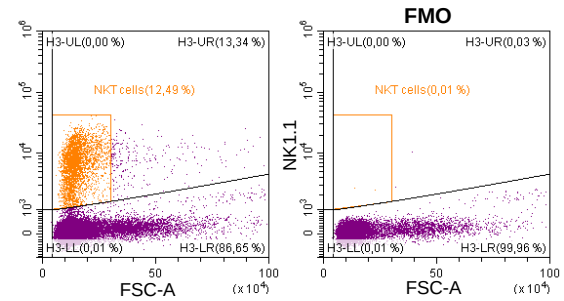

B cells

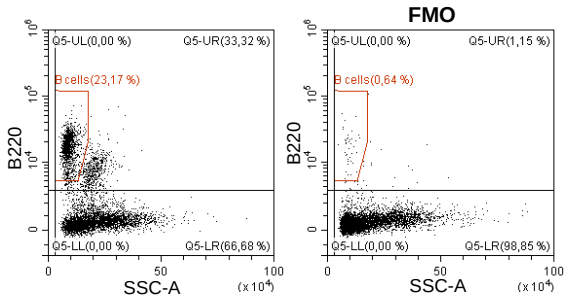

ILCs

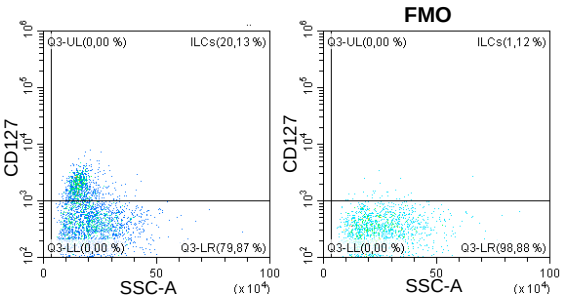

ILC1

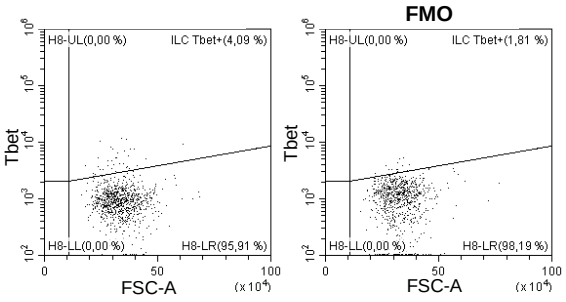

ILC2

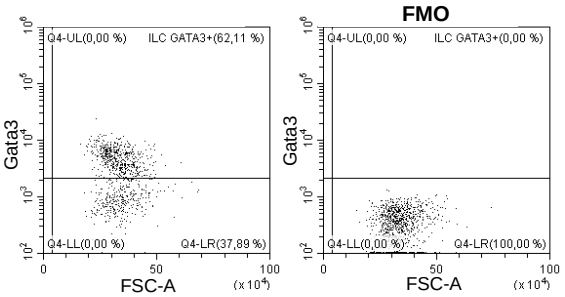

ILC3

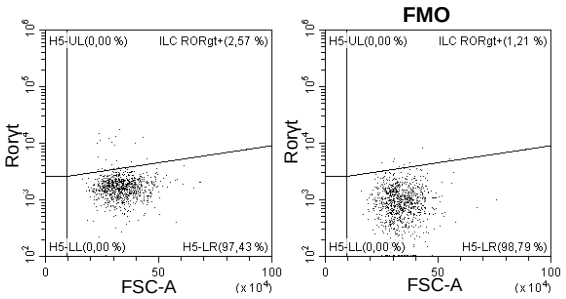

T cells

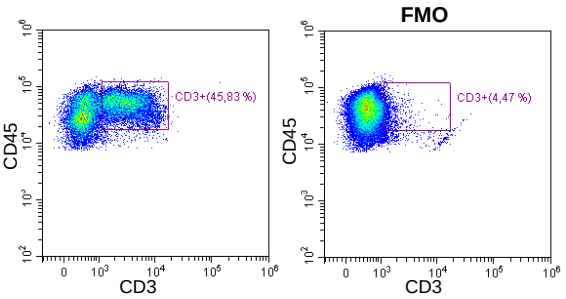

T Thelper / T cytotoxic

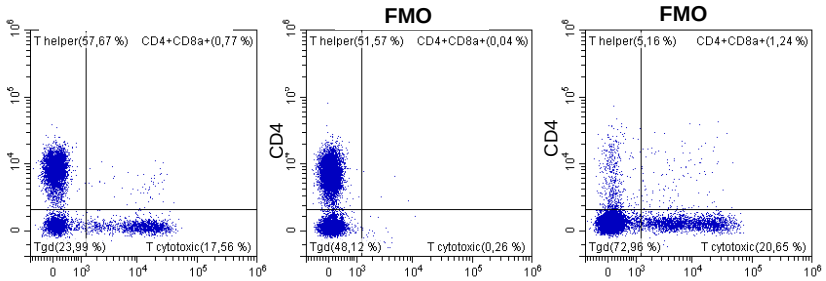

Th1

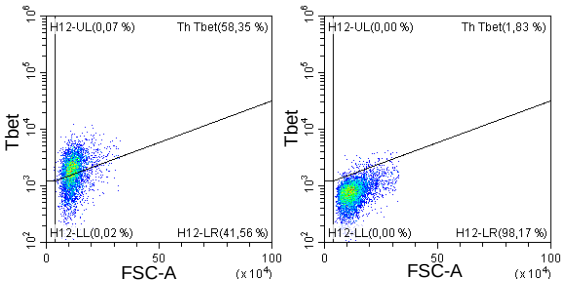

Th2

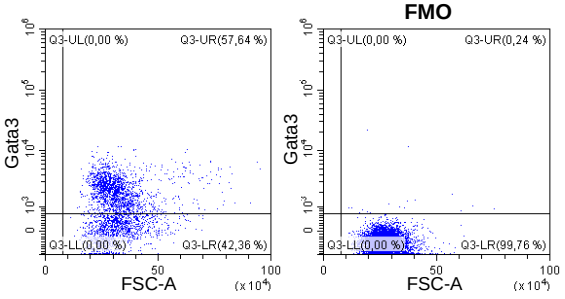

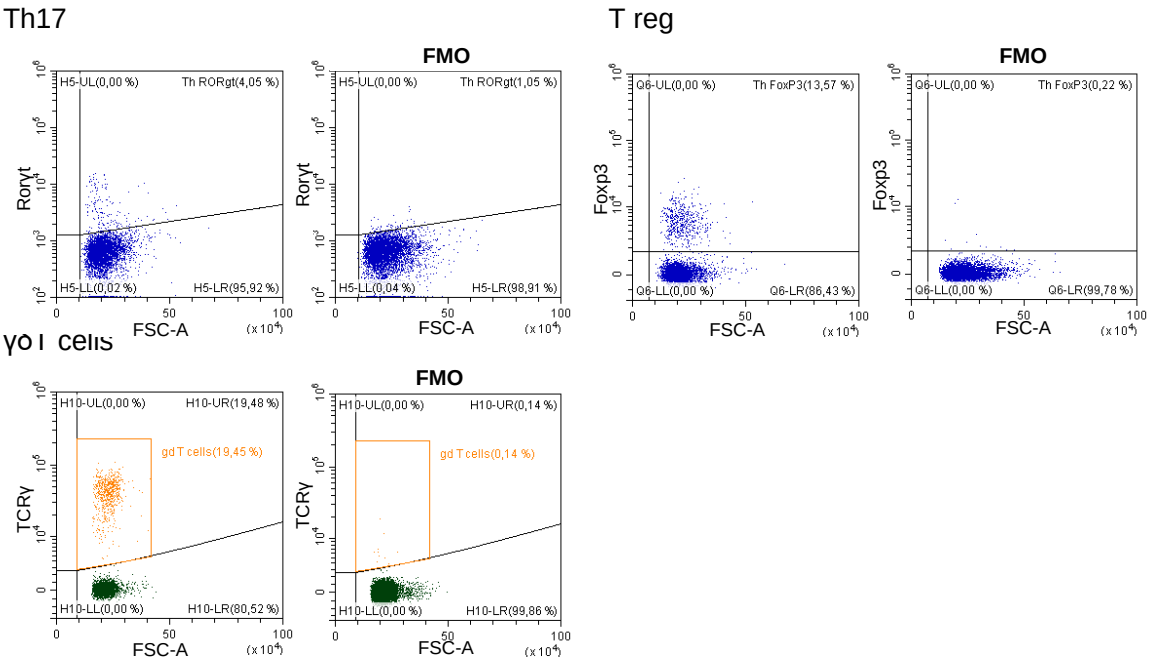

Supplementary figure 1. FMO controls for each immune population. Each FMO control contains all the fluorochromes in the panel, except for the one that is being measured, as well as its respectively isotype.

SUPPLEMENTARY FIGURE 2

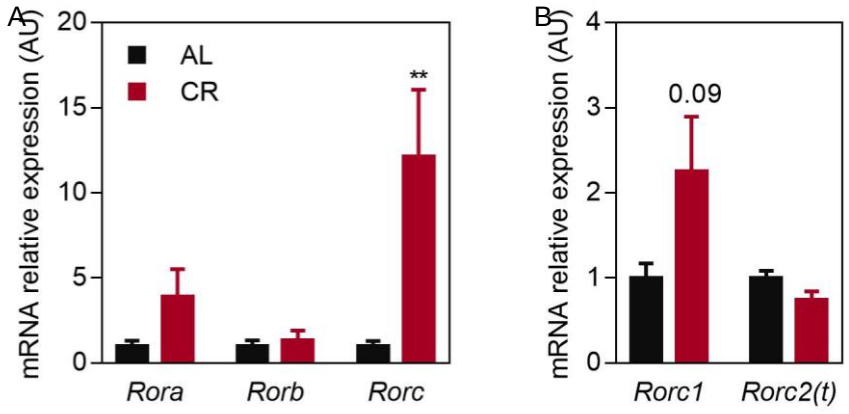

Supplementary figure 2. Effect of CR on RORγ expression levels in gonadal WAT. A) mRNA expression levels of ROR family members in gonadal WAT of AL or CR mice. B) mRNA expression levels of *Rorc1* and *Rorc2(t)* isoforms in gonadal WAT of AL or CR mice. AL, *ad libitum*; CR, calorie restriction. ** *P*≤ 0.01.

SUPPLEMENTARY FIGURE 3

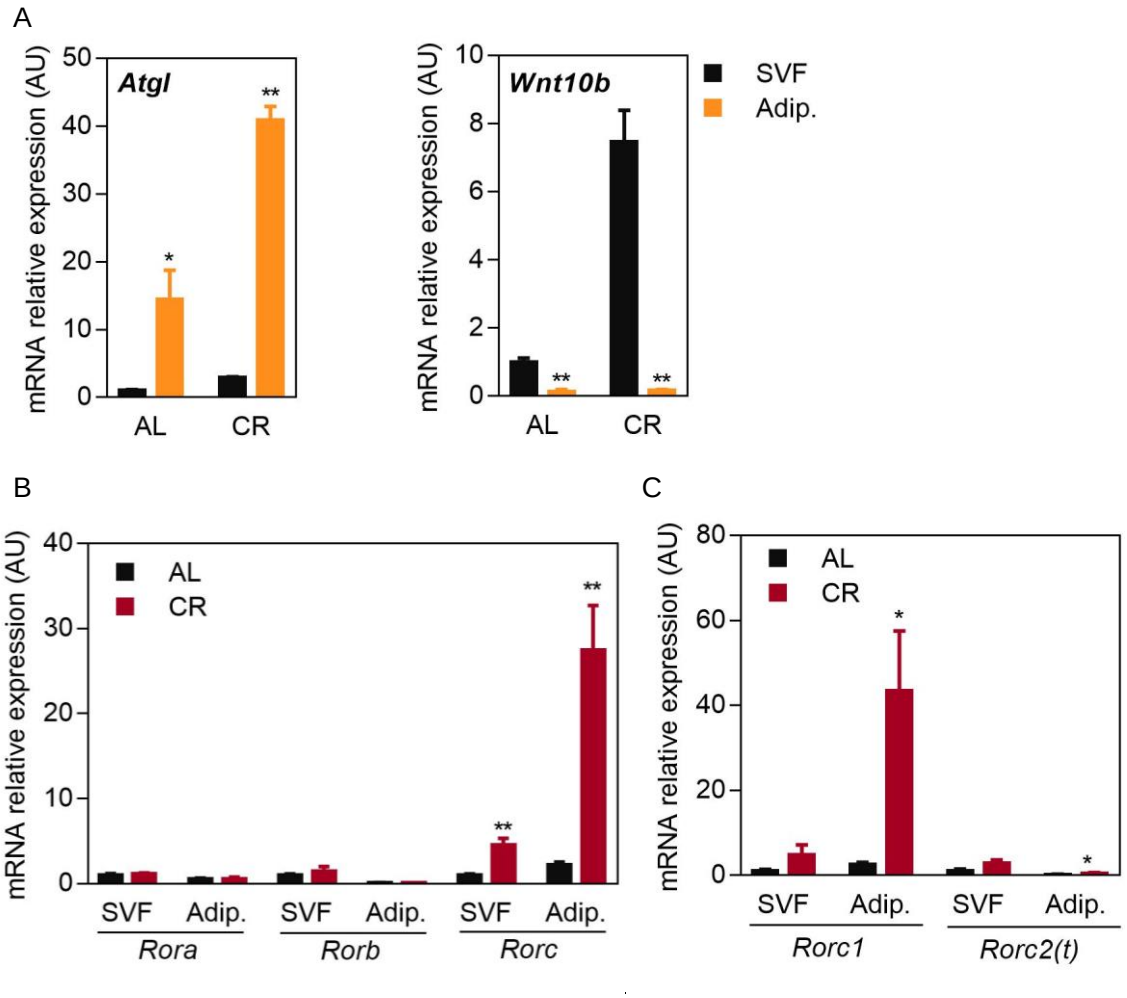

Supplementary figure 3. Expression of ROR family members in adipocyte and SVF fractions from gonadal WAT of AL or CR mice. Adipocyte and SVF fractions were obtained by collagenase digestion. A) mRNA expression levels of mature adipocyte and preadipocyte makers *Atgl* and *Wnt10b*, respectively. B) mRNA expression levels of ROR family members in adipocyte and SVF fractions in response to CR. C) mRNA expression of *Rorc1* and *Rorc2(t)* isoforms in adipocyte and SVF fractions in response to CR. mRNA expression was assessed by qPCR. Results are expressed as mean ± SEM (n=3-5 animals/group). Adip., adipocytes; SVF, stromal vascular fraction; AL, *ad libitum*; CR, calorie restriction. * Indicates statistical significance between AL and CR or adipocytes and SVF. * $P \leq 0.05$; ** $P \leq 0.01$.

ANNEX

SUPPLEMENTARY FIGURE 4

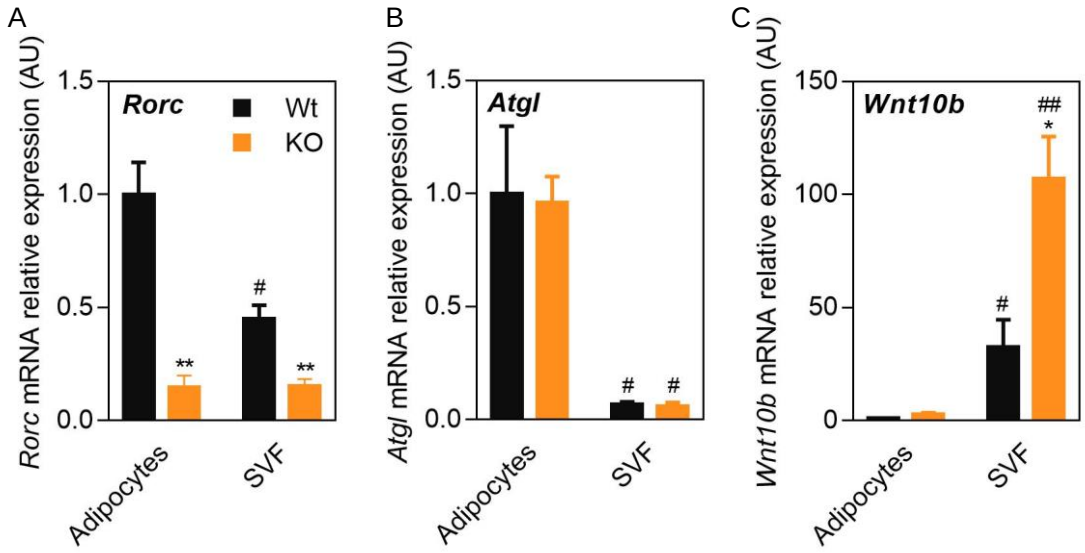

Supplementary figure 4. Gene expression analysis of mature adipocyte markers and *Rorc* in cell fractions of gonadal WAT. Expression of (A) *Rorc* (B) *Atgl* and (C) *Wnt10b* was assessed by qPCR in white adipocytes and SVF isolated from gonadal WAT of Wt and RORγ-FAT-KO mice. Results are expressed as mean ± SEM (n=4-5 animals/group). * Indicates statistical significance between Wt and RORγ-FAT-KO mice; # indicates statistical significance between adipocytes and SVF. *,# $P \leq 0.05$; **,## $P \leq 0.01$.

► 8.2 Supplementary tables

SUPPLEMENTARY TABLE 1: LIST OF ANTIBODIES FOR FLOW CYTOMETRY USED IN THIS STUDY

Antibody	Clone	Cat. Number	Supplier
FITC CD45R/B220	RA3-6B2	553088	BD Biosciences
PE F4/80	T45-2342	565410	BD Biosciences
PerCP-Cy5.5 CD45	30-F11	550994	BD Biosciences
PE-Cy7 CD11b	M1/70	25-0112-81	eBioscience
BV605 NK-1.1	PK136	108753	BioLegend
BV510 CD3	17A2	100233	BioLegend
APC Foxp3	FJK-16s	17-5773-82	eBioscience
APC-H7 CD4	GK1.5	560181	BD Biosciences
FITC CD45	30-F11	103108	BioLegend
PE GATA3	16E10A23	653804	BioLegend
PerCPeFluor710 RORγt	B2D	46-6981-82	Invitrogen
BV421 Tbet	4B10	644816	BioLegend
APC CD127	SB/199	564175	BD Biosciences
APC-eFluor 780 CD45R (B220)	RA3-6B2	47-0452-82	Invitrogen
FITC-Ly6G	1A8	551460	BD Biosciences
BV421 Siglec-F	E50-2440	562681	BD Biosciences
APC TCR gamma/delta	eBioGL3	17-5711-82	Invitrogen
BV605 CD8a	53-6.7	563152	BD Biosciences
FITC Rat IgG2a,k	RTK2758	400505	BioLegend
PE Rat IgG2a,k	RTK2758	400507	BioLegend
PerCP-Cy5.5 Rat IgG2b,k	A95-1	550764	BD Biosciences
PE-Cy7 Rat IgG2b,k	eB149/10H5	25-4031-81	eBioscience
eFluor450 Rat IgG1 K	eBRG1	48-4301-80	eBioscience
BV605 Mouse IgG2a,k	G155-178	562778	BD Biosciences
BV510 Rat IgG2b,k	RTK4530	400645	BioLegend
APC Rat IgG2a,k	R35-95	553932	BD Biosciences
APC-H7 Rat IgG2a,k	R35-95	560197	BD Biosciences
FITC Rat IgG2b,k	A95-1	556923	BD Biosciences
PE Mouse IgG2b,k	MPC-11	400314	BioLegend
PerCP-eFluor710 Rat IgG1,k	MOPC-21	400157	BioLegend
BV421 Mouse IgG1,k	eBRG1	46-4301-80	Invitrogen
APC Rat IgG2b,k	eB149/10H5	17-4031-81	eBioscience
APCeF780 Rat IgG2a,k	eBR2a	47-4321-80	eBioscience
BV421 Rat IgG 2a,k	R35-95	562602	BD Biosciences
APC A.hamster IgG	HTK888	400911	BioLegend
BV605 Rat IgG 2a,k	R35-95	563144	BD Biosciences

Supplementary table 1. List of antibodies for flow cytometry used in this study.

SUPPLEMENTARI TABLE 2: LIST OF PRIMERS USED IN THIS STUDY FOR REAL-TIME QUANTITATIVE PCR

Gene symbol	Entrez ID	FORWARD PRIMER	REVERSE PRIMER
Acadl	**11363**	GTGGAAAACGGAATGAAAGGA	GAACTCACAGGCAGAAATCGC
Acadvl	**11370**	CCAGATAGAAGCCGCCATCAG	ACTCAAACCACTGCCGATTCC
Aco2	**11429**	TCTCTAACAACCTGCTCATCGG	TCATCTCCAATCACCACCCACC
Acox2	**93732**	CCTCTTACAATTCTTCCACAG	ACAGAAGTCTGAAGACATGG
Adam12	**11489**	CACACGGATCATTGTTACTACCA	ATTGGCTCTAAGCTGTACGTTTT
Adamts5	**23794**	GGAGCGAGGCCATTTACAAC	CGTAGACAAGGTAGCCCACTTT
Angptl8/Gm6484	**624219**	AGATTCAGGTGGAAGAGG	CTCAAATTCTTGGTGGGC
Ano6	**105722**	CTCTCTGTCTTCAACATCAC	TAGATGATGTGCTCCATGAC
Apol6	**71939**	GCAGCAAGTTAGAAGACAAG	CATCATCTTCAACATCCAGAG
Apol9b	**71898**	ACTCAAGAAAGAGAGCAGAC	TATACAGGTATCCACTGCTTG
Arg1	**11846**	CTGACCTATGTGTCATTTGG	CATCTGGGAACTTTCCTTTC
Atgl/Pnpla2	**66853**	CCTGATGACCACCCTTTCCAAC	ACCCGTCTGCTCTTTCATCCAC
ATP5a1	**11946**	TTAGAGACAACGGCAAGCACG	ACATCTGGCGGTAAGCGACAG
Bcl3	**12051**	GTGAACGCTCAGATGTATTC	CCTTAAGATATCAATGACCCTG
Btla	**208154**	CACTAACCTGGTTGATATTCC	TCCTTCCAATAACACAATGG
Ccl19	**24047**	TTCTTAATGAAGATGGCTGC	CTTTGTTCTTGGCAGAAGAC
Ccl2	**20296**	CAAGATGATCCCAATGAGTAG	TTGGTGACAAAAACTACAGC
Ccl22	**20299**	GTTCTTCTGGACCTCAAAATC	CCTAGGACAGTTTATGGAGTAG
Ccl3	**20302**	TTCTCTGTACCATGACACTC	CTCTTAGTCAGGAAAATGACAC
Ccl7	**20306**	GCTGCTTTCAGCATCCAAGTG	CCAGGGACACCGACTACTG
Cd11c/Itgax	**16411**	CTGGATAGCCTTTCTTCTGCTG	GCACACTGTGTCCGAACTCA
Cd2	**12481**	AGAAAGGTCTGTCCTTCTATG	TCTTCATCTTTTCTCCTCCTG
Cd206/Mrc1	**17533**	CTCTGTTCAGCTATTGGACGC	CGGAATTTCTGGGATTCAGCTTC
Cd301/Clec10a	**17312**	GAAAGGCTTTAAGAACTGGG	ATAAATTACTTGGCGAGAGC
Cd37	**12493**	CTTTCTTTGCCCACTATTCC	GCCTAGTACAAAGAAGAAGAG
Cd3e	**12501**	ATCTTGGTAGAGAGAGCATTC	CCCATTTTAAGTTCTCGTCAC
Cd4	**12504**	TCTACTGAGTGAAGGTGATAAG	CTCTTGATCTGAGACATTCG
Cd86	**12524**	ACAGAGAGACTATCAACCTG	GAATTCCAATCAGCTGAGAAC
Cd8b1	**12526**	CCGTCTACTTTTACTGTGTG	GCTTTGATTGAGTTACAGTCC
Col3a1	**12825**	CCTGGCTCAAATGGCTCAC	CAGGACTGCCGTTATTCCCG
Cox5a	**12858**	AACAAGCCAGACATTGATGCC	CAACCTCCAAGATGCGAACAG
Cox8b	**12869**	CGAAGTTCACAGTGGTTCCC	TCTCCAAGTGGGCTAAGACC
Cpt1b	**12895**	TCTAGGCAATGCCGTTCAC	GAGCACATGGGCACCATAC
Ctla4	**12477**	TGTTTCTTTGAGCAAGATGC	GCTTTTAGAGACTGAAGTATGC
Cxcl10	**15945**	AAAAAGGTCTAAAAGGGCTC	AATTAGGACTAGCCATCCAC
Cyp46a1	**13116**	TGTCTGAATGTGACTATGGG	GCCTTAGCTTCTAGGATTTC
Cypa/Ppia	**268373**	CAAGACTGAATGGCTGGATG	ATGGGGTAGGGACGCTCTCC
Dio2	**13371**	CAGCTTCCTCCTAGATGCCTA	CTGATTCAGGATTGGAGACGTG
Dll4	**54485**	TGACCAAGATCTCAACTACTG	CTATTCTCCTGGTCCTTACAG
Fam57b/Tlcd3b	**68952**	GGAGATTTCTTTCTAGGCTG	CTTGTACTGAATGAGGATCTTG
Foxp3	**20371**	CACCTATGCCACCCTTATCCG	CATGCGAGTAAACCAATGGTAGA
Gpat3	**231510**	TTTGTGGGTGGACGATGTGC	CCGTTTGCAGAATACGATCTCT
Hmgcr	**15357**	GATTATGTCTTTAGGCTTGGTC	CATCTTGGAGAGATAAAACTGC
Icos	**54167**	AGTGAATACATGTTCATGGC	CAGCAGAATGTTGTCTGTAG
Ifit2	**15958**	ACCAAGATGAGACTTAGAGG	ACTCCTTACTCGTTGTACTC
Ikbke	**56489**	GATCATGTACAGAATCACCAC	CACTTATCCTCTTCCACCTC

Il10	**16153**	GCTGGACAACATACTGCTAACC	ATTTCCGATAAGGCTTGGCAA
Il13	**16163**	CTTAAGGAGCTTATTGAGGAG	CATTGCAATTGGAGATGTTG
Il15	**16168**	TTCATGTCTTCATTTTGGGC	TCTCCAGGTCATATCTTACATC
IL18r1	**16182**	CTTCGTCTTGGTGAGAAAAG	GCATATTACCTGTTAGTGTCTC
Il1b	**16176**	GAAATGCCACCTTTTGACAGTG	TGGATGCTCTCATCAGGACAG
Il1rl1	**17082**	AAACAACCAATTGATCACCG	CTATATCTCTCCAGAACAGAGC
Il33	**77125**	GCTACTACGCTACTATGAGTC	CAGATGTCTGTGTCTTTGATG
Il4ra	**16190**	GAATAGGCCGGTCCAATCAGA	CAGCCATTCGTCGGACACATT
Il6	**16193**	TCTATACCACTTCACAAGTCGGA	GAATTGCCATTGCACAACTCTTT
Irf4	**16364**	CCGACAGTGGTTGATCGACC	CCTCACGATTGTAGTCCTGCTT
Irf7	**54123**	TAAGGTGTACGAACTTAGCC	TACTGCAGAACCTGTGTG
Itgb2	**16414**	GAATGCCTACTATAAACTCTCC	GATTTGCCTATACTCGATGC
Lbp	**16803**	CACTCCCCAGATATACAAAAAG	AGGCAAATACATTAGTGACC
LepR	**16847**	TGCTGAATTATACGTGATCG	AGACGTAGGATGAATAGATGG
Leptin	**16846**	GACACCAAAACCCTCATCAAGAC	GGTGAAGCCCAGGAATGAAGT
Mmp19	**58223**	CTGTGGCTGGCATTCTTACTT	GGGCAGTCCAGATGCTTCC
Mx1	**17857**	CATACTTCAGCATTCTTCTGG	GTTCTGTCATCTTCTGGTATG
Nfufa9	**66108**	GCAAGGCAGTGGGAGAGAAGG	AGGCACAGCAAGAAACCAACG
Nos2	**18126**	TTTTGCATGACACTCTTCAC	ACTGGTTGATGAACTCAATG
Oas1a	**246730**	ATTAAAAAGGATGGTTCCCG	ATGTCCAGTTCTCTTCTACC
Oas2	**246728**	CGGGAAACAGCCCTAAGAGG	AGCGTAGAGGATTGAAGACTGG
PGC1a	**19017**	AAGGCTATCCCAGGCTTTGC	TTTAGAAGGCCAGGCCGATCTC
Pla2g2e	**26970**	TTCTCTATCACTCGAGACAAC	CATACTTGCGGTTGTAAGTG
Plcd3	**72469**	CCTCTCACAATACCTACCTG	CAAAGGCCCTAATATAAGCC
Pnpla3	**116939**	GTGAATATCACCAACCTCAG	TTACAGATGCCATTCTCCTC
Prdm1	**12142**	AACAGCAAAGAGGTTATTGG	GGAACTCCTCTCTGGAATAG
Ptger4	**19219**	GAAAGCAAGATACTCTGACC	CTAGGAATGGTACCTCCAAC
Rora	**19883**	GTGGAGACAAATCGTCAGGAAT	GACATCCGACCAAACTTGACA
Rorb	**225998**	GCAGCATTAGCAATGGCCTC	GACGGCTGACCGGAATCTATG
Rorc	**19885**	CGACTGGAGGACCTTCTACG	AGAGCTCCATGAAGCCTGAA
Sdhb	**67680**	TACCGATGGGACCCAGACA	CGTGTGCACGCCAGAGTAT
Sell	**20343**	ATCTGGAAACTGGTCATCTC	GGATCATCCATCCTTTCTTG
Slc27a1	**26457**	AGGGACCCACCAGCTAGGCC	CAGGAGCCCGCATCCTGTGC
Sqle	**20775**	TTTGGTCAAGAAAAAGGACC	GGTGAGGAGACAATATTGAAAG
Tcf7	**21414**	GGGATAACTACGGAAAGAAG	TGCATTTCTTTTTCCTCCTG
Themis	**210757**	TAAATCTGCCCAAGTCTCTC	AGAGTTATGTAGTCACAGTGG
Tnf	**21926**	CTTCTCATTCCTGCTTGTGGC	ACTTGGTGGTTTGCTACGACG
Tnfrsf26	**244237**	AATATTCAGCTCTCCTCCAC	GTTTGCAAATACATTCCTGC
Ucp1	**22227**	AGCCATCTGCATGGGATCAAA	GGGTCGTCCCTTTCCAAAGTG
Uqcr10	**66152**	CGAGCGAGCCTTCGATCAG	GTTTCCCCTCGTTGATGTGCT
Wnt10b	**22410**	TGCGGATGGAAGGGTAGTG	CCATGTCGTGGTTACAGCCA
Zap70	**22637**	CAGAAGCCCTACAAGAAAATG	GTCACTCATAAGTGCATACATC

Supplementary table 2. List of primers used in this study for real-time quantitative PCR.

SUPPLEMENTARY TABLE 3: LIST OF ANTIBODIES FOR WESTERN BLOD USED IN THIS STUDY

Antibody	Type	Source	Working dilution	Incubation solution	Supplier	Cat. Number
Primary antibodies						
CYPA	Polyclonal	Rabbit	1:10000	Milk	Enzo	BML-SA296
RORA	Polyclonal	Rabbit	1:1000	Milk	Invitrogen	PA1-812
RORC	Monclonal	Rabbit	1:1000	Milk	Abcam	ab207082
VINCULIN	Monoclonal	Human	1:7000	Milk	Santa Cruz Biotechnology	sc-73614
UCP1	Polyclonal	Rabbit	1:1000	Milk	Abcam	ab10983
Secondary antibodies						
Rabbit IgG	-----	Goat	1:10000	Milk	BioRad	170-6517
Mouse IgG	-----	Goat	1:10000	Milk	BioRad	172-1011

Supplementary table 3. List of antibodies for Western Blod used in this study.

SUPPLEMENTARY TABLE 4: LIST OF DOWN- AND UP- REGULATED GENES IN siRORc 3T3-L1 ADIPOCYTES

Down-regulated genes			
Entrez	Gene Symbol	logFC	P.Value
19885	Rorc	-2.2642	1.45E-08
72325	Vps9d1	-0.7643	4.23E-05
16185	Il2rb	-0.7442	6.71E-06
109032	Sp110	-0.6930	2.87E-03
16673	Krt36	-0.6907	1.94E-04
16497	Kcnab1	-0.6871	1.04E-02
68352	Aspdh	-0.6653	7.53E-04
109075	Exosc4	-0.6516	5.38E-03
72404	Wdr44	-0.6378	1.67E-04
13864	Nr2f6	-0.6349	4.07E-05
320226	Ccdc171	-0.6278	2.26E-03
20563	Slit2	-0.6191	2.76E-03
71968	Wdr73	-0.6165	6.38E-03
81000	Rad54l2	-0.6017	7.13E-05
16371	Irx1	-0.5689	8.81E-04
214579	Aldh5a1	-0.5682	1.97E-03
17231	Mcpt8	-0.5640	1.66E-03
30800	Mmp20	-0.5632	1.07E-03
209361	Taf3	-0.5554	4.81E-04
15431	Hoxd11	-0.5545	7.84E-04
231440	Parm1	-0.5535	2.69E-04
50754	Fbxw7	-0.5483	3.63E-03
19301	Pxmp2	-0.5419	1.88E-03
17884	Myh4	-0.5398	3.73E-03
67966	Zcchc10	-0.5386	1.25E-03
56489	Ikbke	-0.5349	5.43E-05
100040533	Btbd35f5	-0.5335	7.64E-04
16328	Cep250	-0.5297	3.79E-04
74370	Rptor	-0.5202	3.81E-04
72149	Strada	-0.5201	3.51E-03
259050	Olfr652	-0.5165	5.67E-03
433926	Lrrc8b	-0.5141	6.74E-03
381126	Garem1	-0.5131	1.04E-02
271424	Ip6k3	-0.5099	2.14E-03
407812	Zfp941	-0.5081	6.52E-03
192188	Stab2	-0.5053	1.02E-02
14534	Kat2a	-0.5041	5.30E-04
52856	Mtg2	-0.5037	1.09E-02
71947	Tmem94	-0.4939	1.60E-02
77622	Apex2	-0.4801	6.66E-03
68267	Slc25a22	-0.4775	5.14E-04
18667	Pgr	-0.4769	1.92E-02
18844	Plxna1	-0.4753	5.83E-04
381549	Zfp69	-0.4735	2.07E-02
23794	Adamts5	-0.4734	5.39E-04
19679	Pitpnm2	-0.4706	4.05E-03
72388	Ripk4	-0.4704	3.17E-02
381680	Nxpe5	-0.4683	7.38E-03
16004	Igf2r	-0.4656	3.23E-04
19274	Ptprm	-0.4655	7.36E-03

Up-regulated genes			
Entrez	Gene Symbol	logFC	P.Value
244682	Cntn5	0.9307	1.48E-05
22700	Zfp40	0.8426	1.25E-03
237711	Eml6	0.8412	2.83E-03
68549	Sgo2a	0.6797	8.17E-04
60406	Sap30	0.6650	3.86E-04
70061	Sdr9c7	0.5993	5.45E-04
243653	Clec1a	0.5875	1.10E-03
105377	Slf1	0.5820	2.10E-03
70918	Nsun7	0.5814	3.04E-03
58522	Trim54	0.5789	2.31E-03
107569	Nt5c3	0.5762	1.49E-02
654824	Ankrd37	0.5721	1.01E-03
16168	Il15	0.5689	4.40E-03
16538	Kcns1	0.5675	1.31E-04
67578	Patl2	0.5606	7.93E-03
78390	Pla2g4d	0.5513	2.21E-02
53858	Rwdd2b	0.5498	9.25E-03
241950	Bbs12	0.5480	2.51E-03
66695	Aspn	0.5467	2.74E-04
18741	Pitx2	0.5453	3.60E-02
19363	Rad51b	0.5403	3.04E-03
228421	Kif18a	0.5380	3.48E-03
67552	H2afy3	0.5376	2.09E-03
66795	Atg10	0.5314	1.19E-02
20535	Slc4a2	0.5234	2.63E-03
20295	Ccl17	0.5220	3.03E-03
12310	Calca	0.5193	1.45E-04
547109	Trim43a	0.5118	4.77E-03
17919	Myo5b	0.5100	6.53E-03
194908	Pld6	0.5088	5.84E-03
12047	Bcl2a1d	0.5068	2.62E-03
56277	Tmem45a	0.4971	5.54E-04
75581	Yipf7	0.4942	5.76E-03
258544	Olfr788	0.4908	5.53E-03
258686	Olfr1467	0.4899	3.08E-03
237221	Gemin8	0.4891	1.59E-03
21389	Tbx6	0.4778	2.51E-03
217558	G2e3	0.4771	3.72E-02
224893	Zfp959	0.4758	8.36E-03
76217	Jakmip2	0.4751	8.63E-03
268480	Rapgefl1	0.4736	2.36E-02
27205	Podxl	0.4675	1.85E-02
66875	Swt1	0.4650	3.76E-02
12292	Cacna1s	0.4638	3.09E-03
67865	Rgs10	0.4595	1.74E-02
320365	Fry	0.4570	2.84E-02
74934	Armc4	0.4565	2.24E-03
17199	Mc1r	0.4546	8.99E-04
18124	Nr4a3	0.4544	2.33E-02
72685	Dnajc6	0.4536	2.15E-03

Supplementary table 4. List of the first 50 down-regulated and up-regulated genes obtained in a microarray analysis comparing mRNA expression levels in siRorc 3T3-L1 adipocytes compared with siCont 3T3-L1 adipocytes. Genes are listed in descending order of logarithm of fold change.

SUPPLEMENTARY TABLE 5: GENE ENRICHMENT ANALYSIS OF UP- AND DOWN-REGULATED GENES IN siRORc 3T3-L1 ADIPOCYTES

	GO Category	Term	Count	P-Value
UP-REGULATED GENES	BP	response to hypoxia	8	4.6E-3
	BP	mast cell degranulation	3	5.9E-3
	BP	cellular response to tumor necrosis factor	6	6.5E-3
	BP	placenta development	4	1.6E-2
	BP	positive regulation of macroautophagy	3	2.5E-2
	BP	odontogenesis of dentin-containing tooth	4	3.0E-2
	BP	vascular smooth muscle cell differentiation	2	3.2E-2
	BP	female gonad development	3	3.3E-2
	BP	extraocular skeletal muscle development	2	4.2E-2
	BP	detoxification of copper ion	2	4.2E-2
DOWN-REGULATED GENES	BP	lipid metabolic process	17	5.5E-4
	BP	response to virus	7	9,8E-4
	BP	negative regulation of angiogenesis	6	2.9E-3
	BP	negative regulation of delayed rectifier potassium channel activity	3	4.9E-3
	BP	cell cycle arrest	6	4.9E-3
	BP	phosphatidylethanolamine biosynthetic process	3	9.3E-3
	BP	cell differentiation	20	1.0E-2
	BP	histone deubiquitination	3	1.5E-2
	BP	lipid catabolic process	6	1.6E-2
	BP	detection of temperature stimulus involved in sensory perception of pain	3	1.7E-2
	BP	defense response to virus	7	2.6E-2
	BP	negative regulation of endothelial cell migration	3	3.0E-2
	BP	temperature homeostasis	3	3.2E-2
	BP	steroid hormone mediated signaling pathway	4	3.5E-2
	BP	positive regulation of apoptotic process	10	4.0E-2
	BP	protein dephosphorylation	6	4.0E-2
	BP	xenobiotic metabolic process	3	4.1E-2
	BP	cellular response to transforming growth factor beta stimulus	4	5.0E-2

Supplementary table 5. Gene enrichment analysis of up- and down-regulated genes ($P \leq 0.05$) in *Rorc* knockdown 3T3-L1 adipocytes using DAVID bioinformatics source showing the gene ontology term “Biological Process” (BP, biological process).

SUPPLEMENTARY TABLE 6: LIST OF DOWN- AND UP- REGULATED GENES IN siRORa 3T3-L1 ADIPOCYTES

Down-regulated genes			
Entrez	Gene Symbol	logFC	P.Value
19883	Rora	-1.3835	1.03E-07
16497	Kcnab1	-0.7290	7.32E-03
71213	Cage1	-0.7271	5.70E-04
71968	Wdr73	-0.7074	2.54E-03
27222	Atp1a4	-0.6638	8.28E-03
16408	Itgal	-0.6477	9.04E-04
11758	Prdx6	-0.6385	8.26E-05
68352	Aspdh	-0.6321	1.13E-03
54670	Atp8b1	-0.6254	4.70E-04
21331	T2	-0.6241	4.09E-03
11419	Asic1	-0.6067	1.13E-03
216453	Rdh19	-0.5911	5.67E-05
407812	Zfp941	-0.5889	2.42E-03
109032	Sp110	-0.5860	8.54E-03
170780	Cd209e	-0.5829	2.10E-03
71592	Pogk	-0.5801	4.48E-04
240505	Cdc42bpg	-0.5685	1.35E-02
320237	Smim10l2a	-0.5621	7.69E-03
68026	Pclaf	-0.5551	1.52E-02
21926	Tnf	-0.5511	1.03E-02
259105	Olfr549	-0.5466	7.46E-03
107769	Tm6sf1	-0.5452	4.30E-04
66991	Khdc3	-0.5443	2.27E-03
70574	Cpm	-0.5348	2.17E-02
11475	Acta2	-0.5302	8.35E-04
19144	Klk6	-0.5293	8.27E-03
73526	Speer4b	-0.5281	1.08E-02
12316	Aspm	-0.5275	4.70E-02
20302	Ccl3	-0.5222	6.46E-03
23850	Pappa2	-0.5112	1.96E-03
110902	Chrna2	-0.5107	3.56E-03
18779	Pla2r1	-0.5049	7.87E-03
19194	Bpifa2	-0.5028	5.60E-03
18742	Pitx3	-0.4957	3.61E-02
216011	Lrrc20	-0.4931	1.54E-03
21378	Tbrg3	-0.4927	7.45E-03
259161	Olfr688	-0.4920	2.39E-03
381680	Nxpe5	-0.4877	5.72E-03
16185	Il2rb	-0.4840	4.28E-04
327762	Dna2	-0.4778	3.36E-03
241943	Ccdc144b	-0.4760	3.59E-03
320226	Ccdc171	-0.4753	1.33E-02
67109	Zfp787	-0.4734	6.70E-03
208258	Ankrd33	-0.4677	4.85E-02
403180	Ccdc121	-0.4669	9.82E-03
68214	Gsto2	-0.4664	4.21E-03
50754	Fbxw7	-0.4639	1.04E-02
108682	Gpt2	-0.4633	7.18E-03
11567	Avil	-0.4630	3.00E-02
665119	Sec14l5	-0.4625	5.61E-03

Up-regulated genes			
Entrez	Gene Symbol	logFC	P.Value
68549	Sgo2a	0.7326	4.39E-04
67578	Patl2	0.6842	2.10E-03
104681	Slc16a6	0.6719	1.15E-02
100502887	Olfr331	0.6552	7.20E-05
384569	Nova2	0.6017	1.71E-03
64095	Gpr35	0.6014	3.11E-04
654824	Ankrd37	0.5932	7.55E-04
244682	Cntn5	0.5865	1.03E-03
60406	Sap30	0.5837	1.13E-03
16523	Kcnj8	0.5790	1.86E-02
30953	Schip1	0.5785	1.33E-03
239659	C1ql4	0.5774	3.97E-02
23832	Xcr1	0.5752	7.12E-04
12876	Cpe	0.5672	6.72E-03
245695	Tceanc	0.5592	1.37E-03
66337	Fam229b	0.5494	1.22E-03
236663	H2al1j	0.5416	1.49E-03
11535	Adm	0.5367	5.44E-04
11565	Adssl1	0.5338	8.09E-03
67983	Pdzd9	0.5331	1.27E-02
17349	Mlf1	0.5312	3.96E-02
14783	Grb10	0.5224	2.64E-02
74393	Map10	0.5176	4.02E-04
11856	Arhgap6	0.5147	1.21E-02
66469	Fam213b	0.5085	3.82E-03
14447	Gapdhs	0.5014	6.76E-03
433809	Rnf207	0.4890	1.30E-02
15902	Id2	0.4834	1.90E-02
57764	Ntn4	0.4833	2.62E-02
67865	Rgs10	0.4819	1.35E-02
78806	Stpg1	0.4816	2.64E-03
243653	Clec1a	0.4733	5.15E-03
20365	Serf1	0.4680	4.89E-02
246228	Vwa1	0.4680	4.84E-03
229927	Clca3b	0.4643	1.65E-02
14979	H2-Ke6	0.4618	4.28E-02
74478	Snx29	0.4602	1.20E-03
229499	Fcrl1	0.4523	1.42E-02
20855	Stc1	0.4486	2.09E-03
67050	Nkap	0.4479	1.21E-02
433022	Plcxd2	0.4467	1.53E-02
15413	Hoxb5	0.4463	1.99E-02
242608	Podn	0.4406	1.43E-02
207474	Kctd12b	0.4392	2.59E-02
224044	Cyp2ab1	0.4337	1.47E-02
258101	Olfr1137	0.4326	3.91E-02
320365	Fry	0.4322	3.65E-02
244416	Ppp1r3b	0.4301	1.77E-03
76002	Ms4a18	0.4299	1.55E-02
241489	Pde11a	0.4291	4.06E-02

Supplementary table 6. List of the first 50 down-regulated and up-regulated genes obtained in a microarray analysis comparing mRNA expression levels in siRora 3T3-L1 adipocytes compared with siCont 3T3-L1 adipocytes. Genes are listed in descending order of logarithm of fold change.

SUPPLEMENTARY TABLE 7 GENE ENRICHMENT ANALYSIS OF UP- AND DOWN-REGULATED GENES IN siRORa 3T3-L1 ADIPOCYTES

	GO Category	Term	Count	P-Value
UP-REGULATED GENES	BP	response to hypoxia	11	3.5E-5
	BP	cellular response to hypoxia	8	1.0E-4
	BP	heart development	10	1.7E-3
	BP	autophagic cell death	3	2.9E-3
	BP	embryo implantation	5	3.6E-3
	BP	oxidation-reduction process	16	5.0E-3
	BP	extracellular matrix organization	6	6.9E-3
	BP	response to vitamin D	3	1.2E-2
	BP	kidney development	6	1.2E-2
	BP	positive regulation of cAMP biosynthetic process	4	1.5E-2
	BP	negative regulation of phosphorylation	3	1.5E-2
	BP	anatomical structure development	3	1.5E-2
	BP	positive regulation of macroautophagy	3	2.4E-2
	BP	intrinsic apoptotic signaling pathway	3	2.6E-2
	BP	G1/S transition of mitotic cell cycle	4	2.7E-2
	BP	odontogenesis of dentin-containing tooth	4	2.8E-2
	BP	cellular response to tumor necrosis factor	5	2.8E-2
	BP	negative regulation of cardiac muscle cell apoptotic process	3	3.0E-2
	BP	regulation of angiogenesis	3	3.4E-2
	BP	positive regulation of release of cytochrome c from mitochondria	3	3.9E-2
	BP	mitochondrial protein catabolic process	2	4.1E-2
	BP	ion transport	12	4.3E-2
	BP	brown fat cell differentiation	3	4.9E-2
	BP	negative regulation of cell proliferation	9	4.9E-2
DOWN-REGULATED GENES	BP	lipid transport	7	8.1E-4
	BP	immune response	9	5.6E-3
	BP	cation transport	5	5.8E-3
	BP	regulation of protein phosphorylation	4	2.3E-2
	BP	cellular response to tumor necrosis factor	5	2.3E-2
	BP	positive regulation of inflammatory response	4	2.4E-2
	BP	regulation of cellular pH	2	2.9E-2
	BP	sodium ion transport	5	3.4E-2
	BP	calcium activated phosphatidylserine scrambling	2	3.9E-2
	BP	negative regulation of neuron differentiation	4	3.9E-2
	BP	lipoprotein metabolic process	3	3.9E-2
	BP	signal transduction	20	4.1E-2
	BP	lymphocyte chemotaxis	3	4.2E-2
	BP	calcium activated phosphatidylcholine scrambling	2	4.8E-2
	BP	PML body organization	2	4.8E-2
	BP	calcium activated galactosylceramide scrambling	2	4.8E-2
	BP	calcium activated phospholipid scrambling	2	4.8E-2
	BP	positive regulation of apoptotic process	8	4.8E-2
	BP	adaptive immune response	5	4.9E-2
	BP	sodium ion transmembrane transport	3	4.9E-2
	BP	response to virus	4	5.0E-2

Supplementary table 7. Gene enrichment analysis of up- and down-regulated genes ($P \leq 0.05$) in *Rora* knockdown 3T3-L1 adipocytes using DAVID bioinformatics source showing the gene ontology term “Biological Process” (BP, biological process).

SUPPLEMENTARY TABLE 8: LIST OF DOWN- AND UP- REGULATED GENES IN siRORa/c 3T3-L1 ADIPOCYTES

Down-regulated genes			
Entrez	Gene Symbol	logFC	P.Value
19885	Rorc	-1.8165	2.02E-07
19883	Rora	-1.4900	4.24E-08
11783	Apaf1	-0.8344	2.31E-05
109032	Sp110	-0.8183	8.20E-04
108682	Gpt2	-0.7677	1.46E-04
71972	Dnmbp	-0.7332	1.02E-03
320237	Smim10l2a	-0.7048	1.66E-03
16193	Il6	-0.6940	1.73E-03
71968	Wdr73	-0.6871	3.12E-03
21926	Tnf	-0.6860	2.50E-03
20768	Sephs2	-0.6718	1.36E-04
66991	Khdc3	-0.6410	6.41E-04
246730	Oas1a	-0.6261	3.33E-05
81000	Rad54l2	-0.6053	6.73E-05
243385	Gprin3	-0.6052	1.74E-03
14308	Fshb	-0.5958	1.52E-03
14943	Gzmf	-0.5785	6.01E-04
234847	Spg7	-0.5769	1.20E-03
70574	Cpm	-0.5746	1.50E-02
15945	Cxcl10	-0.5729	2.30E-04
16185	Il2rb	-0.5727	9.42E-05
109108	Slc30a9	-0.5690	4.59E-04
11475	Acta2	-0.5641	5.02E-04
11761	Aox1	-0.5612	1.95E-04
231440	Parm1	-0.5579	2.51E-04
94214	Spock2	-0.5553	1.77E-03
11758	Prdx6	-0.5487	3.29E-04
76282	Gpt	-0.5438	2.42E-04
17136	Mag	-0.5432	5.44E-04
71213	Cage1	-0.5414	5.07E-03
14421	B4galnt1	-0.5375	9.82E-03
407812	Zfp941	-0.5311	4.91E-03
212974	Pgghg	-0.5306	1.03E-03
67712	Slc25a37	-0.5277	2.58E-02
76251	Ercc6l2	-0.5234	3.46E-03
102098	Arhgef18	-0.5221	1.27E-04
17857	Mx1	-0.5156	7.62E-05
71069	Stox2	-0.5135	3.18E-02
217995	Heatr1	-0.5097	9.85E-04
71592	Pogk	-0.5096	1.28E-03
239559	A4galt	-0.5083	1.54E-03
93887	Pcdhb16	-0.5081	9.64E-03
56790	Supt20	-0.5052	5.14E-03
77905	Fate1	-0.5048	1.14E-02
15958	Ifit2	-0.5013	4.90E-04
258246	Olfr594	-0.4997	2.14E-02
384695	Vmn1r123	-0.4973	6.55E-03
104110	Adcy4	-0.4969	9.53E-03
54670	Atp8b1	-0.4959	2.84E-03
54194	Akap8l	-0.4895	2.26E-03

Up-regulated genes			
Entrez	Gene Symbol	logFC	P.Value
23832	Xcr1	0.7290	8.75E-05
13166	Dbh	0.7117	2.50E-03
74753	Trmo	0.6810	2.52E-02
20365	Serf1	0.6407	1.07E-02
21389	Tbx6	0.6384	2.45E-04
58994	Smpd3	0.6219	6.33E-05
15206	Hes2	0.6211	1.79E-04
237711	Eml6	0.6176	1.85E-02
12448	Ccne2	0.6132	7.88E-03
245126	Tarm1	0.6027	1.25E-04
105377	Slf1	0.5984	1.71E-03
18089	Nkx2-3	0.5788	4.39E-03
170786	Cd209a	0.5776	1.14E-03
65971	Tbata	0.5712	2.00E-03
17199	Mc1r	0.5577	1.55E-04
403174	Msantd1	0.5445	2.90E-03
404310	Olfr199	0.5378	1.67E-04
228802	Bpifb5	0.5355	4.55E-03
66695	Aspn	0.5352	3.30E-04
12623	Ces1g	0.5334	2.04E-03
16819	Lcn2	0.5323	2.28E-03
30953	Schip1	0.5317	2.48E-03
20295	Ccl17	0.5301	2.72E-03
78390	Pla2g4d	0.5230	2.85E-02
319480	Itga11	0.5224	4.90E-03
11856	Arhgap6	0.5199	1.14E-02
68028	Rpl22l1	0.5127	1.16E-03
630146	Cd101	0.5115	1.86E-02
330485	Tmem145	0.5112	1.71E-02
383491	Prdm14	0.5103	5.77E-03
14447	Gapdhs	0.5025	6.67E-03
244682	Cntn5	0.4988	3.39E-03
19713	Ret	0.4985	2.49E-03
269701	Wdr66	0.4937	2.39E-02
16523	Kcnj8	0.4919	3.99E-02
239114	Il17d	0.4917	4.19E-03
67552	H2afy3	0.4915	3.93E-03
243634	Ano2	0.4870	4.78E-03
16538	Kcns1	0.4864	5.11E-04
244431	Sgcz	0.4857	2.48E-03
105785	Kdelr3	0.4801	1.01E-03
19130	Prox1	0.4784	1.24E-02
58869	Pex5l	0.4777	1.67E-02
328035	Fads6	0.4754	9.15E-03
56309	Mycbp	0.4739	1.65E-03
194908	Pld6	0.4725	9.19E-03
271305	Phf21b	0.4706	1.63E-02
50706	Postn	0.4678	1.20E-03
277743	Fam131c	0.4670	1.14E-02
100502887	Olfr331	0.4667	1.36E-03

Supplementary table 8. List of the first 50 down-regulated and up-regulated genes obtained in a microarray analysis comparing mRNA expression levels in siRora/c 3T3-L1 adipocytes compared with siCont 3T3-L1 adipocytes. Genes are listed in descending order of logarithm of fold change.

SUPPLEMENTARY TABLE 9: GENE ENRICHMENT ANALYSIS OF UP- AND DOWN-REGULATED GENES IN siRORa/c 3T3-L1 ADIPOCYTES

	GO Category	Term	Count	P-Value
UP-REGULATED GENES	BP	positive regulation of nitric oxide biosynthetic process	5	2.0E-3
	BP	response to lipopolysaccharide	9	2.7E-3
	BP	bone development	5	4.6E-3
	BP	positive regulation of inflammatory response	5	6.9E-3
	BP	signal transduction	26	8.7E-3
	BP	cellular response to tumor necrosis factor	6	1.1E-2
	BP	peptide metabolic process	3	1.2E-2
	BP	negative regulation of glucose import	3	1.7E-2
	BP	regulation of ion transmembrane transport	6	2.3E-2
	BP	response to pain	3	2.6E-2
	BP	embryo implantation	4	3.5E-2
	BP	sphingomyelin metabolic process	2	3.6E-2
	BP	immune system process	10	4.2E-2
	BP	positive regulation of NF-kappaB transcription factor activity	5	4.2E-2
	BP	cellular response to retinoic acid	4	4.3E-2
	BP	immune response	8	4.6E-2
DOWN-REGULATED GENES	BP	response to virus	13	1.3E-9
	BP	defense response to virus	16	8.3E-9
	BP	immune system process	18	1.9E-5
	BP	innate immune response	18	3.2E-5
	BP	negative regulation of viral genome replication	5	8.6E-4
	BP	necroptotic signaling pathway	3	2.6E-3
	BP	immune response	11	3.9E-3
	BP	steroid hormone mediated signaling pathway	5	5.6E-3
	BP	positive regulation of apoptotic process	12	6.0E-3
	BP	negative regulation of endothelial cell proliferation	4	7.5E-3
	BP	phosphatidylethanolamine biosynthetic process	3	9.2E-3
	BP	positive regulation of histone deacetylation	3	1.3E-2
	BP	positive regulation of I-kappaB kinase/NF-kappaB signaling	7	1.6E-2
	BP	positive regulation of transcription from RNA pol II promoter	23	1.6E-2
	BP	negative regulation of angiogenesis	5	1.6E-2
	BP	regulation of protein secretion	3	1.7E-2
	BP	extrinsic apoptotic signaling pathway	4	1.8E-2
	BP	lipid homeostasis	4	1.8E-2
	BP	positive regulation of endothelial cell apoptotic process	3	1.9E-2
	BP	positive regulation of smooth muscle cell proliferation	5	2.3E-2
	BP	cell cycle G2/M phase transition	2	2.7E-2
	BP	regulation of histone phosphorylation	2	2.7E-2
	BP	cellular response to sterol	2	2.7E-2
	BP	organelle fission	2	2.7E-2
	BP	purine nucleotide biosynthetic process	3	2.9E-2
	BP	positive regulation of chemokine production	3	2.9E-2
	BP	apoptotic signaling pathway	4	3.1E-2
	BP	positive regulation of interleukin-6 production	4	3.3E-2
	BP	phosphatidylserine exposure on apoptotic cell surface	2	4.0E-2
	BP	T-helper 17 cell differentiation	2	4.0E-2
	BP	L-alanine catabolic process	2	4.0E-2
	BP	peptidyl-tyrosine dephosphorylation	3	4.1E-2
	BP	positive regulation of interferon-beta production	3	4.4E-2
	BP	apoptotic process	14	4.5E-2
	BP	regulation of transcription, DNA-templated	41	4.8E-2
	BP	circadian regulation of gene expression	4	4.9E-2

Supplementary table 9. Gene enrichment analysis of up- and down-regulated genes ($P \leq 0.05$) in simultaneously *Rora* and *Rorc* knockdown 3T3-L1 adipocytes using DAVID bioinformatics source showing the gene ontology term "Biological Process" (BP, biological process).

SUPPLEMENTARY TABLE 10: LIST OF DOWN- AND UP- REGULATED GENES IN INGUINAL WAT OF WT MICE SUBJECTED TO 40% OF CR

Down-regulated genes			
Entrez	Gene Symbol	logFC	P.Value
Lipf	67717	-5.4459	4.11E-10
Mmp12	17381	-5.2723	9.81E-06
Atp6v0d2	242341	-5.0301	3.06E-07
Slc5a7	63993	-4.2446	1.60E-07
Gpr50	14765	-4.0911	3.24E-08
Ubd	24108	-3.9603	1.82E-11
Oxtr	18430	-3.8034	6.83E-10
Itgad	381924	-3.1202	6.56E-08
Fgf13	14168	-2.4405	6.76E-07
Il1rn	16181	-2.3849	7.04E-08
Fam83d	71878	-2.3785	5.89E-08
C6	12274	-2.3700	3.36E-06
Angptl8	624219	-2.3628	2.35E-07
Fam122b	78755	-2.3081	9.13E-09
Lcn2	16819	-2.2718	1.99E-05
Mrc2	17534	-2.1833	4.44E-08
Paqr9	75552	-2.1544	8.64E-09
Spc25	66442	-2.1317	1.20E-06
S100a8	20201	-2.0960	2.83E-06
Chrm4	12672	-2.0900	1.87E-06
Fam110c	104943	-2.0709	9.18E-06
Marc1	66112	-2.0263	6.28E-06
Ncan	13004	-2.0000	7.56E-07
Lctl	235435	-1.9469	3.99E-06
Hephl1	244698	-1.9358	1.12E-06
Tm4sf19	277203	-1.8974	3.39E-07
Cdkl4	381113	-1.8944	1.15E-05
Dpep2	319446	-1.8808	6.14E-07
Lgals3	16854	-1.8707	2.13E-07
Dnajc6	72685	-1.8586	5.72E-07
Krt79	223917	-1.8415	3.69E-06
Kcnc2	268345	-1.8278	4.85E-06
Pla2g2e	26970	-1.8174	5.50E-07
Slc16a12	240638	-1.8157	1.20E-06
Tekt1	21689	-1.8123	3.89E-05
Tfpi2	21789	-1.7981	9.93E-08
Fam83a	239463	-1.7723	8.07E-05
Trem2	83433	-1.7635	8.90E-06
Thbs1	21825	-1.7612	1.45E-05
Lbp	16803	-1.7497	5.29E-06
Olfr735	257909	-1.7180	3.73E-05
Kcnj15	16516	-1.7156	1.50E-05
Tfr2	50765	-1.7156	3.31E-05
Duoxa1	213696	-1.7087	9.98E-07
Nectin3	58998	-1.6874	4.24E-08
Kcne1l	66240	-1.6682	2.86E-06
Fcgr4	246256	-1.6643	2.11E-05
Unc79	217843	-1.6635	1.57E-04
Dusp15	252864	-1.6486	3.83E-07
Fam20c	80752	-1.6333	5.66E-07

Up-regulated genes			
Entrez	Gene Symbol	logFC	P.Value
Sell	20343	2.6644	5.46E-03
Cd3e	12501	2.4384	7.17E-03
Sidt1	320007	2.3953	1.13E-03
Cd8b1	12526	2.2996	4.25E-03
Cxcl13	55985	2.2394	1.02E-04
Cd3g	12502	2.2377	1.61E-02
Tcf7	21414	2.1381	7.59E-03
Slc43a1	72401	2.0817	1.53E-07
Ms4a4b	60361	2.0731	1.93E-02
Cr2	12902	2.0104	5.15E-03
Ccl22	20299	1.9898	4.99E-02
Btla	208154	1.9500	1.22E-02
Bank1	242248	1.8538	3.26E-03
Dennd2d	72121	1.8433	4.77E-05
Icos	54167	1.8263	1.46E-03
H2-M2	14990	1.7889	1.12E-02
Ifi208	100033459	1.7586	1.77E-03
Prkcq	18761	1.7346	1.02E-03
Ccr6	12458	1.7304	2.26E-03
Cd4	12504	1.7177	9.80E-03
Ipcef1	320495	1.7079	1.31E-02
Dapl1	76747	1.7068	1.71E-03
Ccl19	24047	1.6772	1.46E-02
Serpina1e	20704	1.6768	9.52E-03
Cd69	12515	1.6593	2.21E-02
Themis	210757	1.6414	3.76E-02
Ifi213	623121	1.6124	3.23E-03
Acsm3	20216	1.6121	3.10E-04
Sit1	54390	1.6046	4.90E-03
Adrb3	11556	1.5788	1.35E-05
Fcrl1	229499	1.5769	5.51E-03
Trim7	94089	1.5603	7.04E-04
Cyfip2	76884	1.5450	2.47E-02
Ltb	16994	1.5407	3.21E-03
Cyp2e1	13106	1.5390	4.00E-05
Alb	11657	1.5283	2.07E-02
Rorc	19885	1.5170	4.31E-04
Dgka	13139	1.5061	9.26E-04
Apol7e	666348	1.4834	4.56E-03
Mmp9	17395	1.4649	2.11E-04
Cfd	11537	1.4553	3.48E-08
Skap1	78473	1.4280	5.42E-03
Cd2	12481	1.4174	1.76E-02
Clu	12759	1.4164	4.42E-04
Spib	272382	1.4060	8.62E-03
Timd4	276891	1.3981	1.19E-03
Rasal3	320484	1.3975	1.15E-02
Il18r1	16182	1.3916	2.51E-03
Ctla4	12477	1.3853	3.25E-03
Adgrg2	237175	1.3482	1.77E-04

Supplementary table 10. List of the first 50 down-regulated and up-regulated genes obtained in a microarray analysis comparing mRNA expression levels in siRorc 3T3-L1 adipocytes compared with siCont 3T3-L1 adipocytes. Genes are listed in descending order of logarithm of fold change.

SUPPLEMENTARY TABLE 11: GENE ENRICHMENT ANALYSIS OF UP- AND DOWN-REGULATED GENES IN INGUINAL WAT OF WT MICE SUBJECTED TO 40% OF CR

	GO Category	Term	Count	P-Value
UP-REGULATED GENES	BP	metabolic process	43	1.8E-11
	BP	glutathione metabolic process	13	7.0E-9
	BP	response to toxic substance	16	1.4E-8
	BP	oxidation-reduction process	44	4.4E-7
	BP	lipid metabolic process	30	3.9E-5
	BP	immune system process	26	7.8E-5
	BP	fatty acid metabolic process	14	4.4E-4
	BP	adaptive immune response	13	5.2E-4
	BP	response to drug	22	5.8E-4
	BP	dibenzo-p-dioxin metabolic process	3	7.3E-3
	BP	complement activation	4	7.6E-3
	BP	positive regulation of T cell proliferation	7	8.7E-3
	BP	steroid metabolic process	8	9.0E-3
	BP	aging	12	9.3E-3
	BP	immune response	16	9.6E-3
	CC	membrane	255	7.0E-9
	CC	mitochondrion	84	1.9E-7
	CC	extracellular space	70	1.3E-5
	CC	extracellular exosome	108	2.0E-5
	CC	mitochondrial inner membrane	25	1.7E-4
	CC	mitochondrial matrix	16	2.0E-4
	CC	extracellular region	71	7.3E-4
	MF	glutathione transferase activity	11	1.9E-8
	MF	oxidoreductase activity	43	1.3E-7
	MF	catalytic activity	37	1.7E-7
	MF	glutathione binding	6	4.6E-5
	MF	protein homodimerization activity	43	1.3E-4
	MF	glutathione peroxidase activity	6	2.1E-4
	MF	structural constituent of myelin sheath	4	2.3E-4
	MF	serine-type peptidase activity	15	2.7E-4
	MF	transferase activity	65	6.0E-4
	MF	receptor binding	25	9.1E-4
	MF	pyridoxal phosphate binding	8	9.7E-4
DOWN-REGULATED GENES	BP	angiogenesis	57	6.8E-18
	BP	cell adhesion	74	5.8E-12
	BP	mitotic nuclear division	46	6.6E-9
	BP	cell division	54	3.9E-8
	BP	cell cycle	76	4.4E-8
	BP	sterol biosynthetic process	12	3.5E-7
	BP	positive regulation of angiogenesis	25	5.8E-7
	BP	inflammatory response	47	1.6E-6
	BP	cholesterol biosynthetic process	11	1.9E-5
	BP	lipid metabolic process	54	2.1E-5
	BP	neutrophil chemotaxis	16	2.4E-5
	BP	regulation of cell cycle	21	2.6E-5
	BP	positive regulation of inflammatory response	15	3.4E-5
	BP	regulation of angiogenesis	10	3.9E-5
	BP	chromosome segregation	18	4.2E-5
	BP	mitotic cytokinesis	10	7.3E-5
	BP	ventricular cardiac muscle cell action potential	7	7.8E-5
	BP	response to hypoxia	28	9.4E-5
	BP	nucleosome assembly	19	9.7E-5
	BP	negative regulation of angiogenesis	15	1.6E-4
	BP	apoptotic process	60	1.7E-4
	BP	organ regeneration	13	1.8E-4
	BP	positive regulation of fibroblast proliferation	14	2.0E-4

	BP	positive regulation of apoptotic process	40	2.1E-4
	BP	regulation of cell migration	15	3.3E-4
	BP	positive regulation of gene expression	44	5.5E-4
	BP	positive regulation of cell migration	27	5.6E-4
	BP	cardiac muscle contraction	11	7.7E-4
	BP	monocyte chemotaxis	10	7.8E-4
	BP	steroid metabolic process	15	8.3E-4
	BP	regulation of gene silencing	6	8.8E-4
	BP	positive regulation of ERK1 and ERK2 cascade	25	9.4E-4
	BP	positive regulation of long-term neuronal synaptic plasticity	5	9.4E-4
	CC	membrane	620	2.2E-26
	CC	extracellular exosome	287	6.8E-21
	CC	extracellular matrix	49	1.4E-9
	CC	cell surface	80	4.1E-9
	CC	cytoplasm	515	6.1E-9
	CC	focal adhesion	57	8.5E-9
	CC	endoplasmic reticulum	137	9.3E-9
	CC	nuclear nucleosome	16	3.9E-8
	CC	cytoskeleton	116	1.1E-7
	CC	nucleosome	24	2.3E-7
	CC	proteinaceous extracellular matrix	46	2.9E-7
	CC	chromosome	48	5.4E-7
	CC	chromosome, centromeric region	27	7.5E-7
	CC	kinetochore	24	1.6E-6
	CC	spindle pole	22	2.6E-6
	CC	sarcolemma	23	4.4E-6
	CC	cell-cell adherens junction	43	4.4E-6
	CC	cell-cell junction	31	1.0E-5
	CC	extracellular region	155	1.6E-5
	CC	plasma membrane	372	2.0E-5
	CC	integral component of plasma membrane	107	2.4E-5
	CC	external side of plasma membrane	41	2.5E-5
	CC	extracellular space	135	3.0E-5
	CC	lamellipodium	26	3.9E-5
	CC	condensed chromosome kinetochore	17	6.5E-5
	CC	lysosome	41	6.8E-5
	CC	cell junction	73	7.5E-5
	CC	basement membrane	18	1.2E-4
	CC	adherens junction	13	1.4E-4
	CC	microtubule	39	2.3E-4
	CC	basolateral plasma membrane	27	4.9E-4
	CC	axon	41	6.9E-4
	CC	cytosol	146	9.6E-4
	CC	condensed nuclear chromosome outer kinetochore	4	9.7E-4
	CC	neuronal cell body	49	9.3E-3
	MF	protein binding	333	4.2E-8
	MF	calcium ion binding	78	9.2E-7
	MF	cadherin binding involved in cell-cell adhesion	38	1.3E-5
	MF	collagen binding	14	5.9E-5
	MF	heparin binding	23	1.9E-4
	MF	enzyme binding	42	6.2E-4

Supplementary table 11. Gene enrichment analysis of up- and down-regulated genes ($P \leq 0.0001$) in inguinal WAT of Wt mice subjected to 40% of CR using DAVID bioinformatics source showing the gene onthology terms “Biological Process”, “Cellular Component” and “Molecular Function”. (BP, biological process; CC, cellular component; MF, molecular function).

SUPPLEMENTARY TABLE 12: LIST OF UP-REGULATED GENES IN INGUINAL WAT OF RORγ-FAT-KO MICE FED AL

Down-regulated genes			
Entrez	Gene Symbol	logFC	P.Value
20201	S100a8	-0.9547	2.30E-03
574437	Xlr3b	-0.9393	1.13E-02
76633	Lrmda	-0.8217	2.87E-02
22446	Xlr3c	-0.7648	3.63E-02
12236	Bub1b	-0.7577	3.20E-02
246256	Fcgr4	-0.6880	1.17E-02
12047	Bcl2a1d	-0.6871	1.76E-02
12801	Cnr1	-0.6805	1.36E-03
71988	Esco2	-0.6749	1.59E-02
258360	Olfr731	-0.6636	2.93E-02
244209	Cyp2r1	-0.6602	3.86E-03
633285	Rbm46	-0.6591	3.65E-02
11629	Aif1	-0.6517	8.17E-03
215387	Ncaph	-0.6269	2.61E-03
244698	Hephl1	-0.6264	3.44E-03
16551	Kif11	-0.6175	1.42E-02
69270	Gins1	-0.6166	2.78E-03
71819	Kif23	-0.6155	1.31E-03
668166	Zxdb	-0.6099	6.43E-04
57814	Kcne4	-0.6082	4.07E-03
72415	Sgo1	-0.5924	4.05E-03
53320	Folh1	-0.5892	4.53E-02
57442	Kcne3	-0.5891	4.02E-03
75178	Meiob	-0.5884	2.15E-02
27405	Abcg3	-0.5859	1.56E-02
317758	Gimap9	-0.5793	7.27E-03
12289	Cacna1d	-0.5787	1.00E-02
213208	Il20rb	-0.5715	3.01E-02
233406	Prc1	-0.5714	2.91E-03
233878	Sez6l2	-0.5669	3.42E-02
68187	Fam135a	-0.5624	4.77E-03
16633	Klra2	-0.5507	3.20E-03
14051	Eya4	-0.5381	1.76E-02
78755	Fam122b	-0.5172	7.74E-03
78697	Pus7	-0.5162	9.27E-03
110196	Fdps	-0.5161	2.71E-02
13605	Ect2	-0.5081	1.43E-02
258783	Olfr920	-0.5004	1.83E-02
20135	Rrm2	-0.4997	6.22E-03
12663	Chml	-0.4954	5.62E-03
68743	Anln	-0.4897	1.35E-02
15957	Ifit1	-0.4878	4.70E-03
236576	Spry3	-0.4825	7.66E-03
319189	Hist2h2bb	-0.4819	1.70E-02
243385	Gprin3	-0.4781	1.81E-02
56068	Ammecr1	-0.4766	9.51E-04
66949	Trim59	-0.4757	2.06E-02
225825	Cd226	-0.4729	3.24E-02
72836	Pot1b	-0.4710	3.24E-02
330301	Zfp786	-0.4699	4.70E-02

Up-regulated genes			
Entrez	Gene Symbol	logFC	P.Value
16644	Kng1	2.0427	1.65E-02
20702	Serpina1c	2.0064	2.25E-02
230163	Aldob	1.8195	2.08E-02
20701	Serpina1b	1.6696	4.50E-02
381531	Mup21	1.6248	5.25E-03
14473	Gc	1.6057	4.26E-02
18703	Pigr	1.6007	8.07E-03
11657	Alb	1.5619	2.27E-02
17842	Mup3	1.5232	6.20E-03
20703	Serpina1d	1.4871	2.51E-02
76971	Sult2a8	1.4323	2.58E-02
20700	Serpina1a	1.3720	4.33E-02
238055	Apob	1.3702	2.86E-02
83702	Akr1c6	1.3163	1.08E-02
56373	Cpb2	1.3037	8.42E-03
20704	Serpina1e	1.2858	3.24E-02
12007	Azgp1	1.2831	2.92E-02
17840	Mup1	1.2647	8.34E-04
11905	Serpinc1	1.2624	4.08E-02
76279	Cyp2d26	1.2551	4.59E-02
18815	Plg	1.2360	2.85E-03
13884	Ces1c	1.2351	2.16E-02
381530	Mup20	1.2207	6.71E-03
18416	Otc	1.1791	1.75E-03
56720	Tdo2	1.1624	6.95E-03
382053	Ces3a	1.1505	2.46E-02
15445	Hpd	1.1339	1.41E-02
13109	Cyp2j5	1.1321	1.64E-02
26458	Slc27a2	1.1213	1.83E-02
13112	Cyp3a11	1.1194	1.54E-02
170942	Erdr1	1.1059	4.74E-02
94175	Hrg	1.0506	4.67E-02
54326	Elovl2	1.0450	7.65E-03
11818	Apoh	1.0374	2.59E-02
18478	Pah	1.0331	2.00E-02
243168	Hsd17b13	1.0267	1.44E-02
107141	Cyp2c50	0.9580	1.94E-02
14860	Gsta4	0.9553	1.37E-05
14711	Gnmt	0.9492	6.82E-03
217847	Serpina10	0.9387	9.48E-03
22262	Uox	0.9172	4.77E-02
13119	Cyp4a14	0.8980	4.28E-03
11808	Apoa4	0.8953	3.74E-02
12116	Bhmt	0.8813	3.36E-02
434764	Rhox2f	0.8737	2.17E-03
71640	Zfp949	0.8684	2.83E-05
28248	Slco1a1	0.8538	8.99E-03
12944	Crp	0.8420	3.06E-02
227231	Cps1	0.8322	4.24E-02
59083	Fetub	0.8243	6.42E-03

Supplementary table 12. List of the first 50 down-regulated and up-regulated genes obtained in a microarray analysis comparing mRNA expression levels in in inguinal WAT from Wt and RORγ-FAT-KO mice fed AL. Genes are listed in descending order of logarithm of fold change.

SUPPLEMENTARY TABLE 13: GENE ENRICHMENT ANALYSIS OF UP- AND DOWN-REGULATED GENES IN WAT OF RORγ-FAT-KO MICE FED AL

	GO Category	Term	Count	P-Value
UP-REGULATED GENES	BP	response to peptide hormone	9	9.30E-08
	BP	negative regulation of fibrinolysis	5	1.20E-07
	BP	negative regulation of lipid storage	6	2.80E-07
	BP	negative regulation of gluconeogenesis	6	9.80E-07
	BP	oxidation-reduction process	20	1.20E-06
	BP	hemostasis	7	1.40E-06
	BP	blood coagulation	8	4.00E-06
	BP	heat generation	5	4.40E-06
	BP	cellular response to lipid	5	4.40E-06
	BP	positive regulation of lipid metabolic process	5	4.40E-06
	BP	negative regulation of lipid biosynthetic process	5	5.80E-06
	BP	positive regulation of glucose metabolic process	5	1.90E-05
	BP	negative regulation of insulin secretion involved in cellular response to glucose stimulus	5	2.30E-05
	BP	energy reserve metabolic process	5	2.30E-05
	BP	negative regulation of peptidase activity	8	3.50E-05
	BP	locomotor rhythm	5	4.50E-05
	BP	epoxygenase P450 pathway	5	8.10E-05
	BP	mitochondrion morphogenesis	5	1.00E-04
	BP	negative regulation of blood coagulation	4	1.20E-04
	BP	response to zinc ion	5	1.50E-04
	BP	acute-phase response	5	1.50E-04
	BP	arachidonic acid metabolic process	5	1.70E-04
	BP	aerobic respiration	5	2.30E-04
	BP	response to cytokine	6	4.10E-04
	BP	triglyceride catabolic process	4	4.70E-04
	BP	response to stilbenoid	4	9.20E-04
	BP	positive regulation of gene expression	11	1.10E-03
	BP	glucose homeostasis	6	3.80E-03
	BP	response to toxic substance	5	4.50E-03
	BP	cholesterol metabolic process	5	5.10E-03
	BP	fibrinolysis	3	5.90E-03
	BP	positive regulation of protein kinase B signaling	5	6.80E-03
	BP	complement activation, classical pathway	4	8.90E-03
	BP	lipid transport	5	1.10E-02
	BP	flavonoid biosynthetic process	3	1.10E-02
	BP	flavonoid glucuronidation	3	1.10E-02
	BP	anion homeostasis	2	1.50E-02
	BP	retina homeostasis	3	1.60E-02
	BP	response to drug	8	1.70E-02
	BP	cholesterol efflux	3	2.00E-02
	BP	sodium-independent organic anion transport	3	2.00E-02
	BP	lipoprotein metabolic process	3	2.50E-02
	BP	steroid metabolic process	4	2.70E-02
	BP	metabolic process	9	2.80E-02
	BP	vitamin transport	2	3.10E-02
	BP	protein N-linked glycosylation	3	3.20E-02
	BP	regulation of gene expression	7	3.30E-02
	BP	negative regulation of plasminogen activation	2	3.80E-02
	BP	triglyceride mobilization	2	4.60E-02
	CC	extracellular region	48	4.5E-15
	CC	extracellular space	44	1.0E-14
	CC	blood microparticle	12	5.6E-9
	CC	organelle membrane	10	4.0E-8
	CC	extracellular exosome	46	1.1E-7
	CC	endoplasmic reticulum	29	6.4E-7
	CC	intracellular membrane-bounded organelle	21	1.0E-6

	CC	chylomicron	4	1.2E-4
	CC	endoplasmic reticulum membrane	16	3.3E-4
	CC	very-low-density lipoprotein particle	4	3.8E-4
	CC	high-density lipoprotein particle	3	1.1E-2
	CC	intermediate-density lipoprotein particle	2	3.7E-2
	MF	oxidoreductase activity, acting on paired donors, with incorporation or reduction of molecular oxygen	12	5.6E-10
	MF	monooxygenase activity	12	1.4E-9
	MF	heme binding	14	2.2E-9
	MF	aromatase activity	8	1.5E-8
	MF	iron ion binding	14	2.3E-8
	MF	arachidonic acid epoxygenase activity	8	1.1E-7
	MF	oxidoreductase activity	21	1.2E-7
	MF	small molecule binding	7	2.2E-7
	MF	steroid hydroxylase activity	8	2.9E-7
	MF	serine-type endopeptidase inhibitor activity	10	8.2E-7
	MF	oxidoreductase activity, acting on paired donors, with incorporation or reduction of molecular oxygen, reduced flavin or flavoprotein as one donor, and incorporation of one atom of oxygen	7	1.2E-6
	MF	insulin-activated receptor activity	5	3.0E-6
	MF	glycoprotein binding	8	4.0E-6
	MF	endopeptidase inhibitor activity	6	5.1E-6
	MF	transporter activity	11	1.3E-5
	MF	oxygen binding	5	5.8E-5
	MF	peptidase inhibitor activity	8	7.2E-5
	MF	protease binding	7	4.2E-4
	MF	phospholipid binding	6	8.1E-4
	MF	pheromone binding	6	2.2E-3
	MF	serine-type peptidase activity	7	2.3E-3
	MF	cysteine-type endopeptidase inhibitor activity	4	6.1E-3
	MF	heparin binding	6	8.4E-3
	MF	serine-type endopeptidase activity	7	8.4E-3
	MF	sodium-independent organic anion transmembrane transporter activity	3	2.1E-2
	MF	glucuronosyltransferase activity	3	2.4E-2
	MF	lipid binding	7	2.5E-2
	MF	amino acid binding	3	2.5E-2
	MF	fatty acid transporter activity	2	3.3E-2
	MF	linoleic acid epoxygenase activity	2	3.3E-2
DOWN-REGULATED GENES	BP	cell cycle	22	1.0E-07
	BP	cell division	17	2.0E-07
	BP	mitotic nuclear division	14	1.1E-06
	BP	chromosome segregation	6	1.1E-03
	BP	positive regulation of cytokinesis	4	3.0E-03
	BP	protein localization to kinetochore	3	3.3E-03
	BP	cytokinesis	4	4.2E-03
	BP	mitotic chromosome condensation	3	5.6E-03
	BP	oxidation-reduction process	14	6.8E-03
	BP	regulation of potassium ion transmembrane transport	3	7.5E-03
	BP	chromosome condensation	3	8.5E-03
	BP	inflammatory response to antigenic stimulus	3	9.6E-03
	BP	putrescine catabolic process	2	2.6E-02
	BP	mitotic cytokinesis	3	2.8E-02
	BP	regulation of ion transmembrane transport	5	3.1E-02
	BP	plus-end-directed vesicle transport along microtubule	2	3.5E-02
	BP	development of primary female sexual characteristics	2	3.5E-02
	BP	spermine catabolic process	2	4.3E-02
	BP	meiotic chromosome segregation	2	4.3E-02
	BP	chromosome organization	3	4.4E-02
	BP	potassium ion transmembrane transport	4	4.5E-02
	BP	T cell differentiation	3	5.0E-02

	CC	chromosome	13	3.1E-5
	CC	spindle	8	5.2E-5
	CC	midbody	7	7.6E-4
	CC	voltage-gated potassium channel complex	5	4.2E-3
	CC	spindle microtubule	4	4.4E-3
	CC	mitotic spindle	4	6.9E-3
	CC	mitochondrial outer membrane	6	9.0E-3
	CC	cytoskeleton	18	1.1E-2
	CC	cytoplasm	69	2.0E-2
	CC	centralspindlin complex	2	2.5E-2
	CC	chromosome, centromeric region	5	3.0E-2
	CC	nucleus	62	3.7E-2
	CC	condensin complex	2	4.1E-2
	MF	oxidoreductase activity	13	4.8E-3
	MF	microtubule binding	7	6.8E-3

Supplementary table 13. Gene enrichment analysis of up- and down-regulated genes ($P \leq 0.001$) in inguinal WAT of RORγ-FAT-KO mice fed AL using DAVID bioinformatics source showing the gene onthology terms “Biological Process”, “Cellular Component” and “Molecular Function”. (BP, biological process; CC, cellular component; MF, molecular function).

SUPPLEMENTARY TABLE 14: LIST OF GENES UP-REGULATED BY CR AND DOWN-REGULATED IN WAT OF RORγ-FAT-KO MICE UNDER CR

		AL-Wt vs AL-CR		CR-Wt vs CR-KO	
Gene Symbol	Entrez	logFC	P.Value	logFC	P.Value
AI467606	101602	0.82968	0.00291	-1.04275	0.00055
Akna	100182	0.72889	0.04776	-1.09944	0.00619
Ano7	404545	0.56031	0.00145	-0.44430	0.00675
Apol7b	278679	0.83425	0.00729	-0.96989	0.00281
Apol7e	666348	1.48344	0.00456	-1.73152	0.00160
Arhgap15	76117	1.07950	0.04922	-1.68913	0.00518
B4galnt1	14421	1.29657	0.04890	-2.00179	0.00557
Bank1	242248	1.85377	0.00326	-1.85840	0.00320
Bin2	668218	1.20248	0.04183	-1.72734	0.00680
Boll	75388	0.76572	0.01872	-0.81462	0.01361
Btla	208154	1.95005	0.01223	-2.42585	0.00329
Cacnb3	12297	1.29424	0.04267	-1.68305	0.01233
Ccl19	24047	1.67723	0.01464	-2.01500	0.00511
Ccl22	20299	1.98976	0.04989	-3.08183	0.00564
Ccr6	12458	1.73037	0.00226	-1.36260	0.01009
Cd2	12481	1.41741	0.01763	-1.86975	0.00354
Cd209b	69165	1.21192	0.00439	-1.04599	0.01056
Cd37	12493	1.17269	0.02380	-1.66392	0.00328
Cd3e	12501	2.43837	0.00717	-2.71222	0.00370
Cd3g	12502	2.23768	0.01612	-3.09833	0.00227
Cd4	12504	1.71770	0.00980	-2.24176	0.00180
Cd69	12515	1.65935	0.02215	-2.16368	0.00513
Cd7	12516	0.96812	0.02557	-0.92029	0.03216
Cd72	12517	0.97024	0.03142	-1.66961	0.00131
Cd8b1	12526	2.29964	0.00425	-2.73670	0.00129
Clcf1	56708	0.65604	0.02911	-0.88543	0.00596
Clu	12759	1.41636	0.00044	-1.07747	0.00328
Cmah	12763	0.92763	0.00590	-1.04299	0.00278
Coro1a	12721	0.96192	0.02699	-1.72224	0.00075
Cr2	12902	2.01036	0.00515	-2.30003	0.00212
Cst7	13011	1.17776	0.00074	-0.99368	0.00253
Ctla4	12477	1.38531	0.00325	-1.46892	0.00218
Cyfip2	76884	1.54504	0.02471	-1.75699	0.01295
Dapl1	76747	1.70676	0.00171	-1.59139	0.00278
Dennd2d	72121	1.84334	0.00005	-0.66033	0.04460
Dgka	13139	1.50612	0.00093	-1.12751	0.00661
Dlg2	23859	0.56868	0.00812	-0.43380	0.03223
Dnase1l3	13421	1.30815	0.03987	-1.98946	0.00445
Far2	330450	0.43566	0.02476	-0.41288	0.03161
Fcmr	69169	0.97211	0.01387	-1.06930	0.00817
Fcrl1	229499	1.57689	0.00551	-1.62610	0.00455
Flt3	14255	0.94736	0.02692	-1.24123	0.00642
Gja6	414089	0.60856	0.00360	-0.55009	0.00678
Gstp3	225884	1.27015	0.01549	-1.40286	0.00901
H2-M2	14990	1.78887	0.01121	-2.31373	0.00227
Haao	107766	1.34232	0.00854	-1.32385	0.00925
Hpse2	545291	0.52864	0.01274	-0.51091	0.01525
Icos	54167	1.82631	0.00146	-1.71670	0.00226
Ifi208	100033459	1.75861	0.00177	-1.84983	0.00123
Ifi209	236312	1.23643	0.03522	-1.64098	0.00851
Ifi213	623121	1.61244	0.00323	-1.78554	0.00160
Ikbke	56489	0.68843	0.01228	-0.76216	0.00688
Il18r1	16182	1.39159	0.00251	-1.10591	0.01043
Il1a	16175	0.70929	0.01186	-0.55354	0.03899
Ipcef1	320495	1.70790	0.01310	-1.70670	0.01315
Isyna1	71780	0.54076	0.02729	-0.54587	0.02614

Itgae	16407	0.93914	0.00660	-0.79976	0.01616
Klhl6	239743	0.99240	0.01600	-1.32402	0.00290
Klrd1	16643	1.06127	0.03123	-1.53381	0.00429
Lepr	16847	0.83625	0.01461	-0.94784	0.00726
Lrp8	16975	0.52632	0.02270	-0.82828	0.00150
Ltb	16994	1.54069	0.00321	-1.63226	0.00217
Mapk10	26414	0.44098	0.04292	-0.51430	0.02169
Ms4a4b	60361	2.07312	0.01934	-2.79265	0.00348
Ndst3	83398	0.55406	0.00411	-0.35978	0.03987
Nrn1	68404	0.82114	0.00041	-0.38794	0.03990
Olfr1259	258338	0.73694	0.00063	-0.47410	0.01187
Olfr1427	258674	0.56967	0.00394	-0.37986	0.03468
Parvg	64099	0.90597	0.02986	-0.87953	0.03402
Patj	12695	0.72053	0.00044	-0.36352	0.03140
Pla2g2d	18782	0.92766	0.00423	-0.85119	0.00719
Prf1	18646	0.39859	0.01311	-0.77172	0.00012
Prkcq	18761	1.73464	0.00102	-1.55708	0.00222
Proc	19123	0.39073	0.01809	-0.37938	0.02092
Ptprc	19264	1.13959	0.04582	-1.85524	0.00358
Rasal3	320484	1.39749	0.01150	-1.77111	0.00269
Rasgrp1	19419	1.27731	0.04558	-2.19515	0.00247
Rhoh	74734	1.02286	0.02114	-1.38358	0.00382
Rorc	19885	1.51701	0.00043	-1.19762	0.00250
Sash3	74131	0.84457	0.04829	-1.17612	0.01003
Sell	20343	2.66444	0.00546	-3.36221	0.00112
Sema4d	20354	0.77030	0.03804	-0.78110	0.03586
Serpina10	217847	0.90334	0.03465	-0.85144	0.04432
Sidt1	320007	2.39526	0.00113	-2.03213	0.00355
Siglech	233274	1.28146	0.00012	-0.81482	0.00375
Sit1	54390	1.60461	0.00490	-1.45227	0.00892
Skap1	78473	1.42799	0.00542	-1.63008	0.00228
Slc14a1	108052	0.69853	0.01608	-1.08114	0.00102
Spata31	78124	0.49484	0.00232	-0.37367	0.01296
Spib	272382	1.40599	0.00862	-1.71611	0.00246
Sprr2j-ps	20764	0.39172	0.02469	-0.39389	0.02405
Srd5a2	94224	0.38908	0.03934	-0.40578	0.03288
Tcf7	21414	2.13811	0.00759	-2.48709	0.00293
Themis	210757	1.64143	0.03759	-2.38468	0.00543
Timd4	276891	1.39807	0.00119	-0.92670	0.01573
Tmem163	72160	0.49878	0.00841	-0.75786	0.00047
Tnfrsf18	21936	0.71896	0.00088	-0.49702	0.01010
Tnfrsf26	244237	0.49155	0.02546	-0.88634	0.00065
Tnfsf8	21949	0.79408	0.03109	-0.83726	0.02441
Tnik	665113	1.07213	0.00502	-0.84200	0.01941
Traf1	22029	0.88086	0.04935	-1.65987	0.00149
Trat1	77647	1.24059	0.01237	-1.44837	0.00502
Trim30b	244183	0.65793	0.01394	-0.54527	0.03432
Trim7	94089	1.56032	0.00070	-0.80890	0.03606
Xkrx	331524	0.86790	0.01848	-0.89239	0.01605
Xlr4c	72891	1.12355	0.04129	-1.57073	0.00784
Zap70	22637	22637.00000	0.00960	-0.92410	0.02144
Zmynd15	574428	0.39722	0.02436	-0.67536	0.00095

Supplementary table 14. List of the common genes up-regulated by CR (AL-Wt vs CR-Wt) and down-regulated by *Rorc* knockout mice compared to Wt mice under CR conditions (CR-Wt vs CR-KO).

SUPPLEMENTARY TABLE 15: GENE ENRICHMENT ANALYSIS OF GENES UP-REGULATED BY CR AND DOWN-REGULATED IN WAT OF RORγ-FAT-KO MICE UNDER CR

Category	Term	Count	P-Value
BP	adaptive immune response	10	4.0E-08
BP	immune system process	14	7.9E-08
BP	positive regulation of T cell proliferation	7	9.3E-07
BP	immune response	11	1.4E-06
BP	T cell receptor signaling pathway	6	6.3E-06
BP	positive regulation of T cell activation	4	8.5E-05
BP	positive regulation of tumor necrosis factor production	5	2.4E-04
BP	positive regulation of calcium-mediated signaling	4	2.5E-04
BP	T cell costimulation	4	2.8E-04
BP	cell chemotaxis	5	7.0E-04
BP	positive regulation of immunoglobulin production	3	9.2E-04
BP	homeostasis of number of cells within a tissue	4	9.8E-04
BP	T cell differentiation	4	1.2E-03
BP	positive regulation of interferon-gamma secretion	3	1.4E-03
BP	positive regulation of alpha-beta T cell proliferation	3	1.40E-03
BP	positive regulation of interleukin-2 biosynthetic process	3	1.7E-03
BP	cellular response to virus	3	2.3E-03
BP	negative thymic T cell selection	3	2.3E-03
BP	positive regulation of interferon-gamma production	4	2.4E-03
BP	B cell receptor signaling pathway	4	2.8E-03
BP	positive regulation of NF-kappaB import into nucleus	3	4.2E-03
BP	positive regulation of interleukin-4 production	3	4.2E-03
BP	cell surface receptor signaling pathway	6	5.5E-03
BP	B cell differentiation	4	8.4E-03
BP	inflammatory response	7	8.7E-03
BP	lymph node development	3	1.0E-02
BP	positive regulation of peptidyl-tyrosine phosphorylation	4	1.5E-02
BP	negative regulation of T cell proliferation	3	1.8E-02
BP	positive regulation of B cell proliferation	3	2.1E-02
BP	regulation of extrinsic apoptotic signaling pathway	2	2.5E-02
BP	regulation of platelet aggregation	2	3.0E-02
BP	positive regulation of GTPase activity	4	4.0E-02
BP	protein localization to plasma membrane	3	4.1E-02
CC	external side of plasma membrane	18	7.2E-13
CC	membrane	69	3.1E-10
CC	immunological synapse	6	8.8E-7
CC	T cell receptor complex	4	6.1E-5
CC	cell surface	12	4.6E-4
CC	integral component of membrane	51	3.1E-3
CC	cell-cell junction	6	4.1E-3
CC	plasma membrane	39	4.1E-3
CC	extracellular space	15	2.5E-2
CC	alpha-beta T cell receptor complex	2	2.6E-2
CC	receptor complex	4	3.3E-2
CC	extracellular region	16	3.9E-2
MF	core promoter binding	4	7.7E-3
MF	heparan sulfate proteoglycan binding	3	7.9E-3
MF	carbohydrate binding	6	8.0E-3
MF	tumor necrosis factor receptor binding	3	1.3E-2
MF	transmembrane signaling receptor activity	6	2.8E-2
MF	cytokine activity	5	2.9E-2
MF	protein binding	31	3.8E-2

Supplementary table 15. Gene enrichment analysis ($P \leq 0.05$) of the common genes up-regulated by CR (AL-Wt vs CR-Wt) and down-regulated by *Rorc* knockout mice compared to Wt mice under CR conditions (CR-Wt vs CR-KO) using DAVID bioinformatics source. (BP, biological process; CC, cellular component; MF, molecular function).

SUPPLEMENTARY TABLE 16: LIST OF GENES DOWN-REGULATED BY CR AND UP-REGULATED IN WAT OF RORγ-FAT-KO MICE UNDER CR

		AL-Wt vs AL-CR		CR-Wt vs CR-KO	
Gene Symbol	Entrez	logFC	P.Value	logFC	P.Value
Abca5	217265	-0.30761	0.04956	0.56484	0.00181
Acp2	11432	-0.65072	0.00023	0.28925	0.03864
Ahsa2	268390	-0.35363	0.03083	0.39171	0.01906
Alg13	67574	-0.66236	0.00874	0.48921	0.03908
Arhgef26	622434	-0.49513	0.00200	0.29694	0.03544
Arxes1	76219	-1.03096	0.00000	0.38616	0.00509
Atp2c1	235574	-0.53623	0.00130	0.29409	0.04011
Atp6v0d2	242341	-5.03014	0.00000	1.27424	0.02173
B3galt1	26877	-1.04914	0.00026	0.45380	0.04590
Bcl2l13	94044	-0.63265	0.00011	0.29370	0.02165
Calr4	108802	-1.51533	0.00000	0.51457	0.00540
Car4	12351	-0.60720	0.00070	0.40842	0.00996
Ccdc71l	72123	-0.78836	0.00025	0.40646	0.02050
Coq10b	67876	-1.27121	0.00000	0.34891	0.04485
Cyp4b1	13120	-0.51123	0.00183	0.29451	0.03978
Ddah1	69219	-1.44531	0.00000	0.54291	0.01109
Dhrs7b	216820	-0.77732	0.00026	0.39101	0.02380
Dhrs9	241452	-1.54950	0.00001	0.62039	0.01263
Elmod2	244548	-0.74341	0.00003	0.31906	0.01581
Fads3	60527	-0.89359	0.00007	0.36322	0.03192
Fbxo4	106052	-0.87724	0.00006	0.51539	0.00389
Galc	14420	-0.95434	0.00000	0.32968	0.01613
Gpc4	14735	-0.97410	0.00001	0.29762	0.04514
Gskip	66787	-0.57913	0.00049	0.28515	0.03681
Gsto1	14873	-0.69113	0.00016	0.44977	0.00408
Hephl1	244698	-1.93584	0.00000	0.50559	0.03349
Hist1h1c	50708	-0.37755	0.00652	0.42697	0.00299
Hist1h2bj	319183	-0.90408	0.00003	0.34958	0.02740
Hist1h2bm	319186	-0.94081	0.00001	0.29195	0.04133
Hspb1	15507	-0.90907	0.00006	0.44006	0.01228
Ica1	15893	-0.49533	0.00197	0.27879	0.04571
Kcne1l	66240	-1.66824	0.00000	0.48379	0.03166
Kcnip4	80334	-0.41196	0.01752	0.34402	0.04007
Kctd12b	207474	-1.26690	0.00002	0.50930	0.01843
L3hypdh	67217	-0.63895	0.00045	0.41524	0.00882
Lamb3	16780	-1.61046	0.00000	0.38776	0.00905
Lig4	319583	-0.55078	0.00663	0.41470	0.02932
Mal2	105853	-1.56970	0.00000	0.45846	0.00539
Map9	213582	-0.75065	0.00192	0.57635	0.01019
March3	320253	-0.62085	0.00108	0.43630	0.01071
Mecom	14013	-0.69712	0.00009	0.39633	0.00613
Mfap3l	71306	-0.88343	0.00033	0.39330	0.04596
Mmp12	17381	-5.27233	0.00001	1.66124	0.03793
Mpv17l	93734	-0.52442	0.00542	0.36484	0.03587
Mutyh	70603	-0.59731	0.00039	0.29173	0.03359
Myrip	245049	-0.54209	0.01099	0.62052	0.00496
Nectin3	58998	-1.68738	0.00000	0.40812	0.01057
Olfr1396	258334	-1.24683	0.00018	0.61592	0.02119
Olfr735	257909	-1.71800	0.00004	0.71399	0.02047
Olfr747	258264	-0.47254	0.00636	0.50047	0.00445
Pex13	72129	-0.48600	0.00084	0.33241	0.01040
Pex7	18634	-0.39911	0.02270	0.44032	0.01384
Phlda3	27280	-0.60576	0.00023	0.27593	0.03440
Pter	19212	-0.80651	0.00009	0.39177	0.01497
Ptger3	19218	-1.08838	0.00003	0.38576	0.03779
Rgs4	19736	-0.80728	0.00022	0.35705	0.03828

Rmdn3	67809	-0.75008	0.00007	0.39763	0.00803
Rnf144b	218215	-0.74983	0.00032	0.34694	0.03852
Rnf149	67702	-0.57211	0.00069	0.32457	0.02375
Rnf152	320311	-0.52290	0.01090	0.38336	0.04720
S100b	20203	-1.14948	0.00001	0.52982	0.00349
Sat2	69215	-0.34570	0.01637	0.48316	0.00217
Sgcb	24051	-0.62019	0.00020	0.28076	0.03352
Slc16a12	240638	-1.81573	0.00000	0.45170	0.04220
Slc44a5	242259	-0.39193	0.03236	0.39221	0.03226
Slfn3	20557	-0.75169	0.00064	0.37378	0.04068
Sowahc	268301	-0.45249	0.00367	0.35497	0.01522
Spry3	236576	-0.81234	0.00010	0.32046	0.04203
Stk38l	232533	-1.02967	0.00000	0.27457	0.04150
Sumf1	58911	-0.58024	0.00052	0.33111	0.01931
Syn2	20965	-0.51599	0.00305	0.61835	0.00084
Tmem62	96957	-0.47164	0.01003	0.35574	0.03961
Tnfrsf23	79201	-1.40448	0.00000	0.24246	0.04252
Triap1	69076	-0.69643	0.00101	0.42871	0.02047
Trim13	66597	-0.36073	0.03544	0.34629	0.04204
Try4	22074	-0.48673	0.00640	0.56141	0.00256
Ttc23	67009	-0.37512	0.04521	0.41410	0.02974
Ttyh2	117160	-0.74731	0.00015	0.37976	0.01613
Wasf1	83767	-0.58931	0.00111	0.35415	0.02434
Wdr93	626359	-0.93296	0.00001	0.45174	0.00350
Wwtr1	97064	-0.59257	0.00022	0.28505	0.02667
Ypel2	77864	-0.60321	0.00037	0.43338	0.00414
Zwint	52696	-0.69193	0.00030	0.33526	0.03053

Supplementary table 16. List of the common genes down-regulated by CR (AL-Wt vs CR-Wt) and up-regulated by *Rorc* knockout mice compared to Wt mice under CR conditions (CR-Wt vs CR-KO).

SUPPLEMENTARY TABLE 17: GENE ENRICHMENT ANALYSIS OF GENES DOWN-REGULATED BY CR AND UP-REGULATED IN WAT OF RORγ-FAT-KO MICE UNDER CR

Category	Term	Count	P-Value
BP	bounding membrane of organelle	12	1.3E-3
BP	negative regulation of signal transduction	12	2.9E-3
BP	negative regulation of cell communication	12	7.3E-3
BP	negative regulation of signaling	12	7.5E-3
BP	negative regulation of intracellular signal transduction	7	1.1E-2
BP	regulation of cell communication	20	1.5E-2
BP	regulation of signaling	20	1.6E-2
BP	regulation of signal transduction	18	2.0E-2
BP	negative regulation of response to stimulus	12	2.1E-2
BP	ether biosynthetic process	2	2.4E-2
BP	glycerol ether biosynthetic process	2	2.4E-2
BP	ether lipid biosynthetic process	2	2.4E-2
BP	negative regulation of cation transmembrane transport	3	2.5E-2
BP	regulation of potassium ion transmembrane transport	3	2.7E-2
BP	cellular lipid biosynthetic process	2	3.2E-2
BP	negative regulation of ion transmembrane transport	3	3.4E-2
BP	ether lipid metabolic process	2	3.6E-2
BP	negative regulation of transmembrane transport	3	4.0E-2
BP	regulation of response to stimulus	21	4.3E-2
BP	regulation of potassium ion transport	3	4.7E-2
CC	organelle membrane	24	1.1E-5
CC	whole membrane	14	1.1E-3
CC	cytoplasmic part	42	1.1E-3
CC	bounding membrane of organelle	15	1.3E-3
CC	intracellular organelle part	42	2.5E-3
CC	cytoplasm	53	3.0E-3
CC	organelle part	42	4.2E-3
CC	membrane	52	8.8E-3
CC	protein complex	26	1.1E-2
CC	membrane part	42	2.3E-2
CC	endomembrane system	22	3.0E-2
CC	microbody part	3	3.1E-2
CC	peroxisomal part	3	3.1E-2
CC	transport vesicle	5	3.1E-2
CC	membrane-bounded vesicle	21	3.2E-2
CC	membrane-bounded organelle	54	3.4E-2
CC	lysosome	6	3.4E-2
CC	lytic vacuole	6	3.4E-2
CC	mitochondrial envelope	7	3.8E-2
CC	membrane protein complex	9	4.1E-2
CC	secretory granule membrane	3	4.3E-2
CC	organelle	57	4.7E-2
CC	vesicle	21	5.0E-2
CC	organelle envelope	9	5.0E-2
MF	transition metal ion binding	13	9.0E-3
MF	catalytic activity	34	1.5E-2
MF	peroxisome targeting sequence binding	2	2.0E-2
MF	ligase activity	6	2.0E-2
MF	zinc ion binding	10	2.7E-2
MF	oxidoreductase activity	8	4.6E-2
MF	ubiquitin protein ligase activity	4	4.9E-2

Supplementary table 17. Gene enrichment analysis ($P \leq 0.05$) of the common genes down-regulated by CR (AL-Wt vs CR-Wt) and up-regulated by *Rorc* knockout mice compared to Wt mice under CR conditions (CR-Wt vs CR-KO) using DAVID bioinformatics source. (BP, biological process; CC, cellular component; MF, molecular function).